Journal of the Serbian Chemical Society

*e*rsion
*e*lectronic

Available on line at

СХД
1897

www.shd.org.rs/JSCS/

The full search of JSCS
is available through

DOAJ DIRECTORY OF
OPEN ACCESS
JOURNALS

www.doaj.org

INSTRUCTIONS FOR AUTHORS (2021)

GENERAL

The *Journal of the Serbian Chemical Society* (the *Journal* in further text) is an international journal publishing papers from all fields of chemistry and related disciplines. Twelve issues are published annually. The Editorial Board expects the editors, reviewers, and authors to respect the well-known standard of professional ethics.

Types of Contributions

Original scientific papers	(up to 15 typewritten pages, including Figures, Tables and References) report original research which must not have been previously published.
Short communications	(up to 8 pages) report unpublished preliminary results of sufficient importance to merit rapid publication.
Notes	(up to 5 pages) report unpublished results of short, but complete, original research
Authors' reviews	(up to 40 pages) present an overview of the author's current research with comparison to data of other scientists working in the field
Reviews[a]	(up to 40 pages) present a concise and critical survey of a specific research area. Generally, these are prepared at the invitation of the Editor
Surveys	(about 25 pages) communicate a short review of a specific research area.
Book and Web site reviews	(1 - 2 pages)
Extended abstracts	(about 4 pages) of Lectures given at meetings of the Serbian Chemical Society Divisions
Letters to the Editor	report miscellaneous topics directed directly to the Editor

[a]Generally, Authors' reviews, Reviews and Surveys are prepared at the invitation of the Editor.

Submission of manuscripts

Manuscripts should be submitted using the **OnLine Submission Form**, available on the JSCS Web Site (**http://www.shd-pub.org.rs/index.php/JSCS**). The manuscript must be uploaded as a Word.doc or .rtf file, with tables and figures (including the corresponding captions – above Tables and below Figures), placed within the text to follow the paragraph in which they were mentioned for the first time.

Please note that **Full Names (**First Name, Last Name), **Full Affiliation** and **Country** (from drop down menu) of **ALL OF AUTHORS** (written in accordance with English spelling rules - the first letter capitalized) must be entered in the manuscript Submission Form (Step 3). Manuscript Title, authors' names and affiliations, as well as the Abstract, **WILL APPEAR** in the article listing, as well as in **BIBLIOGRAPHIC DATABASES (WoS, SCOPUS...)**, in the form and in the order entered in the author details

Graphical abstract

Graphical abstract is a one-image file containing the main depiction of the authors work and/or conclusion and must be supplied along with the manuscript. It must enable readers to quickly gain the main message of the paper and to encourage browsing, help readers identify which papers are most relevant to their research interests. Authors must provide an image that clearly represents the research described in the paper. The most relevant figure from the work, which summarizes the content, can also be submitted. The image should be submitted as a separate file in **Online Submission Form - Step 2**.

Specifications: The graphical abstract should have a clear start and end, reading from top to bottom or left to right. Please omit unnecessary distractions as much as possible.

- **Image size:** minimum of 500×800 pixels (W×H) and a minimum resolution of 300 dpi. If a larger image is sent, then please use the same ratio: 16 wide × 9 high. Please note that your image will be scaled proportionally to fit in the available window in TOC; a 150x240 pixel rectangle. Please be sure that the quality of an image cannot be increased by changing the resolution from lower to higher, but only by rescanning or exporting the image with a higher resolution, which can be set in usual "settings" option.
- **Font:** Please use Calibri and Symbol font with a large enough font size, so it is readable even from the image of a smaller size (150 × 240 px) in TOC.
- **File type:** JPG and PNG only.

No additional text, outline or synopsis should be included. Please do not use white space or any heading within the image.

Cover Letter

Manuscripts must be accompanied by a cover letter (strictly uploaded in **Online Submission Step 2**) in which the type of the submitted manuscript and a warranty as given below are given. The Author(s) has(have) to warranty that the manuscript submitted to the *Journal* for review is original, has been written by the stated author(s) and has not been published elsewhere; is currently not being considered for publication by any other journal and will not be submitted for such a review while under review by the *Journal*; the manuscript contains no libellous or other unlawful statements and does not contain any materials that violate any personal or proprietary rights of any other person or entity. All manuscripts will be acknowledged on receipt (by e-mail).

Illustrations

Illustrations (Figs, schemes, photos…) in TIF or EPS format (JPG format is acceptable for colour and greyscale photos, only), must be additionally uploaded (Online Submission Step 2) as a separate file or one archived (.zip, .rar or .arj) file. Figures and/or Schemes should be prepared according to the **Artwork Instructions -** http://www.shd.org.rs/JSCS/jscs-pdf/Artwork_Instructions.pdf!

For any difficulties and questions related to **OnLine Submission Form -** https://www.shd-pub.org.rs/index.php/JSCS/submission/wizard, please refer to **User Guide -** https://openjournal-systems.com/ojs-3-user-guide/ , Chapter **Submitting an Article -** https://openjournalsystems.com/ojs-3-user-guide/submitting-an-article/. If difficulties still persist, please contact JSCS Editorial Office at **JSCS@shd.org.rs**

A manuscript not prepared according to these instructions will be returned for resubmission without being assigned a reference number.

Conflict-of-Interest Statement*: Public trust in the peer review process and the credibility of published articles depend in part on how well a conflict of interest is handled during writing, peer review, and editorial decision making. A conflict of interest exists when an author (or the author's institution), reviewer, or editor has financial or personal relationships that inappropriately influence (bias) his or her actions (such relationships are also known as dual commitments, competing interests, or competing loyalties). These relationships vary from those with negligible potential to those with great potential to influence judgment, and not all relationships represent true conflict of interest. The potential for a conflict of interest can exist whether or not an individual believes that the relationship affects his or her scientific judgment. Financial relationships (such as employment, consultancies, stock ownership, honoraria, paid expert testimony) are the most easily identifiable conflicts of interest and the most likely to undermine the credibility of the journal, the authors, and of science itself. However, conflicts can occur for other reasons, such as personal relationships, academic competition, and intellectual passion.

Informed Consent Statement*: Patients have a right to privacy that should not be infringed without informed consent. Identifying information, including patients' names, initials, or hospital numbers, should not be published in written descriptions, photographs, and pedigrees unless the information is essential for scientific purposes and the patient (or parent or guardian) gives written informed consent for publication. Informed consent for this purpose requires that a patient who is identifiable be shown the manuscript to be published. Authors should identify Individuals who provide writing assistance and disclose the funding source for this assistance. Identifying details should be omitted if they are not essential. Complete anonymity is difficult to achieve, however, and informed consent should be obtained if there is any doubt. For example, masking the eye region in photographs of patients is inadequate protection of anonymity. If identifying characteristics are altered to protect anonymity, such as in genetic pedigrees, authors should provide assurance that alterations do not distort scientific meaning and editors should so note. The requirement for informed consent should be included in the journal's instructions for authors. When informed consent has been obtained it should be indicated in the published article.

Human and Animal Rights Statement* When reporting experiments on human subjects, authors should indicate whether the procedures followed were in accordance with the ethical standards of the responsible committee on human experimentation (institutional and national) and with the Helsinki Declaration of 1975, as revised in 2000 (5). If doubt exists whether the research was conducted in accordance with the Helsinki Declaration, the authors must explain the rationale for their approach, and demonstrate that the institutional review body explicitly approved the doubtful aspects of the study. When reporting experiments on animals, authors should be asked to indicate whether the institutional and national guide for the care and use of laboratory animals was followed.

---

*International Committee of Medical Journal Editors ("Uniform Requirements for Manuscripts Submitted to Biomedical Journals"), February 2006

PROCEDURE

All contributions will be peer reviewed and only those deemed worthy and suitable will be accepted for publication. The Editor has the final decision. To facilitate the reviewing process, authors are encouraged to suggest up to three persons competent to review their manuscript. Such suggestions will be taken into consideration but not always accepted. If authors would prefer a specific person not be a reviewer, this should be announced. The Cover Letter must be accompanied by these suggestions. Manuscripts requiring revision should be returned according to the requirement of the Editor, within 60 days upon reception of the reviewing comments by e-mail.

The *Journal* maintains its policy and takes the liberty of correcting the English as well as false content of manuscripts **provisionally accepted** for publication in the first stage of reviewing process. In this second stage of manuscript preparation by JSCS Editorial Office, the author(s) may be required to supply some **additional clarifications and corrections**. This procedure will be executed during copyediting actions, with a demand to author(s) to perform corrections of unclear parts before the manuscript would be published OnLine as **finally accepted manuscript (OLF Section of the JSCS website)**. Please note that the manuscript can receive the status of **final rejection** if the author's corrections would not be satisfactory.

When finally accepted manuscript is ready for printing, the corresponding author will receive a request for proof reading, which should be performed within 2 days. Failure to do so will be taken as the authors agree with any alteration which may have occurred during the preparation of the manuscript for printing.

Accepted manuscripts of active members of the Serbian Chemical Society (all authors) have publishing priority.

MANUSCRIPT PRESENTATION

Manuscripts should be typed in English (either standard British or American English, but consistent throughout) with 1.5 spacing (12 points Times New Roman; Greek letters in the character font Symbol) in A4 format leaving 2.5 cm for margins. For Regional specific, non-standard characters that may appear in the text, save documents with Embed fonts Word option: *Save as -> (Tools) -> Save Options... -> Embed fonts in the text.*

The authors are requested to seek the assistance of competent English language expert, if necessary, to ensure their English is of a reasonable standard. The Serbian Chemical Society can provide this service in advance of submission of the manuscript. If this service is required, please contact the office of the Society by e-mail (jscs-info@shd.org.rs).

Tables, figures and/or schemes must be embedded in the main text of the manuscript and should follow the paragraph in which they are mentioned for the first time. **Tables** must be prepared with the aid of the **WORD table function**, without vertical lines. The minimum size of the font in the tables should be **10 pt**. Table columns must not be formatted using multiple spaces. Table rows must not be formatted using any returns (enter key; ↵ key) and are **limited to 12 cm width**. Tables should not be incorporated as graphical objects. **Footnotes to Tables** should follow them and are to be indicated consequently (in a single line) in superscript letters and separated by semi-column.

Table caption must be placed above corresponding Table, while **Captions of the Illustrations** (Figs. Schemes...) must follow the corresponding item. **The captions, either for Tables or Illustrations**, should make the items comprehensible without reading of the main text (but clearly referenced in), must follow numerical order (Roman for Tables, Arabic for Illustrations), and should not be provided on separate sheets or as separate files.

High resolution Illustrations (named as Fig. 1, Fig. 2... and/or Scheme 1, Scheme 2...) in **TIF or EPS format** (JPG format is acceptable for photos, only) **must be additionally uploaded as a separate files or one archived (.zip, .rar) file.**

Illustrations should be prepared according to the <u>ARTWORK INSTRUCTIONS</u> - http://www.shd.org.rs/JSCS/jscs-pdf/Artwork_Instructions.pdf. **!**

All pages of the manuscript must be numbered continuously.

DESIGNATION OF PHYSICAL QUANTITIES AND UNITS

IUPAC recommendations for the naming of compounds should be followed. SI units, or other permissible units, should be employed. The designation of physical quantities must be in italic throughout the text (including figures, tables and equations), whereas the units and indexes (except for indexes having the meaning of physical quantities) are in upright letters. They should be in Times New Roman font. In graphs and tables, a slash should be used to separate the designation of a physical quantity from the unit

(example: p / kPa, j / mA cm^{-2}, t / °C, T_0 / K, τ / h, ln (j / mA cm^{-2})…). Designations such as: p (kPa), t [min]…, are not acceptable. However, if the full name of a physical quantity is unavoidable, it should be given in upright letters and separated from the unit by a comma (example: Pressure, kPa; Temperature, K; Current density, mA cm^{-2}…). Please do not use the axes of graphs for additional explanations; these should be mentioned in the figure captions and/or the manuscript (example: "pressure at the inlet of the system, kPa" should be avoided). The axis name should follow the direction of the axis (the name of y-axis should be rotated by 90°). Top and right axes should be avoided in diagrams, unless they are absolutely necessary.

Latin words, as well as the names of species, should be in *italic*, as for example: *i.e., e.g., in vivo, ibid, Calendula officinalis* L., *etc*. The branching of organic compound should also be indicated in *italic*, for example, *n*-butanol, *tert*-butanol, *etc*.

Decimal numbers must have decimal points and not commas in the text (except in the Serbian abstract), tables and axis labels in graphical presentations of results. Thousands are separated, if at all, by a comma and not a point.

Mathematical and chemical equations should be given in separate lines and must be numbered, Arabic numbers, consecutively in parenthesis at the end of the line. All equations should be embedded in the text Complex equations (fractions, integrals, matrix…) should be prepared with the aid of the **Microsoft Equation 3.0** (or higher) or **MathType** (Do not use them to create simple equations and labels). **Using the Insert -> Equation option, integrated in MS Office 2010 and MS Office 2013, as well as insertion of equation objects within paragraph text IS NOT ALLOWED.**

ARTICLE STRUCTURE
- TITLE PAGE;
- MAIN TEXT – including Tables and Illustrations with corresponding captions;
- SUPPLEMENTARY MATERIAL (optional)

Title page
- **Title** in bold letters, should be clear and concise, preferably 12 words or less. The use of non-standard abbreviations, symbols and formulae is discouraged.
- AUTHORS' NAMES in capital letters with the full first name, initials of further names separated by a space and surname. Commas should separate the author's names except for the last two names when 'and' is to be used. In multi-affiliation manuscripts, the author's affiliation should be indicated by an Arabic number placed in superscript after the name and before the affiliation. Use * to denote the corresponding author(s).
- *Affiliations* should be written in italic. The e-mail address of the corresponding author should be given after the affiliation(s).
- *Abstract:* A one-paragraph abstract written of 150 – 200 words in an impersonal form indicating the aims of the work, the main results and conclusions should be given and clearly set off from the text. Domestic authors should also submit, on a separate page, an Abstract - Izvod, the author's name(s) and affiliation(s) in Serbian (Cyrillic letters). (Домаћи аутори морају доставити Извод (укључујући имена аутора и афилијацију) на српском језику, исписане ћирилицом, иза Захвалнице, а пре списка референци.) For authors outside Serbia, the Editorial Board will provide a Serbian translation of their English abstract.
- *Keywords:* Up to 6 keywords should be given. Do not use words appearing in the manuscript title
- RUNNING TITLE: A one line (maximum five words) short title in capital letters should be provided.

Main text – should have the form:
- **INTRODUCTION,**
- **EXPERIMENTAL (RESULTS AND DISCUSSION),**
- **RESULTS AND DISCUSSION (EXPERIMENTAL),**
- **CONCLUSIONS,**
- **NOMENCLATURE (optional) and**
- *Acknowledgements*: **If any.**
- REFERENCES (Citation of recent papers published in chemistry journals that highlight the significance of work to the general readership is encouraged.)

The sections should be arranged in a sequence generally accepted for publication in the respective fields. They subtitles should be in capital letters, centred and NOT numbered.

- The INTRODUCTION should include the aim of the research and a concise description of background information and related studies directly connected to the paper.
- The EXPERIMENTAL section should give the purity and source of all employed materials, as well as details of the instruments used. The employed methods should be described in sufficient detail to enable experienced persons to repeat them. Standard procedures should be referenced and only modifications described in detail. On no account should results be included in the experimental section.

Chemistry

Detailed information about instruments and general experimental techniques should be given in all necessary details. If special treatment for solvents or chemical purification were applied that must be emphasized.

Example: Melting points were determined on a Boetius PMHK or a Mel-Temp apparatus and were not corrected. Optical rotations were measured on a Rudolph Research Analytical automatic polarimeter, Autopol IV in dichloromethane (DCM) or methanol (MeOH) as solvent. IR spectra were recorded on a Perkin-Elmer spectrophotometer FT-IR 1725X. ^{1}H and ^{13}C NMR spectra were recorded on a Varian Gemini-200 spectrometer (at 200 and 50 MHz, respectively), and on a Bruker Ultrashield Advance III spectrometer (at 500 and 125 MHz, respectively) employing indicated solvents (*vide infra*) using TMS as the internal standard. Chemical shifts are expressed in ppm (δ / ppm) values and coupling constants in Hz (J / Hz). ESI-MS spectra were recorded on Agilent Technologies 6210 Time-Of-Flight LC-MS instrument in positive ion mode with CH_3CN/H_2O 1/1 with 0.2 % HCOOH as the carrying solvent solution. Samples were dissolved in CH_3CN or MeOH (HPLC grade purity). The selected values were as follows: capillary voltage = 4 kV, gas temperature = 350 °C, drying gas flow 12 L min^{-1}, nebulizer pressure = 310 kPa, fragmentator voltage = 70 V.The elemental analysis was performed on the Vario EL III- C,H,N,S/O Elemental Analyzer (Elementar Analysensysteme GmbH, Hanau-Germany). Thin-layer chromatography (TLC) was performed on precoated Merck silica gel 60 F254 and RP-18 F254 plates. Column chromatography was performed on Lobar LichroPrep Si 60 (40-63 μm), RP-18 (40-63 μm) columns coupled to a Waters RI 401 detector, and on Biotage SP1 system with UV detector and FLASH 12+, FLASH 25+ or FLASH 40+ columns pre packed with KP-SIL [40-63 μm, pore diameter 6 nm (60 Å)], KP-C18-HS (40-63 μm, pore diameter 9 nm (90 Å) or KP-NH [40-63 μm, pore diameter 10 nm (100 Å)] as adsorbent. Compounds were analyzed for purity (HPLC) using a Waters 1525 HPLC dual pump system equipped with an Alltech, Select degasser system, and dual λ 2487 UV-VIS detector. For data processing, Empower software was used (methods A and B). Methods C and D: Agylent Technologies 1260 Liquid Chromatograph equipped with Quat Pump (G1311B), Injector (G1329B) 1260 ALS, TCC 1260 (G1316A) and Detector 1260 DAD VL+ (G1315C). For data processing, LC OpenLab CDS ChemStation software was used. For details, see Supporting Information.

1. Synthesis experiments

Each paragraph describing a synthesis experiment should begin with the name of the product and any structure number assigned to the compound in the Results and Discussions section. Thereafter, the compound should be identified by its structure number. Use of standard abbreviations or unambiguous molecular formulas for reagents and solvents, and of structure numbers rather than chemical names to identify starting materials and intermediates, is encouraged.

When a new or improved synthetic method is described, the yields reported in key experimental examples, and yields used for comparison with existing methods, should represent amounts of isolated and purified products, rather than chromategraphically or spectroscopically determined yields. Reactant quantities should be reported in weight and molar units and for product yields should be reported in weight units; percentage yields should only be reported for materials of demonstrated purity. When chromatography is used for product purification, both the support and solvent should be identified.

2. Microwave experiments

Reports of syntheses conducted in microwave reactors must clearly indicate whether sealed or open reaction vessels were used and must document the manufacturer and model of the reactor, the method of monitoring the reaction mixture temperature, and the temperature-time profile. Reporting a wattage rating or power setting is not an acceptable alternative to providing temperature data. Manuscripts describing work done with domestic (kitchen) microwave ovens will not be accepted except for studies where the unit is used for heating reaction mixtures at atmospheric pressure.

3. Compound characterization

The Journal upholds a high standard for compound characterization to ensure that substances being added to the chemical literature have been correctly identified and can be synthesized in known yield and purity by the reported preparation and isolation methods. For **all new** compounds, evidence adequate to establish both **identity** and **degree of purity** (homogeneity) must be provided.

Identity - Melting point. All homogeneous solid products (*e.g.* not mixtures of isomers) should be characterized by melting or decomposition points. The colors and morphologies of the products should also be noted.

Specific rotations. Specific rotations based on the equation $[\alpha]^t;D = (100\ \alpha) / (l\ c)$ should be reported as unitless numbers as in the following example: $[\alpha]^{20};\ D = -25.4$ (*c* 1.93, CHCl$_3$), where c / g mL^{-1} is concentration and l / dm is path length. The units of the specific rotation, (deg mL) / (g dm), are implicit and are not included with the reported value.

Spectra/Spectral Data. Important IR adsorptions should be given.

For all new diamagnetic substances, NMR data should be reported (^{1}H, ^{13}C, and relevant heteronuclei). ^{1}H NMR chemical shifts should be given with two digits after the decimal point. Include the number of protons represented by the signal, signal multiplicity, and coupling constants as needed (*J* italicized, reported with up to one digit after the decimal). The number of bonds through which the coupling is operative, ^xJ, may be specified by the author if known with a high degree of certainty. ^{13}C NMR signal shifts should be rounded to the nearest 0.01 ppm unless greater precision is needed to distinguish closely spaced signals. Field strength should be noted for each spectrum, not as a comment in the general experimental section. Hydrogen multiplicity (C, CH, CH$_2$, CH$_3$) information obtained from routine DEPT spectra should be included. If detailed signal assignments are made, the type of NOESY or COSY methods used to establish atom connectivity and spatial relationships should be identified in the Supporting Information. Copies of spectra should also be included where structure assignments of complex molecules depend heavily on NMR interpretation. Numbering system used for assignments of signals should be given in the Supporting Information with corresponding general structural formula of named derivative.

HPLC/LCMS can be substituted for biochemistry papers where the main focus is not on compound synthesis.

HRMS/elemental analysis. To support the molecular formula assignment, HRMS data accurate within 5 ppm, or combustion elemental analysis [carbon and hydrogen (and nitrogen, if present)] data accurate within 0.5 %, should be reported for new compounds. HRMS data should be given in format as is usually given for combustion analysis: calculated mass for given formula following with observed mass: (+)ESI-HRMS *m/z*: [molecular formula + H]$^+$ calculated mass, observed mass. Example: (+)ESI-HRMS *m/z*: calculated for [C$_{13}$H$_8$BrCl$_2$N + H$^+$] 327.92899, observed 327.92792.

NOTE: in certain cases, a crystal structure may be an acceptable substitute for HRMS/elemental analysis.

Biomacromolecules. The structures of biomacromolecules may be established by providing evidence about sequence and mass. Sequences may be inferred from the experimental order of amino acid, saccharide, or nucleotide coupling, from known sequences of templates in enzyme-mediated syntheses, or through standard sequencing techniques. Typically, a sequence will be accompanied by MS data that establish the molecular weight.

Example: Product was isolated upon column chromatography [dry flash (SiO$_2$, eluent EA, EA/MeOH gradient 95/5 → 9/1, EA/MeOH/NH$_3$ gradient 18/0.5/0.5 → 9/1/1, and flash chromatography (Biotage SP1, RP column, eluent MeOH/H$_2$O gradient 75/25 → 95/5, N-H column, eluent EA/Hex gradient 6/3 → EA). was obtained after flash column chromatography (Biotage SP NH column, eluent hexane/EA 4:6 → 2:6). Yield 968.4 mg (95 %). Colorless foam softens at 96-101 °C. $[\alpha]^{20};\ D = +0,163$ (*c* =2.0×10^{-3} g/mL, CH$_2$Cl$_2$). IR (ATR): 3376w, 2949m, 2868w, 2802w, 1731s, 1611w, 1581s, 1528m, 1452m, 1374s, 1331w, 1246s, 1171m, 1063w, 1023m, 965w, 940w, 881w, 850w, 807w, cm^{-1}. ^{1}H NMR (500 MHz, CDCl$_3$, δ): 8.46 (*d*, 1H, *J* = 5.4, H-2'), 7.89 (*s*, 1H, *J* = 2.0, H-8'), 7.71 (*d*, 1H, *J* = 8.9, H-5'), 7.30 (*dd*, 1H, *J$_1$* = 8.8, *J$_2$* = 2.1, H-6'), 6.33 (*d*, 1H, *J* = 5.4, H-3'), 6.07 (*s*, HN-Boc, exchangeable with D$_2$O), 5.06 (*s*, 1H, H-12), 4.92-4.88 (*m*, 1H, H-7), 4.42 (*bs*, H-3), 3.45 (*s*,CH$_3$-N), 3.33 (*bs*, H-9'), 3.05-2.95 (*m*, 2H, H-11'), 2.70-2.43 (*m*, 2H, H-24) and HN, exchangeable with D$_2$O), 2.07 (*s*, CH$_3$COO), 2.04 (*s*, CH$_3$COO), 1.42 (*s*, 9H, (CH$_3$)$_3$C-N(Boc)), 0.88 (*s*, 3H, CH$_3$-10), 0.79 (*d*, 3H,*J* = 6.6, CH$_3$-20), 0.68 (*s*, 3H, CH$_3$-13). ^{13}C NMR (125 MHz, CDCl$_3$, δ): 170.34, 170.27, 151.80, 149.92, 148.87, 134.77, 128.36, 125.11, 121.43, 117.29, 99.98, 75.41, 70.82, 50.43, 49.66, 47.60, 47.33, 44.97, 43.30, 41.83, 41.48, 37.65, 36.35, 35.44, 34.89,

34.19, 33.23, 31.24, 28.79, 28.35, 27.25, 26.45, 25.45, 22.74, 22.63, 21.57, 21.31, 17.85, 12.15. (+)ESI-HRMS (m/z): calculated for $[C_{45}H_{67}ClN_4O_6 + H]^+$ 795.48219, observed 795.48185. Combustion analysis for $C_{45}H_{67}ClN_4O_6$: Calculated. C 67.94, H 8.49, N 7.04; found C 67.72, H 8.63, N 6.75. HPLC purity: method A: RT 1.994, area 99.12 %; method C: RT 9.936, area 98.20 %.

Purity - Evidence for documenting compound purity should include one or more of the following:

a) Well-resolved high field 1D ^{1}H NMR spectrum showing at most only trace peaks not attributable to the assigned structure and a standard 1D proton-decoupled ^{13}C NMR spectrum. Copies of the spectra should be included as figures in the Supporting Information.

b) Quantitative gas chromatographic analytical data for distilled or vacuum-transferred samples, or quantitative HPLC analytical data for materials isolated by column chromatography or separation from a solid support. HPLC analyses should be performed in two diverse systems. The stationary phase, solvents (HPLC), detector type, and percentage of total chromatogram integration should be reported; a copy of the chromatograms may be included as a figure in the Supporting Information.

c) Electrophoretic analytical data obtained under conditions that permit observing impurities present at the 5 % level.

HRMS data may be used to support a molecular formula assignment **but cannot be used as a criterion of purity**.

4. Biological Data

Quantitative biological data are required for all tested compounds. Biological test methods must be referenced or described in sufficient detail to permit the experiments to be repeated by others. Detailed descriptions of biological methods should be placed in the experimental section. Standard compounds or established drugs should be tested in the same system for comparison. Data may be presented as numerical expressions or in graphical form; biological data for extensive series of compounds should be presented in tabular form. Tables consisting primarily of negative data will not usually be accepted; however, for purposes of documentation they may be submitted as supporting information. Active compounds obtained from combinatorial syntheses should be resynthesized and retested to verify that the biology conforms to the initial observation.

Statistical limits (statistical significance) for the biological data are usually required. If statistical limits cannot be provided, the number of determinations and some indication of the variability and reliability of the results should be given. References to statistical methods of calculation should be included. Doses and concentrations should be expressed as molar quantities (*e.g.*, mol/kg, μmol/kg, M, mM). The routes of administration of test compounds and vehicles used should be indicated, and any salt forms used (hydrochlorides, sulfates, *etc.*) should be noted. The physical state of the compound dosed (crystalline, amorphous; solution, suspension) and the formulation for dosing (micronized, jet-milled, nanoparticles) should be indicated. For those compounds found to be inactive, the highest concentration (*in vitro*) or dose level (*in vivo*) tested should be indicated.

- The RESULTS AND DISCUSSION should include concisely presented results and there significance discussed and compared to relevant literature data. The results and discussion may be combined or kept separate.

- The inclusion of a CONCLUSION section, which briefly summarizes the principal conclusions, is recommended.

- NOMENCLATURE is optional but, if the authors wish, a list of employed symbols may be included.

- REFERENCES should be numbered sequentially as they appear in the text. Please note that any reference numbers appearing in the Illustrations and/or Tables and corresponding captions must follow the numbering sequence of the paragraph in which they appear for the first time. When cited, the reference number should be superscripted in Font 12, following any punctuation mark. In the reference list, they should be in normal position followed by a full stop. Reference entry must not be formatted using Carriage returns (enter key; ↵ key) or multiple space key. The formatting of references to published work should follow the *Journal's* style as follows:

Journals[a]:   A. B. Surname1, C. D. Surname2, *J. Serb. Chem. Soc.* **Vol** (Year) first page Number (https://doi.org/doi)[b]

Books: A. B. Surname1, C. D. Surname2, *Name of Book*, Publisher, City, Year, pp. 100-101 (https://doi.org/doi)[b]

Compilations:A. B. Surname1, C. D. Surname2, in *Name of Compilation*, A. Editor1, C. Editor2, Ed(s)., Publisher, City, Year, p. 100 (https://doi.org/doi)[b]

Proceedings: A. B. Surname1, C. D. Surname2, in *Proceedings of Name of the Conference or Symposium*, (Year), Place of the Conference, Country, *Title of the Proceeding*, Publisher, City, Year, p. or Abstract No. 100

Patents: A. B. Inventor1, C. D. Inventor2, (Holder), Country Code and patent number (registration year)

Chemical Abstracts: A. B. Surname1, C. D. Surname2, *Chem. Abstr.* CA 234 567a; For non-readily available literature, the Chemical Abstracts reference should be given in square brackets: [C.A. 139/2003 357348t] after the reference

Standards: EN ISO 250: *Name of the Standard* (Year)

Websites: Title of the website, URL in full (date accessed)

[a] When citing Journals, the International Library Journal abbreviation is required. Please consult, *e.g.*, https://images.webofknowledge.com/WOK46/help/WOS/A_abrvjt.html

[b] doi should be replaced by doi number of the Article, for example: http://dx.doi.org/10.2298/JSC161212085B (as active link). If doi do not exist, provide the link to the online version of the publication.

Only the last entry in the reference list should end with a full stop.

The names of all authors should be given in the list of references; the abbreviation *et al.* may only be used in the text. The original journal title is to be retained in the case of publications published in any language other than English (please denote the language in parenthesis after the reference). Titles of publications in non-Latin alphabets should be transliterated. Russian references are to be transliterated using the following transcriptions:

ж→zh, х→kh, ц→ts, ч→ch, ш→sh, щ→shch, ы→y, ю→yu, я→ya, э→e, й→i, ь→'.

Supplementary material

Authors are encouraged to presentthe information and results non-essential to the understanding of their paper as SUPPLEMENTARY MATERIAL (can be uploaded inStep 4 of Online Submission). This material may include as a rule, but is not limited to, the presentation of analytical and spectral data demonstrating the identity and purity of synthesized compounds, tables containing raw data on which calculations were based, series of figures where one example would remain in the main text, etc. The Editorial Board retain the right to assign such information and results to the Supplementary material when deemed fit. Supplementary material does not appear in printed form but can be downloaded from the web site of the JSCS.

Mathematical and chemical equations should be given in separate lines and must be numbered, Arabic numbers, consecutively in parenthesis at the end of the line. All equations should be embedded in the text Complex equations (fractions, integrals, matrix…) should be prepared with the aid of the Microsoft Equation 3.0 (or higher) or MathType (Do not use them to create simple equations and labels). Using the Insert -> Equation option, integrated in MS Office 2010 and MS Office 2013, as well as insertion of equation objects within paragraph text IS NOT ALLOWED.

Deposition of crystallographic data

Prior to submission, the crystallographic data included in a manuscript presenting such data should be deposited at the appropriate database. Crystallographic data associated with organic and metal-organic structures should be deposited at the Cambridge Crystallographic Data Centre (CCDC) by e-mail to **deposit@ccdc.cam.ac.uk**

Crystallographic data associated with inorganic structures should be deposited with the Fachinformationszentrum Karlsruhe (FIZ) by e-mail to **crysdata@fiz-karlsruhe.de**. A deposition number will then be provided, which should be added to the reference section of the manuscript.

For detailed instructions please visit the JSCS website:
https://www.shd-pub.org.rs/index.php/JSCS/Instructions

ARTWORK INSTRUCTIONS

JSCS accepts only **TIFF** or **EPS** formats, as well as **JPEG** format (only for colour and greyscale photographs) for electronic artwork and graphic files. **MS files** (Word, PowerPoint, Excel, Visio) **NOT acceptable**. Generally, scanned instrument data sheets should be avoided. Authors are responsible for the quality of their submitted artwork. Every single Figure or Scheme, as well as any part of the Figure (A, B, C…) should be prepared according to following instructions (every part of the figure, A, B, C…, must be submitted as an independent single graphic file):

TIFF

Virtually all common artwork and graphic creation software is capable of saving files in TIFF format. This 'option' can normally be found under 'the 'Save As...' or 'Export...' commands in the 'File' menu.

TIFF (Tagged Image File Format) is the recommended file format for bitmap, greyscale and colour images.

- Colour images should be in the RGB mode
- When supplying TIFF files, please ensure that the files are supplied at the correct resolution:
    1. Line artwork: minimum of 1000 dpi
    2. RGB image: minimum of 300 dpi
    3. Greyscale image: minimum of 300 dpi
    4. Combination artwork (line/greyscale/RGB): minimum of 500 dpi
- Images should be tightly cropped, without frame and any caption.
- If applicable please re-label artwork with a font supported by JSCS (Arial, Helvetica, Times, Symbol) and ensure it is of an appropriate font size.
- Save an image in TIFF format with LZW compression applied.
- It is recommended to remove Alpha channels before submitting TIFF files.
- It is recommended to flatten layers before submitting TIFF files.

Please be sure that quality of an image cannot be increased by changing the resolution from lower to higher, but only by rescanning or exporting the image with higher resolution, which can be set in usual "settings" facilities.

EPS

Virtually all common artwork creation software, such as Canvas, ChemDraw, CorelDraw, SigmaPlot, Origin Lab…, are capable of saving files in EPS format. This 'option' can normally be found under the 'Save As...' or 'Export...' commands in the 'File' menu.

For vector graphics, EPS (Encapsulated PostScript) files are the preferred format as long as they are provided in accordance with the following conditions:

- when they contain bitmap images, the bitmaps should be of good resolution (see instructions for TIFF files)
- when colour is involved, it should be encoded as RGB
- an 8-bit preview/header at a resolution of 72 dpi should always be included
- embed fonts should always included and only the following fonts should be used in artwork: Arial, Helvetica, Times, Symbol
- the vertical space between the parts of an illustration should be limited to the bare necessity for visual clarity
- no data should be present outside the actual illustration area
- line weights should range from 0.35 pt to 1.5 pt
- when using layers, they should be reduced to one layer before saving the image (Flatten Artwork)

JPEG

Virtually all common artwork and graphic creation software is capable of saving files in JPEG format. This 'option' can normally be found under 'the 'Save As...' or 'Export...' commands in the 'File' menu.

JPEG (Joint Photographic Experts Group) is the acceptable file format **only for colour and greyscale photographs**. JPEG can be created with respect to photo quality (low, medium, high; from 1 to 10), ensuring file sizes are kept to a minimum to aid easy file transfer. Images should have a minimum resolution of 300 dpi. Image width: minimum 3.0 cm; maximum 12.0 cm.

Please be sure that quality of an image cannot be increased by changing the resolution from lower to higher, but only by rescanning or exporting the image with higher resolution, which can be set in usual "settings" facilities.

SIZING OF ARTWORK

- JSCS aspires to have a uniform look for all artwork contained in a single article. Hence, it is important to be aware of the style of the journal.
- Figures should be submitted in black and white or, if required, colour (charged). If coloured figures or photographs are required, this must be stated in the cover letter and arrangements made for payment through the office of the Serbian Chemical Society.
- As a general rule, the lettering on an artwork should have a finished, printed size of 11 pt for normal text and no smaller than 7 pt for subscript and superscript characters. Smaller lettering will yield a text that is barely legible. This is a rule-of-thumb rather than a strict rule. There are instances where other factors in the artwork, (for example, tints and shadings) dictate a finished size of perhaps 10 pt. Lines should be of at least 1 pt thickness.
- When deciding on the size of a line art graphic, in addition to the lettering, there are several other factors to address. These all have a bearing on the reproducibility/readability of the final artwork. Tints and shadings have to be printable at the finished size. All relevant detail in the illustration, the graph symbols (squares, triangles, circles, *etc.*) and a key to the diagram (to explain the explanation of the graph symbols used) must be discernible.
- The sizing of halftones (photographs, micrographs,...) normally causes more problems than line art. It is sometimes difficult to know what an author is trying to emphasize on a photograph, so you can help us by identifying the important parts of the image, perhaps by highlighting the relevant areas on a photocopy. The best advice that can be given to graphics suppliers is not to over-reduce halftones. Attention should also be paid to magnification factors or scale bars on the artwork and they should be compared with the details inside. If a set of artwork contains more than one halftone, again please ensure that there is consistency in size between similar diagrams.

General sizing of illustrations which can be used for the Journal of the Serbian Chemical Society:

- Minimum fig. size: 30 mm width
- Small fig. size - 60 mm width
- Large fig. size - 90 mm width
- Maximum fig. size - 120 mm width

Pixel requirements (width) per print size and resolution for bitmap images:

	Image width	A	B	C
Minimal size	30 mm	354	591	1181
Small size	60 mm	709	1181	2362
Large size	90 mm	1063	1772	3543
Maximal size	120 mm	1417	2362	4724

A: 300 dpi > RGB or Greyscale image
B: 500 dpi > Combination artwork (line/greyscale/RGB)
C: 1000 dpi> Line artwork

The designation of physical quantities and graphs formatting

The designation of physical quantities on figures must be in italic, whereas the units are in upright letters. They should be in Times New Roman font. In graphs a slash should be used to separate the designation of a physical quantity from the unit (example: p / kPa, t °C, T_0 / K, τ / h, ln (j / mA cm^{-2})…). Designations such as: p (kPa), t [min]…, are not acceptable. However, if the full name of a physical quantity is unavoiable, it should be given in upright letters and separated from the unit by a comma (example: Pressure, kPa, Temperature, K…). Please do not use the axes of graphs for additional explanations; these should be mentioned in the figure captions and/or the manuscript (example: "pressure at the inlet of the system, kPa" should be avoided). The axis name should follow the direction of the axis (the name of y-axis should be rotated by 90°). Top and right axes should be avoided in diagrams, unless they are absolutely necessary. Decimal numbers must have decimal points and not commas in the axis labels in graphical presentations of results. Thousands are separated, if at all, by a comma and not a point.

INCORRECT

CORRECT

CONTENTS*

* For colored figures in this issue please see electronic version at the Journal Home Page:
http://www.shd.org.rs/JSCS/

New 4-aminoquinolines as moderate inhibitors of *P. falciparum* malaria

IGOR OPSENICA[1#], MILICA SELAKOVIĆ[2#], MIKLOŠ TOT[1], TATJANA VERBIĆ[1#],
JELENA SRBLJANOVIĆ[3], TIJANA ŠTAJNER[3], OLGICA DJURKOVIĆ DJAKOVIĆ[3]
and BOGDAN ŠOLAJA[1,4*#]

[1]*University of Belgrade – Faculty of Chemistry, Studentski trg 16, P.O. Box 51, 11158
Belgrade, Serbia,* [2]*Innovative Centre, Faculty of Chemistry, Ltd. Studentski Trg 12–16, 11158
Belgrade, Serbia,* [3]*Institute for Medical Research, University of Belgrade, Dr. Subotića 4,
P.O. Box 39, 11129 Belgrade, Serbia and* [4]*Serbian Academy of Sciences and Arts,
Knez Mihailova 35, 11000 Belgrade, Serbia*

Abstract: Synthesis of novel aminoquinoline derivatives has been accomplished and their activity against malaria strains has been examined. The compounds showed moderate *in vitro* antimalarial activity against two *P. falciparum* strains, 3D7 (CQ susceptible clone) and Dd2 (CQ resistant clone). Three aminoquinolines were further examined for antimalarial efficacy in a mouse model using a modified Thompson test. In this model, mice were infected with *P. berghei*-infected red blood cells, and drugs were administered orally. Antimalarial **3** was found toxic at a dose of 320 (mg/kg)/day in 3/6 mice, however, 2/6 mice of the same group survived through day 31, and one of them was cured.

Keywords: quinoline; bromobenzyl derivatives; antimalarials; *β*-hematin inhibitory activity.

INTRODUCTION

Climate change and global warming are closely associated with growing threat from infectious diseases. Increase in global temperatures favors the development and spread of tropical diseases and the associated vector organisms.[1] Warming will contribute to area expansion populated with malaria-transmitting mosquitoes. With 300–500 million clinical cases and nearly one million deaths every year, malaria is a major global public health problem.[2] Among the five known species of the *Plasmodium* genus that cause human malaria (*Plasmodium* species: *P. falciparum*, *P. ovale*, *P. vivax*, *P. malarie* and *P. knowlesi*), *P. falci-*

parum is th-e major cause of mortality. Malaria parasites use hemoglobin (Hb) as a source of nutrients, and after digestion of host Hb in the acidic food vacuole (FV) of *P. falciparum* amino acids and heme are released. The parasites use Hb amino acids as building blocks for their own protein synthesis. The heme moiety ferriprotoporphyrin-IX is toxic to the host, and the parasite has developed several mechanisms of detoxification: sequestration of heme into insoluble hemozoin,[3] and degradation of heme with hydrogen peroxide[4,5] and glutathione-mediated mechanisms[6] in the FV and cytosol, respectively. The clinical symptoms of malaria appear during the asexual intraerythrocytic stage; consequently, efforts to develop an effective drug have mainly focused on this stage of infection.[7] Malaria has been known for centuries, and there is a lot of information regarding transmission, prevention and treatment of the disease. Despite this, it is still one of the most widespread infectious diseases in the world.[8] One of the main causes is development of widespread drug resistance[9,10] especially to chloroquine (CQ), the most widely used antimalarial (Fig. 1).[11,12] Most of 4-amino-7-chloroquino-line based compounds (ACQs) act as inhibitors of hemozoin formation,[8] but it is also reported that they may act as inhibitors of oxidative[13] and gluthatione--mediated[14] heme degradation. Resistance to ACQs is closely related to reduced accumulation of drugs caused by mutations in drug transporters (PfCRT, Pgh1, and PfMRP).[15,16] The synthesis and development of novel ACQ-based derivatives has been the subject of extensive research. Efforts have focused mostly on three subclasses: bisquinolines, sidechain modified 4-aminoquinolines, and hybrid 4-aminoquinolines.[17,18]
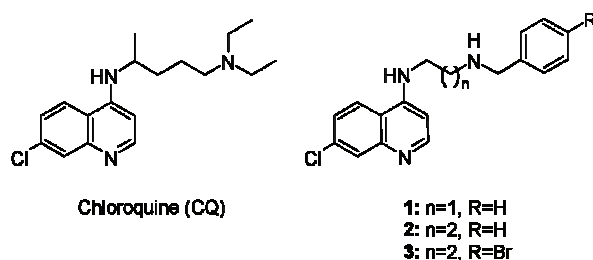
Fig. 1. Structures of CQ and potent antimalarials.

During our studies a variety of ACQ-based compounds were identified as potential antimalarial agents.[19–22] Recently, we synthesized a series of simplified analogues with the ACQ component attached via an ethylene or propylene linker to different benzyl or pyridyl-groups (Fig. 1).[23] The synthesized compounds showed promising antimalarial activities, and exhibited better potencies against CQ susceptible (CQS) and CQ resistant (CQR) strains as compared to CQ and mefloquine. The structure–activity data indicated that a substitution on the benzene ring had a significant influence on the antimalarial activity.

In order to better understand the possible influence of bromine substituents on the antimalarial activity, we synthesized ten new aminoquinoline derivatives and here we analyze their activity (Scheme 1).

ACQ2: n=1, X=Cl
ACQ3: n=2, X=Cl
ACQ4: n=3, X=Cl
ACQ6: n=5, X=Cl
DCACQ2: n=1, X=H
DCACQ4: n=3, X=H

4: n=1, X=Cl, R^1=H, R^2=Br, R^3=H, 90%
5: n=2, X=Cl, R^1=H, R^2=Br, R^3=H, 78%
6: n=2, X=Cl, R^1=Br, R^2=H, R^3=H, 85%
7: n=1, X=Cl, R^1=H, R^2=Br, R^3=Br, 78%
8: n=2, X=Cl, R^1=H, R^2=Br, R^3=Br, 63%
9: n=3, X=Cl, R^1=H, R^2=Br, R^3=Br, 69%
10: n=5, X=Cl, R^1=H, R^2=Br, R^3=Br, 61%
11: n=1, X=H, R^1=H, R^2=Br, R^3=Br, 73%
12: n=3, X=H, R^1=H, R^2=Br, R^3=Br, 63%
13: n=2, X=Cl, R^1=H, R^2=Br, R^3=NO_2, 65%

I) ArCHO, CH_2Cl_2, MeOH, AcOH, $NaBH_4$, r.t., 18 h
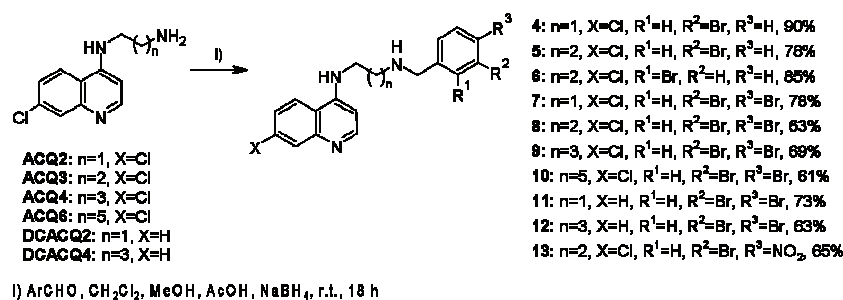
Scheme 1. Synthesis of aminoquinoline derivatives **4–13**.

In addition, we have synthesized four hybrid derivatives (Fig. 2) that include previously established antimalarial pharmacophores-aminoquinoline[24] and tetrahydroimidazo[1,2-*a*]pyrazine.[12]

14: R = H
15: R = CH_3

16: R = H
17: R = CH_3
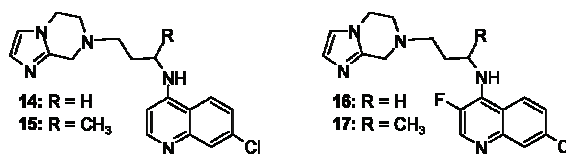
Fig. 2. Structures of hybrid derivatives.

EXPERIMENTAL

For the sake of journal space the full experimental details for the synthesis of tested compounds are given in the Supplementary material to this paper.

In vitro *antimalarial activity*

In vitro cultures of *P. falciparum*, chloroquine-sensitive 3D7 and chloroquine-resistant Dd2 strains were maintained as described previously.[25] For drug assays, parasites were synchronized with 5 % sorbitol and ring-stage parasites were seeded in 96-well plates at a 2 % parasitemia and 0.75 % hematocrit. The compounds were initially dissolved in DMSO at a concentration of 50 mM and further dilutions were made in complete culture medium (final DMSO concentration was ≤0.2 %). After an initial screen at 0.5 μM concentration, compounds that inhibited parasite growth for at least 50 % were further titrated to obtain IC_{50} and IC_{90} values at eight two-fold dilutions (3 independent experiments were performed for each compound, each with 3 replicates per condition). Control experiments using chloroquine and/or artemisinin were performed in parallel with the tested compounds. Parasite inhibition was assayed after 48 h of incubation in the presence of a drug by the colorimetric LDH assay. The test is based on the evaluation of plasmodial lactate dehydrogenase (pLDH) activity and was performed according to the previously described method.[26] IC_{50} and IC_{90} values were obtained using a sigmoidal dose–response model with the variable slope fitted to results using GraphPad Prism.

In vivo *antimalarial activity*

Antimalarial activity of novel compounds was tested in mice infected with *Plasmodium berghei* ANKA strain using a modified version of the Thompson test.[27] Prior to antimalarial efficacy experiments, all compounds were tested for toxicity.

Female C57BL/6 mice aged 12 to 14 weeks and weighing 19–21 g were used. Mice were housed at 5 to 6 animals per cage at the Institute for Medical Research Animal Facility under a natural photo period and were offered drinking water and standard feed *ad libitum*.

Mice were infected intraperitoneally (i.p.) with 250 μL of a PBS suspension containing 10^6 parasitized erythrocytes from the peripheral blood of a donor mouse. Compounds were suspended in 0.5 % hydroxyethylcellulose–0.1 % Tween 80 and administered orally at designated doses in a volume of 200 μL once a day (on day 3, 4 and 5 post-infection (p.i.)).

Mice were monitored daily and any clinical symptoms (*e.g.*, ruffled fur, decreased locomotion, lethargy, loss of appetite, lacrimation, salivation, diarrhoea, convulsions and weight loss) were noted. Parasitaemia was monitored by microscopic examination of Giemsa-stained peripheral blood smears using mouse tail blood twice a week, starting immediately before the initiation of treatment. The first time point served to check the efficacy of experimental infections, whereas all later points served to monitor compound efficacy. Mice were observed for 30 days from the day of infection. Cure was defined as the survival of treated mice with parasite clearance at 31 days p.i.

For toxicity experiments, naive mice were treated according to the described protocol of compound administration. Mice were observed daily during a period of 30 days after the first day of drug administration.

All animal studies were approved by a local (Institute for Medical Research) ethics committee. *In vivo* experiments were approved by the Veterinary Directorate of the Ministry of Agriculture and Environmental Protection of Serbia (decision no. 323-07-02444/2014--05/1).

β-*Hematin inhibitory activity assay*. The inhibition of *β*-hematin formation is expressed as the molar equivalent of compound, relative to hemin, that inhibits *β*-hematin formation by 50 % and determined by slightly modified BHIA assay introduced by Parapini *et al.*[28] Briefly, as described previously,[29] 50.0 μL of 16 mM solution of hemin in DMSO was distributed to 1.5 mL centrifuge tubes; compound dissolved in DMSO ($C_{comp} \approx 80$ mM) was added to hemin in doses ranging from 0.125 to 5 mole equivalents (pure DMSO was added to control samples). 100.0 μL of ultrapure water was added to each tube, and β-hematin formation initiated by the addition of 200.0 μL of 8 M acetate buffer (pH 5.2). The final concentration of DMSO per tube was kept constant at 25 %. Tubes were incubated at 37.0 ± 0.1 °C for 18 h and then centrifuged. The remaining pellet was resuspended in 0.500 mL DMSO to remove unreacted hematin. Tubes were then centrifuged again, DMSO-soluble fraction removed and the pellet, consisting of a pure precipitate of *β*-hematin, dissolved in 1.000 mL 0.1 M NaOH. 10.0 μL aliquots were transferred to 96-well microplate and diluted with 190.0 μl 0.1 M NaOH (200.0 μl of 0.1 M NaOH was used as a blank). The absorbance was measured at 405 nm, with correction at 670 nm (LKB 5060-006 Micro Plate Reader, Vienna, Austria). Experiments were performed in duplicate. A calibration curve of hemin dissolved in 0.1 M NaOH was made in the c_{HE} range of 0.4×10^{-5}–4.0×10^{-5} M, samples were diluted, if needed, to fit the calibration curve range.

RESULTS AND DISCUSSION

Synthesis

All compounds were synthesized in high yield by coupling commercially available aryl aldehydes with aminoquinolines via reductive amination using sodium borohydride and acetic acid (Scheme 1). Each of the final compounds was then purified by dry-flash chromatography, and tested as > 95 % pure based on m.a. and/or HPLC analysis.

Antimalarial activity

The *in vitro* antimalarial activity of the synthesized compounds was evaluated against the CQS 3D7 and the CQR Dd2 *P. falciparum* strains, using CQ and artemisinin (ART) as positive controls (Table I). Eight compounds (**1**–**3**, **5**, **6**, **8**, **11** and **12**) were quite potent, with IC_{50} values within 19–48 nM range and appeared more active against the CQR Dd2 strain than CQ. Among them, derivatives **3** and **6** were 5-fold more active than CQ.[30] In addition, **2** and **6** were as active as CQ and ART against the CQS 3D7 strain (**2**: IC_{50} = 22.05 nM; **6**: IC_{50} = 14.02 nM). The results indicate that the length of the methylene chain affects the antiplasmodial activity. The potency of our compounds against the CQS 3D7 strain was increased up to C4 spacer, and further chain lengthening resulted in a decrease of the activity (**7**–**9** *vs.* **10**). On the other hand, the substitution of chlorine atom with hydrogen at the 7-position of the quinoline ring did not significantly affect the *in vitro* antimalarial activity against the CQS strain (**9**: IC_{50} = 30.04 nM; **12**: IC_{50} = 25.45 nM).

TABLE I. *In vitro* antimalarial activity, IC_{50} / nM (geometric mean)

Compound	Strain	
	3D7[a]	Dd2[b]
1	32.20[c]	40.82[c]
2	22.05[c]	37.97[c]
3	30.11[c]	18.81[c]
4	N.D. (>500)[d]	N.D.[d]
5	43.50	34.04
6	14.02	26.07
7	41.08	N.D.[e]
8	45.75	35.22
9	30.04	N.D.[d]
10	61.66	N.D.[d]
11	291.10	48
12	25.45	30.72
13	76.22	216.71
CQ	16.17(5)[e]	129.18(5)[e]
ART	13.09(3)[e]	15.93(2)[e]

[a]*P. falciparum* CQ susceptible clone; [b]*P. falciparum* CQ resistant clone; [c]taken from reference[25]; [d]N.D. – not determined; [e]number of replicates

In order to get an initial insight into the compound's antimalarial mechanism of action, antimalarials **2**, **3** and **8** were submitted to BHIA.[28] The results showed that **3** and **8** interfered with hematin polymerization with the same potency as CQ (**3**: IC_{50} = 1.40; **8**: IC_{50} = 0.81 *vs*. CQ: IC_{50} = 1.23), indicating the same mechanism of action. On the other hand, compound **2** (without bromine attached to benzene ring) showed significantly lower BHIA (**2**: IC_{50} = 3.46). This difference in blocking the hemozoin formation requires further research, and we will pay full attention to this issue in the near future.

Reported results of *in vitro* antimalarial activity for **2** and **3** showed that these compounds are good candidates for *in vivo* testing. Additionally, low toxicities to human liver carcinoma cell line HepG2 and high metabolic stability in mouse and human liver microsomes of antimalarial **2** further supported antimalarial efficacy studies in a mouse model.[23] The bromo derivatives **3** and **8** were examined for antimalarial efficacy. A modified Thompson test model of malaria was used to determine the blood schizonticidal efficacy of the test compounds. Mice were infected with *P. berghei*-infected red blood cells. The test compounds were administered orally at doses of 80, 160 and 320 (mg/kg)/day on days 3, 4, and 5 after parasite inoculation; infection was confirmed by positive blood smear results for all the mice on study day 3 (prior to drug administration).

At a dose of 320 (mg/kg)/day, compound **3** appeared active, since it afforded survival of 2/6 mice, with parasite clearance in one and parasite recrudescence in the other mouse. However, these results should be taken with caution since 3 experimental animals died on day 7 (D7), indicating no activity. Of the two mice that survived to D31, one had a positive blood smear and was therefore not cured, but the other one (1/6 tested) was cured based on a negative blood smear as well as absence of detection of *P. berghei* DNA by PCR (performed as previously described[31]) of blood, liver and spleen. At concentrations of 160 and 80 (mg/kg)/ /day only suppression activity was observed. No acute toxicity of compound **3** was detected, the mice that died or were euthanized prior to day 31 showed typical gross lesions such as gray swollen liver, dark spleen, and pale emaciated carcass (like the control mice group), which indicated fatal malaria infection. Antimalarial **8** was tested at doses of 160 and 80 (mg/kg)/day. At 160 mg/kg/day it was found toxic, and at the lower concentration only suppression activity was observed, Table II.

The hybrid derivatives **14**–**17** did not meet our expectations as they exhibited extremely poor *in vitro* activity, of IC_{50} > 1000 nM, against the CQR strain. However, their BHIA (IC_{50} ≈ 1) indicated that they may interfere with hematin polymerization to the same extent as CQ (CQ: IC_{50} = 1.23; **14**: IC_{50} = 0.95; **15**: IC_{50} = 1.19; **16**: IC_{50} = 0.72; **17**: IC_{50} = 0.96). The inconsistency between *in vitro* activity and BHIA could indicate the inability of hybrid derivatives to accumulate in the food vacuole of the parasite.

TABLE II. *In vivo* antimalarial activity; groups of four, five, or six, *P. berghei* (ANKA strain) infected mice were treated p.o. once per day on days 3–5 post infection with aminoquinolines suspended in 0.5 % hydroxyethylcellulose-0.1 % Tween 80. Mice alive on day 31 with no parasites as detected by PCR are considered cured

Compd.	Dose, (mg/kg)/day	Mice dead/day died	Mice alive on day 31/total	Mean survival time, day
2[b]	160c	1/13, 1/14, 1/15, 1/17	1/5	18
	80	1/12, 2/13, 1/14, 1/28	0/5	16
3	320	3/7, 1/22	2/6	18
	160c	1/15, 1/16, 2/17, 1/21, 1/24	0/6	18
	80	1/12, 1/13, 2/14	0/4	13
8	80	2/14, 2/15, 1/19, 1/26	0/6	17
Infected controls	0	All mice died on day 6–8		

[a]Taken from reference[22]

CONCLUSIONS

In this manuscript we reported our findings on the antimalarial activity of simple aminoquinoline tethered benzyl derivatives with introduced bromines in positions C3 and C4. Although the synthesized compounds showed acceptably low *in vitro* activities, the antimalarial **3** was found toxic *in vivo* at a dose of 320 (mg/kg)/day in 3/6 mice, however, 2/6 mice of the same group survived through day 31, and one of them was cured. The detected toxicity of compound **3** indicates that the basic structure of presented aminoquinolines has yet to be improved in the near future.

SUPPLEMENTARY MATERIAL

Additional data are available electronically at the pages of journal website:.https://www.shd-pub.org.rs/index.php/JSCS/index, or from the corresponding author on request.

ИЗВОД

НОВИ ДЕРИВАТИ 4-АМИНОХИНОЛИНА КАО УМЕРЕНИ ИНХИБИТОРИ ПАРАЗИТА *Plasmodium falciparum*

ИГОР ОПСЕНИЦА[1], МИЛИЦА СЕЛАКОВИЋ[2], МИКЛОШ ТОТ[1], ТАТЈАНА ВЕРБИЋ[1], ЈЕЛЕНА СРБЉАНОВИЋ[3], ТИЈАНА ШТАЈНЕР[3], ОЛГИЦА ЂУРКОВИЋ ЂАКОВИЋ[3] и БОГДАН ШОЛАЈА[1,4]

[1]*Универзитет у Београду-Хемијски факултет, Студентски трг 16, 11158 Београд, [2]Иновациони центар Хемијског факултета, Студентски трг 12–16, 11158 Београд, [3]Институт за медицинска истраживања Универзитета у Београду, Др. Суботића 4, 11129 Београд и [4]Српска академија наука и уметности, Кнез Михаилова 35, 11000 Београд*

Синтетисани су нови деривати аминохинолина и испитана је антималаријска активност једињења на два соја *P. falciparum*, хлорокин осетљивом клону 3D7 и хлорокин резистентом клону Dd2. У наставку истраживања испитана је *in vivo* активност деривата који су у *in vitro* условима испољили највећу активност. Применом аминохинолина **3** у дози 320 (mg/kg)/дан преживела су два од шест мишева, при чему је један миш излечен.

Међутим, при истој дози у 3/6 тестиране животиње исказана је токсичност аминохино-лина **3**, што указује да је потребно даље истраживање на побољшању структуре овог типа једињења.

REFERENCES

1. S. Altizer, R. S. Ostfeld, P. T. J. Johnson, S. Kutz, C. D. Harvell, *Science* **341** (2013) 514 (https://doi.org/10.1126/science.1239401)
2. WHO_TDR (2019), http://www.who.int/tdr/diseases-topics/malaria/en/index.html (accessed December 22, 2020)
3. D. Rathore, D. Jani, R. Nagarkatti, S. Kumar, *Drug Discov. Today Ther. Strategy* **3** (2006) 153 (https://doi.org/10.1016/j.ddstr.2006.06.003)
4. P. Loria, S. Miller, M. Foley, L. Tilley, *Biochem. J.* **339** (1999) 363 (https://doi.org/10.1042/bj3390363)
5. V. Papalexis, M. A. Siomos, N. Campanale, X. guo Guo, G. Kocak, M. Foley, L. Tilley, *Mol. Biochem. Parasitol.* **115** (2001) 77 (https://doi.org/10.1016/S0166-6851(01)00271-7)
6. H. Ginsburg, O. Famin, J. Zhang, M. Krugliak, *Biochem. Pharmacol.* **56** (1998) 1305 (https://doi.org/10.1016/s0006-2952(98)00184-1)
7. M. Delves, D. Plouffe, C. Scheurer, S. Meister, S. Wittlin, E. A. Winzeler, R. E. Sinden, D. Leroy, *PLoS Med.* **9** (2012) e1001169 (https://doi.org/10.1371/journal.pmed.1001169)
8. *Treatment and Prevention of Malaria: Antimalarial Drug Chemistry, Action and Use*, H. M. Staines, S. Krishna (Eds.), Series: Milestones in Drug Therapy; M. J. Parnham, J. Bruinvels (Series Eds.), Springer, Basel, 2012 (https://www.springer.com/series/4991)
9. N. J. White, *J. Clin. Invest.* 2**113** (2004) 1084 (https://doi.org/10.1172/JCI21682)
10. J. K. Baird, *N. Engl. J. Med.* **352** (2005) 1565 (https://doi.org/10.1056/NEJMra043207)
11. J. Wiesner, R. Ortmann, H. Jomaa, M. Schlitzer, *Angew. Chem. Int. Ed.* **42** (2003) 5274 (https://doi.org/10.1002/anie.200200569)
12. M. A. Phillips, J. N. Burrows, C. Manyando, R. H. Van Huijsduijnen, W. C. Van Voorhis, T. N. C. Wells, *Nat. Rev. Dis. Prim.* **3** (2017) 17050 (https://doi.org/10.1038/nrdp.2017.50)
13. M. Foley, L. Tilley, *Pharmacol. Ther.* **79** (1998) 55 (https://doi.org/10.1016/s0163-7258(98)00012-6)
14. O. Famin, M. Krugliak, H. Ginsburg, *Biochem. Pharmacol.* **58** (1999) 59 (https://doi.org/10.1016/S0006-2952(99)00059-3)
15. S. A. W. I. M. Hastings, P. G. Bray, *Science* **298** (2002) 74 (https://doi.org/10.1126/science.1077573)
16. M. Henry, S. Alibert, C. Rogier, J. Barbe, B. Pradines, *Curr. Top. Med. Chem.* **8** (2008) 563 (https://doi.org/10.2174/156802608783955593)
17. V. V. Kouznetsov, A. Gómez-Barrio, *Eur. J. Med. Chem.* **44** (2009) 3091 (https://doi.org/10.1016/j.ejmech.2009.02.024)
18. K. Kaur, M. Jain, R. P. Reddy, R. Jain, *Eur. J. Med. Chem.* **45** (2010) 3245 (https://doi.org/10.1016/j.ejmech.2010.04.011)
19. J. C. Burnett, D. Opsenica, K. Sriraghavan, R. G. Panchal, G. Ruthel, A. R. Hermone, T. L. Nguyen, T. A. Kenny, D. J. Lane, C. F. McGrath, J. J. Schmidt, J. L. Vennerstrom, R. Gussio, B. A. Šolaja, S. Bavari, *J. Med. Chem.* **50** (2007) 2127 (https://doi.org/10.1021/jm061446e)

20. B. A. Šolaja, D. Opsenica, K. S. Smith, W. K. Milhous, N. Terzić, I. Opsenica, J. C. Burnett, J. Nuss, R. Gussio, S. Bavari, *J. Med. Chem.* **51** (2008) 4388 (https://doi.org/10.1021/jm800737y)
21. M. Videnović, D. M. Opsenica, J. C. Burnett, L. Gomba, J. E. Nuss, Z. Selaković, J. Konstantinović, M. Krstić, S. Šegan, M. Zlatović, R. J. Sciotti, S. Bavari, B. A. Šolaja, *J. Med. Chem.* **57** (2014) 4134 (https://doi.org/10.1021/jm500033r)
22. J. Konstantinović, M. Videnović, J. Srbljanović, O. Djurković-Djaković, K. Bogojević, R. Sciotti, B. Šolaja, *Molecules* **22** (2017) 343 (https://doi.org/10.3390/molecules22030343)
23. I. M. Opsenica, M. Tot, L. Gomba, J. E. Nuss, R. J. Sciotti, S. Bavari, J. C. Burnett, B. A. Šolaja, *J. Med. Chem.* **56** (2013) 5860 (https://doi.org/10.1021/jm4006077)
24. N. Terzić, J. Konstantinović, M. Tot, J. Burojević, O. Djurković-Djaković, J. Srbljanović, T. Štajner, T. Verbić, M. Zlatović, M. Machado, I. S. Albuquerque, M. Prudêncio, R. J. Sciotti, S. Pecic, S. D'Alessandro, D. Taramelli, B. A. Šolaja, *J. Med. Chem.* **59** (2016) 264 (https://doi.org/10.1021/acs.jmedchem.5b01374)
25. W. Trager, J. B. Jensen, *Science* **193** (1976) 673 (https://doi.org/10.1126/science.781840)
26. M. T. Makler, J. M. Ries, J. A. Williams, J. E. Bancroft, R. C. Piper, B. L. Gibbins, D. J. Hinrichs, *Am. J. Trop. Med. Hyg.* **48** (1993) 739 (https://doi.org/10.4269/ajtmh.1993.48.739)
27. I. Opsenica, J. C. Burnett, R. Gussio, D. Opsenica, N. Todorović, C. A. Lanteri, R. J. Sciotti, M. Gettayacamin, N. Basilico, D. Taramelli, J. E. Nuss, L. Wanner, R. G. Panchal, B. A. Šolaja, S. Bavari, *J. Med. Chem.* **54** (2011) 1157 (https://doi.org/10.1021/jm100938u)
28. S. Parapini, N. Basilico, E. Pasini, T. J. Egan, P. Olliaro, D. Taramelli, D. Monti, *Exp. Parasitol.* **96** (2000) 249 (https://doi.org/10.1006/expr.2000.4583)
29. I. M. Opsenica, T. Verbić, M. Tot, R. J. Sciotti, B. S. Pybus, O. Djurković-Djaković, K. Slavić, B. A. Šolaja, *Bioorg. Med. Chem.* **23** (2015) 2176 (https://doi.org/10.1016/j.bmc.2015.02.061)
30. J. Srbljanović, B. Bobić, T. Štajner, A. Uzelac, I. Opsenica, N. Terzić-Jovanović, N. Bauman, B. A. Šolaja, O. Djurković-Djaković, *J. Glob. Antimicrob. Resist.* **23** (2020) 20 (http://dx.doi.org/10.1016/j.jgar.2020.07.027)
31. J. Srbljanović, T. Štajner, J. Konstantinović, N. Terzić-Jovanović, A. Uzelac, B. Bobić, B. A. Šolaja, O. Djurković-Djaković, *Int. J. Antimicrob. Agents* **50** (2017) 461 (https://doi.org/10.1016/j.ijantimicag.2017.06.002).

Journal of the Serbian Chemical Society

New 4-aminoquinolines as moderate inhibitors of *P. falciparum* malaria

IGOR OPSENICA[1#], MILICA SELAKOVIĆ[2#], MIKLOŠ TOT[1], TATJANA VERBIĆ[1#],
JELENA SRBLJANOVIĆ[3], TIJANA ŠTAJNER[3], OLGICA DJURKOVIĆ DJAKOVIĆ[3]
and BOGDAN ŠOLAJA[1,4*#]

[1]*University of Belgrade – Faculty of Chemistry, Studentski trg 16, P.O. Box 51, 11158
Belgrade, Serbia,* [2]*Innovative Centre, Faculty of Chemistry, Ltd. Studentski Trg 12–16, 11158
Belgrade, Serbia,* [3]*Institute for Medical Research, University of Belgrade, Dr. Subotića 4,
P.O. Box 39, 11129 Belgrade, Serbia and* [4]*Serbian Academy of Sciences and Arts,
Knez Mihailova 35, 11000 Belgrade, Serbia*

EXPERIMENTAL DETAILS

Melting points were determined on a Boetius PMHK apparatus and were not corrected. IR spectra were recorded on a Thermo-Scientific Nicolet 6700 FT-IR Diamond Crystal. NMR: ^{1}H and ^{13}C NMR spectra were recorded on a Varian Gemini-200 spectrometer (at 200 and 50 MHz, respectively) and/or a Bruker Ultrashield Advance III spectrometer (at 500 and 125 MHz, respectively) in the indicated solvent using TMS as the internal standard. Chemical shifts are expressed in ppm (δ) values and coupling constants (J) in Hz. The elemental analysis was performed on the Vario EL III – C, H, N, S/O elemental analyzer (Elementar Analysensysteme GmbH, Hanau, Germany). ESI MS spectra of the synthesized compounds were recorded on an Agilent Technologies 6210 Time-of-Flight LC/MS instrument in positive ion mode using $CH_3CN/H_2O = 1/1$ with 0.2 % HCOOH as the carrying solvent solution. The samples were dissolved in pure acetonitrile (HPLC grade). The selected values were as follows: capillary voltage = 4 kV; gas temperature = 350 °C; drying gas = 12.l min^{-1}; nebulizer pressure = 45 psig; fragmentor voltage =70 V. Compounds were analyzed for purity using Waters 1525 HPLC dual pump system equipped with an Alltech Select degasser system, and a dual λ 2487 UV-VIS detector, and Agilent 1200 HPLC system equipped with Quat Pump (G1311B), Injector (G1329B) 1260 ALS, TCC 1260 (G1316A) and Detector 1260 DAD VL+(G1315C). All analyzed compounds were >95 % pure. HPLC analysis was performed in two diverse systems for each analyzed compound. Compounds were dissolved in methanol, final concentrations were ~ 1 mg/mL. Applied HPLC methods were as follows:

Method A: Zorbax Eclipse Plus C18 2.1 × 100 mm, 1.8μ, S.N.USUXU04444 was used as the stationary phase. Eluent was made of the following solvents: 0.2 % formic acid in water (A) and acetonitrile (B). The analysis were performed at 330 nm for compounds **14** and **17**, and at 320 nm for compounds **15** and **16**. Flow rate was 0.5 mL/min.

* Corresponding author. E-mail: bogdan.solaja@sanu.ac.rs

Compounds **14-17** were eluted using gradient protocol: 0–1 min 95 % A, 1–2 min 95 % A → 5 % A, 2–10 min 5 % A, 10–11 min 5 % A → 95 % A, 11–13 min 95 % A.

Method B: Zorbax Eclipse Plus C18 2.1 × 100 mm, 1.8μ, S.N.USUXU04444 was used as the stationary phase. Eluent was made of the following solvents: 0.2 % formic acid in water (A) and methanol (B). The analysis were performed at 330 nm for compounds **14** and **17**, and at 320 nm for compounds **15** and **16**. Flow rate was 0.2 mL/min.

Compounds **14-17** were eluted using gradient protocol: 0–1 min 95 % A, 1–2 min 95 % A → 5 % A, 2–10 min 5 % A, 10–11 min 5 % A → 95 % A, 11–13 min 95 % A.

General procedure

3-Bromobenzaldehyde (200 mg, 1.08 mmol) and **ACQ2 (**359 mg, 1.62 mmol) were dissolved in dry CH_2Cl_2/MeOH mixture (18 mL, 1:2 v/v), anh. AcOH (93 μL, 1.62 mmol) was added and mixture was stirred under Ar atmosphere at room temperature. After 2 h, $NaBH_4$ (245 mg, 6.48 mmol) was added and stirring at r.t. was continued for another 18 h. Solvents were removed under reduced pressure and the residue was dissolved in CH_2Cl_2 (40 mL). The organic layer was washed with 2M NH_4OH (15 mL). The layers were separated, and water layer was extracted with CH_2Cl_2 (2×15 mL). Combined organic layers were washed with brine and dried over anh. Na_2SO_4. Finally, the solvent was removed under reduced pressure and crude product was purified by dry-flash chromatography (SiO_2: CH_2Cl_2/MeOH).

N-(3-Bromobenzyl)-N'-(7-chloroquinolin-4-yl)ethane-1,2-diamine (4)

The crude product was purified using dry-flash chromatography (SiO_2: CH_2Cl_2/MeOH = 95/5). Yield: 380 mg (90 %). Pale yellow amorphous powder. m.p. 137-138 °C; IR (ATR, cm^{-1}): 3314*w*, 3184*w*, 3032*w*, 2953*s*, 2896*m*, 2843*m*, 1606*w*, 1581*s*, 1540*m*, 1450*m*, 1390*w*, 1364*m*, 1331*w*, 1279*w*, 1230*w*, 1200*w*, 1170*w*, 1141*w*, 1107*w*, 1080*w*, 1045*w*, 1009*w*, 928*w*, 891*w*, 831*w*; ^{1}H-NMR (200 MHz, CDCl$_3$, δ / ppm): 8.53-8.48 (1H, *m*), 7.96-7.92 (1H, *m*), 7.73-7.65 (1H, *m*), 7.52 (1H, *s*), 7.43-7.33 (2H, *m*), 7.26-7.13 (2H, *m*), 6.37-6.31 (1H, *m*), 5.84 (1H, *m*, -NH), 3.81 (2H, *s*), 3.36-3.24 (*m*, CH$_2$NHCH$_2$C$\underline{H}_2$NHAr), 3.08-2.96 (*m*, CH$_2$NHC$\underline{H}_2$CH$_2$NHAr), 1.82 (1H, *m*, -NH); ^{13}C-NMR (50 MHz, CDCl$_3$, δ / ppm): 152.01, 149.78, 149.05, 142.36, 134.81, 131.02, 130.29, 130.07, 128.64, 126.63, 125.32, 122.68, 121.22, 117.31, 99.16, 52.60, 46.70, 41.95; (+)ESI-HRMS (*m/z*): [M + H]$^+$ 390.03666 (error -0.15 ppm); Anal. Calcd. for C$_{18}$H$_{17}$BrClN$_3$ × 0.5H$_2$O: C, 54.09; H, 4.54; N, 10.51 %. Found: C, 54.00; H, 4.34; N, 10.62 %.

N-(3-Bromobenzyl)-N'-(7-chloroquinolin-4-yl)propane-1,3-diamine (5)

3-Bromobenzaldehyde (200 mg, 1.08 mmol) and **ACQ3 (**381 mg, 1.62 mmol) were coupled to afford **5** (340 mg, 78 %) using AcOH (93 μL, 1.62 mmol) and $NaBH_4$ (245 mg, 6.48 mmol). The crude product was purified by dry-flash chromatography (SiO_2: CH_2Cl_2/MeOH = 95/5). **5**: Pale yellow amorphous powder; m.p. 70-72 °C; IR (ATR, cm^{-1}): 3285*s*, 3070*m*, 2944*m*, 2848*m*, 1691*w*, 1609*w*, 1579*s*, 1539*m*, 1483*w*, 1450*m*, 1364*m*, 1329*m*, 1284*w*, 1248*w*, 1195*w*, 1139*w*, 1112*w*, 1076*w*, 988*w*, 903*w*, 857*m*, 823*w*; ^{1}H-NMR (200 MHz, CDCl$_3$, δ / ppm): 8.46 (1H, *d*, *J* = 5.4 Hz), 7.93-7.89 (1H, *m*), 7.55-7.31 (4H, *m*), 7.30-7.17 (3H, *m*), 6.29 (1H, *d*, *J* = 5.4 Hz), 3.80 (2H, *s*), 3.44-3.32 (*m*, CH$_2$NHCH$_2$CH$_2$C$\underline{H}_2$NHAr), 2.99-2.90 (*m*, CH$_2$NHC$\underline{H}_2$CH$_2$CH$_2$NHAr), 2.11 (1H, *m*, -NH), 2.01-1.87 (*m*, CH$_2$NHCH$_2$C$\underline{H}_2$CH$_2$NHAr); ^{13}C-NMR (50 MHz, CDCl$_3$, δ / ppm): 151.83, 150.43, 148.81, 141.78, 134.70, 131.28, 130.50, 130.22, 128.20, 126.94, 125.07, 122.70, 121.88, 117.38, 98.28, 53.68, 49.11, 43.74, 27.31; (+)ESI-HRMS (*m/z*): [M + 2H]$^{2+}$ 202.52934 (error -2.36 ppm), [M + H]$^+$ 404.05203 (error -0.83 ppm); Anal. Calcd. for 4C$_{19}$H$_{19}$BrClN$_3$ × 5H$_2$O: C, 53.41; H, 5.07; N, 9.84 %. Found: C, 53.38; H, 4.73; N, 9.94 %.

N-*(2-Bromobenzyl)*-N'-*(7-chloroquinolin-4-yl)propane-1,3-diamine* **(6)**

2-Bromobenzaldehyde (100 mg, 0.54 mmol) and **ACQ3** (191 mg, 0.81 mmol) were coupled to afford **6** (187 mg, 85 %) using AcOH (46 µL, 0.81 mmol) and $NaBH_4$ (123 mg, 3.24 mmol). The crude product was purified by dry-flash chromatography (SiO_2: CH_2Cl_2/MeOH = 95/5). **6**: Yellow amorphous powder; m.p. 110-112 °C; IR (ATR, cm^{-1}): 3426m, 3219m, 3064w, 3009w, 2923w, 2850w, 1676w, 1610m, 1582s, 1463m, 1436m, 1383w, 1365w, 1331w, 1308w, 1280w, 1254w, 1230w, 1200w, 1167w, 1137w, 1110w, 1080w, 1023w, 896w, 852w, 825w, 802w; ^{1}H-NMR (200 MHz, $CDCl_3$, δ / ppm): 8.49-8.43 (1H, m), 7.91-7.88 (1H, m), 7.71 (1H, m, -NH), 7.64-7.57 (1H, m), 7.47-7.32 (3H, m), 7.31-7.17 (1H, m), 7.08-7.00 (1H, m), 6.31-6.25 (1H, m), 3.92 (2H, s), 3.45-3.34 (m, $CH_2NHCH_2CH_2C\underline{H}_2NHAr$), 3.02-2.93 ($m$, $CH_2NHC\underline{H}_2CH_2CH_2NHAr$), 2.26 (1H, m, -NH), 2.03-1.88 (m, $CH_2NHCH_2C\underline{H}_2CH_2NHAr$); ^{13}C-NMR (50 MHz, $CDCl_3$, δ / ppm): 151.83, 150.52, 148.81, 138.47, 134.55, 133.10, 130.68, 129.20, 128.14, 127.69, 124.72, 124.19, 122.21, 117.40, 98.14, 54.06, 49.12, 43.99, 27.13; (+)ESI-HRMS (*m/z*): $[M + 2H]^{2+}$ 202.52993 (error +0.53 ppm), $[M + H]^+$ 404.05151 (error -2.12 ppm); Anal. Calcd. for $C_{19}H_{19}BrClN_3 \times 0.5H_2O$: C, 55.16; H, 4.87; N, 10.16 %. Found: C, 54.97; H, 4.53; N, 10.23 %

N-*(7-Chloroquinolin-4-yl)*-N'-*(3,4-dibromobenzyl)ethane-1,2-diamine* **(7)**

3,4-Dibromobenzaldehyde (100 mg, 0.38 mmol) and **ACQ2** (126 mg, 0.56 mmol) were coupled to afford **7** (139 mg, 78 %) using AcOH (36 µL, 0.62 mmol) and $NaBH_4$ (84 mg, 2.22 mmol). The crude product was purified by dry-flash chromatography (SiO_2: CH_2Cl_2/MeOH = 95/5). **7**: Yellow amorphous powder; m.p. 136-139 °C; IR (ATR, cm^{-1}): 3748w, 3302w, 3074w, 2931w, 2848w, 2359w, 1611m, 1583s, 1534w, 1457w, 1371w, 1332w, 1277w, 810w; ^{1}H-NMR (500 MHz, $CDCl_3$, δ / ppm): 8.51 (1H, d, J = 5.4 Hz), 7.94 (1H, d, J = 2.0 Hz), 7.67 (1H, d, J = 9.0 Hz), 7.63 (1H, d, J = 1.9 Hz), 7.54 (1H, d, J = 8.1 Hz), 7.37 (1H, dd, J = 9.0 Hz, J = 2.0 Hz), 7.12 (1H, dd, J = 8.1 Hz, J = 1.9 Hz), 6.35 (1H, d, J = 5.4 Hz), 5.78 (1H, m, -NH), 3.78 (2H, s), 3.35-3.30 (m, $CH_2NHCH_2C\underline{H}_2NHAr$), 3.04-3.00 ($m$, $CH_2NHC\underline{H}_2CH_2NHAr$); ^{13}C-NMR (125 MHz, $CDCl_3$, δ / ppm): 151.92, 149.74, 148.97, 141.06, 134.89, 133.63, 133.09, 128.65, 128.17, 125.40, 124.94, 123.21, 121.09, 117.27, 99.19, 52.08, 46.83, 42.06; (+)ESI-HRMS (*m/z*): $[M + H]^+$ = 467.94639 (error -1.78 ppm); Anal. Calcd. for $C_{18}H_{16}Br_2ClN_3 \times H_2O$: C, 44.34; H, 3.72; N, 8.62 %. Found: C, 44.55; H, 3.56; N, 8.77 %.

N-*(7-Chloroquinolin-4-yl)*-N'-*(3,4-dibromobenzyl)propane-1,3-diamine* **(8)**

3,4-Dibromobenzaldehyde (100 mg, 0.38 mmol) and **ACQ3** (134 mg, 0.57 mmol) were coupled to afford **8** (115 mg, 63 %) using AcOH (36 µL, 0.62 mmol) and $NaBH_4$ (84 mg, 2.22 mmol). The crude product was purified by dry-flash chromatography (SiO_2: CH_2Cl_2/MeOH = 95/5). **8**: Yellow amorphous powder; m.p. 111-113 °C; IR (ATR, cm^{-1}): 3269m, 2930w, 2846w, 1986w, 1610m, 1584s, 1539w, 1457w, 1369w, 1332w, 1140w, 809w; ^{1}H-NMR (500 MHz, $CDCl_3$, δ / ppm): 8.50 (1H, d, J = 5.4 Hz), 7.93 (1H, d, J = 2.1 Hz), 7.61 (1H, d, J =2.1 Hz), 7.57 (1H, d, J = 8.1 Hz), 7.51 (1H, d, J = 8.8 Hz), 7.23 (1H, dd, J = 8.8 Hz, J = 2.1 Hz), 7.12 (1H, dd, J = 8.1 Hz, J = 2.1 Hz), 7.06 (1H, m, -N*H*), 6.33 (1H, d, J = 5.4 Hz), 3.78 (2H, s), 3.42-3.38 (m, $CH_2NHCH_2CH_2C\underline{H}_2NHAr$), 2.94-2.90 ($m$, $CH_2NHC\underline{H}_2CH_2CH_2NHAr$), 1.98-1.91 ($m$, $CH_2NHCH_2C\underline{H}_2CH_2NHAr$), 1.78 (1H, m, -NH); ^{13}C-NMR (125 MHz, $CDCl_3$, δ / ppm): 152.00, 150.23, 149.02, 140.63, 134.74, 133.77, 133.33, 128.57, 128.44, 125.14, 125.03, 123.46, 121.54, 117.39, 98.48, 53.10, 48.91, 43.61, 27.61; (+)ESI-HRMS (*m/z*): $[M + H]^+$ = 481.96289 (error +0.02 ppm); Anal. Calcd. for $C_{19}H_{18}Br_2ClN_3$: C, 47.19; H, 3.75; N, 8.69 %. Found: C, 47.19; H, 3.80; N, 8.74 %.

N-*(7-Chloroquinolin-4-yl)*-N'-*(3,4-dibromobenzyl)butane-1,4-diamine* (*9*)

3,4-Dibromobenzaldehyde (100 mg, 0.38 mmol) and **ACQ4** (142 mg, 0.57 mmol) were coupled to afford **9** (130 mg, 69 %) using AcOH (36 μL, 0.62 mmol) and NaBH$_4$ (84 mg, 2.22 mmol). The crude product was purified by dry-flash chromatography (SiO$_2$: CH$_2$Cl$_2$/MeOH = 95/5). **9**: Pale yellow amorphous powder; m.p. 121-122 °C; IR (ATR, cm^{-1}): 3232*w*, 3114*w*, 3063*w*, 3012*w*, 2958*w*, 2874*w*, 2816*w*, 1612*w*, 1581*s*, 1550*w*, 1456*m*, 1430*w*, 1368*w*, 1341*w*, 1320*w*, 1279*w*, 1249*w*, 1147*w*, 1014*w*, 896*w*, 871*w*, 850*w*, 815*m*; ^{1}H-NMR (500 MHz, MeOD, *δ* / ppm): 8.32 (1H, *d*, *J* = 5.7 Hz), 8.05 (1H, *d*, *J* = 9.0 Hz), 7.75 (1H, *d*, *J* = 2.1 Hz), 7.65 (1H, *d*, *J* =2.0 Hz), 7.56 (1H, *d*, *J* = 8.2 Hz), 7.35 (1H, *dd*, *J* = 9.0 Hz, *J* = 2.1 Hz), 7.17 (1H, *dd*, *J* = 8.2 Hz, *J* = 2.0 Hz), 6.46 (1H, *d*, *J* = 5.7 Hz), 3.68 (2H, *s*), 3.36-3.30   (*m*,   CH$_2$NHCH$_2$CH$_2$CH$_2$C<u>H</u>$_2$NHAr),   2.63-2.58   (*m*, CH$_2$NHC<u>H</u>$_2$CH$_2$CH$_2$CH$_2$NHAr), 1.80-1.72 (*m*, CH$_2$NHCH$_2$CH$_2$C<u>H</u>$_2$CH$_2$NHAr), 1.69-1.62 (*m*, CH$_2$NHCH$_2$C<u>H</u>$_2$CH$_2$CH$_2$NHAr); ^{13}C-NMR (125 MHz, MeOD, *δ* / ppm): 152.83, 152.49, 149.75, 142.56, 136.42, 134.88, 134.84, 130.22, 127.70, 126.05, 125.63, 124.43, 123.99, 118.89, 99.76, 53.26, 43.94, 28.14, 27.26; (+)ESI-HRMS (*m/z*): [M + 2H]$^{2+}$ 248.49354 (error +2.55 ppm), [M + H]$^+$ 495.97832 (error -0.43 ppm); Anal. Calcd. for C$_{20}$H$_{20}$Br$_2$ClN$_3$: C, 48.27; H, 4.05; N, 8.44 %. Found: C, 47.94; H, 4.06; N, 8.35 %.

N-*(7-Chloroquinolin-4-yl)*-N'-*(3,4-dibromobenzyl)hexane-1,6-diamine* (*10*)

3,4-Dibromobenzaldehyde (100 mg, 0.38 mmol) and **ACQ6** (158 mg, 0.57 mmol) were coupled to afford **10** (122 mg, 61 %) using AcOH (36 μL, 0.62 mmol) and NaBH$_4$ (84 mg, 2.22 mmol). The crude product was purified by dry-flash chromatography (SiO$_2$: CH$_2$Cl$_2$/MeOH = 95/5). **10**: Pale yellow amorphous powder; m.p. 105-106 °C; IR (ATR, cm^{-1}): 3211*m*, 3108*m*, 3062*m*, 2933*m*, 2848*m*, 1583*s*, 1546*m*, 1490*w*, 1451*s*, 1366*m*, 1328*w*, 1279*w*, 1256*w*, 1220*w*, 1200*w*, 1140*w*, 1113*w*, 1079*w*, 1010*w*, 900*w*, 884*w*, 850*w*, 832*w*, 811*m*; ^{1}H-NMR (500 MHz, MeOD, *δ* / ppm): 8.32 (1H, *d*, *J* =5.7 Hz), 8.07 (1H, *d*, *J* = 9.0 Hz), 7.75 (1H, *d*, *J* = 2.2 Hz), 7.65 (1H, *d*, *J* = 2.0 Hz), 7.57 (1H, *d*, *J* = 8.2 Hz), 7.36 (1H, *dd*, *J* = 9.0 Hz, *J* = 2.2 Hz), 7.17 (1H, *dd*, *J* = 8.2 Hz, *J* = 2.0 Hz), 6.46 (1H, *d*, *J* = 5.7 Hz) 3.65 (2H, *s*), 3.38-3.29 (*m*, CH$_2$NH(CH$_2$)$_5$C<u>H</u>$_2$NHAr), 2.55-2.51 (*m*, CH$_2$NHC<u>H</u>$_2$(CH$_2$)$_5$NHAr) 1.77-1.69 (*m*, CH$_2$NH(CH$_2$)$_4$C<u>H</u>$_2$CH$_2$NHAr), 1.57-1.50 (*m*, CH$_2$NHCH$_2$C<u>H</u>$_2$(CH$_2$)$_4$NHAr), 1.47-1.36 (*m*, CH$_2$NH(CH$_2$)$_2$C<u>H</u>$_2$C<u>H</u>$_2$(CH$_2$)$_2$NHAr); ^{13}C-NMR (125 MHz, MeOD, *δ* / ppm): 152.85, 152.51, 149.81, 142.58, 136.39, 134.89, 134.83, 130.23, 127.72, 126.02, 125.61, 124.43, 123.97, 118.89, 99.72, 53.29, 49.96, 44.08, 30.47, 29.44, 28.27, 28.21; (+)ESI-HRMS (*m/z*): [M + 2H]$^{2+}$ 262.50876 (error +0.79 ppm), [M + H]$^+$ 524.00906 (error -1.46 ppm); Anal. Calcd. for C$_{22}$H$_{24}$Br$_2$ClN$_3$: C, 50.26; H, 4.60; N, 7.99 %. Found: C, 50.07; H, 4.66; N, 8.05 %.

N-*(3,4-Dibromobenzyl)*-N'-*quinolin-4-ylethane-1,2-diamine* (*11*)

3,4-Dibromobenzaldehyde (100 mg, 0.38 mmol) and **DCACQ2** (106 mg, 0.57 mmol) were coupled to afford **11** (120 mg, 73 %) using AcOH (112 μL, 1.94 mmol) and NaBH$_4$ (84 mg, 2.22 mmol). The crude product was purified by dry-flash chromatography (SiO$_2$: CH$_2$Cl$_2$/MeOH = 9/1). **11**: Yellow oil; IR (ATR, cm^{-1}): 3257*m*, 3065*m*, 2907*m*, 2840*m*, 1581*s*, 1539*m*, 1457*m*, 1391*w*, 1336*m*, 1252*w*, 1129*w*, 1112*w*, 1013*w*, 809*m*; ^{1}H-NMR (500 MHz, CDCl$_3$, *δ* / ppm): 8.56-8.54 (1H, *m*), 7.99-7.97 (1H, *m*), 7.78-7.76 (1H, *m*), 7.66-7.62 (2H, *m*), 7.57-7.53 (1H, *m*), 7.48-7.43 (1H, *m*), 7.15-7.11 (1H, *m*), 6.41-6.39 (1H, *m*), 5.76 (1H, *m*, -NH), 3.79 (2H, *s*), 3.39-3.34 (*m*, CH$_2$NHCH$_2$C<u>H</u>$_2$NHAr), 3.05-3.01 (*m*, CH$_2$NHC<u>H</u>$_2$CH$_2$NHAr), 1.85 (1H, *m*, -NH); ^{13}C NMR (125 MHz, CDCl$_3$, *δ* / ppm): 150.89, 149.76, 148.24, 141.14, 133.63, 133.13, 129.75, 129.08, 128.19, 124.92, 124.77, 123.17,

119.45, 118.86, 98.91, 52.13, 46.98, 42.15; (+)ESI-HRMS (m/z): $[M + H]^+$ 433.98624 (error +0.10 ppm); Anal. Calcd. for $C_{18}H_{17}Br_2N_3$: C, 49.68; H, 3.94; N, 9.66 %. Found: C, 49.29; H, 4.00; N, 9.46 %.

N-*(3,4-Dibromobenzyl)*-N'-*quinolin-4-ylbutane-1,4-diamine (12)*

3,4-Dibromobenzaldehyde (100 mg, 0.38 mmol) and **DCACQ4** (123 mg, 0.57 mmol) were coupled to afford **12** (109 mg, 63 %) using AcOH (112 µL, 1.94 mmol) and NaBH$_4$ (84 mg, 2.22 mmol). The crude product was purified by dry-flash chromatography (SiO$_2$: CH$_2$Cl$_2$/MeOH = 9/1). **12**: Yellow oil; IR (ATR, cm^{-1}): 3278m, 3072m, 2928m, 2856m, 2361w, 1618w, 1581s, 1542m, 1457m, 1376w, 1341m, 1258w, 1129w, 1013w, 866w, 810m; ^{1}H NMR (500 MHz, CDCl$_3$, δ / ppm): 8.54-8.52 (1H, m), 7.99-7.95 (1H, m), 7.74-7.71 (1H, m), 7.62-7.58 (2H, m), 7.55-7.52 (1H, m), 7.38-7.35 (1H, m), 7.12-7.10 (1H, m), 6.40-6.38 (1H, m), 5.54 (1H, m, -NH), 3.73 (2H, s), 3.35-3.29 (m, CH$_2$NHCH$_2$CH$_2$CH$_2$C$\underline{H}_2$NHAr), 2.72-2.66 (m, CH$_2$NHC$\underline{H}_2$CH$_2$CH$_2$CH$_2$NHAr), 1.88-1.80 (m, CH$_2$NHCH$_2$CH$_2$C$\underline{H}_2$CH$_2$NHAr), 1.71-1.64 (m, CH$_2$NHCH$_2$C$\underline{H}_2$CH$_2$CH$_2$NHAr); ^{13}C NMR (125 MHz, CDCl$_3$, δ / ppm): 150.82, 149.82, 148.18, 141.34, 133.53, 133.11, 129.69, 128.99, 128.18, 124.76, 124.50, 122.92, 119.41, 118.70, 98.63, 52.70, 48.63, 43.10, 27.65, 26.41; (+)ESI-HRMS (m/z): $[M + 2H]^{2+} = 231.51308$ (error +3.00 ppm) $[M + H]^+ = 462.01695$ (error -1.19 ppm); Anal. Calcd. for $C_{20}H_{21}Br_2N_3$: C, 51.86; H, 4.57; N, 9.07 %. Found: C, 52.49; H, 4.83; N, 8.73 %.

N-*(3-Bromo-4-nitrobenzyl)*-N'-*(7-chloroquinolin-4-yl)propane-1,3-diamine (13)*

3-Bromo-4-nitrobenzaldehyde (100 mg, 0.43 mmol) and **ACQ3** (153 mg, 0.64 mmol) were coupled to afford **13** (127 mg, 65 %) using AcOH (37 µL, 0.65 mmol) and NaBH$_4$ (99 mg, 2.62 mmol). The crude product was purified by dry-flash chromatography (SiO$_2$: CH$_2$Cl$_2$/MeOH = 95/5). **13**: Yellow oil; IR (ATR, cm^{-1}): 3431m, 2924m, 2851m, 1581s, 1524s, 1449m, 1333s, 1280m, 1240m, 1201w, 1135m, 1078w, 1037w, 877w, 849w, 806m; ^{1}H NMR (200 MHz, CDCl$_3$, δ / ppm): 8.51-8.45 (1H, m), 7.92 (1H, d, J = 2.2 Hz), 7.81 (1H, d, J = 8.4 Hz), 7.72 (1H, d, J = 1.6 Hz), 7.55 (1H, d, J = 9.0 Hz), 7.39 (1H, dd, J = 8.4 Hz, J = 1.6 Hz), 7.24 (1H, dd, J = 9.0 Hz, J = 2.2 Hz), 6.76 (1H, m, -NH), 6.37-6.31 (1H, m), 3.89 (2H, s), 3.47-3.35 (m, CH$_2$NHCH$_2$CH$_2$C$\underline{H}_2$NHAr), 2.96-2.86 (m, CH$_2$NHC$\underline{H}_2$CH$_2$CH$_2$NHAr), 2.15 (1H, m, -NH), 2.05-1.90 (m, CH$_2$NHCH$_2$C$\underline{H}_2$CH$_2$NHAr); ^{13}C NMR (50 MHz, CDCl$_3$, δ / ppm): 151.80, 150.19, 148.77, 148.56, 146.15, 134.86, 134.37, 128.38, 127.71, 125.87, 125.18, 121.37, 117.26, 114.84, 98.59, 52.84, 48.58, 43.13, 27.80; (+)ESI-HRMS (m/z): $[M + 2H]^{2+}$ 225.02285 (error +2.18 ppm), $[M + H]^+$ 449.03705 (error -0.88 ppm); Anal. Calcd. for $C_{19}H_{18}BrClN_4O_2 \times 0.5H_2O$: C, 49.75; H, 4.17; N, 12.21 %. Found: C, 49.68; H, 3.96; N, 12.27 %.

a) NaH, DMF, 100 °C b) H$_2$ (30 Psi), Pd/C, CH$_3$OH
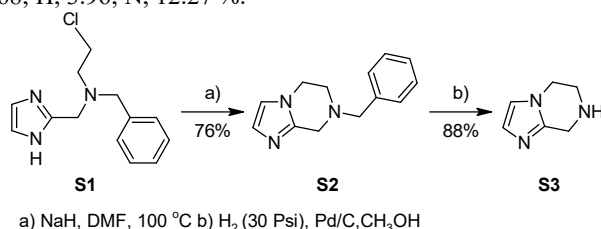
Scheme S-1.

The synthesis of **S1** has been previously reported.[1]

OPSENICA *et al.*

7-Benzyl-5,6,7,8-tetrahydroimidazo[1,2-a]pyrazine *(S2)*

To a suspension of NaH (673 mg, 0.017 mol, 60 % dispersion in mineral oil) in dry DMF (20 mL) was added solution of **S1** (3.82 g, 0.015 mol) in DMF (39 mL), and the mixture was stirred under Ar atmosphere at 100 °C. After 24 h, water was added and solvent was removed under reduced pressure, and crude product was purified using dry-flash chromatography (SiO$_2$: CH$_2$Cl$_2$/MeOH). Yield 2.47 g (76 %), brown oil. IR (ATR): 3352*s*, 3196*s*, 2929*w*, 2816*w*, 1666*s*, 1501*m*, 1450*m*, 1391*m*, 1348*m*, 1279*w*, 1188*w*, 1132*w*, 1106*w*, 1067*w*, 1001*w*, 865*w*, 742*m*, 700*m*, 675*m*, 571*m*, 460*w*, cm^{-1}. ^{1}H NMR (500 MHz, CDCl$_3$, δ): 7.40-7.27 (m, 5H), 7.10–7.02 (m, 1H), 6.90–6.85 (m, 1H), 4.01 (t, *J* = 5.5 Hz, 2H), 3.87 (s, 2H), 3.74 (s, 2H), 2.97–2.85 (m, 2H). ^{13}C NMR (125 MHz, CDCl$_3$, δ): 142.52; 136.30; 128.94; 128.61; 127.83; 122.87; 118.58; 61.47; 49.91; 48.14; 44.95. GC/MS (m/z (%)): 213.1 ([M$^+$], 50); 122.0 (100); 91.0 (90).

5,6,7,8-Tetrahydroimidazo[1,2-a]pyrazine *(S3)*

In a Parr reaction bottle, **S2** (2.12 g, 9.94 mmol) was dissolved in deoxygenated methanol (150 mL) and Pd/C (2.12 g, 10 mol% Pd) was added. The reactor was pressurized with 30 psi H$_2$ and the closed system was stirred at room temperature for 5 h. The reaction mixture was filtered through a pad of Celite. The solvents were removed under the reduced pressure, and crude product was purified using dry-flash chromatography (SiO$_2$: CH$_2$Cl$_2$/MeOH/NH$_3$). Yield 1.07 g (88 %), brown oil. IR (ATR): 3296s, 2959s, 1660m, 1532m, 1502s,1448m, 1369m, 1325m, 1301m, 1274m, 1199w, 1178m, 1118m, 1082m, 996w, 961m, 936m, 896m, 853m, 741m, 693m, 671m, 528m, 467w cm^{-1}. ^{1}H NMR (500 MHz, (CD$_3$)$_2$SO, δ): 7.10 (s,1H), 6.89 (s, 1H), 4.10–3.90 (m, 4H), 3.30–3.10 (m, 2H). ^{13}C NMR (125 MHz, CD$_3$OD, δ): 142.44; 126.08; 118.30; 44.19; 43.13; 42.11. GC/MS (m/z (%)): 123.1 ([M$^+$], 70); 122.1 (100).
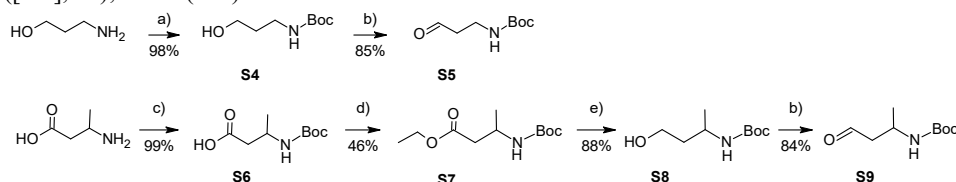
a) Boc$_2$O, CH$_2$Cl$_2$, 0 °C - r.t.; b) PCC, CH$_2$Cl$_2$, r.t.; c) 1. Boc$_2$O, NaOH (1M), NaHCO$_3$, H$_2$O, dioxane, 0 °C - r.t. 2. KHSO$_4$, 0 °C;

d) ClCO$_2$Et, Et$_3$N, CH$_2$Cl$_2$, r.t.; e) LiAlH$_4$, THF, 0 °C - r.t.

Scheme S-2.

tert-*Butyl (3-hydroxypropyl)carbamate (S4)*[2]

To a solution of 3-aminopropan-1-ol (400 mg, 5.32 mmol) in CH$_2$Cl$_2$ (18 mL) di-*tert*--butyl dicarbonate (1.22 g, 5.59 mmol) was added at 0 °C. The reaction was stirred at r.t. for 2.5 h. The reaction mixture was extracted with CH$_2$Cl$_2$. The organic layer was washed with brine and dried over anhydrous Na$_2$SO$_4$. The organic solvent was removed under reduced pressure and the crude residue was purified by dry-flash chromatography (SiO$_2$: hexane/EtOAc and EtOAc/MeOH) to yield **S4** (913 mg, 98 %) as colorless oil. ^{1}H NMR (500 MHz, CDCl$_3$, δ): 4.85 (bs, 1H), 3.85–3.50 (m, 2H), 3.40–3.20 (m, 2H), 1.75–1.62 (m, 2H), 1.44 (s, 9H). ^{13}C NMR (125 MHz, CDCl$_3$, δ): 157.16; 79.58; 59.19; 36.86; 32.84; 28.32.

tert-*Butyl (3-oxopropyl)carbamate (S5)*

Alcohol **S4** (1.18 g, 6.73 mmol) was dissolved in CH_2Cl_2 (36 mL) followed by the addition of pyridinium chlorochromate (3.19 g, 14.8 mmol). After 2 h the mixture was transferred to a silica gel column and eluted with hexane/EtOAc to afford **S5** (989 mg, 85 %) as a colorless oil.

*3-[(*tert-*Butoxycarbonyl)amino]butanoic acid (S6)*[3]

To a solution of 3-aminobutanoic acid (755 mg, 7.32 mmol) in dioxane/water (2:1, v/v, 22.5 mL), 1M NaOH (aq) (3.8 mL) was added. The reaction mixture was cooled in an ice-bath, and di-*tert*-butyl dicarbonate (2.396 g, 10.98 mmol) and $NaHCO_3$ (615 mg, 7.32 mmol) were added. The reaction mixture was stirred for 16 h at r.t. and was then evaporated to half the initial volume. The residue was diluted with EtOAc, cooled in an ice-bath and acidified to pH 2–3 with 1M $KHSO_4$ (aq). The layers were separated and water layer was extracted with EtOAc. Combined organic layers were washed with brine and dried over anh. Na_2SO_4. Finally, the solvent was removed under reduced pressure, and crude product was purified by dry-flash chromatography (SiO_2: CH_2Cl_2/MeOH) to yield **S6** (1.47 g, 99 %) as colorless oil. IR (ATR): 3330m, 2980s, 2936m, 1809m, 1715s, 1516m, 1456m, 1398m, 1370s, 1303m, 1251m, 1213m, 1169s, 1120s, 1068m, 952w, 847m, 779w cm^{-1}. ^{1}H NMR (500 MHz, CDCl$_3$, δ): 4.95 (bs, H-N), 4.05 (bs, 1H), 2.80–2.40 (m,2H), 1.44 (s, 9H), 1.24 (d, $J = 6.7$ Hz, 3H). ^{13}C NMR (125 MHz, CDCl$_3$, δ): 176.37; 155.30; 79.58; 43.32; 40.74; 28.35; 20.44.

Ethyl 3-[(tert-butoxycarbonyl)amino]butanoate (S7)

To a solution of **S6** (1.47 g, 7.23 mmol) in dry CH_2Cl_2 (40 mL) Et$_3$N (2.0 mL, 14.4 mmol), and ClCO$_2$Et (1.4 mL, 14.4 mL) were added. The reaction mixture was stirred for 18 h at r.t. and was then evaporated to dryness. The crude product was purified by dry-flash chromatography (SiO_2: CH_2Cl_2/MeOH) to yield **S7** (772 mg, 46 %). IR (ATR): 3365m, 2978s, 2934m, 1714s, 1517s, 1456m, 1369s, 1299m, 1249s, 1171s, 1094m, 1058m, 1030m, 887w, 851w, 783w, 593w cm^{-1}. ^{1}H NMR (500 MHz, CDCl$_3$, δ): 4.94 (bs, H-N); 4.15 (q, $J = 7.0$ Hz, 2H); 4.04 (bs, 1H); 2.60–2.30 (m, 2H); 1.44 (s, 9H); 1.26 (t, $J = 7.2$ Hz, 3H); 1.21 (d, $J = 6.7$ Hz, 3H). ^{13}C NMR (125 MHz, CDCl$_3$, δ): 171.73; 155.31; 79.47; 60.69; 43.68; 41.04; 28.58; 20.67; 14.38.

tert-*Butyl (4-hydroxybutan-2-yl)carbamate (S8)*

To a suspension of LiAlH$_4$ (122.7 mg, 3.235 mmol) in dry THF (3 mL) solution of **S7** (299 mg, 1.29 mmol) in dry THF (3 mL) was added at 0 °C, and the mixture was stirred for 1 h under Ar atmosphere. The reaction mixture was diluted with THF/H$_2$O (8 mL, 3 : 1, v/v), filtrated, and solvent was removed under reduced pressure. The crude product was purified using dry-flash chromatography (SiO_2: hexane/EtOAc) to yield **S8** (214 mg, 88 %) as colorless oil. IR (ATR): 3334m, 2974s, 2934m,1686s, 1530s, 1454m, 1390m, 1366m, 1276m, 1250m, 1173s, 1077m, 1052m, 987w, 967w, 853w, 782w, 751w, 648w cm^{-1}. ^{1}H NMR (500 MHz, CDCl$_3$, δ): 4.57 (bs, H-N), 3.88 (bs, 1H), 3.70–3.56 (m, 2H), 1.90–1.72 (m, 1H), 1.45 (s, 9H), 1.40–1.30 (m, 1H), 1.19 (d, $J = 6.7$ Hz, 3H). ^{13}C NMR (125 MHz, CDCl$_3$, δ): 156.71; 79.66; 58.85; 43.01; 40.61; 28.28; 21.39.

tert-*Butyl (4-oxobutan-2-yl)carbamate (S9)*

Alcohol **S8** (299 mg, 1.58 mmol) was dissolved in CH_2Cl_2 (10 mL) followed by the addition of pyridinium chlorochromate (749 g, 3.47 mmol). After stirring for 2 h at r.t. the mixture was transferred to a silica gel column and eluted with hexane/EtOAc to afford **S9** (232 mg, 84 %) as a colorless oil. IR (ATR): 3340m, 2977s, 2933m, 2731w, 1692s, 1522s,

1455m, 1391m, 1368s, 1250s, 1172s, 1068m, 856w, 782w cm^{-1}. ^{1}H NMR (500 MHz, CDCl$_3$, δ): 9.76 (s, 1H), 4.69 (bs, H-N), 4.20–4.10 (m, 1H), 2.80–2.40 (m, 2H), 1.43 (s, 9H), 1.30–1.20 (m, 3H). ^{13}C NMR (125 MHz, CDCl$_3$, δ): 200.86; 155.00; 79.69; 50.46; 42.26; 28.26; 20.87.

a) 1. **S5** or **S9**, AcOH, CH$_2$Cl$_2$/CH$_3$OH, r.t; 2. NaBH$_4$;
b) TFA, CH$_2$Cl$_2$, r.t.;
c) 4,7-DCQ, MW, 85 °C - 95 °C - 140 °C;
d) **S14**, Pd$_2$(dba)$_3$, SPhos, NaO^{t}Bu, PhMe, 100 °C
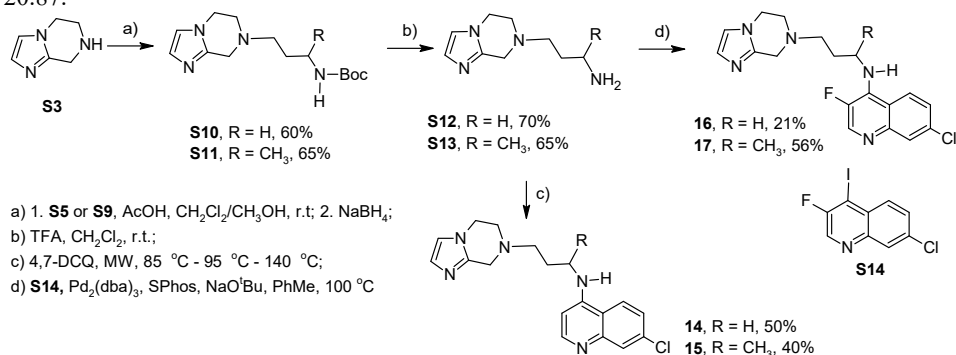
Scheme S-3.

The synthesis of **S14**[4] has been previously reported.

General procedure for reductive amination

tert-*Butyl [3-(5,6-dihydroimidazo[1,2-a]pyrazin-7(8H)-yl)propyl]carbamate (S10)*

Aldehyde **S5** (343.2 mg, 1.981 mmol) and 5,6,7,8-tetrahydroimidazo[1,2-*a*]pyrazine **S3** (292.8 mg, 2.377 mmol) were dissolved in dry MeOH/CH$_2$Cl$_2$ mixture (24 mL, 2 : 1, v/v), anh. AcOH (143 μL, 2.377 mmol) was added, and the mixture was stirred under Ar atmosphere at rt. After 3 h, NaBH$_4$ (450 mg, 11.9 mmol) was added, and stirring was continued for another 18 h at rt. Solvent was removed under reduced pressure, and the residue was dissolved in CH$_2$Cl$_2$. The organic layer was washed with 2 M NH$_4$OH. The layers were separated and water layer was extracted with CH$_2$Cl$_2$. Combined organic layers were washed with brine and dried over anh. Na$_2$SO$_4$. Finally, the solvent was removed under reduced pressure, and crude product was purified by dry-flash chromatography (SiO$_2$: hexane/EtOAc and CH$_2$Cl$_2$/MeOH). Yield 311.4 mg (60 %), colorless oil. IR (ATR): 3336w, 3112w, 3048w, 2973m, 2934m, 2873w, 2816w, 2772w, 1700s, 1528m, 1505m, 1452m, 1390w, 1366m, 1323w, 1275m, 1251m, 1172s, 1110m, 1077w, 994w, 943w, 858w, 734m, 698w, 676w cm^{-1}. ^{1}H NMR (500 MHz, CDCl$_3$, δ): 6.99 (s, 1H), 6.81 (s, 1H), 5.00 (bs, H-N), 4.00 (t, J = 5,5 Hz, 2H), 3.70 (s, 2H), 3.30–3.15 (m, 2H), 2.87 (t, J = 5,3 Hz, 2H), 2.62 (t, J = 6,9 Hz, 2H), 1.85-1.65 (m, 2H), 1.43 (s, 9H). ^{13}C NMR (125 MHz, CDCl$_3$, δ): 157.55; 144.33; 129.78; 119.05; 80.66; 57.06; 53.55; 51.38; 45.55; 40.64; 29.97; 28.64.

tert-*Butyl [4-(5,6-dihydroimidazo[1,2-a]pyrazin-7(8H)-yl)butan-2-yl]carbamate (S11)*

Aldehyde **S9** (451.7 mg, 2.41 mmol) and 5,6,7,8-tetrahydroimidazo[1,2-*a*]pyrazine **S3** (386.2 mg, 3.133 mmol) were coupled to afford **S11** (406.2 mg, 65 %) using AcOH (188 μL, 3.133 mmol) and NaBH$_4$ (547 mg, 11.9 mmol). The crude product was purified by dry-flash chromatography (SiO$_2$: hexane/EtOAc and CH$_2$Cl$_2$/MeOH). Yield 406.2 mg (65 %), colorless oil. The product was used for the next reactions without further purification.

3-(5,6-Dihydroimidazo[1,2-a]pyrazin-7(8H)-yl)propan-1-amine **(S12)**

To a solution of **S10** (311.4 mg, 1.112 mmol) in CH_2Cl_2 (7 mL, degassed) TFA (1.3 mL) was added. The reaction was stirred at r.t. for 3 h. The solvent was removed under reduced pressure, the reaction mixture was suspended in CH_2Cl_2/MeOH, and NaOH (aq) was added until pH 10. The organic layer was washed with brine, dried (anh. Na_2SO_4), filtered, and concentrated in vacuo. Yield 139.4 mg (70 %), brown oil. IR (ATR): 3361s, 2946s, 2821s, 1689m, 1572m, 1502s, 1469m, 1374m, 1324m, 1279m, 1199m, 1110m, 1077m, 994w, 939m, 824w, 741m, 676m cm^{-1}. ^{1}H NMR (500 MHz, CD_3OD, δ): 6.99 (s, 1H), 6.90 (s, 1H), 4.08-3.98 (m, 2H), 3.66 (s, 2H), 2.97-2.85 (m, 2H), 2.77 (t, J = 7.0 Hz, 2H), 2.65 (t, J = 7.2 Hz, 2H), 1.85-1.70 (m, 2H). ^{13}C NMR (125 MHz, $CDCl_3$ + CD_3OD, δ): 144.25; 129.27; 119.21; 57.02; 53.02; 51.42; 45.48; 41.42; 30.83. (+)ESI-HRMS (m/z): $[M + H]^+$ = 181.14477 (error +3.04 ppm).

4-(5,6-Dihydroimidazo[1,2-a]pyrazin-7(8H)-yl)butan-2-amine **(S13)**

To a solution of **S11** (406.2 mg, 1.853 mmol) in CH_2Cl_2 (10 mL, degassed) and MeOH (0.5 mL), TFA (2 mL) was added. The reaction was stirred at r.t. for 3 h. The solvent was removed under reduced pressure, the reaction mixture was suspended in CH_2Cl_2/MeOH, and NaOH (aq) was added until pH 10. The organic layer was washed with brine, dried (anh. Na_2SO_4), filtered, and concentrated in vacuo. Yield 174 mg (65 %), pale-brown oil. IR (ATR): 3417w, 2972m, 2830m, 1677s, 1540w, 1506m, 1460w, 1424w, 1393w, 1327w, 1280w, 1201s, 1133s, 1034w, 942w, 834w, 801w, 743w, 723w, 676w cm^{-1}. ^{1}H NMR (500 MHz, $(CD_3)_2SO$, δ): 7.78 (bs, 2H, NH_2), 7.14 (s, 1H), 6.97 (s, 1H), 4.05–3.95 (m, 2H), 3.75–3.55 (m, 2H), 3.35–3.25 (m,1H), 2.90–2.75 (m, 2H), 2.70–2.55 (m, 2H), 1.90–1.55 (m, 2H), 1.19 (d, J = 6.4 Hz, 3H). ^{13}C NMR (125 MHz, $(CD_3)_2SO$, δ): 142.33; 126.10; 118.96; 53.07; 50.85; 49.24; 46.01; 43.99; 31.08; 18.62. (+)ESI-HRMS (m/z): $[M + H]^+$ = 195.16053 (error +2.26 ppm).

7-Chloro-N-[3-(5,6-dihydroimidazo[1,2-a]pyrazin-7(8H)-yl)propyl]quinolin-4-amine **(14)**

A reaction vessel containing **S12** (19.1 mg, 0.105 mmol) and 4,7-dichloroquinoline (17.4 mg, 0.088 mmol) was stirred for 15 min at 80 °C, 30 min at 95 °C and 2 h at 140 °C in a MW reactor. The reaction mixture was suspended in CH_2Cl_2, transferred to a separation funnel, and washed well with 1M NaOH (aq). The organic layer was collected, dried with anh. Na_2SO_4, and filtered. Subsequently, the solvent was removed under reduced pressure and product **14** was purified by dry-flash chromatography (SiO$_2$: EtOAc/MeOH). Yield 15.1 mg (50 %), pale-yellow amorphous powder, mp = 71 °C. IR (ATR): 3274m, 2925s, 2853m, 1673m, 1609m, 1582s, 1541m, 1502m, 1452m, 1370m, 1329m, 1281m, 1246w, 1202w, 1137m, 1111m, 1080w, 942w, 900w, 879w, 850w, 809w, 767w, 731w, 677w, 647w cm^{-1}. ^{1}H NMR (500 MHz, $CDCl_3$, δ): 8.49 (d, J = 5.2 Hz, 1H), 7.90 (s, 1H), 7.22–7.07 (m, 2H), 7.05–6.92 (m, 2H), 6.33 (d, J = 5.2 Hz, 1H), 4.09 (t, J = 5.5 Hz, 2H), 3.88 (s, 2H), 3.50–3.42 (m, 2H), 3.01 (t, J = 5.7 Hz, 2H), 2.95–2.85 (m, 2H), 2.10–2.00 (m, 2H). ^{13}C NMR (125 MHz, $CDCl_3$, δ): 151.88; 150.24; 148.87; 142.23; 134.56; 128.97; 128.45; 125.10; 121.23; 117.75; 117.36; 98.44; 57.30; 51.81; 50.47; 44.01; 43.55; 24.22. (+)ESI-HRMS (m/z): $[M + H]^+$ = 342.14700 (error +4.53 ppm). HPLC purity, method A: t_R = 3.872, area 99.36 %. Method B: t_R = 4.504, area 99.20 %.

7-Chloro-N-[(2R)-4-(5,6-dihydroimidazo[1,2-a]pyrazin-7(8H)-yl)butan-2-yl]quinolin-4-amine **(15)**

A reaction vessel containing **S13** (63.8 mg, 0.328 mmol) and 4,7-dichloroquinoline (32.5 mg, 0.164 mmol) was stirred for 15 min at 80 °C, 30 min at 95 °C and 2 h at 140 °C in a

MW reactor. The reaction mixture was suspended in CH_2Cl_2, transferred to a separation funnel, and washed well with 1M NaOH (aq). The organic layer was collected, dried with anh. Na_2SO_4, and filtered. Subsequently, the solvent was removed under reduced pressure and product **15** was purified by dry-flash chromatography (SiO_2: EtOAc/MeOH and CH_2Cl_2/MeOH (NH_3)) and flash chromatography (Biotage SP, NH: hexane/EtOAc and EtOAc/MeOH). Yield 23.5 mg (40 %), pale-yellow oil. IR (ATR): 3269m, 2963m, 2818m, 1610m, 1578s, 1538m, 1501m, 1450m, 1374m, 1329m, 1277m, 1193w, 1153w, 1110w, 1078w, 933w, 880w, 850w, 810w, 734m, 699w, 678w, 648w cm^{-1}. ^{1}H NMR (500 MHz, $CDCl_3$, δ): 8.47 (d, $J = 5.5$ Hz, 1H), 7.88 (d, $J = 2.1$ Hz, 1H), 7.20 (d, $J = 8.9$ Hz, 1H), 7.11 (s, 1H), 7.02–6.90 (m, 3H), 6,37 (d, $J = 5.5$ Hz, 1H), 4.10–3.98 (m, 2H), 3.95–3.78 (m, 3H), 3.05–2.85 (m, 3H), 2.78–2.69 (m, 1H), 2.12–2.00 (m, 1H), 1.86–1.75 (m, 1H), 1.34 (d, $J = 6.1$ Hz, 3H). ^{13}C NMR (125 MHz, $CDCl_3$, δ): 151.88; 149.33; 149.23; 142.26; 134.53; 128.89; 128.61; 124.92; 121.26; 117.72; 117.49; 98.71; 54.38; 51.90; 50.38; 48.00; 43.93; 31.73; 19.28. (+)ESI-HRMS (m/z): $[M + H]^+ = 356.16272$ (error +4.15 ppm). HPLC purity, method A: $t_R = 3.490$, area 95.35 %. Method B: $t_R = 7.515$, area 97.30 %.

General procedure for Buchwald-Hartwig amination

7-Chloro-N-[3-(5,6-dihydroimidazo[1,2-a]pyrazin-7(8H)-yl)propyl]-3-fluoroquinolin-4-amine (16)

To a flame-dried reaction tube, $Pd_2(dba)_3$ (8 mg, 0.009 mmol, 5 mol% Pd), SPhos (7.2 mg, 0.017 mmol) and PhMe (1.5 mL) were added. The solution was stirred at r.t. under an inert atmosphere for 3 min, and was then added to a mixture of **S14** (53.7 mg, 0.175 mmol), **S12** (63 mg, 0.35 mmol), NaO*t*-Bu (47 mg, 0.49 mmol, 2.8 equiv) and PhMe (1.5 mL), the tube was sealed and the mixture was heated at 100 °C in an oil bath for 19 h. The crude product **16** was purified by dry-flash column chromatography (SiO_2: hexane/EtOAc and EtOAc/MeOH) and furthermore by flash column chromatography (Biotage SP, NH, hexane/EtOAc and EtOAc/MeOH). Yield 13.4 mg (21 %), pale-yellow oil. IR (ATR): 3270s, 2952s, 2822m, 1700m, 1597s, 1575s, 1539s, 1501s, 1455s, 1420s, 1372s, 1324m, 1298m, 1270m, 1191m, 1139m, 1110m, 1077m, 992w, 942m, 892w, 814m, 762m, 735m, 700w, 676w, 656w, 622w, 542w cm^{-1}. ^{1}H NMR (500 MHz, $CDCl_3$ + D_2O, δ): 8.45 (d, $J = 5.8$ Hz, 1H), 7.88 (s, 1H), 7.21 (d, $J = 9.2$ Hz, 1H), 7.15–7.12 (m, 1H), 6.97–6.91 (m, 2H), 4.07 (t, $J = 5.5$ Hz, 2H), 3.90–3.80 (m, 4H), 3.05–2.95 (m, 2H), 2.90–2.80 (m, 2H), 2.05–1.95 (m, 2H). ^{13}C NMR (125 MHz, $CDCl_3$, δ): 146.44; 143.58 (d, $J = 238.3$ Hz); 142.50 (d, $J = 27.1$ Hz); 142.88; 136.67 (d, $J = 5.4$ Hz); 133.80; 129.05; 128.85; 125.90; 121.74 (d, $J = 5.4$ Hz); 119.15 (d, $J = 5.4$ Hz); 117.85; 57.61; 52.13; 50.49; 46.59; 44.01; 25.52. (+)ESI-HRMS (m/z): $[M + H]^+ = 360.13767$ (error +4.04 ppm). HPLC purity, method A: $t_R = 3.471$, area 95.05 %. Method B: $t_R = 7.381$, area 97.14 %.

7-Chloro-N-[4-(5,6-dihydroimidazo[1,2-a]pyrazin-7(8H)-yl)butan-2-yl]-3-fluoroquinolin-4-amine (17)

Following the general procedure for Buchwald-Hartwig amination, compound **17** was obtained after dry-flash column chromatography (SiO_2: hexane/EtOAc and EtOAc/MeOH) as a pale-yellow oil (31.5 mg, 56 %) from **S13** (43.5 mg, 0.224 mmol) and **S14** (46 mg, 0.015 mmol) using $Pd_2(dba)_3$ (6.8 mg, 0.007 mmol), SPhos (6.1 mg, 0.015 mmol), NaO*t*-Bu (40.2 mg, 0.419 mmol) and PhMe (2 mL). IR (ATR): 3271s, 2966s, 2822m, 1596s, 1574s, 1540m, 1502m, 1449m, 1421m, 1380s, 1350m, 1298m, 1270m, 1192m, 1142m, 1112m, 1078m, 992w, 927w, 879w, 815w, 762w, 734m, 675w, 622w, 540w cm^{-1}. ^{1}H NMR (500 MHz, $CDCl_3$ + CD_3OD, δ): 8.42 (d, $J = 5.8$ Hz, 1H), 7.86 (d, $J = 2.1$ Hz, 1H), 7.48 (d,

J = 8.9 Hz, 1H), 7.10–7.00 (m, 2H), 6.93 (d, J = 1.2 Hz, 1H), 4.41–4.32 (m, 1H), 4.10–3.92 (m, 2H), 3.87–3.75 (m, 2H), 3.10–3.00 (m, 1H), 2.99–2.89 (m, 2H), 2.80–2.70 (m, 1H), 2.15-2.05 (m, 1H), 1.87–1.75 (m, 1H), 1.36 (d, J = 6.1 Hz, 3H). ^{13}C NMR (125 MHz, CDCl$_3$ + CD$_3$OD, δ): 146.15; 143.05 (d, J = 239.2 Hz); 142.43; 142.12 (d, J = 28.0 Hz); 136.38 (d, J = 4.5 Hz); 134.21; 128.26; 128.14; 125.94; 122.10 (d, J = 5.4 Hz); 119.33 (d, J = 4.5 Hz); 118.02; 54.23; 51.66; 50.37; 50.19; 44.05; 32.62; 21.63. (+)ESI-HRMS (m/z): [M + H]$^+$ = 374.15307 (error +4,56 ppm). HPLC purity, method A: t_R = 3.520, area 97.15 %. Method B: t_R = 7.549, area 98.21 %.
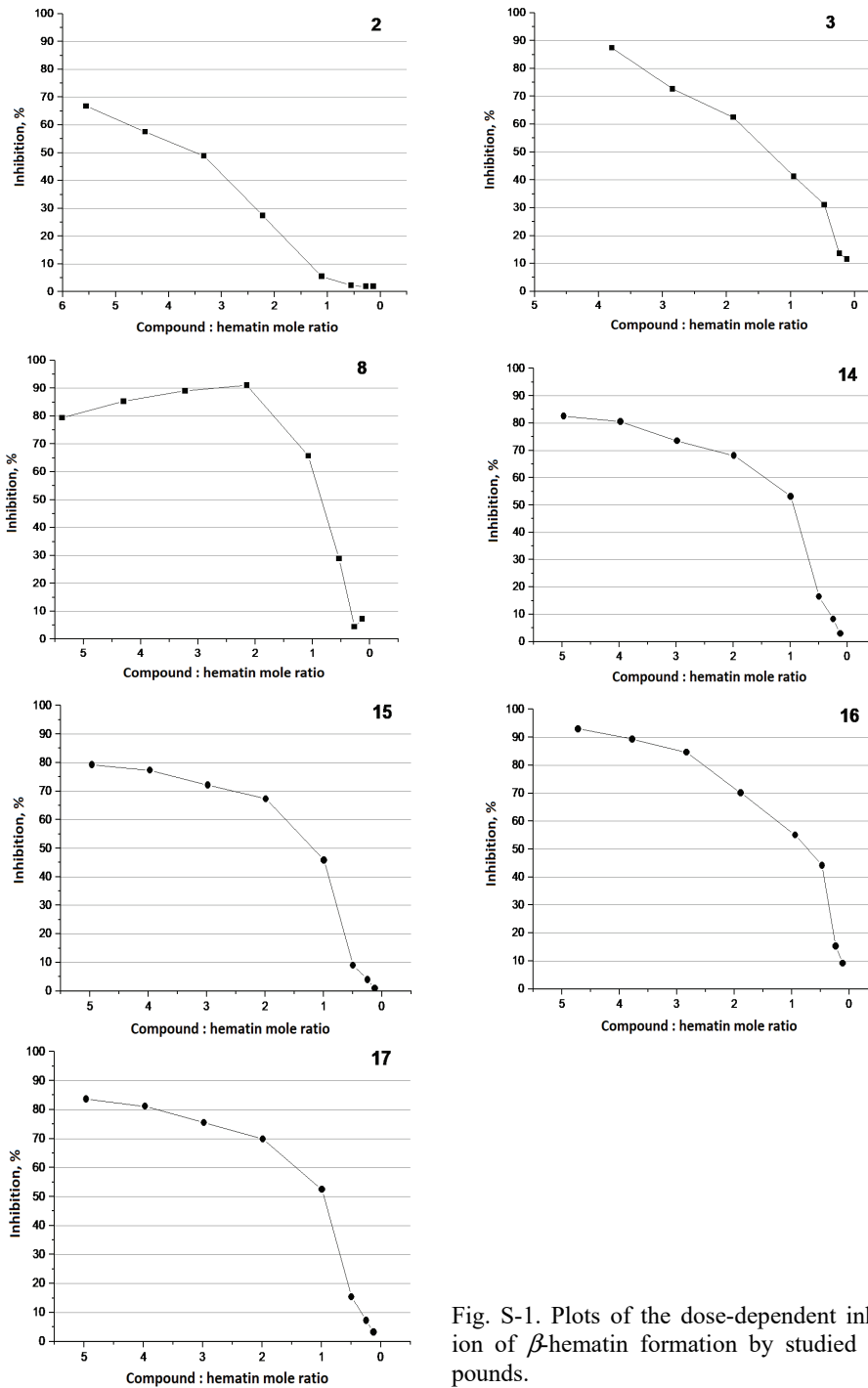
Fig. S-1. Plots of the dose-dependent inhibition of β-hematin formation by studied compounds.

REFERENCES

1. a) E. Regel, *Justus Liebigs Ann. Chem*. **1977** (1977) 159 (https://doi.org/-10.1002/jlac.197719770116); b) L. A. M. Bastiaansen, E. Godefroi, *J. Org. Chem*.**43** (1978) 1603 (https://doi.org/10.1021/jo00402a032), c) L. Gong, Y-C. Tan, (Holder), Inhibitors of JNK, WO 2011/151357, December 8, 2011

2. T. James, I. Simpson, J. A. Grant, V. Sridharan, A. Nel, *Org. Lett*. **15** (2013) 6094 (https://doi.org/10.1021/ol402988s)

3. V. Čaplar, M. Žinić, J-L. Pozzo, F. Fages, G. Mieden-Gundert, F. Vogtle, *Eur. J. Org. Chem*. **2004** (2004) 4048 (https://doi.org/10.1002/ejoc.200400105)

4. a) N. D. Heindel, S. A. Fine, *Org. Prep. Proced*. **1** (1969) 279 (https://doi.org/-10.1080/00304946909458399); b) N. Terzić, J. Konstantinović, M. Tot, J. Burojević, O. Djurković-Djaković, J. Srbljanović, T. Štajner, T. Verbić, M. Zlatović, M. Machado, I. S. Albuquerque, M. Prudêncio, R. J. Sciotti, S. Pecic, S. D'Alessandro, D. Taramelli, B. A. Šolaja, *J. Med. Chem*. **59** (2016) 264 (https://doi.org/10.1021/acs.jmedchem.5b01374).

Molecular docking study on biomolecules isolated from endophytic fungi

JANKO IGNJATOVIĆ[1], NEVENA ĐAJIĆ[1], JOVANA KRMAR[1], ANA PROTIĆ[1], BORUT ŠTRUKELJ[2] and BILJANA OTAŠEVIĆ[1]*

[1]*Department of Drug Analysis, University of Belgrade – Faculty of Pharmacy, Vojvode Stepe 450, 11221 Belgrade, Serbia and* [2]*Faculty of Pharmacy, University of Ljubljana, Aškerčeva cesta 7, 1000 Ljubljana, Slovenia*

Abstract: Recently, growing interest has been devoted to the investigation of compounds with antimicrobial activity due to rising cases of resistance of microbes to known therapies. A reliable and versatile source of novel drug discovery was recently found among endophytic fungi. Hitherto, the research usually enclosed the *in vitro* evaluation of antimicrobial activity and chemical structure elucidation of biomolecules extracted from fungal material. Therefore, this research was designed as an extension to previous investigations of endophytic fungi growing on conifer needles by means of conducting a molecular docking study. The *in silico* methods were used with the main goal to make a contribution to the understanding of the mechanisms underlying the interaction of biomolecules isolated from fungus *Phomopsis species* and eight different types of receptors that belong to usually multidrug resistant bacterial pathogens. The results revealed valuable interactions with receptors 3G7B (*Staphylococcus aureus*'s gyrase B), 1F0K (1.9 Å structure of *Escherichia coli*'s transferase) and 1SHV (*Klebsiella pneumoniae*'s SHV-1 *β*-lactamase) thus pointing out the receptors that trigger antibiotic response upon activation by the most potent compounds 325-3, 325-5, phomoenamide and phomol. These findings also recommended further discovery of novel potent and broadspectrum antibiotics based on the structure of selected molecules.

Keywords: endophytes; antibacterial activity; *in silico* drug discovery.

INTRODUCTION

Antimicrobial drug resistance represents a global health problem. In order to effectively undertake the challenge of antimicrobial resistance, indispensable and sustainable use of antibiotics is necessary in order to control the disease, but also fostering innovation and development of new molecules with antibiotic potential. Development of novel antimicrobial therapies is necessary in order to enable

substitution for the declining effectiveness of already existing antibiotics.[1] Endophytic fungi were recently recognised as a naturally occurring repository of potent compounds for novel drug discovery regarding the fact that they represent microorganisms that usually inhabit medicinally potent plants and thus may inherit their medicinal abilities.[2–5] Endophytic fungi are defined as non-pathogenic microorganisms (bacteria or fungi) that are present in the inner tissues of plants and have a symbiotic relationship with their plant host by helping the host plant to overcome the invasion of pathogenic microorganisms by producing secondary metabolites.[6–11] A literature survey revealed that for these molecules, a variety of pharmacological activities, such as antifungal, antibacterial, antiviral, cytotoxic, anti-oxidant, *etc*. have already been reported.[12] In this regard, the authors have reported significant antibacterial activity coming from secondary metabolites of endophytic fungus *Phomopsis species* growing in Slovenian conifer forests.[13]

It is common knowledge that many antimicrobials express their effect through specific interaction with receptor targets that are present in microbes.[14,15] Nowadays, in line with experimental *in vitro* testing of the activity and interactions between potential ligands and receptors, achievements in the field of computer science allow a unique opportunity for computer aided drug design and simulation.[16–18] *In silico* methods enable high throughput screening for potential drug candidates and introduce scientifically more informative and rationalized pharmaceutical research. Bearing this in mind, as well as the already proven activity of biomolecules isolated from endophytic fungus *Phomopsis species* growing on conifer needles against *Staphylococcus aureus* and *Escherichia coli*,[13] the present study undertook consideration of common target receptors of known antibiotics related to these pathogens. It was decided that the antimicrobial activity against G$^+$ bacteria *S. aureus* should be investigated using receptors 3VSL (penicillin-binding protein 3 from methicilin-resistant *S. aureus*),[19] 3G7B (*S. aureus* gyrase B)[20] and 1JIJ (tyrosyl-tRNA synthetase of *S. aureus*).[20] In addition, receptor 3K3P from *Streptococcus mutans* (apo-form of D-alanine: D-alanine ligase),[21] was included as a valuable clue in further understanding of the resistance of G$^+$ type bacteria to known drugs. On the other hand, widely tested receptor targets for evaluation of antimicrobial activity on *E. coli*, as the most common representative of G$^-$ bacteria, were 1F0K (1.9 Å structure of *E. coli*'s transferase),[22] 1KZN (24 kDa domain of *E. coli*'s isomerase)[21] and 4EMV (structure of *E. coli*'s topoisomerase ATP inhibitor).[22] Furthermore, the authors emphasized the importance of 1SHV receptor from *Klebsiella pneumoniae* (SHV-1 *β*-lactamase)[22] as an additional target for inhibition of G$^-$ type bacteria.

Bioactive compounds labelled as 325-3 and 325-5, isolated from endophytic fungus *Phomopsis species* growing on conifer needles,[13] were used as a reference for a thorough literature search for secondary metabolites from other *Phomopsis species* strains, as well as structurally similar bioactive compounds.[23–32]

A set of molecules was selected that comprised phomoenamide and phomonitro-ester, secondary metabolites from endophyte *Phomopsis species* strain PSU-D15 with records on moderate *in vitro* antibacterial activity against *Mycobacterium tuberculosis*.[23,24] Five structurally similar compounds, hybrid peptide–polyketides named as curvularides A–E, obtained from the endophytic fungus *Curvularia geniculate* and isolated from the limbs of *Catunaregam tomentosa* were further selected because of their demonstrated antifungal activity against *Candida albicans*.[25] The set was complemented with compounds **6** and **7** isolated from endophytic fungus *Phomopsis species* from *Notobasis syriaca*, which also showed considerate antibacterial, anti-algal and antifungal activity.[26] Finally, phomol was recently promoted as a novel antibiotic isolated from *Phomopsis species* from the medicinal plant *Erythrina crista-galli*.[27]

EXPERIMENTAL

Molecular docking

Molecular docking is a practical *in silico* method employed in order to predict the orientation of a ligand in a receptor binding pocket.[33,34] Freely available software Autodock v4.2 (The Scripps Research Institute, La Jolla, CA, USA) was used to perform the docking studies, while analyses of the docking simulation was performed in AutoDockTools 1.5.6 (The Scripps Research Institute, La Jolla, CA, USA). Prior to docking simulation, the ligands and receptors were adequately prepared. The structures of the ligands were optimized to achieve the conformations with the minimum energy, while structures of the receptor were retrieved from Brookhaven protein data bank. Pre-calculation of a 3D grid of interaction energies was performed by AutoGrid based on a macromolecular target. Within this procedure, a cubic grid box and grid maps were created in order to represent the active region in which the native molecular structure is embedded.[35] A grid of 40 points in *x*-, *y*- and *z*-direction with grid spacing of 0.375 Å was built centred on a ligand. The maximum number of energy evaluations was 2.500.000. The Lamarckian genetic algorithm was used to identify the best conformers.[36,37] A maximum of 100 independent conformers for each compound were considered during the simulation. The docking exercise was executed between flexible ligands (tested molecular structures) and rigid protein receptors, allowing an evaluation of the free binding energy of the ligand and the macromolecule. Docked conformations with best *RMSD* (root mean square deviation) scoring function of all docked conformation were evaluated together with established key interactions.[38,39]

Preparation of receptors and ligand molecules

Crystal structures of G+ and G- bacterial type receptors were obtained from the Protein Data Bank (https://www.rcsb.org/).[20-22] A set of ligand molecules included compounds 325-3 and 325-5, curvularides A–E, compounds **6** and **7**, phomol, phomoenamide and phomonitro-ester (Fig. 1).[23-27] The antibiotic ampicillin served as the control ligand. All ligand molecules were set in their minimum energy conformations obtained by the MOPAC/AM1 method (job type: minimising the *RMS* gradient to 0.100; display: each iteration; AM1 theory; wave function: closed shell) in Chem 3D Ultra 7.0.0 (Surrey, UK).
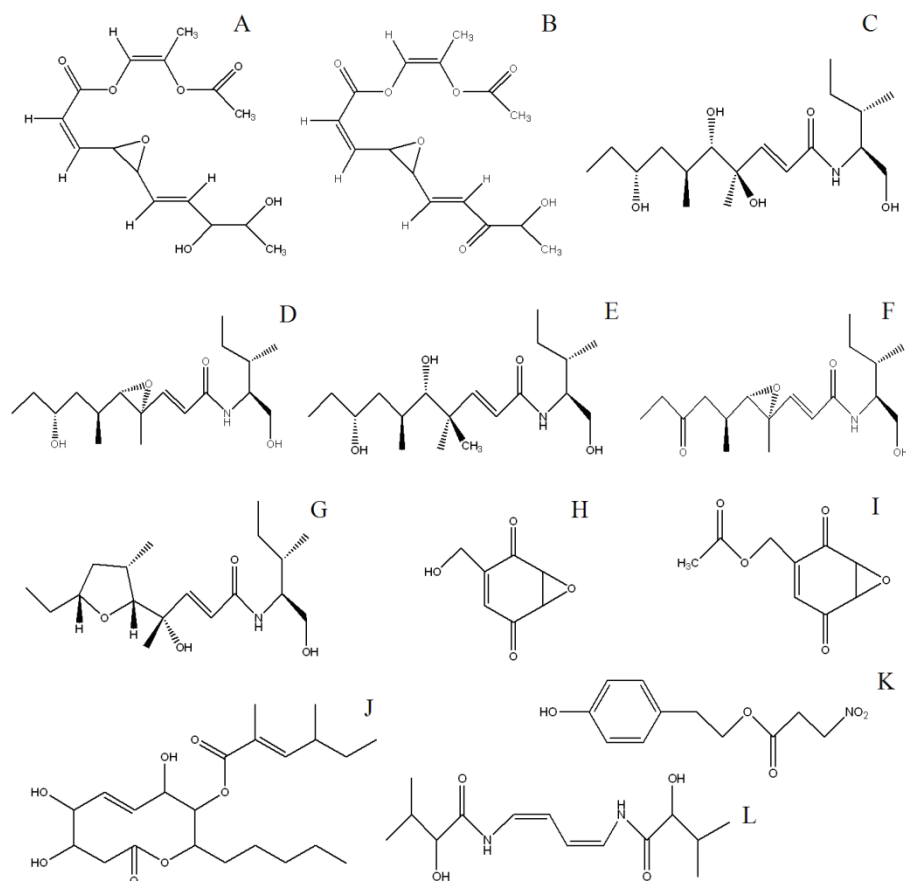
Fig. 1. Chemical structure of compound 325-3 (A), 325-5 (B), curvularide A (C), curvularide B (D), curvularide C (E), curvularide D (F), curvularide E (G), compound 6 (H), compound 7 (I), phomol (J), phomoenamide (K) and phomonitroester (L).

RESULTS AND DISCUSSION

As a result of the authors' previous research attempts, compounds 325-3 and 325-5 were isolated from endophytic fungus *Phomopsis* sp. and their activity against *Escherichia coli* and *Staphylococcus aureus* strains was experimentally evaluated. To understand the mechanism underlying the interaction between 325-3 or 325-5 and different type of receptors and to identify the receptor that triggers antibiotic response upon activation, a molecular docking study was further performed. Additionally, the pool of ligands was enriched with ten more endophytic biomolecules found through a literature surveillance. The most stable conformations proposed by docking study were selected based on the minimum binding energy contributing to more thermodynamically favoured pathway of the formation of the docked structure.

Each interaction was evaluated through certain parameters, *i.e.*, inhibition constant (K_i), *RMSD* value, free binding energy and potential presence of hydrogen bonds between the tested ligand and the receptor. In general, lower values of final and binding energies, lower values of inhibition constant, root mean square deviation (*RMSD*) with a threshold value of 2 Å and, in case of close interaction of the ligand and receptor, the potential for the formation of hydrogen bonds between them, may be considered as reliable indicators of potential binding of the tested ligand to a receptor.[40] The coordinates of the central grid point of the maps for all the tested ligands are provided in Table S-I of the Supplementary material to this paper.

The outcomes of the docking simulation for the 1F0K receptor with ligands (Table I and Table S-II of the Supplementary material) demonstrated that of the tested ligands, ampicillin exhibited the highest bonding potential by establishing 2 hydrogen bonds (Fig. 2), and having the lowest free binding energy of –6.47 kcal* mol^{-1}, an inhibition constant (K_i) of 18.08 μM and an *RMSD* value of 5.08. When comparing the affinity of the other ligands to ampicillin, 325-3, 325-5, phomoenamide and phomol stood out. Of the afore-mentioned compounds, lowest free binding energies were observed for compound 325-3 (–5.14 kcal mol^{-1}), phomoenamide (–4.97 kcal mol^{-1}) and 325-5 (–4.78 kcal mol^{-1}). Interestingly, the lowest K_i value, which implies high binding potential for the 1F0K receptor, was noted for phomol ($K_i = 60.52$ μM), followed by compounds 325-3 ($K_i = 172.04$ μM) and phomoenamide ($K_i = 227.74$ μM). The lowest *RMSD* value was observed in case of phomol (*RMSD* = 3.26), followed compounds 325-3 and 325-5, which had the same *RMSD* value of 3.72 and phomoenamide with *RMSD* value of 4.46. Four hydrogen bonds were observed in case of compound 325-5 and curvularide A, though both compounds bind only to the GLN289 amino acid on the receptor, while additional hydrogen bonds were established with the other amino acids LEU265, SER192 and GLN193. This may imply that the 2 binding pockets of receptor 1F0K were in close vicinity. Compound 325-3, phomol and phomoenamide established 3 hydrogen bonds with the receptor. Since 325-5 and phomoenamide formed hydrogen bonds through THR266 amino acid and both compound 325-3 and 325-5 formed hydrogen bonds with amino acid GLN289 on the 1F0K receptor, it is suspected that compounds 325-3, 325-5 and phomoenamide bind to the same receptor pocket. On the other hand, phomol formed hydrogen bonds with amino acids GLY190 and GLN193, implying that it did not bond to the same place as the other compounds.

The analysis of docking results of ligands to 3G7B receptor showed, as expected, that among the investigated ligands, the lowest binding energy of –6.10 kcal mol^{-1} was observed for the ampicillin control (Table II and Table S-III of the Supplementary material). Of all tested ligands, compound 325-3 had the low-

---

* 1 kcal = 4184 J

TABLE I. Extracted crystal and experimental data for the molecular complexes with the 1F0K receptor

Tested ligand	Free binding energy, kcal mol⁻¹	Inhibition constant, µM	*RMSD*	Hydrogen bonds with receptor amino acids
Ampicillin	–6.47	18.08	5.08	THR266
325-3	–5.14	172.04	3.72	GLN289
325-5	–4.78	313.49	3.72	THR266 GLN289
Curvularide A	–4.76	324.52	6.17	LEU265, SER192, GLN193, GLN289
Curvularide B	–4.10	994.76	6.79	GLN289
Curvularide C	–4.70	361.64	4.74	VAL189
Curvularide D	–4.74	334.92	6.42	LEU265
Curvularide E	–4.73	343.80	4.90	GLU269
Phomoenamide	–4.97	227.74	4.46	THR266
Compound **6**	–3.88	1430	7.35	LEU265, THR266
Compound **7**	–4.56	454.39	5.83	ARG164, THR266
Phomol	–5.75	60.52	3.26	GLY190, GLN193
Phomonitroester	–4.81	296.63	5.89	GLU269, GLN289
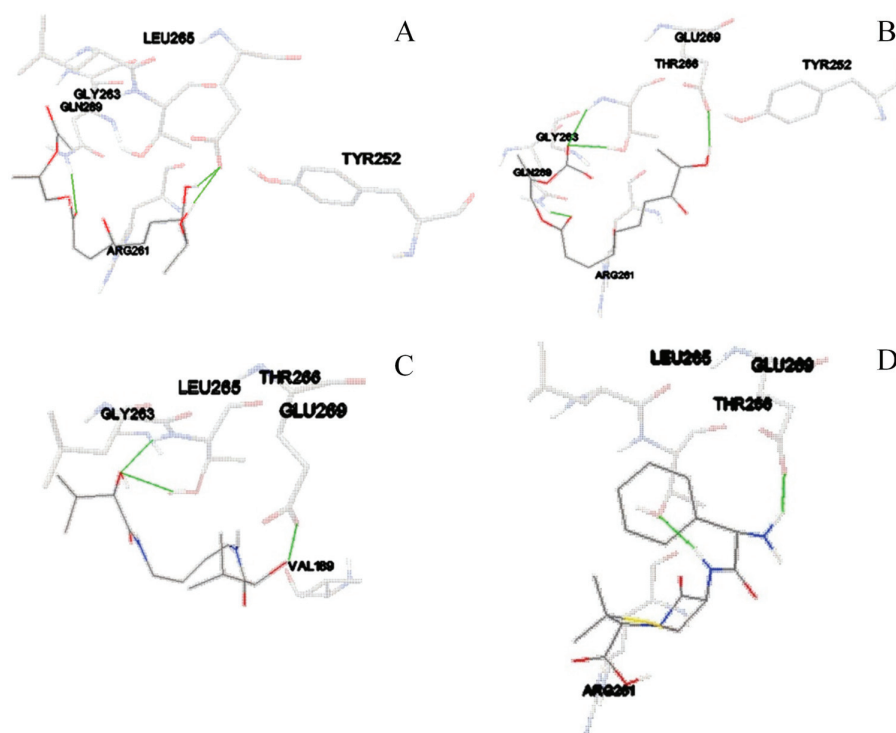
Fig. 2. Docking pose of ligands 325-3 (A), 325-5 (B), phomoenamide (C) and ampicillin (D) with binding pocket of 1F0K receptor. Only the portion of the receptor with interacting amino acid residues is displayed. Main hydrogenic bonds between ligand amino acid residues in receptor pocket are emphasized in green.

est binding energy of –5.27 kcal mol^{-1}. Moreover, a low binding energy with the 3G7B receptor was also observed for phomoenamide and the 325-5 ligand.

In addition, docking simulation revealed the establishment of 4 hydrogen bonds between the receptor 3G7B and both the ligand 325-3 and phomoenamide. Furthermore, 3 hydrogen bonds were observed between compound 325-3 and the 3G7B receptor. Similar binding spots on the 3G7B receptor (amino acids on positions ASP57, ASN54 and VAL131 of 3G7B receptor, Table S-III) were observed for both compounds 325-3 and 325-5 (Fig. 3), which may explain the antimicrobial activity against *S. aureus* experimentally observed in previous research. This also implied that compounds 325-3 and 325-5 interact with the same binding spot on the receptor, while phomoenamide or ampicillin bind to the other pockets of the 3G7B receptor. The lowest *RMSD* values were noted for phomoenamide (*RMSD* 3.27) and compound 325-5 (*RMSD* 3.92). Moreover, other tested ligands showed potential for interaction and binding with the 3G7B receptor. However, according to the free binding energy, the constant of inhibition and the *RMSD* value, compounds 325-3 ($K_i = 135.56$ µM, *RMSD* 5.04), 325-5 ($K_i = 425.42$ µM, *RMSD* 3.92) and phomoenamide ($K_i = 397.98$ µM, *RMSD* 3.27) showed the greatest potential.

TABLE II. Extracted crystal and experimental data for molecular complexes with the 3G7B receptor

Tested ligand	Free binding energy, kcal mol^{-1}	Inhibition constant, µM	*RMSD*	Hydrogen bonds with receptor amino acids
Ampicillin	–6.10	33.93	5.77	ASP53, GLU50
325-3	–5.27	135.56	5.04	ASP57, ASN54, VAL131
325-5	–4.60	425.42	3.92	ASP57VAL131, ASN54
CurvularideA	–2.58	12930	4.21	ASP53, GLU50, ASN54
CurvularideB	–4.36	632.03	3.98	GLU50, HIS46
CurvularideC	–3.21	4440	4.50	ASP57
CurvularideD	–4.51	495.24	4.19	ASP53, ASN54, VAL131
CurvularideE	–4.47	532.45	4.15	ASP52, ASN54
Phomoenamide	–4.64	397.98	3.27	ASN54, GLU50
Compound 6	–3.75	1790	6.72	VAL131, ASN54, GLU50
Compound 7	–4.20	838.08	4.80	ASN54, VAL131
Phomol	–3.74	1800	4.89	ASP53, ASN206
Phomonitroester	–3.88	1440	6.80	VAL130, GLU50, HIS46, VAL131

These results suggest that the highest affinity for the receptor 3G7B was observed for the ampicillin antibiotic control. Of the tested ligands, slightly lower affinity was noted for ligands 325-3, 325-5 and phomoenamide. Interestingly, binding places for ampicillin and phomoenamide included interactions in the receptor pocket in the vicinity of amino acid GLU50, while both compounds 325-3 and 325-5 included interactions with amino acids ASP57, ASP54 and

VAL131 on different receptor spot (Fig. 3). There was a difference in binding locations of the aforementioned compounds, which implied potential differences in mechanism of action of ampicillin and phomoenamide in comparison to 325-3 and 325-3.
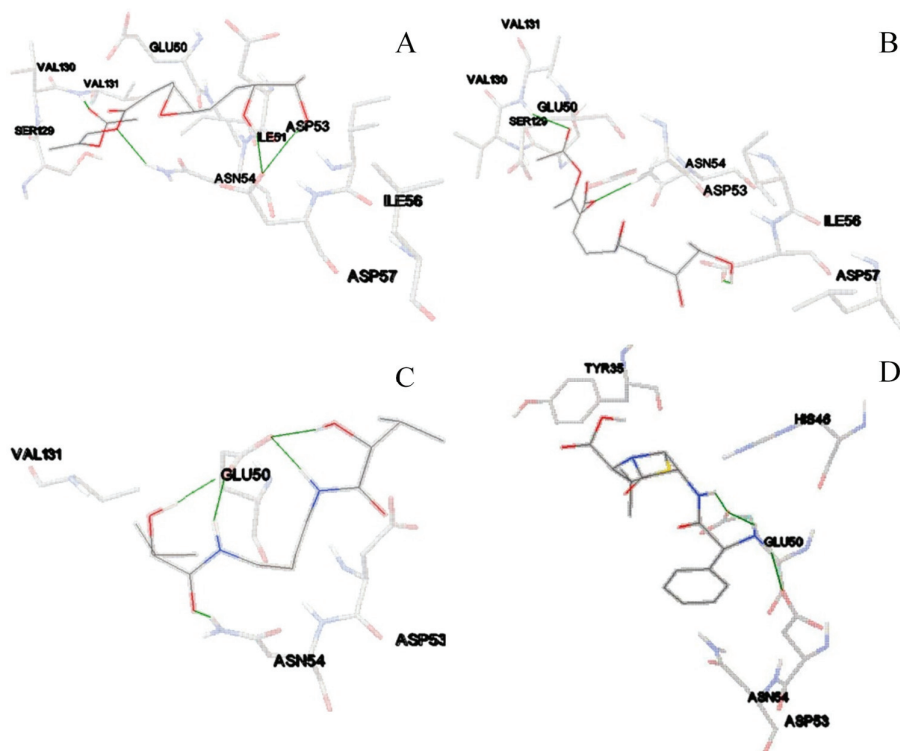
Fig. 3. Docking pose of ligands 325-3 (A), 325-5 (B), phomoenamide (C) and ampicillin (D) with 3G7B receptor binding pocket. Only the portion of the receptor with interacting amino acid residues is displayed. The main hydrogenic bonds between ligand amino acid residues in the receptor pocket are emphasized in green.

It is known that antibiotics can exhibit their effect through inhibition of β-lactamase. Therefore, docking simulations between SHV-1 β-lactamase as receptor and all the investigated ligands were performed and evaluated (Tables III and S-IV (Supplementary material)). Ampicillin exhibited the lowest free binding energy of –1.90 kcal mol^{-1} and an *RMSD* of 5.08. However, compounds **6** and phomonitroester had the lowest free binding energy (–2.85 and –2.67 kcal mol^{-1}, respectively), followed by compound **6** (–2.48 kcal mol^{-1}) and compound 325-5 (–1.79 kcal mol^{-1}). This might imply that they potentially have greater affinity for the receptor in comparison to the ampicillin control. For all compounds, higher values for the inhibition constants were observed, with the lowest value of

8.10 mM for compound **7**. Moreover, 4 hydrogen bonds were obtained in the case of compound **7** and phomonitroester, while 3 potential hydrogen bonds were formed between compound 325-5 and amino acids ARG202 and ARG205 on the 1SHV receptor.

TABLE III. Crystal and experimental data for molecular complexes with the 1SHV receptor

Tested ligand	Free binding energy, kcal mol^{-1}	Inhibition constant, μM	RMSD	Hydrogen bonds with receptor amino acids
Ampicillin	−1.90	40320	5.08	ARG205
325-3	0.33	N.A.	7.26	ARG205
325-5	−1.79	48870	5.65	ARG202, ARG205
CurvularideA	−0.41	497240	5.07	ARG202
CurvularideB	−0.92	210410	7.41	ARG202ARG205
CurvularideC	0.75	N.A.	4.74	None
CurvularideD	−1.57	70350	6.97	ARG202, ARG205
CurvularideE	−1.27	116590	5.05	ARG202, ARG205
Phomoenamide	−1.78	49500	6.51	GLU92
Compound **6**	−2.48	15230	7.48	ARG202, ARG205
Compound **7**	−2.85	8100	5.97	ARG202, ARG205
Phomol	−0.55	395820	5.28	ARG202, ARG205
Phomonitroester	−2.67	11060	7.46	ARG202, ARG205

Overall, a lower binding potential was observed in case of docking of all the tested ligands with 1SHV receptor in comparison to both the 1F0K and 3G7B receptors. Moreover, the highest affinity for the 1SHV receptor was observed for compound **7** followed by phomonitroester, the ampicillin control and compound 325-5. For all ligands, the binding pocket within the receptor seemed to be the same, since all hydrogen bonds were formed with amino acids on position ARG202 and ARG205 (Fig. 4).

In docking simulations with receptor 3VSL, all compounds showed a weak potential for interaction (Table S-V). None of the compounds had the potential to form hydrogen bonds, also the values of the free binding energy were high, implying a weak potential for any interaction, and hence the inhibition constant could not be calculated. A similar lack of interaction potential for all tested compounds with 4EMV, 1JIJ, 1KZN and 3K3P receptor was also evident (Tables S-VI–IX of the supplementary material). According to the obtained data, it seemed that none of the investigated compounds interacted with these receptors.

CONCLUSIONS

As an extension of practical *in vitro* experiments for antimicrobial evaluation, separation and characterization of the biomolecules of endophytic fungi, *in silico* molecular docking was proposed with the aim to introduce additional effort and to reliably recognize which active structures could serve as leading molecules for further *in silico* antibiotic drug discovery. Within this study, light was shed on
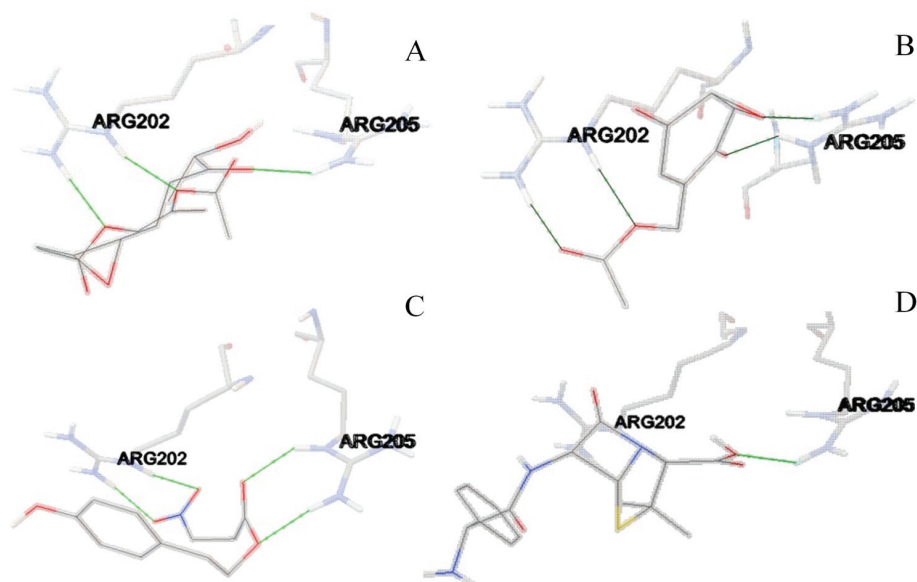
Fig. 4. Docking pose of ligands 325-5 (A), compound **7** (B), phomonitroester (C) and ampicillin (D) with the 1SHV receptor binding pocket. Only the portion of the receptor with interacting amino acid residues is displayed. The main hydrogenic bonds between the ligand amino acid residues in receptor pocket are emphasized in green.

the interactions between a series of twelve compounds and their potential targeted receptors. According to the overall criteria for docking evaluations, which included the value of the free binding energy, constant of inhibition, *RMSD* value and potential for establishment of hydrogen bonds with the receptor, it was concluded that the highest potential for docking interaction was observed in case of 3G7B, 1F0K and 1SHV receptors located in pathogens *Staphylococcus aureus*, *Escherichia Coli* and *Klebsiella pneumonia*. The results from this docking study suggest that structural similarities as well as some specific properties of compounds 325-3, 325-5, phomoenamide and phomol may hopefully be used as directions for the further development of their derivatives as novel antibiotics with potent, broad-spectrum activity. In addition, these findings may also indicate how to perform further optimization of biomolecule production by endophytic fungi and/or more effective processing of gathered biomaterial. Moreover, the investigated compounds might also interact with other targets involving different mechanisms of action.

SUPPLEMENTARY MATERIAL

Tables S-I–S-IX, containing coordinates of central grid point of maps for all tested ligands and overall docking results of twelve antimicrobial structures and control ligand against eight receptors, are available electronically at the pages of journal website: https://www.shd-pub.org.rs/index.php/JSCS/index, or from the corresponding author on request.

И З В О Д

СТУДИЈА МОЛЕКУЛСКОГ ДОКИНГА СА БИОМОЛЕКУЛИМА ИЗОЛОВАНИМ ИЗ ЕНДОФИТНИХ ГЉИВА

ЈАНКО ИГЊАТОВИЋ[1], НЕВЕНА ЂАЈИЋ[1], ЈОВАНА КРМАР[1], АНА ПРОТИЋ[1], БОРУТ ШТРУКЕЉ[2] и БИЉАНА ОТАШЕВИЋ[1]

[1]*Кашедра за аналишику лекова, Универзишеш у Беоīраду – Фармацеушски факулшеш, Војводе Сшеūе 450, 11221 Беоīрад и* [2]*Faculty of Pharmacy, University of Ljubljana, Aškerčeva cesta 7, 1000 Ljubljana, Slovenia*

У последње време, као одговор на повећање резистенције микроорганизама на познату терапију, све већа пажња се поклања истраживању једињења са антимикробном активношћу. Ендофитне гљиве су недавно представљене као поуздан и богат извор за развој нових лекова. До сада, истраживања су се углавном ограничавала на *in vitro* процену антимикробне активности и разоткривање хемијске структуре биомолекула изолованих из материјала гљива. Из тог разлога, ово истраживање је осмишљено као проширење претходно спроведених испитивања ендофита које расту на иглицама четинара путем *in silico* студије молекулског докинга. Главни циљ употребе *in silico* метода је био да се направи прилог разумевању механизама који стоје иза интеракције биомолекула изолованих из гљиве *Phomopsis species* са осам различитих типова рецептора који припадају патогеним бактеријама уобичајено мултирезистентних на лекове. Резултати су указали на важне интеракције са рецепторима 3G7B (*Staphylococcus aureus* гираза Б), 1F0K (структура *Escherichia Coli* трансферазе величине 1,9 Å) и 1SHV (SHV-1 *β*-лактамаза *Klebsiella pneumoniae*) указујући на тај начин на рецепторе путем којих се започиње антибиотски одговор након активације најпотентнијим једињењима, 325-3, 325-5, фомоенамидом и фомолом. Овим открићем се такође препоручује будући развој нових моћних антибиотика са широким спектром деловања базиран на структури изабраних молекула.

(Примљено 15. августа 2020, ревидирано 10. јануара, прихваћено 23. јануара 2021)

REFERENCES

1. V. L. Simpkin, M. J. Renwick, R. Kelly, E. Mossialos, *J. Antibiot.* **70** (2017) 1087 (https://doi.org/10.1038/ja.2017.124)
2. E. D. Brown, G. D. Wright, *Nature* **529** (2016) 336 (https://doi.org/10.1038/nature17042)
3. D. J. Newman, G. M. Cragg, K. M. Snader, *Nat. Prod. Rep.* **17** (2000) 215 (https://doi.org/10.1039/a902202c)
4. P. Saha, A. D. Talukdar, M. D. Choudhury, D. Nath, in *Advances in Endophytic Fungal Research*, B. Singh, Ed., Springer, Cham, 2019, p. 35 (https://doi.org/10.1007/978-3-030-03589-1_3)
5. A. Stierle, G. Strobel, D. Stierle, *Science* **260** (1993) 214 (https://doi.org/10.1126/science.8097061)
6. P. P. Pal, A. B. Shaik, A. S. Begum, *Planta Med.* (2020) 1 (https://doi.org/10.1055/a-1140-8388)
7. D. Udayanga, X. Liu, E. H. McKenzie, E. Chukeatirote, A. H. Bahkali, K. D. Hyde, *Fungal Divers.* **50** (2011) 189 (https://doi.org/10.1007/s13225-011-0126-9)

8.   A. E. Arnold, L. C. Mejía, D. Kyllo, E. I. Rojas, Z. Maynard, N. Robbins, E. A. Herre, *Proc. Nat. Acad. Sci.* **100** (2003) 15649 (https://doi.org/10.1073/pnas.2533483100)
9.   G. A. Strobel, *Microbes Infect.* **5** (2003) 535 (https://doi.org/10.1016/s1286-4579(03)00073-x)
10. R. P. Ryan, K. Germaine, A. Franks, D. J. Ryan, D. N. Dowling, *FEMS Microbiol. Lett.* **278** (2008) 1 (https://doi.org/10.1111/j.1574-6968.2007.00918.x)
11. R. X. Tan, W. X. Zou, *Nat. Prod. Rep.* **18** (2001) 448 (https://doi.org/10.1039/b100918o)
12. M. Jia, L. Chen, H. L. Xin, C. J. Zheng, K. Rahman, T. Han, L. P. Qin, *Front. Microbiol.* **7** (2016) 1 (https://doi.org/10.3389/fmicb.2016.00906)
13. J. Ignjatović, N. Maljurić, J. Golubović, M. Ravnikar, M. Petković, N. Savodnik, B. Štrukelj, B. Otašević, *Acta Chim. Slov.* **68** (2020) 445 (http://dx.doi.org/10.17344/acsi.2019.5389)
14. K. J. Simmons, I. Chopra, C. W. Fishwick, *Nat. Rev. Microbiol.* **8** (2010) 501 (https://doi.org/10.1038/nrmicro2349)
15. E. K. Jagusztyn-Krynicka, A. Wyszynska, *Pol. J. Microbiol.* **57** (2008) 91 (http://www.pjm.microbiology.pl/archive/vol5722008091.pdf)
16. J. D. Durrant, R. E. Amaro, *Chem. Biol. Drug Des.* **85** (2015) 14 (https://doi.org/10.1111/cbdd.12423)
17. N. Okimoto, N. Futatsugi, H. Fuji, A. Suenaga, G. Morimoto, R. Yanai, Y. Ohno, T. Narumi, M. Taiji, *PLoS Comput. Biol.* **5** (2009) 1 (https://doi.org/10.1371/journal.pcbi.1000528)
18. X. Liu, D. Shi, S. Zhou, Liu, H., H. Liu, X. Yao, *Expert Opin. Drug Discovery* **13** (2018) 23 (https://doi.org/10.1080/17460441.2018.1403419)
19. T. B. Emran, M. A. Rahman, M. M. N. Uddin, R. Dash, M. F. Hossen, M. Mohiuddin, M. R. Alam, *DARU J. Pharm. Sci.* **23** (2015) 1 (https://doi.org/10.1186/s40199-015-0106-9)
20. K. Gullapelli, G. Brahmeshwari, M. Ravichander, U. Kusuma, Egypt. *J. Basic Appl. Sci.* **4** (2017) 303 (https://doi.org/10.1016/j.ejbas.2017.09.002)
21. G. Ashtalakshmi, P. Prabakaran, *Eur. J. Pharm. Med. Res.* **3** (2016) 458 (https://storage.googleapis.com/journal-uploads/ejpmr/article_issue/1456728800.pdf)
22. W. Wang, R. Chen, Z. Luo, W. Wang, J. Chen, *Nat. Prod. Res.* **32** (2018) 558 (https://doi.org/10.1080/14786419.2017.1329732)
23. V. Rukachaisirikul, U. Sommart, S. Phongpaichit, J. Sakayaroj, K. Kirtikara, *Phytochem.* **69** (2008) 783 (https://doi.org/10.1016/j.phytochem.2007.09.006)
24. H. Yu, L. Zhang, L. Li, C. Zheng, L. Guo, W. Li, P. Sun, L. Qin, *Microbiol. Res.* **165** (2010) 437 (https://doi.org/10.1016/j.micres.2009.11.009)
25. P. Chomcheon, S. Wiyakrutta, T. Aree, N. Sriubolmas, N. Ngamrojanavanich, C. Mahidol, S. Ruchirwat, P. Kittakoop, *Chem. Eur. J.* **16** (2010): 11178 (https://doi.org/10.1002/chem.201000652)
26. H. Hussain, M. K. Tchimene, I. Ahmed, K. Meier, M. Steinert, S. Draeger, B. Schulz, K. Krohn, *Nat. Prod. Commun.* **6** (2011) 1905 (https://doi.org/10.1177%2F1934578X1100601228)
27. D. Weber, O. Sterner, T. Anke, S. Gorzalczancy, V. Martino, C. Acevedo, *J. Antibiot.* **57** (2004) 559 (https://doi.org/10.7164/antibiotics.57.559)
28. M. Corrado, K. F. Rodrigues, *J. Basic Microbiol.* **44** (2004) 157 (https://doi.org/10.1002/jobm.200310341)
29. M. Isaka, A. Jaturapat, K. Rukseree, K. Danwisetkanjana, M. Tanticharoen, Y. Thebtaranonth, *J. Nat. Prod.* **64** (2001) 1015 (https://doi.org/10.1021/np010006h)

30. G. Jayanthi, S. Kamalraj, K. Karthikeyan, J. Muthumary, *Int. J. Curr. Sci.* **1** (2011) 85 (https://scinapse.io/papers/2188762895)
31. D. Rakshith, P. Santosh, S. Satish, *Int. J. Chem. Anal. Sci.* **4** (2013) 156 (https://doi.org/10.1016/j.ijcas.2013.08.006)
32. M. A. Abdalla, J. C. Matasyoh, *Nat. Prod. Bioprospect.* **4** (2014) 257 (https://dx.doi.org/10.1007%2Fs13659-014-0038-y)
33. R. Huey, G. M. Morris, A. J. Olson, D. S. Goodsell, *J. Comput. Chem.* **28** (2007) 1145 (https://doi.org/10.1002/jcc.20634)
34. G. M. Morris, R. Huey, W. Lindstorm, M. Sanner, M. F. Belew, D. S. Goodsell, A. J. Olson, *J. Comput. Chem.* **16** (2009) 2785 (https://dx.doi.org/10.1002%2Fjcc.21256)
35. M. R. Simić, A. Damjanović, M. Kalinić, G. Tasić, S. Erić, J. Antić-Stanković, V. Savić, *J. Serb. Chem. Soc.* **81** (2016) 103 (https://doi.org/10.2298/JSC150525090S)
36. G. M. Morris, R. Huey, W. Lindstrom, M. F. Sanner, R. K. Belew, D. S. Goodsell, A. J. Olson, *J. Comput. Chem.* **30** (2009) 2785 (https://dx.doi.org/10.1002%2Fjcc.21256)
37. J. Fuhrmann, A. Rurainski, H. P. Lenhof, D. Neumann, *J. Comput. Chem.* **31** (2010) 1911 (https://doi.org/10.1002/jcc.21478)
38. M. K. Paul, A. K. Mukhopadhyay, *Int. J. Med. Sci.* **1** (2004) 101 (https://dx.doi.org/10.7150%2Fijms.1.101)
39. K. Cheng, Q. Z. Zheng, Y. Qian, L. Shi, J. Zhao, H. L. Zhu, *Bioorg. Med. Chem.* **17** (2009) 7861 (https://doi.org/10.1016/j.bmc.2009.10.037)
40. M. J. Alves, H. J. Froufe, A. F. Costa, A. F. Santos, L. G. Oliveira, S. R. Osório, R. M. V. Abreu, M. Pintado, I. C. Ferreira, *Molecules* **19** (2014) 1672 (https://doi.org/10.3390/molecules19021672).
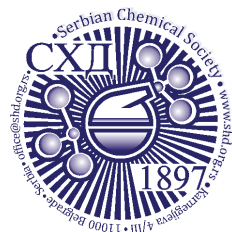
Molecular docking study on biomolecules isolated from endophytic fungi

JANKO IGNJATOVIĆ[1], NEVENA ĐAJIĆ[1], JOVANA KRMAR[1], ANA PROTIĆ[1],
BORUT ŠTRUKELJ[2] and BILJANA OTAŠEVIĆ[1]*

[1]Department of Drug Analysis, University of Belgrade – Faculty of Pharmacy, Vojvode Stepe 450, 11221 Belgrade, Serbia and [2]Faculty of Pharmacy, University of Ljubljana, Aškerčeva cesta 7, 1000 Ljubljana, Slovenia

TABLE S-I. Crystal and experimental data for molecular complexes with 1F0K receptor

Tested ligand	Free binding energy, kcal/mol	Ligand efficiency, kcal/mol	Inhibition constant, µM	Intermolar energy, kcal/mol	VdW HB desol- vatation energy, kcal/mol	Electrostatic energy, kcal/mol	Total internal, kcal/mol	Torsional energy, kcal/mol	Unbound energy, kcal/mol	*RMSD*	Mean binding energy, kcal/mol	Hydrogen bonds
Ampicillin*	–6.47	–0.27	18.08	–8.26	–6.50	–1.76	–2.95	1.79	–2.95	5.08	–6.09	Ampicilin:0:1:H Ampicilin:0:1:H
325-3	–5.14	–0.23	172.04	–8.42	–7.94	–0.48	–2.30	3.28	–2.30	3.72	–3.85	325-3:0:1:H; 325-3:0:1:H; 1f0k:A:GLN289:HE22

* Corresponding author. E-mail: biljana.otasevic@pharmacy.bg.ac.rs

325-5	−4.78	−0.22	313.49	−7.76	−7.35	−0.41	−1.14	2.98	−1.14	3.72	−3.99	325-5:0:1:H; 1f0k:A:THR266:HN 1f0k:A:THR266:HG1; 1f0k:A:GLN289:HE22
Curvul-arideA	−4.76	−0.20	324.52	−9.23	−9.02	−0.21	−2.48	4.47	−2.48	6.17	−4.37	1f0k:A:LEU265:HN: Civularide-A:0:1:O Cuvularide-A:0:1H: 1f0k:A:SER192:OG 1f0k:A:GLN193:HN: Cuvularide-A:0:1:O 1f0k:A:GLN289:HE22 Cuvularide-A:0:1:O
Curvul-arideB	−4.10	−0.18	994.76	−7.68	−7.54	−0.14	−1.85	3.58	−1.85	6.79	−2.85	1f0k:A:GLN289:HE22
Curvul-arideC	−4.70	−0.20	361.64	−8.87	−8.52	−0.35	−2.97	4.18	−2.97	4.74	−3.55	Cuvularide-C:0 1:H; Cuvularide-C:0 1:H
Curvul-arideD	−4.74	−0.21	334.92	−8.02	−8.08	0.06	−0.81	3.28	−0.81	6.42	−3.81	1f0K:A:LEU265:HN
Curvul-arideE	−4.73	−0.21	343.80	−7.71	−7.52	−0.19	−1.79	2.98	−1.79	4.90	−3.91	Cuvularide-E: 0: 1:H; Cuvularide-E: 0: 1:H
Phomo-enamide	−4.97	−0.25	227.74	−7.65	−7.38	−0.27	−2.25	2.68	−2.25	4.46	−3.66	Phomoenamide:0: 1:H; 1f0k:A:THR266:HN 1f0k:A:THR266:HG1
Compound 6	−3.88	−0.35	1430	−4.48	−4.37	−0.11	−0.27	0.60	−0.27	7.35	−3.73	1f0h:A:LEU265:HN: Compound_6:0: 1:O 1f0k:A:THR266:HN: Compound_6:0: 1:O
Compound 7	−4.56	−0.33	454.39	−5.45	−4.97	−0.48	−0.18	0.89	−0.18	5.83	−4.32	1f0k:A:ARG164:HH11: Compound_7:0: 1:O 1f0k:A:THR266:HN: Compound_7:0: 1:O

Phomol	–5.75	–0.20	60.52	–9.33	–9.14	–0.19	–4.48	3.58	–4.48	3.26	–4.95	Phomol:0: 1:H: 1f0k:A:GLY190:O Phomol:0: 1:H: 1f0k:A:GLY190:O 1f0k:A:GLN193:HN: Phomol:0: 1:O
Phomonitro-ester	–4.81	–0.28	296.63	–7.20	–5.96	–1.24	–0.33	2.39	–0.33	5.89	–4.37	Phomonitroester:0: 1:H: 1f0k:A:GLU269:OE2 1f0k:A:GLN289:HE22: Phomonitroester:0: 1:O,O

*Control ligand

TABLE S-II. Crystal and experimental data for molecular complexes with 3G7B receptor

Tested ligand	Free binding energy, kcal/mol	Ligand efficiency, kcal/mol	Inhibition constant, μM	Intermolar energy, kcal/mol	VdW HB desol-vation energy, kcal/mol	Electrostatic energy, kcal/mol	Total internal, kcal/mol	Torsional energy, kcal/mol	Unbound energy, kcal/mol	RMSD	Mean binding Energy, kcal/mol	Hydrogen bonds
Ampicillin*	–6.10	–0.25	33.93	–7.89	–5.25	–2.63	–1.71	1.79	1.71	5.77	–5.63	Ampicilin:0: 1:H: 3G7B:B:ASP53:OD1 Ampicilin:0: 1:H: 3G7B:B:GLU50:OE1 Ampicilin:0: 1:H: 3G7B:B:GLU50:OE1
325-3	–5.27	–0.24	135.56	–8.55	–7.83	–0.72	–2.26	3.28	–2.26	5.04	–4.50	325-3:0: 1:H: 3G7B:N:ASP57:OD2 325-3:0: 1:H: 3G7B:N:ASP57:OD2 3G7B:B:ASN54:HD21: 325-3:0 1:O 3G7B:B:VAL131:HN:

												325-3:0 1:O
325-5	−4.60	−0.21	425.42	−7.58	−7.42	−0.16	−1.58	2.98	−1.58	3.92	−3.74	325-5:0 :1:H: 3G7B:B:ASP57:OD2 3G7B:B:VAL131:HN: 325-5:0 1:O 3G7B:B:ASN54:HD21: 325-5:0: 1:O
CurvularideA	−2.58	−0.11	12930	−7.05	−6.30	−0.75	−3.36	4.47	−3.36	4.21	−0.86	Cuvularide-A:0: 1:H: 3G7B:B:ASP53:OD1 Cuvularide-A:0: 1:H: 3G7B:B:ASP53:OD1 Cuvularide-A:0: 1:H: 3G7B:B:GLU50:OE2 Cuvularide-A:0: 1:H: 3G7B:B:ASN54:OD1
CurvularideB	−4.36	−0.19	632.03	−7.94	−7.31	−0.64	−1.85	3.58	−1.85	3.98	−3.34	Cuvularide-B:0 1:H: 3G7B:B:GLU50:OE1 Cuvularide-B:0 1:H: 3G7B:B:GLU50:OE1 3g7B:B:HIS46:HE2: Cuvularide-B:0 1:O
CurvularideC	−3.21	−0.13	4440	−7.39	−6.72	−0.67	−0.62	4.18	−0.62	4.50	−1.79	Cuivularide-C:0: 1:H: 3G7B:B:ASP57:OD2 Cuivularide-C:0: 1:H: 3G7B:B:ASP57:OD1 Cuivularide-C:0: 1:H: 3G7B:B:ASP57:OD2
CurvularideD	−4.51	−0.20	495.24	−7.79	−7.63	−0.16	−1.24	3.28	−1.24	4.19	−3.34	Cuvularide-D:0: 1:H: 3G7B:ASP53:O 3G7B:B:ASN54:HD21: Cuvularide-D:0: 1:O 3G7B:B:VAL131:HN:

CurvularideE	−4.47	−0.19	532.45	−7.45	−7.36	−0.09	−1.01	2.98	−1.01	4.15	−3.54	Cuvularide-D:0: 1:O Cuvularide-E:0: 1:H: 3G7B:B:ASP52:OD1 3G7B:B:ASN54:HD21: Cuvularide-E:0: 1:O
Phomoenamide	−4.64	−0.23	397.98	−7.32	−6.76	−0.56	−2.44	2.68	−2.44	3.27	−3.40	3G7B:B:ASN54:HD21: Phomoenamide:0: 1:O Phomoenamide:0: 1:H: 3G7B:B:GLU50:OE2 Phomoenamide:0: 1:H: 3G7B:B:GLU50:OE1 Phomoenamide:0: 1:H: 3G7B:B:GLU50:OE1
Compound **6**	−3.75	−0.34	1790	−4.35	−4.08	−0.27	0.05	0.6	0.05	6.72	−3.37	3g7b:B:VAL131:HN: Compound_6:0 1:O 3g7b:B:ASN54:HD21: Compound_6:0 1:O Compound_6:0 1:H: 3g7b:B:GLU50:OE2
Compound **7**	−4.20	−0.30	838.08	−5.09	−4.83	−0.26	0.15	0.89	0.15	4.80	−3.79	3g7b:B:ASN54:HD21: Compound:7:0 1:O 3g7b:B:VAL131:HN: Compound_7:0: 1:O
Phomol	−3.74	−0.13	1800	−7.32	−7.14	−0.19	−3.51	3.58	−3.51	4.89	−2.43	Phomol:0 1:H: 3g7b:B:ASP53:OD2 3g7b:B:ASN206:HD22: Phomol:0 1:O

| Phomonitroester | –3.88 | –0.23 | 1440 | –6.26 | –6.25 | –0.01 | –0.41 | 2.39 | –0.41 | 6.80 | –3.05 | 3g7b:B:VAL130:HN: Phomonitroester:0: 1:O Phomonitroester:0: 1:H: 3g7b:B:GLU50:OE1 3g7b:B:HIS46:HE2: Phomonitroester:0: 1:O 3g7b:B:VAL131:HN: Phomonitroester:0: 1:O,O |

*Control ligand

TABLE S-III. Crystal and experimental data for molecular complexes with 1SHV receptor

Tested ligand	Free binding energy, kcal/mol	Ligand efficiency, kcal/mol	Inhibition constant, μM	Intermolar energy, kcal/mol	VdW HB desol- vation energy, kcal/mol	Electrostatic energy, kcal/mol	Total internal, kcal/mol	Torsional energy, kcal/mol	Unbound energy, kcal/mol	RMSD	Mean binding Energy, kcal/mol	Hydrogen bonds
Ampicillin*	–1.90	0.08	40320	–3.69	–2.40	–1.29	–3.09	1.79	–3.09	5.08	–1.82	1shv:A:ARG205:HH21
325-3	0.33	0.02	N.A.	–2.95	–2.86	–0.09	–4.75	3.28	–4.75	7.26	1.09	1shv:A:ARG205:HH21
325-5	–1.79	–0.08	48870	–4.77	–4.40	–0.37	–2.19	2.98	–2.19	5.65	–1.30	1shv:A:ARG202:HE; 1shv:A:ARG202:HH21 1shv:A:ARG205:HH21
CurvularideA	–0.41	–0.02	497240	–4.89	–4.68	–0.21	–5.60	4.47	–5.60	5.07	0.91	1shv:A:ARG202:HE
CurvularideB	–0.92	–0.04	210410	–4.50	–4.21	–0.29	–1.96	3.58	–1.96	7.41	–0.17	1shv:A:ARG202:HE; 1shv:A:ARG205:HE 1shv:A:ARG205:HH21
CurvularideC	0.75	0.03	N.A.	–3.43	–3.29	–0.14	–5.10	4.18	–5.10	4.74	1.45	None
CurvularideD	–1.57	–0.07	70350	–4.85	–4.47	–0.38	–2.01	3.28	–2.01	6.97	–0.79	1shv:A_ARG202:HE; 1shv:A_ARG205:HH21
CurvularideE	–1.27	–0.06	116590	–4.26	–3.90	–0.36	–2.87	2.98	–2.87	5.05	–0.53	1shv:A:ARG202:HE; 1shve:A:ARG205:HE 1shv:A:ARG205:HH21

Phomoenamide	−1.78	−0.09	49500	−4.47	−4.13	−0.33	−4.23	2.68	−4.23	6.51	−0.91	Phomoenamide:0: 1:H
Compound **6**	−2.48	−0.23	15230	−3.08	−2.75	−0.33	−0.41	0.60	−0.41	7.48	−2.32	1shv:A:ARG202:HE: Compound_6:0: 1:O 1shv:A:ARG205:HE: Compound_6:0: 1:O
Compound **7**	−2.85	−0.20	8100	−3.75	−3.43	−0.32	−0.21	0.89	−0.21	5.97	−2.67	1shv:A:ARG202:HH21: Compound_7:0: 1:O 1shv:A:ARG205:HE: Compound_7:0: 1:O 1shv:A:ARG205:HH21: Compound_7:0: 1:O 1shv:A:ARG202:HE: Compound_7:0: 1:O
Phomol	−0.55	0.02	395820	−4.13	−3.89	−4.13	−4.47	3.58	−4.47	5.28	−0.17	1shv:A:ARG202:HH21: Phomol:0: 1:O 1shv:A:ARG205:HH21: Phomol:0: 1:O
Phomonitroester	−2.67	−0.16	11060	−5.06	−3.70	−1.35	−0.57	2.39	−0.57	7.46	−2.13	1shv:A:ARG202:HH21: Phomonitroester:0: 1:O 1shv:A:ARG205:HH21: Phomonitroester:0: 1:O 1shv:A:ARG205:HE: Phomonitroester:0: 1:O 1shv:A:ARG202:HE: Phomonitroester:0: 1:O,O

* Control ligand

TABLE S-IV. Crystal and experimental data for molecular complexes with 3VSL receptor

Tested ligand	Free binding energy, kcal/mol	Ligand efficiency, kcal/mol	Inhibition constant, μM	Intermolar energy, kcal/mol	VdW HB desolvatation energy, kcal/mol	Electrostatic energy, kcal/mol	Total internal, kcal/mol	Torsional energy, kcal/mol	Unbound energy, kcal/mol	RMSD	Mean binding Energy, kcal/mol	Hydrogen bonds
Ampicillin*	1.72	0.07	N.A.	–0.06	0.00	–0.06	–3.19	1.79	–3.19	5.36	1.73	None
325-3	3.27	0.15	N.A.	–0.01	0.00	–0.01	–6.12	3.28	–6.12	4.94	3.27	None
325-5	2.98	0.14	N.A.	–0.01	0.00	–0.01	–3.85	2.98	–3.85	5.16	2.98	None
CurvularideA	4.47	0.19	N.A.	–0.01	0.00	–0.01	–6.97	4.47	–6.97	3.74	4.47	None
CurvularideB	3.57	0.16	N.A.	–0.01	0.00	–0.01	–2.94	3.58	–2.94	6.16	3.57	None
CurvularideC	4.17	0.17	N.A.	–0.01	0.00	–0.01	–5.73	4.18	–5.73	4.50	4.17	None
CurvularideD	3.27	0.14	N.A.	–0.01	0.00	–0.01	–2.47	3.28	–2.47	4.85	3.28	None
CurvularideE	2.98	0.13	N.A.	–0.01	0.00	–0.01	–3.32	2.98	–3.32	4.60	2.98	None
Phomoenamide	2.68	0.13	N.A.	–0.01	0.00	–0.01	–5.61	2.68	–5.61	6.41	2.68	None
Compound **6**	0.59	0.05	N.A.	0.00	0.00	0.00	–0.57	0.60	–0.57	7.59	0.59	None
Compound **7**	0.89	0.06	N.A.	–0.01	0.00	–0.01	–0.46	0.89	–0.46	6.34	0.89	None
Phomol	3.57	0.12	N.A.	–0.01	0.00	–0.01	–5.51	3.58	–5.51	4.84	3.57	None
Phomonitroester	2.05	0.12	N.A.	–0.34	0.00	–0.34	–2.37	2.39	–2.37	8.34	2.06	None

*Control ligand

TABLE S-V. Crystal and experimental data for molecular complexes with 4EMV receptor

Tested ligand	Free binding energy, kcal/mol	Ligand efficiency, kcal/mol	Inhibition constant, μM	Intermolar energy, kcal/mol	VdW HB desolvatation energy, kcal/mol	Electrostatic energy, kcal/mol	Total internal, kcal/mol	Torsional energy, kcal/mol	Unbound energy, kcal/mol	RMSD	Mean binding Energy, kcal/mol	Hydrogen bonds
Ampicillin*	1.75	0.07	N.A.	–0.04	0.00	–0.04	–3.19	1.79	–3.19	5.34	1.76	None
325-3	3.28	0.15	N.A.	0.00	0.00	0.00	–5.89	3.28	–5.89	5.31	3.28	None
325-5	2.98	0.14	N.A.	0.00	0.00	0.00	–3.80	2.98	–3.80	6.54	2.98	None
CurvularideA	4.47	0.19	N.A.	0.00	0.00	0.00	–6.94	4.47	–6.94	4.37	4.47	None
CurvularideB	3.58	0.16	N.A.	0.00	0.00	0.00	–2.93	3.58	–2.93	6.32	3.58	None
CurvularideC	4.17	0.17	N.A.	0.00	0.00	0.00	–5.70	4.18	–5.70	3.93	4.17	None
CurvularideD	3.28	0.14	N.A.	0.00	0.00	0.00	–2.48	3.28	–2.48	5.63	3.28	None
CurvularideE	2.98	0.13	N.A.	0.00	0.00	0.00	–3.31	2.98	–3.31	5.38	2.98	None
Phomoenamide	2.68	0.13	N.A.	0.00	0.00	0.00	–5.60	2.68	–5.60	3.50	2.68	None
Compound **6**	0.59	0.05	N.A.	0.00	0.00	0.00	–0.57	0.60	–0.57	8.42	0.59	None
Compound **7**	0.89	0.06	N.A.	0.00	0.00	0.00	–0.46	0.89	–0.46	6.24	0.89	None
Phomol	3.58	0.12	N.A.	0.00	0.00	0.00	–5.49	0.00	–5.49	4.50	3.58	None
Phomonitroester	2.43	0.14	N.A.	0.04	0.00	0.04	–2.39	2.39	–2.39	8.77	2.43	None

* Control ligand

TABLE S-VI. Crystal and experimental data for molecular complexes with 1JIJ receptor

Tested ligand	Free binding energy, kcal/mol	Ligand efficiency, kcal/mol	Inhibition constant, μM	Intermolar energy, kcal/mol	VdW HB desolvatation energy, kcal/mol	Electrostatic energy, kcal/mol	Total internal, kcal/mol	Torsional energy, kcal/mol	Unbound energy, kcal/mol	RMSD	Mean binding Energy, kcal/mol	Hydrogen bonds
Ampicillin*	1.78	0.07	N.A.	–0.01	0.00	–0.01	–3.20	1.79	–3.20	4.28	1.78	None
325-3	3.28	0.15	N.A.	0.00	0.00	0.00	–6.15	3.28	–6.15	3.10	3.28	None
325-5	2.98	0.14	N.A.	0.00	0.00	0.00	–3.73	2.98	–3.73	2.92	2.98	None
CurvularideA	4.47	0.19	N.A.	0.00	0.00	0.00	–6.88	4.47	–6.88	3.88	4.47	None
CurvularideB	3.58	0.16	N.A.	0.00	0.00	0.00	–2.94	3.58	–2.94	3.94	3.58	None
CurvularideC	4.18	0.17	N.A.	0.00	0.00	0.00	–5.74	4.18	–5.74	2.67	4.18	None
CurvularideD	3.28	0.14	N.A.	0.00	0.00	0.00	–2.47	3.28	–2.47	6.52	3.28	None
CurvularideE	2.98	0.13	N.A.	0.00	0.00	0.00	–3.31	2.98	–3.31	3.84	2.98	None
Phomoenamide	2.68	0.13	N.A.	0.00	0.00	0.00	–5.61	2.68	–5.61	3.68	2.68	None
Compound **6**	0.60	0.05	N.A.	0.00	0.00	0.00	–0.57	0.60	–0.57	6.10	0.60	None
Compound **7**	0.89	0.06	N.A.	0.00	0.00	0.00	–0.46	0.89	–0.46	2.45	0.89	None
Phomol	3.58	0.12	N.A.	0.00	0.00	0.00	–5.51	3.58	–5.51	2.61	3.58	None
Phomonitroester	2.46	0.14	N.A.	0.08	0.00	0.08	–2.38	2.39	–2.38	8.62	2.47	None

*Control ligand

TABLE S-VII. Crystal and experimental data for molecular complexes with 1KZN receptor

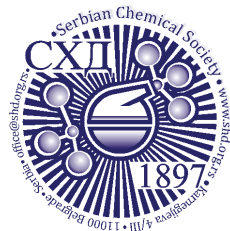| Tested ligand	Free binding energy, kcal/mol	Ligand efficiency, kcal/mol	Inhibition constant, μM	Intermolar energy, kcal/mol	VdW HB desolvatation energy, kcal/mol	Electrostatic energy, kcal/mol	Total internal, kcal/mol	Torsional energy, kcal/mol	Unbound energy, kcal/mol	RMSD	Mean binding Energy, kcal/mol	Hydrogen bonds
Ampicillin*	1.78	0.07	N.A.	–0.01	0.00	–0.01	–3.20	1.79	–3.20	7.86	1.78	None
325-3	3.28	0.15	N.A.	0.00	0.00	0.00	–6.16	3.28	–6.16	4.60	3.28	None
325-5	2.98	0.14	N.A.	0.00	0.00	0.00	–3.65	2.98	–3.65	5.58	2.98	None
CurvularideA	4.47	0.19	N.A.	0.00	0.00	0.00	–6.83	4.47	–6.83	6.28	4.47	None
CurvularideB	3.58	0.16	N.A.	0.00	0.00	0.00	–2.94	3.58	–2.94	3.13	3.58	None
CurvularideC	4.18	0.17	N.A.	0.00	0.00	0.00	–5.76	4.18	–5.76	2.45	4.18	None
CurvularideD	3.28	0.14	N.A.	0.00	0.00	0.00	–2.48	3.28	–2.48	5.24	3.28	None
CurvularideE	2.99	0.13	N.A.	0.00	0.00	0.00	–3.32	2.98	–3.32	4.29	2.98	None
Phomoenamide	2.68	0.13	N.A.	0.00	0.00	0.00	–5.61	2.68	–5.61	6.11	2.68	None
Compound **6**	0.60	0.05	N.A.	0.00	0.00	0.00	–0.57	0.60	–0.57	7.32	0.60	None
Compound **7**	0.89	0.06	N.A.	0.00	0.00	0.00	–0.46	0.89	–0.46	7.31	0.89	None
Phomol	3.58	0.12	N.A.	0.00	0.00	0.00	–5.49	3.58	–5.49	2.86	3.58	None
Phomonitroester	2.43	0.14	N.A.	0.05	0.00	0.05	–2.38	2.39	–2.38	8.21	2.43	None

*Control ligand

TABLE S-VIII. Crystal and experimental data for molecular complexes with 3K3P receptor

Tested ligand	Free binding energy, kcal/mol	Ligand efficiency, kcal/mol	Inhibition constant, μM	Intermolar energy, kcal/mol	VdW HB desolvatation energy, kcal/mol	Electrostatic energy, kcal/mol	Total internal, kcal/mol	Torsional energy, kcal/mol	Unbound energy, kcal/mol	RMSD	Mean binding Energy, kcal/mol	Hydrogen bonds
Ampicillin*	1.75	0.07	N.A.	–0.04	0.00	–0.04	–3.20	1.79	–3.20	5.97	1.76	None
325-3	3.28	0.15	N.A.	0.00	0.00	0.00	–6.11	3.28	–6.11	4.12	3.28	None
325-5	2.98	0.14	N.A.	–0.01	0.00	–0.01	–3.70	2.98	–3.70	3.80	2.98	None
CurvularideA	4.47	0.19	N.A.	0.00	0.00	0.00	–6.87	4.47	–6.87	5.19	4.47	None
CurvularideB	3.58	0.16	N.A.	0.00	0.00	0.00	–2.93	3.58	–2.93	5.82	3.58	None
CurvularideC	4.17	0.17	N.A.	0.00	0.00	0.00	–5.67	4.18	–5.67	2.98	4.17	None
CurvularideD	3.28	0.14	N.A.	0.00	0.00	0.00	–2.47	3.28	–2.47	5.11	3.28	None
CurvularideE	2.98	0.13	N.A.	0.00	0.00	0.00	–3.30	2.98	–3.30	3.58	2.98	None
Phomoenamide	2.68	0.13	N.A.	0.00	0.00	0.00	–5.62	2.68	–5.62	5.59	2.68	None
Compound **6**	0.60	0.05	N.A.	0.00	0.00	0.00	–0.57	0.60	–0.57	6.15	0.60	None
Compound **7**	0.89	0.06	N.A.	0.00	0.00	0.00	–0.46	0.89	–0.46	5.47	0.89	None
Phomol	3.58	0.12	N.A.	0.00	0.00	0.00	–5.53	3.58	–5.53	3.16	3.58	None
Phomonitroester	2.58	0.15	N.A.	0.19	0.00	0.19	–2.37	–2.37	–2.37	9.17	2.58	None

*Control ligand

Microwave-assisted synthesis of 1,2,3,4-tetrahydroisoquinoline sulfonamide derivatives and their biological evaluation

STANIMIR P. MANOLOV, ILIYAN I. IVANOV* and DIMITAR G. BOJILOV

Department of Organic Chemistry, University of Plovdiv, 24 Tzar Assen str., 4000 Plovdiv, Bulgaria

Abstract: Herein we report an alternative eco-friendly method for the synthesis of 1,2,3,4-tetrahydroisoquinoline sulfonamide derivatives. All obtained compounds were screened for their *in vitro* inhibition of albumin denaturation, antioxidant, antitryptic and antibacterial activity, and have shown significant results. The lipophilicity was established using both reversed-phase thin layer chromatography and *in silico* calculations.

Keywords: SiO$_2$/PPA; microwave synthesis; inhibition of albumin denaturation; H$_2$O$_2$ scavenging activity; antitryptic activity; antibacterial activity.

INTRODUCTION

Sulfonamide drugs are the first broad-spectrum chemotherapeutic antibacterial agents to be used in practical medicine. Chemically, they are derivatives of 4-amino sulfonic acid amide. Despite the widespread use of antibiotics in medicine, sulfonamides continue to be used in the treatment of various infectious diseases caused by microorganisms sensitive to sulfonamide preparations.[1] Sulfonamides have a variety of biological activities, such as cytotoxic, anticancer, anticonvulsant, antispasmodic, carbonic anhydrase inhibitors, and others.[2]

Isoquinoline skeleton synthesis is a topic that is contained in many works, including monographs,[3,4] chapters in monographs,[5,6] and review reports.[7,8] The interest in this class of heterocyclic compounds is due to the large number of isoquinoline alkaloids contained in many different plants around the world,[3–8] as well as their diverse and significant biological activity of both the alkaloids themselves and their synthetic derivatives.

In the last decade, new techniques and methods have been used for the synthesis of organic compounds, which significantly improve organic synthesis.[9] Nowadays, the microwave-assisted organic synthesis is widely used.[10,11] The

---

method is "unconventional". The advantage of this technology includes reducing the reaction time by improving the yield and purity of the products, which makes it a "green" and environmentally friendly method. A number of authors have reported microwave-assisted preparation of 1,2,3,4-tetrahydroisoquinoline compounds.[12,13]

Herein, alternative synthesis of sulfonamides (amides and cyclic) and their inhibition of albumin denaturation, antitryptic, antibacterial, and H_2O_2 scavenging activity has been reported. Lipophilicity as R_M value as a fundamental property has also been evaluated. A green method for the synthesis of 1,2,3,4-tetrahydroisoquinoline sulfonamide derivatives was applied as an alternative, using microwave irradiation and heterogeneous catalyst PPA/SiO_2. All compounds have been characterized by physical and spectral analysis.

EXPERIMENTAL

General methods

Chromatographic grade methanol analyses was used for HPLC (VWR, Austria). Water for HPLC was prepared with a Millipore purifier (Millipore, USA). Ibuprofen, potassium dihydrogen phosphate, dipotassium hydrogen phosphate, sodium chloride, potassium chloride, hydrogen peroxide, ascorbic acid, trypsin, egg albumin, Tris–HCl buffer, and perchloric acid were purchased from Sigma–Aldrich. Human albumin 20 % – BB, 200 g/l was purchased from BB-NCIPD Ltd., Bulgaria. Chromatographic plates Kieselgel 60 F_{254} were purchased from Merck.

All the reagents and chemicals for the synthesis were purchased from commercial sources (Sigma–Aldrich) and used as received. Melting points were determined on a Boetius hot stage apparatus and are non-corrected. The spectral data were recorded on a Bruker Avance II + 600 spectrometer (BAS-IOCCP-Sofia, Sofia, Bulgaria). The ^{1}H-NMR and ^{13}C--NMR spectra were taken in $CDCl_3$ or DMSO at 600 MHz and 150.9 MHz, respectively. Chemical shifts are given in ppm relative and were referenced to TMS ($\delta = 0.00$ ppm) as an internal standard with the coupling constants indicated in Hz. The NMR spectra were taken at room temperature (ac. 295 K). Mass analyses were carried out on a QExactive quadrupole--orbitrap mass spectrometer (ThermoFisher Scientific). TLC was carried out on precoated 0.2 mm Fluka silica gel 60 plates.

Synthesis of 2-methylsulfonyl-1,2,3,4-tetrahydroisoquinolines (3)

The starting amides **2** (3mmol), paraformaldehyde (5 mmol), and 0.06 g PPA/SiO_2 catalyst were placed in a Teflon microwave vessel and dissolved in toluene (10 ml). The reaction mixture was irradiated in the microwave reactor at 100ºC at a set microwave power of 1200 W. Maximum conversion of the starting amides to 2-methylsulfonyl-1,2,3,4-isoquinoline compounds was achieved after 60 min. After the reaction was finished, the reaction mixture was cooled and filtered to separate the catalyst (PPA/SiO_2). The filtrate was transferred to a round bottom flask and toluene was removed using a rotary evaporator. The residue was washed with H_2O and extracted with dichloromethane (3×20 ml), dried over anhydrous Na_2SO_4 and the solvent was removed by distillation. The obtained compounds were filtered through short column chromatography (silica gel 60, 70–230 mesh, Merck; diethyl ether) and then recrystallized from the same solvent.

Biological experiments

Hydrogen peroxide scavenging activity (HPSA). The ability of sulfonamide derivatives to scavenge hydrogen peroxide was assessed according to the method reported by Ruch[14] with minor modification. The solution of hydrogen peroxide (43 mM) was prepared in potassium phosphate buffer solution (0.2 M, pH 7.4). The sample analysis was performed as follows: in test tubes were mixed 0.6 ml hydrogen peroxide (43 mM), 0.1 ml sample/standard with different concentrations (15–1000 μg/ml), and 2.4 ml potassium phosphate buffer solution. The mixture was stirred and incubated in dark for 10 min at 37 °C. Absorbance was measured at 230 nm with a spectrophotometer (Camspec M508, England) against a blank solution containing phosphate buffer and hydrogen peroxide without the sample. Ascorbic acid was used as standard. Performing the analysis should be considered if the compounds are UV active in this wavelength, as most of the organic compounds have absorbance at 230 nm. In our case, the control sample absorbance in the absence of hydrogen peroxide is measured, i.e. the absorbance of a sample/standard with phosphate buffer for each concentration. The percentage HPSA of the samples was evaluated by comparing with a blank sample and calculated using the following formula:

$$I(\text{HPSA}) = 100 \frac{A_{\text{blank}} - (A_{\text{TS}} - A_{\text{CS}})}{A_{\text{blank}}} \tag{1}$$

where A_{blank} is the absorbance of the blank sample (phosphate buffer and hydrogen peroxide), A_{CS} is the absorbance of the control sample (test sample + phosphate buffer) and A_{TS} is the absorbance of the test sample (test sample + phosphate buffer + hydrogen peroxide). The mean IC_{50} value was estimated based on three replicates by means of interpolating the graphical dependence of scavenging hydrogen peroxide on concentration.

Inhibition of albumin denaturation. *In vitro* analysis of anti-inflammatory activity was assessed as the inhibition of albumin denaturation.[15] The analysis was performed according to Sakat method[15] with minor modification. The experiment was performed with egg albumin. The solution of albumin (1 %) was prepared in distilled water (pH 7.4). The tested compounds/standard were dissolved firstly in 1.2 ml DMF and PBS up to 25 ml, so the final concentration of the stock solution is 1000 μg/ml. Then a series of working solutions with different concentrations (20–500 μg/ml) in PBS were prepared. The reaction mixture was containing 2 ml test sample/standard of different concentrations and 1 ml albumin (1 %). The mixture was incubated at 37 °C for 15 min and then heated at 70 °C for 15 min in a water bath. After cooling the turbidity was measured at 660 nm with a spectrophotometer (Camspec M508, England). The experiment was performed three times. Percentage inhibition of albumin denaturation (*IAD*) was calculated against control. The control sample is albumin with the same concentration dissolved in distilled water:

$$IAD = 100 \frac{A_{\text{control}} - A_{\text{sample}}}{A_{\text{control}}} \tag{2}$$

Antitryptic activity. This method is known also as an anti-arthritic activity.[16] The analysis was performed according to the method of Oyedapo and Femurewas[16] with minor modification. The reaction mixture was containing 2 ml 0.06 mg/ml trypsin, 1 ml Tris–HCl buffer (20 mM, pH 7.4) and 1 ml test sample/standard (in methanol) of different concentrations (20-500 μg/ml). The mixture was incubated at 37 °C for 5 min. Then 1 ml of human albumin (4 vol. %) was added. The mixture was incubated for an additional 20 min. To the mixture, 2 ml of 70 % perchloric acid was added for termination of the reaction. The cloudy suspension was

cooled and centrifuged at 5000 rpm for 20 min. The absorbance of the supernatant was measured at 280 nm with a spectrophotometer (Camspec M508, England) against the control solution. The UV activity of the test compounds should be considered. The control solution was a test sample/standard in methanol with different concentrations. Ibuprofen was used as standard. The analysis was performed three times. The percentage of the antitryptic activity (*ATA*) of the samples was evaluated by comparing it to a blank sample. The blank sample is prepared as the test sample but with a small exception – perchloric acid is added before albumin:

$$ATA = 100 \frac{A_{\text{blank}} - (A_{\text{TS}} - A_{\text{CS}})}{A_{\text{blank}}} \tag{3}$$

where A_{blank} is the absorbance of the blank sample, A_{CS} is the absorbance of the control solution (test sample in different concentrations) and A_{TS} is the absorbance of the test samples. The mean IC_{50} values were estimated by means of interpolating the graphical dependence of *ATA* on concentration.

Antibacterial activity. The synthesized sulfonamides were screened for antibacterial activity against Gram-positive strains (*Bacillus licheniformis* ATCC 14580) and Gram-negative strain (*Escherichia coli* ATCC 8739), using the hole plate method in Mueller–Hinton agar with 100 µL loading of 1 mg/mL solutions in DMSO–water (1:1 volume ratio).[17]

Physicochemical characterisation

Determination of lipophilicity as R_M *values*. Determination of lipophilicity of sulfonamides was estimated according to the method reported by Pontiki and Hadjipavlou-Litina.[18]

Prediction of anti-inflammatory and anti-arthritic activity. A computerized prediction of biological activity (anti-inflammatory and anti-arthritic) for the obtained compounds was performed using the PASS Online program.[19,20]

Statistical analysis

All the analyses were made in triplicates. Data were expressed as mean±*SD*. The level of significance was set at *p* < 0.05.

<div align="center">RESULTS AND DISCUSSION</div>

Chemistry

In our previous experiments, we have reported the synthesis of 1,2,3,4-tetrahydroisoquinolines, including sulfonamide derivatives, using a conventional intramolecular *α*-amidoalkylation reaction.[21] Herein we aimed to use microwave irradiation as an environmentally friendly method for the synthesis of *N*-methylsulfonyl-1,2,3,4-tetrahydroisoquinoline compounds using SiO_2/PPA as a heterogeneous catalyst.

The main tasks are summarized in the given retrosynthesis Scheme 1: preparation of starting amines, transforming the amines to sulfonamides, and cyclisation of the obtained amides to 1,2,3,4-tetrahydroisoquinolines.

The starting amines **1a** and **b** are commercially available. For the obtaining of amine **1c**, a procedure[21] developed in the Department of Organic Chemistry, University of Plovdiv, was applied.
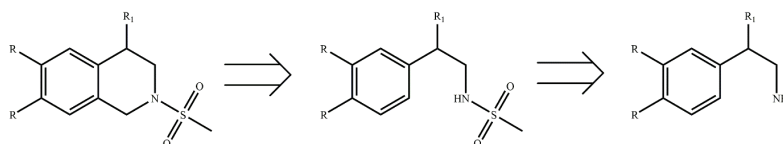
Scheme 1. Retrosynthesis scheme of 1,2,3,4-tetrahydroisoquinoline sulfonamides.

The next step, according to the retrosynthesis scheme above, is the obtaining of amides **2a–c** (Scheme 2). For this purpose, the Schotten–Baumann method was used.[22,23]

a R=OCH$_3$; b R=H;   c R=OCH$_3$
R$_1$=H.   R$_1$=C$_6$H$_5$.   R$_1$=3,4-(CH$_3$O)$_2$-C$_6$H$_3$.
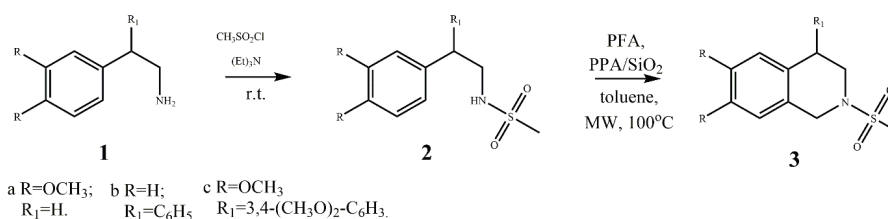
Scheme 2. Synthesis of sulfonamides (**2**) and 1,2,3,4-tetrahydroisoquinolines (**3**).

The possibility of applying PPA/SiO$_2$ as a heterogeneous acid catalyst in the intramolecular α-amidoalkylation reaction was studied. For this purpose, the conventional heating was replaced by the microwave radiation. The PPA/SiO$_2$ system was used for the cyclization step. The reaction is carried out in a Milestone Ethos One microwave reactor, which allows the control of the time, the temperature of the samples, and the power used.

A significant advantage of the use of the heterogeneous catalyst (PPA/SiO$_2$) in the intramolecular α-amidoalkylation reaction for the synthesis of *N*-sulfonyl--1,2,3,4-tetrahydroisoquinolines is the simplified procedure for the isolation of the final product. After completion of the reaction, the reaction mixture was cooled, the catalyst was removed by simple filtration, and the solvent was distilled off on a rotary evaporator. The resulting 1,2,3,4-tetrahydroisoquinolines (**3**) (Scheme 2) were filtered through short column chromatography (silica gel 60, 70–230 mesh, Merck; diethyl ether) and then recrystallized from the same solvent.

After using the PPA/SiO$_2$ system during the reaction, it is regenerated and prepared for its next participation. For this purpose, it is transferred to a 50 ml round-bottomed flask and dried under vacuum at 100 °C for 2 h. The solvent is distilled and there are practically no waste products. The applied method for the synthesis of *N*-sulfonyl-1,2,3,4-tetrahydroisoquinolines offers a convenient, fast, economical, and environmentally friendly synthesis.

Comparing the yields of compounds (**3**) obtained by the proposed microwave-assisted intramolecular α-amidoalkylation reaction with the yields of the same compounds obtained by conventional heating in a mixture of acetic:triflu-

oroacetic acid = 4:1 (volume ratio) or in a polyphosphoric acid/silica gel system (20 wt. % SiO$_2$),[21] we found that the yields of compounds **3b** and **c** were higher and the reaction time shorter when the microwave radiation is used instead of conventional heating in acetic:trifluoroacetic acid in a ratio of 4:1 (volume ratio) at the same temperature (100 °C, Table I). It was also found that, when compared to conventional heating and the use of the heterogeneous PPA/SiO$_2$ catalyst, the yields of the microwave-assisted intramolecular α-amidoalkylation reaction were comparable for the same reaction time.

TABLE I. Comparison of yields (%) of compounds (**3**)

Compound	Reaction conditions		
	t = 100 °C, τ = 1 h (MW, PPA/SiO$_2$)	Room temperature, τ = 8 h (AcOH:TFA = 4:1 volume ratio)	Reflux, τ = 1 h (PPA/SiO$_2$)
3a	81	–	–
3b	93	80	91
3c	95	87	97

The yields of the final *N*-sulfonyl-1,2,3,4-tetrahydroisoquinoline compounds were prepared at a ratio of 3 mmol of the starting amides to 0.06 g of PPA/SiO$_2$ catalyst. The obtained compounds are characterized by their melting points, ^{1}H- and ^{13}C-NMR, IR and HRMS spectra.

Biological evaluation

All synthesized sulfonamides were tested for their *in vitro* inhibition of albumin denaturation (*IAD*), antioxidant and antitryptic activity (*ATA*). The obtained *in vitro* results were compared to the predicted *in silico* ones. The results are presented in Table II.

H₂O₂ scavenging activity

It has been demonstrated that free radicals play an important role in the pathogenesis of specific diseases and aging.[24,25] The obtained synthesized sulfonamides were screened *in vitro* scavenging activity using hydrogen peroxide. The antioxidant activity values of the synthesized sulfonamides vary from 1659.86 to 3160.97 µM. Hydrogen peroxide is an oxidant and is formed continuously in living tissues as a result of a number of metabolic processes. The scavenging of hydrogen peroxide is a very important step that prevents the reaction between iron ions and H$_2$O$_2$, which generate extremely reactive oxygen species – •OH radicals. Compared to ascorbic acid (497.37 µM), the obtained sulfonamides demonstrated lower *in vitro* antioxidant activity. Compound **3c** (1659.86 µM) demonstrate higher antioxidant activity, when compared to the ibuprofen and the rest of the synthesized sulfonamides (Table II, Fig. 1).

TABLE II. *In vitro* and *in silico* biological activity results. Hydrogen peroxide scavenging activity (*HPSA*), inhibition of albumin denaturation (*IAD*), and antitryptic activity (*ATA*) were expressed as IC_{50}. Ascorbic acid (AA) and ibuprofen (Ibu) were used as standards. R_M is a non-dimensional quantity because it is a function of R_f and is determined by thin-layer chromatography. cAnti-I and cAnti-A are expressed as Pa (probability "to be active") estimates the chance that the studied compound is belonging to the sub-class of active compounds (resembles the structures of molecules, which are the most typical in a sub-set of "actives" in PASS training set). The value of the most active compound is 1; Ibu – Ibuprofen; R_M – lipophilicity; cAnti-I – calculated anti-inflammatory activity; cAnti-A – calculated anti-arthritic activity

Compd.	$IC_{50} \pm SD$ / μM			$R_M \pm SD$	Pa	
	HPSA	*IAD*	*ATA*		cAnti-I	cAnti-A
AA	497.37±42.47	–	–	–	–	–
Ibu	1854.78±60.11	336.13±27.10	1259.49±44.31	0.99±0.032	0.903	0.573
2a	2659.52±90.50	2993.77±223.39	143.26±10.14	0.96±0.028	0.341	0.472
2b	2720.93±31.92	1679.44±63.27	506.85±40.82	1.22±0.031	0.270	0.249
2c	1902.01±62.72	840.39±4.63	98.44±9.18	1.16±0.025	0.270	0.298
3a	3160.97±47.97	1424.30±142.75	260.64±14.63	1.11±0.033	0.330	0.598
3b	2753.76±111.57	747.21±24.52	628.17±51.57	0.97±0.025	0.376[a]	0.665
3c	1659.86±25.71	108.45±1.52	75.91±7.14	0.99±0.028	0.306[a]	0.612

[a]Inflammatory Bowel disease treatment – inflammatory bowel disease (IBD) is a term for two conditions (Crohn's disease and ulcerative colitis) that are characterized by the chronic inflammation of the gastrointestinal (GI) tract. Prolonged inflammation results in damage to the GI tract. Biological therapy for inflammatory bowel disease, especially the TNF inhibitors, are used in people with more severe or resistant Crohn's disease and sometimes in ulcerative colitis. The treatment is usually started by administering drugs with high anti-inflammatory effects. The Pass program, which is also available online, was used to determine the predicted anti-inflammatory values of our synthesized compounds. For the determination of the anti-inflammatory activity in the PASS database on the basis of which the theoretical calculations are made, there are data on molecules that affect the treatment of inflammatory processes in the intestine
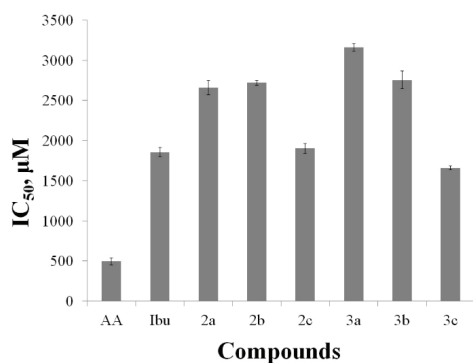

Fig. 1. HPSA of sulfonamides. Ascorbic acid (AA) used as standard. The results of antioxidant activity were expressed as IC_{50}.

Although hydrogen peroxide is not very reactive, it can cause cytotoxicity by generating hydroxyl radicals in the cell.[26] Hydroxy radicals are the most reactive and are thought to be responsible for some tissue damage caused by inflammation. In living organisms, the superoxide anion radical ($O_2^{-\bullet}$) and H_2O_2 are transformed into $^{\bullet}OH$ and $^{\bullet}O_2$, which are responsible for cell damage. The inf-

lammatory process causes the generation of a superoxide anionic radical at the inflammation site and this is associated with the formation of other oxidizing species such as $^{\bullet}OH$. Scavengers of hydroxyl radicals can increase the synthesis of prostaglandins.[18] Therefore, the removal of H_2O_2 is very important in the prevention of the generation of $^{\bullet}OH$.

Inhibition of albumin denaturation

Inflammation is the response of living tissues to injury. It involves a complex array of enzyme activation, mediator release, fluid extravasation, cell migration, tissue breakdown, and repair.[27] The denaturation of proteins is a well-documented cause of inflammation in rheumatoid arthritis. Several anti-inflammatory drugs have shown a dose-dependent ability to inhibit thermally-induced protein denaturation.[28] The obtained sulfonamides were screened for the inhibition of albumin denaturation. This method provides the extent information on to which albumin is protected from denaturation when heated. For this purpose, we have used egg albumin. The percentages of inhibition of synthesized sulfonamides are presented in Fig. 2. The results of the study are presented as IC_{50}. As ibuprofen has proven properties, we have decided to use it as a benchmark to compare the activities of newly synthesized sulfonamides. The IC_{50} values of ibuprofen, estimated as *IAD* is 336.13 μM (Table II, Fig. 2). All the obtained results show the IC_{50} values of sulfonamides are in the range from 108.45 to 2993.73 μM (Table II, Fig. 2). Comparing the compounds to the standard, compound **3c** exhibited the highest degree of albumin protection and compound **2a** is the least active.
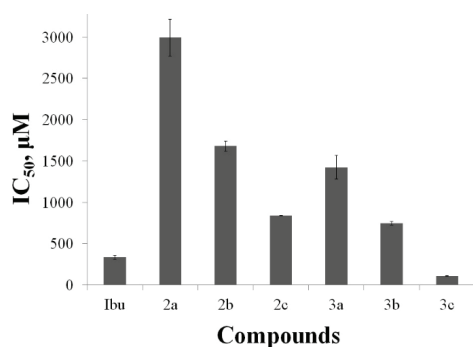

Fig. 2. The inhibition of albumin denaturation activity of synthesized sulfonamides. Ibuprofen is used as standard. The results were expressed as IC_{50}.

Analyzing the results, it can be seen that cyclic sulfonamides (**3a–c**) are characterized by higher albumin protection compared to non-cyclic ones (**2a–c**) (Fig. 2). In addition, it has been observed that the activity of sulfonamides depends on the methoxy group number. As the number of methoxy groups in the structure of sulfonamides increases, so does the stabilization of the albumin molecule. Furthermore, IAD analysis reveals that lipophilicity is a major phys-

icochemical parameter. The studied synthetic sulfonamides show average lipophilicity (R_M) around 1.11 for the non-cyclic sulfonamides and 1.02 for the cyclic sulfonamides, which to some extent affects the albumin protection. Despite their slight difference in R_M values, the cyclic sulfonamides show a greater effect on the stabilization of the albumin molecule. (Table II).

Compound **2c** of the non-cyclic sulfonamides is the most active, while of the cyclic sulfonamides it is **3c**. Although the R_M values of ibuprofen and **3c** did not differ statistically, compound **3c** showed the highest activity (Table II, Fig. 2).

In vitro analysis of sulfonamides by *IAD* is essential for the study of new potential anti-inflammatory agents.

Antitryptic activity

Proteinases have been implicated in arthritic reactions. Neutrophils are known to be a rich source of proteinase which carries many serine proteinases in their lysosomal granules. It was previously reported that leukocyte proteinase plays an important role in the development of tissue damage during inflammatory reactions and that a significant level of protection was provided by proteinase inhibitors.[16,28] *In vitro* anti-arthritic activity was assessed as antitryptic activity.[16] The results present that the sulfonamides show better antitryptic activity compared to ibuprofen (Table II, Fig. 3).
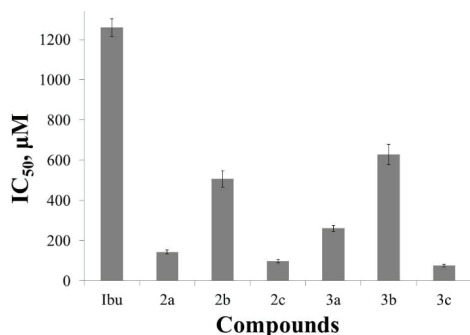

Fig. 3. The antitryptic activity of synthesized sulfonamides. Ibuprofen is used as standard. The results are expressed as IC_{50}.

The IC_{50} results for the *ATA* range from 75.91 to 628.17 μM. The highest activity was demonstrated by compounds **3c** (75.91 μM), **2c** (98.44 μM), **2a** (143.26 μM) and **3a** (260.64 μM). Hence these compounds were shown to be the most promising.

The data from the analysis show that the activity of the sulfonamides depends on the methoxy groups presence. The presence of methoxy groups in the structures of the sulfonamides leads to an increase in their activity. The low activity of **2b** (506.85 μM) and **3b** (628.17 μM) is due to a lack of methoxy groups in their structures. The decreasing order of their antitryptic activity is as follows: **3c** > **2c** > **2a** > **3a** > **2b** > **3b** (Table II, Fig. 3).

Antibacterial activity

The method Mueller–Hinton[17] is intended for testing the sensitivity of fast-growing aerobic bacteria and for demanding microorganisms for which standards have been introduced. For more accurate determination of sensitivity, a method for the determination of the minimum inhibitory concentrations (MIC) of antimicrobial agents by methods with serial dilutions of the preparation in agar is also used. The results show that compound **3c** exhibits antibacterial activity against gram-positive bacteria *Bacillus licheniformis* and gram-negative *Escherichia coli*. The data from the conducted studies are presented in Table III.

TABLE III. Antibacterial activity of the obtained sulfonamides

Compound	*Escherichia coli* ATCC 8739		*B. licheniformis* ATCC 14580	
	Inhibition zone, mm[a]	*MIC*, mg/mL[b]	Inhibition zone, mm[a]	*MIC*, mg/mL[b]
2a–**3b**	–	–	–	–
3c	23	0.06	15	0.06

[a]Assessed by the hole-plate method with 100 µL loading of 1 mg/mL solutions in 1:1 DMSO–water; [b]ampicillin was used as a positive control with *MIC* = 0.0004 mg/mL against both strains

Biological activity is an important factor for any new drug. There is a clear correlation between the *in vitro* tests performed and the antibacterial activity, which showed that compound **3c** is the most active.

Lipophilicity

Lipophilicity is the most regularly applied parameter used in structure activity relationship (SAR) drug discovery studies. It can be experimentally determined or calculated. Lipophilicity has been correlated to permeability, solubility and it increases in target potency and toxicity. We determined the lipophilicity by the reverse phase thin layer chromategraphy (RPTLC) method as R_M values. This is considered to be a reliable, fast, and convenient method for expressing lipophilicity.[29] Aside from the essential role of lipophilicity for the kinetics of biologically active compounds, the antioxidants of hydrophilic or lipophilic character are both needed to act as radical scavengers in the aqueous phase or as chain-breaking antioxidants in biological membranes.[18]

In the present work, we have investigated the antioxidant and *in vitro* biological activity of the newly synthesized sulfonamides. Lipophilicity proved to be an important factor in their activity. The results have shown that sulfonamides are lipophilic compounds with low antioxidant activity. However, it should not be taken as a criterion for whether the compounds will exhibit biological activity. However, the use of lipophilic antioxidants is necessary to neutralize harmful radicals in cell membranes.[18]

In general, the *in vitro* studies results show that the sulfonamides exhibit *IAD* and *ATA*. From both experiments, we have derived the important information

about the properties of potential new drugs, and both experiments are related to preserving the integrity of the albumin molecule. Human serum albumin (HSA) is known to have two major binding sites for drugs: Sudlow sites I and II. Sudlow site I, which is found in subdomain IIA of HSA, binds to bulky heterocyclic compounds such as coumarins, sulfonamides and salicylates. Sudlow site II, found in subdomain IIIA, binds to aromatic carboxylic acids and profens.[30] In addition, it is known that sulfonamides bind to Sudlow site I by stabilizing the structure of the albumin molecule and increasing the anti-oxidant properties of albumin.[31] From the experiment it was found out that the newly synthesized sulfonamides show better expressed ATA activity.

In addition, this result is confirmed by the experimentally performed antibacterial activity, which shows that compound **3c** is the most active. It has high antibacterial, *IAD* and *ATA*, which makes it a reliable and effective drug.

CONCLUSION

To conclude, a microwave-assisted intramolecular α-amidoalkylation reaction as an environmentally friendly method for the synthesis of 1,2,3,4-tetrahydroisoquinoline sulfonamides has been successfully applied. The use of the PPA/ /SiO$_2$ system in this reaction proceeds faster with higher yields of the target compounds compared with conventional heating in a CH$_3$COOH:CF$_3$COOH = 4:1 milieu. The compounds were biologically evaluated *in vitro* and *in silico* for their antioxidant, *ATA*, *IAD* and antibacterial activities. Lipophilicity as R_M values as a fundamental property has also been evaluated. Compound **3c** shows significant high results for all activities.

И З В О Д
МИКРОТАЛАСНА СИНТЕЗА ДЕРИВАТА 1,2,3,4-ТЕТРАХИДРОИЗОХИНОЛИН-
-СУЛФОНАМИДА И ИСПИТИВАЊЕ ЊИХОВЕ БИОЛОШКЕ АКТИВНОСТИ

STANIMIR P. MANOLOV, ILIYAN I. IVANOV и DIMITAR G. BOJILOV

Department of Organic Chemistry, University of Plovdiv, Plovdiv, Bulgaria

У раду је описан алтернативни, еколошки прихватљив, метод за синтезу деривата 1,2,3,4-тетрахидроизохинолин-сулфонамида. Испитана је способност ових једињења да у *in vitro* условима инхибирају денатурацију албумина, као и антиоксидативна, анти-трипсинска и антибактеријска активност, које су биле значајне. Липофилност је утврђена користећи методе реверзно-фазне танкослојне хроматографије и *in silico* израчунавања.

(Примљено 2. августа, ревидирано 18. новембра, прихваћено 27. новембра 2020)

REFERENCES

1. R. N. Shelke, D. N. Pansare, A. P. Sarkate, I. K. Narula, D. K. Lokwani, S. V Tiwari, R. Azad, S. R. Thopate, *Bioorg. Med. Chem. Lett*. **30** (2020) 127246 (https://doi.org/10.1016/j.bmcl.2020.127246)
2. R. Pingaew, P. Mandi, C. Nantasenamat, S. Prachayasittikul, S. Ruchirawat, V. Prachayasittikul, *Eur. J. Med. Chem.* **81** (2014) 192 (https://doi.org/10.1016/j.ejmech.2014.05.019)
3. G. Blaskó, P. Kerekes, S. Makleit, *Reissert Synthesis of Isoquinoline and Indole Alkaloids in The Alkaloids: Chemistry and Pharmacology*, A. Brossi (Ed.), Elsevier, Academic Press, New York, 1987, p. 1 (https://doi.org/10.1016/S0099-9598(08)60256-4)
4. M. Shamma, in *The Isoquinoline Alkaloids. Chemistry and Pharmacology*, Academic Press, New York, 1972, p. 595 (https://doi.org/10.1016/B978-0-12-638250-1.50040-X)
5. G. Jones, in *Comprehensive Heterocyclic Chemistry II*, A. R. Katritzky, C. V. Rees, E. F. V. Scriven (Eds.), Pergamon Press, Elsevier Sci. Ltd., New York, 1997 (https://doi.org/10.1021/jm9706123)
6. R. Kreher, S. Andreae, S. von Angerer, P. Czerney, H. Hartmann, M. A. Kessler, E. Reimann, W.-D. Rudorf, I. Stahl, O. S. Wolfbeis, in *Methoden der Organischen Chemie (Houben-Weyl)*, E7a, 4th ed., Georg Thieme Verlag, Stuttgart, 1991, p. 571 (https://www.thieme-connect.de/products/ebooks/book/10.1055/b-003-115784)
7. K. W. Bentley, *Nat. Prod. Rep*. **9** (1992) 365 (http://dx.doi.org/10.1039/NP9920900365)
8. K. W. Bentley, *Nat. Prod. Rep*. **17** (2000) 247 (http://dx.doi.org/10.1039/A900251K)
9. A. K. Pathak, C. Ameta, R. Ameta, P. B. Punjabi, *J. Heterocycl. Chem.* **53** (2016) 1697 (https://doi.org/10.1002/jhet.2515)
10. B. T. Pérez-Martínez, M. A. Aboudzadeh, U. S. Schubert, J. R. Leiza, R. Tomovska, *Chem. Eng. J.* **399** (2020) 125761 (https://doi.org/10.1016/j.cej.2020.125761)
11. H. M. Nguyen, J. Sunarso, C. Li, G. H. Pham, C. Phan, S. Liu, *Appl. Catal., A* **599** (2020) 117620 (https://doi.org/10.1016/j.apcata.2020.117620)
12. E. Awuah, A. Capretta, *J. Org. Chem.* **75** (2010) 5627 (https://doi.org/10.1021/jo100980p)
13. I. D. Lick, L. Gavernet, L. E. Bruno-Blanch, E. N. Ponzi, *Thermochim. Acta* **501** (2010) 30 (https://doi.org/10.1016/j.tca.2009.12.019)
14. R. J. Ruch, S.-J. Cheng, J. E. Klaunig, *Carcinogenesis* **10** (1989) 1003 (https://doi.org/10.1093/carcin/10.6.1003)
15. S. S. Sakat, A. R. Juvekar, M. N. Gambhire, *Int. J. Pharm. Pharm. Sci.* **2** (2010) 146 (https://innovareacademics.in/journal/ijpps/Vol2Issue1/322.pdf)
16. O. O. Oyedapo, A. J. Famurewa, *Int. J. Pharmacogn.* **33** (1995) 65 (https://doi.org/10.3109/13880209509088150)
17. I. Wiegand, K. Hilpert, R. E. W. Hancock, *Nat. Protoc.* **3** (2008) 163 (https://doi.org/10.1038/nprot.2007.521)
18. E. Pontiki, D. Hadjipavlou-Litina, *Bioorg. Med. Chem.* **15** (2007) 5819 (https://doi.org/10.1016/j.bmc.2007.06.001)
19. A. Sadym, A. Lagunin, D. Filimonov, V. Poroikov, *SAR QSAR Environ. Res.* **14** (2003) 339 (https://doi.org/10.1080/10629360310001623935)
20. D. A. Filimonov, A. A. Lagunin, T. A. Gloriozova, A. V. Rudik, D. S. Druzhilovskii, P. V. Pogodin, V. V. Poroikov, *Chem. Heterocycl. Compd.* **50** (2014) 444 (http://link.springer.com/10.1007/s10593-014-1496-1)
21. S. Manolov, S. Nikolova, I. Ivanov, *Molecules* **18** (2013) 1869 (https://www.mdpi.com/1420-3049/18/2/1869)

22. C. Schotten, *Berichte Der Dtsch. Chem. Gesellschaft* **17** (1884) 2544 (https://doi.org/10.1002/cber.188401702178)
23. E. Baumann, *Berichte Der Dtsch. Chem. Gesellschaft* **19** (1886) 3218 (https://doi.org/10.1002/cber.188601902348)
24. A. A. H. Kadhum, A. A. Al-Amiery, A. Y. Musa, A. B. Mohamad, *Int. J. Mol. Sci.* **12** (2011) 5747 (https://doi.org/10.3390/ijms12095747)
25. J. H. Naama, G. H. Alwan, H. R. Obayes, A. A. Al-Amiery, A. A. Al-Temimi, A. A. H. Kadhum, A. B. Mohamad, *Res. Chem. Intermed.* **39** (2013) 4047 (http://link.springer.com/10.1007/s11164-012-0921-2)
26. M. Ebrahimzadeh, S. Nabavi, S. Nabavi, F. Bahramian, A. Bekhradnia, *Pak. J. Pharm. Sci.* **23** (2010) 29 (https://pubmed.ncbi.nlm.nih.gov/20067863)
27. J. R. Vane, R. M. Botting, *Inflamm. Res.* **44** (1995) 1 (http://link.springer.com/10.1007/BF01630479)
28. V. Jayashree, S. Bagyalakshmi, K. Manjula Devi, D. Richard Daniel, *Asian J. Pharm. Clin. Res.* **9** (2016) 108 (https://doi.org/10.22159/ajpcr.2016.v9s2.12623)
29. C. Hansch, A. Leo, D. Hoekman, *Exploring QSAR: hydrophobic, electronic, and steric constants*, American Chemical Society, Washington, DC, 1995, ISBN-13: 978-0841229914 (https://www.amazon.com/Exploring-QSAR-Hydrophobic-Electronic-Professional/dp/0841229910)
30. K. S. Joseph, J. Anguizola, D. S. Hage, *J. Pharm. Biomed. Anal.* **54** (2011) 426 (https://doi.org/10.1016/j.jpba.2010.09.003)
31. G. R. Behbehani, M. Hossaini Sadr, H. Nabipur, L. Barzegar, *J. Chem.* **2013** (2013) 1 (https://doi.org/10.1155/2013/120480).

Synthesis, characterization, antimicrobial screening and cytotoxic properties of Cu(II) and Zn(II) complexes with a bidentate hydroxylated 1,3-diaryl-2-propene-1-one ligand

PRAVINKUMAR PATIL[1] and SAINATH ZANGADE[2]*

[1]Research Laboratory, Department of Chemistry, N.E.S. Science College, Nanded-431605 (MS), India and [2]Department of Chemistry, Madhavrao Patil, ACS College, Palam, Dist. Parbhani-431720 (MS), India

Abstract: A series of binary metal complexes (halo, hydroxyl and methoxy substituted bis(2-(E)acryloyl)naphthalen-1-yl)oxy)Cu(II) and Zn(II) (**C1**––**C10**)) of Cu^{2+} and Zn^{2+} ions derived from bi-coordinated hydroxylated 1,3--diaryl-2-propene-1-ones were synthesized. The newly synthesized metal complexes were structurally determined by FT-IR, ^{1}H-NMR, ^{13}C-NMR, ESR spectral, XRD and TGA analyses. The FT-IR and ESR studies demonstrated that interactions between metal ions with ligands occur through carbonyl oxygen and deprotonated hydroxyl oxygen and correspond to square-planar geometry for all complexes. The metal complexes were screened *in-vitro* and evaluated for their antimicrobial and cytotoxic activities. The complexes **C1** and **C4** showed significant antimicrobial activity while the remaining complexes showed moderate antimicrobial activity against the tested pathogens. The complexes were evaluated for cytotoxic activity against the organism *Artemia salina*. Complexes **C2**–**C5** exhibited LC_{50} values of 630.45, 969.99, 921.94 and 918.41 $\mu M\ mL^{-1}$, respectively. Furthermore, the complexes were evaluated for their anticancer activity against the liver cancer cell line Hep G2 in comparison with the 5-fluorouracil standard. Complex **C5** showed a significant IC_{50} value of 58.94 $\mu g\ mL^{-1}$. Therefore, the present study is useful for the development of a new class of antimicrobial and anticancer agents.

Keywords: metal complexes; 1,3-diaryl-2-propene-1-one derivatives; antimicrobial activity; cytotoxicity; anticancer activity.

INTRODUCTION

1,3-Diaryl-2-propene-1-ones are recognized as chalcones. Chalcones occur in nature in many plants or are synthesized in laboratories. They serve as biogenic key precursors of flavonoids in higher plants.[1–3] The presence of two elec-

---

trophilic reaction centres enables them to participate in the synthesis of hetero-cyclic compounds.[4] They demonstrate a wide range of biological activities, such as antiviral,[5] anti-inflammatory, anticancer, antimicrobial,[6] antioxidant[7] and antimalerial activities.[8] The biological activity of chalcones may be due to the presence of a reactive keto vinyl group that demonstrates static properties against pathogens.[9]

Chalcones contain an α,β-unsaturated carbonyl system with a reactive keto-ethylenic group. The presence of an α,β-unsaturated carbonyl system makes chalcones very important in organic chemistry.[10] The versatility of chalcones arises from their distinctive combination of functional groups. Chalcones and their derivatives can act as chelating agents towards metals to form stable complexes. They are well known as effective metal ion chelators to form metal-coordinated compounds. They provide three centres to interact with metals, *i.e.*, functional groups present on the aromatic ring, the keto–enol moiety and the olefinic moiety.[11] The heterodiene molecular functionalities form stable complexes with transition and non-transition elements.[12]

In recent years, there have outstanding developments in several areas of pharmaceutical science. The wide range of biological activities associated with chalcone-based complexes has explored their therapeutic potentials.[13–14] Transition metal complexes as medicinal compounds posses a great diversity in their action, such as anticancer, antiviral, antimalarial, antitubercular, anti-amoebic,[15] anti-infective[16] and antidiabetic properties.[17,18] Metal ions play essential roles in biological processes. Thus, on coordination, ligands could increase their bioactive profile or some inactive ligand could posses medicinal properties.[19] Copper plays a key role in several enzymes and coenzyme in biochemical processes, because of its bio-essentiality, its complexes are expected to be less toxic in recent medicinal complexes.[20] Zinc is another important transition metal in living organism that plays a critical role in physiological processes.[21] Zinc can adopt different geometries with different coordination numbers; they have good pharmacological profiles[22] as anti-radio agents and tumour photosensitizes.[23,24] Zinc complexes have been used for the treatment of Alzheimer disease.[25] In view of the above importance of metal complexes, first metal complexes of Cu(II) and Zn(II) ions were synthesised and then their antimicrobial and cytotoxic activities evaluated.

## EXPERIMENTAL

Chemical material and methods

Starting materials, solvents and reagents were purchased from commercial sources and used without purification. FTIR spectra were recorded as KBr pellets on a Perkin Elmer System 2000. ^{1}H-NMR and ^{13}C-NMR spectra were acquired on a Bruker Avance NEO500 spectrometer at 500 and 125 MHz, respectively. XRD was performed on an Ultima IV, Rigaku Corporation, X-ray diffractometer. TGA analysis was realised on a Mettler Toledo instru-

ment under an inert atmosphere. ESR analysis was performed on an ESR-JEOL, JES-FA200 ESR spectrometer with the X band (8.75–9.65 GHz) at room temperature.

The preparation of 1,3-diaryl-2-propene-1-ones ligands were reported in a previous work.[26]

Synthesis of [Cu(Ln)$_2$]and [Zn(Ln)$_2$] complexes (C1–C10)

A warm methanolic solution of metal chloride (CuCl$_2$·2H$_2$O and ZnCl$_2$ (0.25 mmol, 10 mL)) was added drop wise under constant stirring to a sodium methoxide solution (at pH 7.0–8.0) of ligand 2′-hydroxy chalcones (0.50 mmol, 20 mL). Then, the resultant reaction mixture was refluxed continuously for 3 h. On cooling the solution to room temperature, a brown solid mass separated which was filtered and washed with warm methanol and stored in a CaCl$_2$ desiccator (Scheme 1, Table I). All the complexes gave satisfactory characterization data.
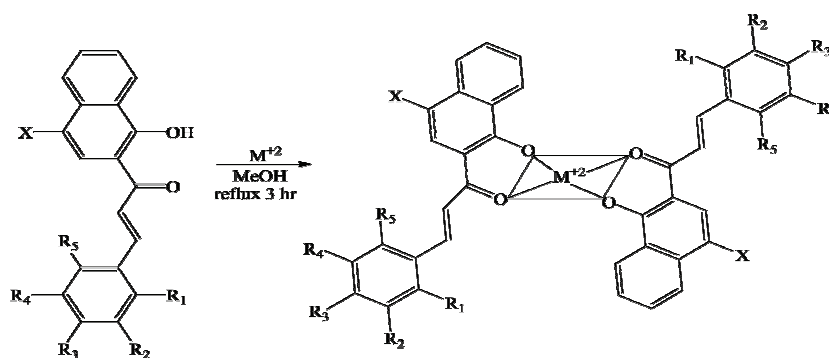
Scheme 1. Representation of the synthesis of Cu(II) and Zn(II) square planar complexes **C1–C10**.

TABLE I. Synthesized Cu(II) and Zn(II) complexes

Complex	X	R$_1$	R$_2$	R$_3$	R$_4$	R$_5$
C1 : [Cu(L$_1$)$_2$]	I	OH	I	H	I	H
C2 : [Cu(L$_2$)$_2$]	Br	H	H	Cl	H	H
C3 : [Cu(L$_3$)$_2$]	Br	Cl	H	H	H	Cl
C4 : [Cu(L$_4$)$_2$]	Br	Cl	H	Cl	H	H
C5 : [Cu(L$_5$)$_2$]	Br	H	OH	OH	H	H
C6 : [Zn(L$_6$)$_2$]	Br	H	H	OCH$_3$	H	H
C7 : [Zn(L$_7$)$_2$]	Br	H	H	Br	H	H
C8 : [Zn(L$_8$)$_2$]	Br	H	H	OH	H	H
C9 : [Zn(L$_9$)$_2$]	Br	H	H	F	H	H
C10 : [Zn(L$_{10}$)$_2$]	I	H	OH	OH	H	H

Antimicrobial activity

In-vitro antimicrobial activity of compounds was evaluated by the Agar cup plate method against the Gram-positive bacteria *Staphylococcus aureus* (ATCC6538) and Gram-negative bacteria *Escherichia coli* (ATCC8739), and the yeast *Candida albicans* (ATCC10231). The activity was evaluated against the antibacterial standard drug ampicillin and the antifungal standard drug fluconazole. Stock solutions of each complex and the standard drugs were pre-

pared in dimethyl sulfoxide to obtain a concentration of 1 mg mL^{-1}. The bacterial slant was incubated at 35 °C for 24 h. Soyabean casein in digest agar media and fungal slant was incubated at 25 °C for 72 h in sabourauds dextrose agar media. After incubation, the well grown slant was inoculated in saline solution and adjusted to a viable count of 10^7 colony forming unit (CFU mL^{-1}). These culture suspensions were inoculated on Mueller–Hinton agar and 100 µL of sample solution was added to each well created on plates with a cork borer. Standard drug controls and a blank control were run for each test. Then the plates were incubated at 35 °C for 24 h for the bacteria and for the yeast and mould at 25 °C for 48 h to examine the zone of inhibition. All the experiments were performed in triplicate and the average zone of inhibition is reported.

The minimum inhibitory concentration of each complex was evaluated against the standard concentrations. The different concentrations of sample and standard of 1, 0.5, 0.25 and 0.12 mg mL^{-1} were prepared in dimethyl sulfoxide by serial dilution. A volume of 100 µL was added into each well. Standard and blank controls were run for each test. After incubation, the lowest concentration of test solution with no visually detectable bacterial growth was considered as the minimum inhibitory concentration.

Cytotoxic activity

In-vitro cytotoxic activity was screened against the organism *Artemia salina*. Test solutions with concentrations 1, 10, 100 and 1000 µM mL^{-1} were prepared in dimethyl sulfoxide. Brine solution 0.1 mL and 10 shrimps were added in different test tubes. Each test tube was treated with test solutions of different concentrations, except the blank control. The blank control and test solutions were incubated at room temperature (28–30 °C) under strong aeration conditions for 24 h. After incubation, the nauplii were counted in the stem of capillary against a light background. The percentage mortality was obtained using the following formula:

Mortality, % = 100(Total nauplii – Alive nauplii)/Total nauplii

The MTT (3-(4,5-dimethylthiazol-2-yl)-2,5-diphenyltetrazolium bromide) assay was performed against the liver cancer cell line Hep G2. The assay was evaluated against a standard 20 µg mL^{-1} solution of 5-fluorouracil prepared in dimethyl sulfoxide. Test solutions with concentrations of 200, 400, 600, 800 and 1000 µg mL^{-1} were prepared in dimethyl sulfoxide. Cell line (HepG2) at a concentration of 10^4 cells per well was cultured in 100 µL culture medium in 96 well flat bottom microplates. Controls were run to determine the control cell survival and the percentage of live cells after culture. Control wells containing DMSO (0.2 % in PBS) and cell line and all sample wells in triplicate were incubated in a 5 % CO$_2$ incubator for 24 h at 37 °C. After incubation, the medium was completely removed and 20 µL of MTT reagent (5 mg mL^{-1} in PBS) was added to each well. Then the cells were incubated for 4 h at 37 °C in a CO$_2$ incubator. The resulting formazan crystals were dissolved in 200 µL DMSO and the absorbance was measured spectrophotometrically at 550 nm after 10 min incubation at 37 °C. The inhibition induced by each tested compound at the indicated concentrations was calculated using the following formula:

Inhibition, % = 100(Control absorbance – Test absorbance)/Control absorbance

RESULTS AND DISCUSSIONS

The Cu(II) and Zn(II) metal complexes were synthesized by the general procedure mentioned above in the experimental section. All the metal complexes were brown coloured and stable towards air and moisture at room temperature.

All these metal complexes are insoluble in most organic solvents except DMSO and DMF.

FT-IR Spectra

FT-IR analysis of the complexes was performed using the KBr pellet technique. The observed results were compared with those of the ligands and are tabulated in Table II. The –OH group in the ligands was confirmed by the presence of corresponding stretching bands at around 3234–3431 cm^{-1} whereas this characteristics band disappeared on complex formation. This is due to deprotonation of the hydroxyl proton and coordination of the central metal ion through the oxygen. The presence of surface or uncoordinated water molecule in the complex was confirmed by the presence of a broad band in the range 3234–3432 cm^{-1}. The vibrational bands observed in the ligands and complexes in the range 1523––1644 cm^{-1}, 1433–1607 and 1207–1294 cm^{-1} confirmed the presence of C=O, C=C and C–O groups, respectively. While the band observed around 468–602 cm^{-1} arises from metal–oxygen bond stretching (M–O) in the formed complexes. The data for the FT-IR analysis of the ligands and synthesized complexes are presented in Table II.

TABLE II. IR frequencies (cm^{-1}) of the ligands and their complexes; * – characteristics IR stretching frequencies of ligand[26]

Ligand and complex	Bond					
	OH	H$_2$O	C=O	C=C	C–O	M–O
L$_1$*	3418.97	–	1627.99	1576.87	1268.25	–
C1 : [Cu(L$_1$)$_2$]	–	3434.8	1643.2	1433.0	1207.2	558.3
L$_2$*	3415.02	–	1630.88	1576.87	1293.33	–
C2 : [Cu(L$_2$)$_2$]	–	3410.6	1523.5	1491.2	1256.5	526.5
L$_3$*	3234.8	–	1624.7	1591.0	1266.80	–
C3 : [Cu(L$_3$)$_2$]	–	3463.7	1635.1	1606.2	1255.7	599.4
L$_4$*	3400.00	–	1621.4	1590.20	1266.00	–
C4 : [Cu(L$_4$)$_2$]	–	3463.8	1633.8	1572.7	1251.2	601.9
L$_5$*	3431.00	–	1625.40	1591.50	1266.40	–
C5 : [Cu(L$_5$)$_2$]	–	3416.3	1611.8	1585.5	1253.5	594.1
L$_9$*	3432.0	–	1625.2	1606.20	1262.30	–
C9 : [Zn(L$_9$)$_2$]	–	3434.6	1635.1	1547.5	1249.8	468.7

Powder X-ray diffraction analysis

The X-ray powder diffraction analysis was performed on an X-ray powder diffractometer with the scanning mode parameters: $2\theta/\theta$, scanning type; continuous, X-ray; 40 kV/20 mA, fixed monochromator within the 2θ range 10 to 90° at a step 0.02°. To observe the novelty of the synthesized complexes, a comparison was made between the observed patterns and reported patterns with peak search method. The measurements showed peaks present at different 2θ

values. From these values, the grain size, dislocation density, strain and unit cell parameters were calculated and are given in Table III.

TABLE III. Crystal data and structure refinement for bis((4-bromo-2-((E)-3-(4-chlorophenyl)acryloyl)naphthalen-1-yl)oxy)copper(II) (**C2**) and bis((4-bromo-2-((E)-3-(4-fluorophenyl)acryloyl)naphthalen-1-yl)oxy)zinc(II) (**C9**)

Complex	$[Cu(C_{19}H_{11}O_2BrCl)_2]$	$[Zn(C_{19}H_{11}O_2BrF)_2]$
Empirical formula	$Cu\ (C_{38}H_{22}O_4Br_2Cl_2)$	$Zn(C_{38}H_{22}O_4Br_2F_2)$
Formula weight	836.84	805.76
Temperature, K	298	298
Crystal system	Cubic	Cubic
Space group	*Fm–3m*	*Fm–3m*
a / Å	5.6384	5.6382
b / Å	5.6384	5.6382
c / Å	5.6384	5.6382
α / °	90	90
β / °	90	90
γ / °	90	90
Volume, Å^3	179.25	179.23
Z	4	4
ρ_{calc} / g cm^{-3}	31.009	29.860
μ / cm^{-1}	330.933	164.189
Crystallite size, nm	29.76360	30.54437
Dislocation density, nm^{-2}	1.12883	1.07186
Micro strain	6.63928	8.52797

Thermogravimetric analysis

The TGA analyses were performed on a Mettler Toledo instrument under an inert atmosphere. From the thermogram, it can be seen that a first weight loss step was observed in the range 30–100 °C. The weight loss continued gradually in second step in the range 100–800 °C. Weight loss in first step was due to the loss of uncoordinated water molecule then further weight loss in second step was due to the removal of ligands from the metal atom. The final residue was undetermined. Thus, the thermograms of studied complexes showed that almost all the complexes started to lose weight at a relatively high temperature, indicating the absence of coordinated water.

Magnetic moments

Zn(II) is diamagnetic, the Cu(II) complexes are paramagnetic and exhibit magnetic moments at room temperature in the solid state. The Cu(II) complexes showed magnetic moments in the range 1.84–1.95 BM, suggesting one electron in a square planar environment.

ESR analysis

The ESR analysis of the synthesized complexes was performed at room temperature. From the spectrum, the calculated value of $g_\parallel$ and $g\perp$ are respectively 2.2497 and 2.0972, and 2.0509 and 2.0066 for the C1 and C9 complexes respectively. The trend $g_\parallel > g\perp > g_e$ observed for the complexes indicates that the observed complexes have square planar geometry and that the unpaired electron lies in a dx^2-y^2 orbital.

^{1}H-NMR and ^{13}C-NMR analysis

In the ^{1}H-NMR analysis, peaks observed at δ values 7.760–8.578 ppm indicate the presence of aromatic protons and the peaks present at $\delta = 7.110$ ppm and $\delta = 7.740$ ppm revealed olefinic H_α and H_β protons, respectively, with a coupling constant value of 16 Hz. The peak present at δ 5.4 ppm indicates the presence of a phenolic –OH group. While the absence of a characteristic peak at $\delta = 14.0$ ppm for 2′-hydroxynapthyl proton confirms the formation of the complexes. In the ^{13}C-NMR analysis, the peaks observed in the δ value range 100 to 183 ppm indicate the presence of aromatic and olefinic carbons, the peak present at δ 188 ppm indicates the presence of a carbonyl carbon and the peak present at 89 ppm indicates the presence of a C–I bond.

Antimicrobial activity

The *in-vitro* antimicrobial activity of the complexes and their ligands are presented in Table IV.

TABLE IV. Antimicrobial activity of the complexes and their ligands; * – growth inhibitory activity of ligand against the tested pathogens[26]

Compound	S. aureus		E. coli		C. albicans	
	Average zone of inhibition, mm	Activity index	Average zone of inhibition, mm	Activity index	Average zone of inhibition, mm	Activity index
L$_1$*	–	1.2471	–	0.8358	–	1.03132
C1 : [Cu(L$_1$)$_2$]	19.84	1.3018	12.97	0.9120	18.63	1.14505
L$_2$*	–	0.5914	–	0.8749	–	0.82447
C2 : [Cu(L$_2$)$_2$]	11.37	0.7460	13.95	0.9810	19.64	1.20712
L$_3$*	–	0.8131	–	0.6981	–	0.86288
C3 : [Cu(L$_3$)$_2$]	14.70	0.9645	11.25	0.7911	15.33	0.94222
L$_4$*	–	0.7841	–	0.8309	–	0.84220
C4 : [Cu(L$_4$)$_2$]	14.15	0.9284	13.55	0.9528	15.92	0.97848
L$_5$*	–	0.8218	–	0.7096	–	0.77069
C5 : [Cu(L$_5$)$_2$]	14.91	0.9783	13.49	0.9486	17.48	1.07437
L$_9$*	–	0.5920	–	0.6826	–	0.76950
C9 : [Zn(L$_9$)$_2$]	11.14	0.7309	12.69	0.8924	15.17	0.93239
DMSO	No zone	–	No zone	–	No zone	–
Ampicilin	15.24	–	14.22	–	–	–
Fluconazole	–	–	–	–	16.27	–

Complexes **C1**, **C4** and **C5** exhibit potent antimicrobial activity against the tested pathogens, complexes **C2** and **C9** display significant antibacterial activity against *Echerchia coli* and antifungal activity against *Candida albicans*, while complex **C3** showed moderate antifungal activity against the pathogen *Candida albicans*. The activity of all complexes was enhanced compared to those of the corresponding ligands. This is because the synthesized complexes are bi-coordinated, and their ligands are associated with multiple halogen or hydroxyl substituents. These substituent supports boost the pharmacological activity.

The minimum inhibitory concentrations of complexes were determined using concentrations of 1.0, 0.5, 0.25 and 0.12 mg mL^{-1}. The observed *MIC* values of complexes and respective ligands are presented in Table V. The complexes **C1** and **C4** exhibited a significant *MIC* value of 0.12 mg mL^{-1} against all pathogens. The complex **C2** and **C5** show a significant *MIC* value of 0.12 mg mL^{-1} against the pathogen *E. coli* and *C. albicans.* The complexes **C3** and **C9** shows a moderate *MIC* value of 0.25 mg mL^{-1} against the pathogen *E. coli* and *C. albicans.* All complexes showed improved *MIC* values with respect to their respective ligands The increased potency is due to the presence of pharmacological active halogens or hydroxyl substituents in the ligands.

TABLE V. *MIC* values (mg mL^{-1}) of complexes and their ligands; a positive sign (+) indicates growth on the plate, a negative sign (–) indicates no growth on the plate; * – *MIC* mg mL^{-1} displayed by the ligands[26]

Ligand and complex	Pathogen											
	S. aureus				*E. coli*				*C. albicans*			
	1.0	0.5	0.25	0.12	1.0	0.5	0.25	0.12	1.0	0.5	0.25	0.12
L$_1$*	–	–	–	–	–	–	–	+	–	–	–	–
C1 : [Cu(L$_1$)$_2$]	–	–	–	–	–	–	–	–	–	–	–	–
L$_2$*	–	–	+	+	–	–	–	+	–	–	–	+
C2 : [Cu(L$_2$)$_2$]	–	–	+	+	–	–	–	–	–	–	–	–
L$_3$*	–	–	–	+	–	–	+	+	–	–	–	+
C3 : [Cu(L$_3$)$_2$]	–	–	–	+	–	–	–	+	–	–	–	+
L$_4$*	–	–	+	+	–	–	–	+	–	–	–	+
C4 : [Cu(L$_8$)$_2$]	–	–	–	–	–	–	–	–	–	–	–	–
L$_5$*	–	–	–	+	–	–	+	+	–	–	+	+
C5 : [Cu(L$_5$)$_2$]	–	–	–	+	–	–	–	–	–	–	–	–
L$_9$*	–	+	+	+	–	+	+	+	–	+	+	+
C9 : [Zn(L$_9$)$_2$]	–	–	+	+	–	–	–	+	–	–	–	+
Ampicilin	–	–	–	+	–	–	–	+				
Fluconazole									+	+	+	+

Cytotoxic activity

In a previous work, a series of ligand was synthesized with different substituent and their biological activity were examined. It was observed that some of them showed significant biological activity. The metal ion plays a significant role

in a bioactive profile. Upon coordination of the ligand with a metal ion, the bioactive profile may be enhanced and so it was our interest to evaluate those complexes which are associated with previously studied biological active ligands. Hence, complexes **C1**–**C5** and **C9** were selected for evaluation and their activities were studied and compared in the respective tables.

The cytotoxic activity of the synthesized complexes was screened in terms of their effect on live cells of the organism *Artemia salina*. Cytotoxic activity was evaluated in percentage mortality after treatment of test solution of different concentrations on live cells of *A. salina.* All the complexes displayed significant cytotoxic activity. The observed results are given in Table VI. Complexes **C3**––**C5** demonstrated LC_{50} values of 630.45, 969.99, 921.24 and 918.41 µM mL^{-1}, respectively. These values show that **C2**–**C5** are more potent than **C1** and **C9**. Complexes **C2**–**C4** contain –Cl and –Br substituents at the *ortho* and *para* position of the aromatic ring, whereas **C5** has –OH at the *meta/para* position of the aromatic ring and –Br substituent at the *para* position of the naphthyl moiety. Complexes **C1** and **C9** possess –OH, –I and –Br, –F substituent, respectively, are potentially active. All complexes are associated with a copper metal ion except complex **C9** that is associated with a zinc metal ion. From these observations, it could be concluded that complexes associated with a copper metal ion and the substituents –Cl, Br, –OH may lead to significant cytotoxic activity.

TABLE VI. Cytotoxic activity in terms of percentage mortality; ND – not detected; * – cytotoxicity and LC_{50} shown by the ligands[26]

| Complex | Mortality, % | | | | LC_{50} / µM mL^{-1} |
| | Sample concentration, µM mL^{-1} | | | | |
	1	10	100	1000	
L$_1$*	70	70	80	80	ND
C1 : [Cu(L$_1$)$_2$]	70	70	80	90	ND
L$_2$*	30	40	40	50	997.14
C2 : [Cu(L$_2$)$_2$]	30	30	40	60	630.45
L$_3$*	90	90	100	100	ND
C3 : [Cu(L$_3$)$_2$]	30	30	40	50	969.99
L$_4$*	90	80	100	100	ND
C4 : [Cu(L$_4$)$_2$]	40	40	50	50	921.94
L$_5$*	100	100	100	100	ND
C5 : [Cu(L$_5$)$_2$]	30	40	50	50	918.41
L$_9$*	90	90	100	100	ND
C9 : [Zn(L$_9$)$_2$]	90	90	100	100	ND

MTT Assay

The *in-vitro* anticancer activity was evaluated by the MTT assay. The growth inhibitory activity of complexes was determined against the liver cancer cells (HepG2). All complexes displayed inhibitory activity against liver cancer

cells. The complexes **C2–C5** were showed IC_{50} values of 392.64, 896.64, 490.40 and 58.94 μg mL^{-1}, respectively (Table VII). These values specify that the **C2–C5** complexes are more potent than the **C1** and **C9** complexes. The complexes **C2–C4** have –Cl and –Br substituents at the *ortho* and *para* position of the aromatic ring, whereas **C5** has –OH at the meta/para position of the aromatic ring and a –Br substituent at the *para* position of the naphthyl moiety. The complexes **C1** and **C9** possessing –OH, –I and –Br, –F substituents at the respective position showed moderate activity. All complexes associated with a copper metal ion and complex **C9**, which is associated with the zinc metal ion, show potency in anticancer activity. From these observations, it was concluded that the complexes associated with the copper metal ion and the attached substituents –Cl, Br, –OH may lead to significant anticancer activity.

TABLE VII. The IC_{50} values of the complexes and their ligands; standard, 5-flurouracil: 97.22 μM mL^{-1}; * – The IC_{50} values shown by the ligands[26]

Complex	IC_{50} / μM mL^{-1}	Ligand	IC_{50}* / μM mL^{-1}
C1 : $[Cu(L_1)_2]$	>1000	L_1	ND
C2 : $[Cu(L_2)_2]$	392.64	L_2	416.66
C3 : $[Cu(L_3)_2]$	896.64	L_3	ND
C4 : $[Cu(L_4)_2]$	490.40	L_4	536.66
C5 : $[Cu(L_5)_2]$	58.94	L_5	91.85
C9 : $[Zn(L_9)_2]$	>1000	L_9	ND

CONCLUSIONS

Novel Cu(II) and Zn(II) complexes with hydroxylated 1,3-diaryl-2-propene-1-ones ligands were synthesized. All the metal complexes were characterized by various spectroscopic and analytical techniques. The data suggested a square planar structure of Cu(II) and Zn(II) complexes with 1:2 (metal:ligand) stoichiometry. Their *in-vitro* antimicrobial activity was evaluated by the agar cup plate method against gram positive bacteria *Staphylococcus aureus* and Gram-negative bacteria *Echerchia coli* and the yeast *Candida albicans*. All complexes showed enhanced antimicrobial activity than its ligands. The complexes **C1** and **C4** showed the significant activity with *MIC* values of 0.12 mg mL^{-1} against all the tested pathogens. The complexes **C2** and **C5** showed significant activity with *MIC* values of 0.12 mg mL^{-1} against the *E. coli* and *C. albicans* and the complexes **C3** and **C9** showed moderate activity with *MIC* values of 0.25 mg mL^{-1} against *E. coli* and *C. albicans*. Their anticancer activity was evaluated against a liver cancer cell line. The complex **C5** showed significant activity with an IC_{50} value 58.94 μg mL^{-1}, while complexes **C2–C4** showed moderate activity with IC_{50} values 392.64, 896.64 and 490.40 μg mL^{-1}, respectively. Hence, the complexes contained pharmacological active substituents, such as hydroxyl, chloro and bromo at the *ortho* and *para* positions of the aromatic ring, shows potentially

antimicrobial and anticancer activity. Therefore, this synthetic methodology and antimicrobial results serve as preliminary screening for the development of new antimicrobial and anticancer agents by new complex synthesis.

SUPPLEMENTARY MATERIAL

Additional data are available electronically at the pages of journal website: https://www.shd-pub.org.rs/index.php/JSCS/index, or from the corresponding author on request.

ИЗВОД

СИНТЕЗА, КАРАКТЕРИЗАЦИЈА, АНТИМИКРОБНА И ЦИТОТОКСИЧНА ИСПИТИВАЊА КОМПЛЕКСА БАКРА(II) И ЦИНКА(II) СА ХИДРОКСИЛОВАНИМ БИДЕНТАТНИМ 1,3-ДИАРИЛ-2-ПРОПЕН-1-ОН ЛИГАНДИМА

PRAVINKUMAR PATIL[1] и SAINATH ZANGADE[2]

[1]*Research Laboratory, Department of Chemistry, N.E.S. Science College, Nanded-431605(MS), India* и
[2]*Department of Chemistry, Madhavrao Patil, ACS College, Palam, Dist. Parbhani-431720 (MS), India*

Описана је синтеза различитих бинарних комплекса метала (халоген, хидроксил и метокси супституисани бис(2-(E)-акрилоил)нафтален-1-ил)окси)-бакар(II) и цинк(II), **C1**–**C10**) који садрже хидроксиловане бидентато координоване 1,3-диарил-2-пропен-1-он лиганде. Синтетисани комплекси су структурно окарактерисани помоћу FT-IR, ^{1}H-NMR, ^{13}C-NMR, ESR спектроскопије, XRD и TGA анализе. На бази FT-IR и ESR испитивања потврђено је да су лиганди преко карбонилног и депротонованог хидроксилног атома кисеоника бидентато координовани за јоне метала и да сви комплекси имају квадратно-планарну геометрију. Извршена су *in-vitro* испитивања антимикробне и цитотоксичне активности комплекса. Комплекси **C1** и **C4** су показали значајну антимикробну активност, док је активност осталих комплекса била осредња. Испитивана је цитотоксична активност комплекса према *Artemia salina*. За комплексе **C2**–**C5** добијене су следеће IC_{50} вредности: 630,45, 969,99, 921,94 и 918,41 µM mL^{-1}. Поред тога, испитивана је антитуморска активност комплекса према туморској ћелијској линији јетре (Hep G2), при чему је комплекс **C5** показао највећу активност у односу 5-флуороурацил стандард (IC_{50} = 58,94 µg mL^{-1}). Добијени резултати су од значаја за развој нове класе антимикробних и антитуморских агенаса.

(Примљено 1. септембра, ревидирано 14. октобра, прихваћено 2. новембра 2020)

REFERENCES

1. W. Dan, J. Dai, *Eur. J. Med. Chem*. 187 (2019) 111980 (https://doi.org/10.1016/j.ejmech.2019.111980)
2. A. M. Asiri, S. A. Khan, *Molecules* **16** (2011) 523 (https://doi.org/10.3390/molecules16010523)
3. D. Kakati, J. C. Sarma, *Chem. Cent. J.* **5** (2011) 1 (http://dx.doi.org/10.1186/1752-153X-5-8)
4. H. Albuquerque, C. Santos, J. Cavaleiro, A. Silva, *Curr. Org. Chem.* **18** (2014) 2750 (https://doi.org/10.2174/1385272819666141013224253)
5. J. S. Biradar, B. S. Sasidhar, R. Parveen, *Eur. J. Med. Chem.* **45** (2010) 4074 (https://doi.org/10.1016/j.ejmech.2010.05.067)

6. B. P. Bandgar, S. S. Gawande, *Bioorgan. Med. Chem.* **18** (2010) 2060
    (https://doi.org/10.1016/j.bmc.2009.12.077)
7. P. S. Bhale, H. V. Chavan, S. B. Dongare, S. N. Shringare, Y. B. Mule, S. S. Nagane, B.
    P. Bandgar, *Bioorg. Med. Chem. Lett.* **27** (2017) 1502
    (https://doi.org/10.1016/j.bmcl.2017.02.052)
8. M. Liu, P. Wilairat, M. L. Go, *J. Med. Chem.* **44** (2001) 4443
    (http://dx.doi.org/10.1021/jm0101747)
9. F. M. Atlam, M. N. El-Nahass, E. A. Bakr, T. A. Fayed, *Appl. Organomet. Chem.* **32**
    (2018) 1 (https://doi.org/10.1002/aoc.3951)
10. P. Patil, G. Bhopalkar, S. Zangade, *Curr. Microwave Chem.* **7** (2020) 145
    (https://doi.org/10.2174/2213335607666200129113827)
11. C. Sulpizio, J. Breibeck, A. Rompel, *Coord. Chem. Rev.* **374** (2018) 497
    (https://doi.org/10.1016/j.ccr.2018.05.023)
12. J. Johnson, A. Yardily, *J. Coord. Chem.* **72** (2019) 2437
    (https://doi.org/10.1080/00958972.2019.1669022)
13. D. Krajčiová, M. Melník, E. Havránek, A. Forgácsová, P. Mikuš, *J. Coord. Chem.* **67**
    (2014) 1493 (https://doi.org/10.1080/00958972.2014.915966)
14. L. Dkhar, V. Banothu, E. Pinder, R. M. Phillips, W. Kaminsky, M. R. Kollipara,
    Polyhedron **185** (2020) 114606 (https://doi.org/10.1016/j.poly.2020.114606)
15. D. K. Mahapatra, S. K. Bharti, V. Asati, S. K. Singh, *Eur. J. Med. Chem.* **174** (2019) 142
    (https://doi.org/10.1016/j.ejmech.2019.04.032)
16. S. Shukla, A. P. Mishra, *Arab. J. Chem.* **12** (2019) 1715
    (https://doi.org/10.1016/j.arabjc.2014.08.020)
17. N. Patel, A. K. Prajapati, R. N. Jadeja, I. P. Tripathi, N. Dwivedi, *J. Coord. Chem.* **73**
    (2020) 1131 (https://doi.org/10.1080/00958972.2020.1774562)
18. A. Levina, P. A. Lay, *Dalton Trans.* **40** (2011) 11675
    (https://doi.org/10.1039/C1DT10380F)
19. O. I. Edozie, O. J. Godday, A. K. Chijioke, I. O. Uchenna, N. F. Chigozie, *Bull. Chem.
    Soc. Ethiop.* **34** (2020) 83 (https://dx.doi.org/10.4314/bcse.v34i1.8)
20. M. Iqbal, S. Ali, M. Tahir, M. Haleem, H. Gulab, N. Shah, *J. Serb. Chem. Soc.* **85** (2020)
    203 (https://doi.org/10.2298/JSC190423065I)
21. A. D. Cort, P. De Bernardin, G. Forte, F. Y. Mihan, *Chem. Soc. Rev.* **39** (2010) 3863
    (http://dx.doi.org/10.1039/B926222A)
22. C. T. Liu, A. A. Neverov, R. S. Brown, *J. Am. Chem. Soc.* **130** (2008) 13870
    (http://dx.doi.org/10.1021/ja805801j)
23. S. J. Hosseinimehr, S. Emami, S. M. Taghdisi, S. Akhlaghpoor, *Eur. J. Med. Chem.* **43**
    (2008) 557 (https://dx.doi.org/10.1016/j.ejmech.2007.04.013)
24. Y. Q. Liu, X. M. Luo, H. J. Jiang, Z. Q. Zhang, *Russ. J. Coord. Chem. (Khimiya)* **44**
    (2018) 317 (https://dx.doi.org/10.1134/S1070328418050032)
25. S. Liu, W. Cao, L. Yu, W. Zheng, L. Li, C. Fan, T. Chen, *J. Chem. Soc. Dalton Trans.* **42**
    (2013) 5932 (http://dx.doi.org/10.1039/C3DT33077J)
26. P. Patil, P. A. Khan, S. Zangade, *Curr. Chem. Lett.* **9** (2020) 1838
    (http://www.growingscience.com/ccl/Vol9/ccl_2020_5.pdf).

Journal of the Serbian Chemical Society

Synthesis, characterization, antimicrobial screening and cytotoxic properties of Cu(II) and Zn(II) complexes with a bidentate hydroxylated 1,3-diaryl-2-propene-1-one ligand

PRAVINKUMAR PATIL[1] and SAINATH ZANGADE[2]

[1]*Research Laboratory, Department of Chemistry, N.E.S. Science College, Nanded-431605 (MS), India and* [2]*Department of Chemistry, Madhavrao Patil, ACS College, Palam, Dist. Parbhani-431720 (MS), India*

TABLE S-I. Preparation of complexes **C1**–**C10**

Metal chloride	Ligand*		Complex[a,b]	
Amount taken for synthesis, mg (0.25 mmol)	Molecular formula	Amount taken for synthesis, mg (0.50 mmol)	Molecular formula	Yield, %
43	$C_{19}H_{11}O_3I_3$	334	$CuC_{38}H_{20}O_6I_6$	58
43	$C_{19}H_{12}O_2$ BrCl	194	$CuC_{38}H_{22}O_4Br_2Cl_2$	60
43	$C_{19}H_{12}O_2$ BrCl$_2$	211	$CuC_{38}H_{20}O_4Br_2Cl_4$	62
43	$C_{19}H_{12}O_2$ BrCl$_2$	211	$CuC_{38}H_{20}O_4Br_2Cl_4$	54
43	$C_{19}H_{13}O_4$ Br	193	$CuC_{38}H_{24}O_8Br_2$	63
34	$C_{19}H_{15}O_2$ Br	192	$ZnC_{40}H_{28}O_6Br_2$	61
34	$C_{19}H_{12}O_2$ Br$_2$	216	$ZnC_{38}H_{22}O_4Br_4$	59
34	$C_{19}H_{13}O_3$ Br	185	$ZnC_{38}H_{24}O_6Br_2$	57
34	$C_{19}H_{12}O_2$ BrF	186	$ZnC_{38}H_{22}O_4Br_2F_2$	58
34	$C_{19}H_{13}O_4$ I	216	$ZnC_{38}H_{24}O_8I_2$	62

* Physical data of ligand.[1]

CHARACTERIZATION

Bis((2-((E)-3-(2-hydroxy-3,5-diiodophenyl)acryloyl)-4-iodonaphthalen-1-yl)oxy)copper(II) (***C1***). Yield: 58 %; brown solid; m.p.: >300 °C decomposition; FTIR (KBr, cm⁻¹): 3434.8 (s, OH), 1643.2 (m, C=O), 1433.2 (m, C=C), 1207.2 (m, CO), 558.3 (m, CuO); ¹H-NMR (500 MHz, DMSO, δ / ppm): 5.41 (2H, *s*), 7.11 (2H, *d*, *J* = 16 Hz), 7.74 (2H, *d*, *J* = 16 Hz), 7.76-8.57 (14H, *m*); ¹³C-NMR (125 MHz, DMSO, δ / ppm): 89.38, 100.22, 108.07, 113.10, 123.62, 136.50, 140.74, 147.81, 151.74, 164.62, 172.00, 183.31, 188.50; ESR: $g_{\parallel}$: 2.2497, $g_{\perp}$: 2.0972.

Bis((4-bromo-2-((E)-3-(4-chlorophenyl)acryloyl)naphthalen-1-yl)oxy)copper(II) (***C2***). Yield: 60 %; brown solid; m.p.: >300 °C decomposition; FTIR (KBr, cm⁻¹): 3410.6 (s, OH), 1523.5 (m, C=O), 1491.2 (m, C=C), 1256.5 (m, C-O), 526.5 (m, Cu-O); ¹H-NMR (500 MHz, DMSO, δ / ppm): 7.28 (2H, *d*, *J* = 16 Hz), 7.60 (2H, *d*, *J* = 16 Hz), 7.76-8.36 (18H, *m*); ¹³C-

NMR (125 MHz, DMSO, δ / ppm): 92.83, 104.14, 109.80, 125.98, 134.46, 145.14, 148.91, 159.75, 174.20, 177.19.

Bis((4-bromo-2-((E)-3-(2,6-dichlorophenyl)acryloyl)naphthalen-1-yl)oxy)copper(II) *(C3)*. Yield: 62 %; brown; m.p.: >300 °C decomposition; FTIR (KBr, cm^{-1}): 3463.7 (s, OH), 1635.1 (m, CO), 1606.2 (m, C=C), 1255.7 (m, C-O), 599.4 (m, Cu-O).

Bis((4-bromo-2-((E)-3-(2,4-dichlorophenyl)acryloyl)naphthalen-1-yl)oxy)copper(II) *(C4)*. Yield: 54 %; brown; m.p.: >300 °C decomposition; FTIR (KBr, cm^{-1}): 3463.8 (s, OH), 1633.8 (m, C=O), 1572.7 (m, C=C), 1251.2 (m, C-O), 601.9 (m, Cu-O); ^{1}H-NMR (500 MHz, DMSO, δ / ppm): 7.10 (2H, *d*, *J* = 16 Hz), 7.53 (2H, *d*, *J* = 16 Hz), 7.67-8.72 (16H, *m*); ^{13}C-NMR (500 MHz, DMSO, δ / ppm): 82.94, 92.21, 106.19, 108.86, 128.18, 131.01, 151.58, 156.77, 160.54, 169.18, 171.69, 180.17, 182.69, 189.28.

Bis((4-bromo-2-((E)-3-(3,4-dihydroxyphenyl)acryloyl)naphthalen-1-yl)oxy)copper(II) *(C5)*: Yield: 63 %; brown; m.p.: >300 °C decomposition; FTIR (KBr, cm^{-1}): 3416.3 (s, OH), 1611.8 (m, C=O), 1585.5 (m, C=C), 1253.5 (m, C-O), 594.1 (m, Cu-O).

Bis((4-bromo-2-((E)-3-(4-fluorophenyl)acryloyl)naphthalen-1-yl)oxy)zinc(II) *(C9)*. Yield: 58 %; brown; m.p.: >300 °C decomposition; FTIR (KBr, cm^{-1}): 3434.6 (s, OH), 1635.1 (m, C=O), 1547.5 (m, C=C), 1249.8 (m, C-O), 468.7 (m, Cu-O); ^{1}H-NMR (500 MHz, DMSO, δ / ppm): 6.88 (2H, *d*, *J* = 16Hz), 7.47 (2H, *d*, *J* = 16 Hz), 7.76-8.58 (18H, m); ^{13}C-NMR (500 MHz, DMSO, δ / ppm): 101.32, 117.34, 125.19, 126.92, 131.95, 141.22, 142.63, 152.84, 156.45, 159.91, 165.09, 170.12, 183.16, 185.20,186.46; ESR: $g_{\parallel}$: 2.0509, $g_{\perp}$: 2.0066.

TABLE S-II. Crystal data and structure refinement

Complex	[Cu(C$_{19}$H$_{10}$O$_3$I$_3$)$_2$]	[Cu(C$_{19}$H$_{10}$O$_2$BrCl$_2$)$_2$]	Zn(C$_{19}$H$_{12}$O$_4$I)$_2$
Empirical formula	Cu(C$_{38}$H$_{20}$O$_6$I$_6$)	Cu(C$_{38}$H$_{20}$O$_4$Br$_2$Cl$_4$)	ZnC$_{38}$H$_{24}$O$_8$I$_2$
Formula weight	1397.53	905.73	927.78
Temperature, K	298	298	298
Crystal system	Orthorhombic	Orthorhombic	Orthorhombic
Space group	P b c a	P c a 21	P n m a
a / Å	16.8478	14.6387	22.2520
b / Å	12.4058	10.2508	17.6363
c / Å	27.8294	18.8246	11.3842
α / °	90	90	90
β / °	90	90	90
γ / °	90	90	90
Volume, Å^3	5816.64	2824.79	4467.65
Z	16	4	4
ρ_{calc} g / cm^{-3}	6.383	2.130	1.379
μ / cm^{-1}	5.744	38.815	30.222
Crystallite size, nm	24.70794	29.28896	13.16591
Dislocation density, nm^{-2}	1.63805	1.16571	5.76897
Micro strain	12.93231	7.72544	19.39073

MTT Assay

In-vitro anticancer activity was evaluated by MTT assay. The growth inhibitory activity of complexes was determined against liver cancer cells (HepG2). Activity data is presented in Fig. 26.
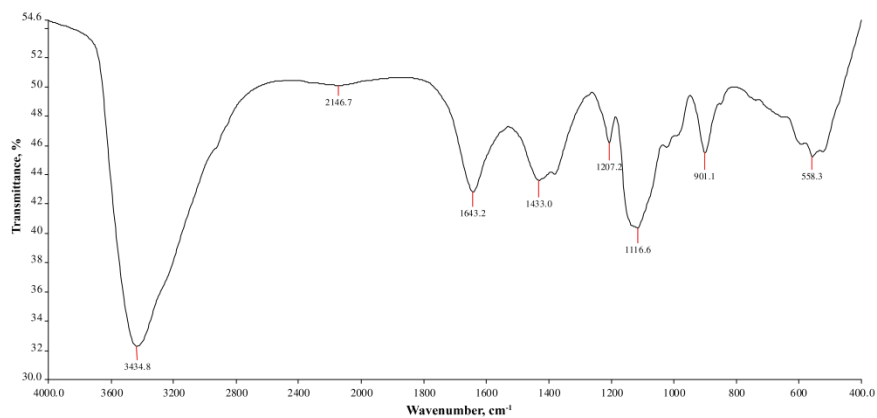
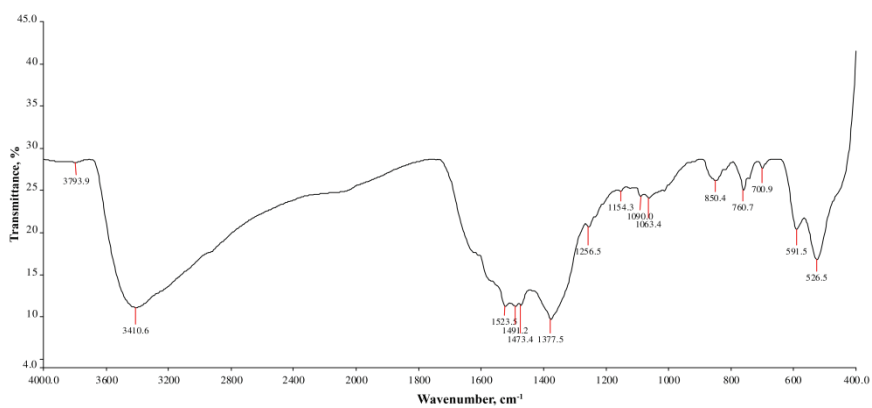Figure S-1. FTIR Spectrum of complex C1
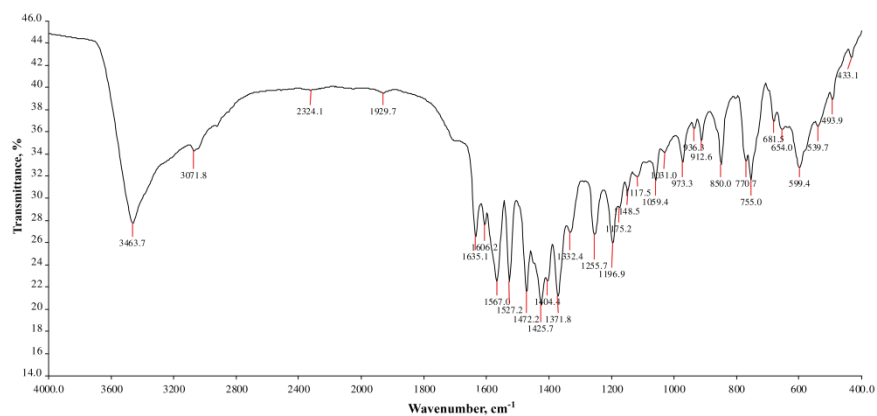

Figure S-2. FTIR Spectrum of complex C2

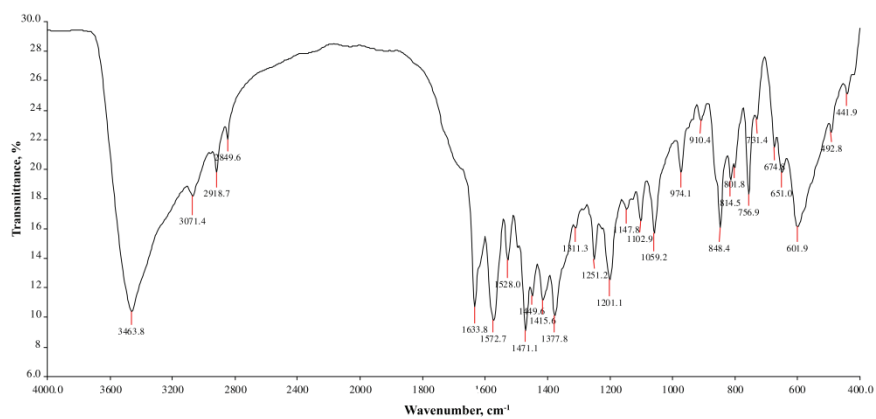Figure S-3. FTIR Spectrum of complex C3

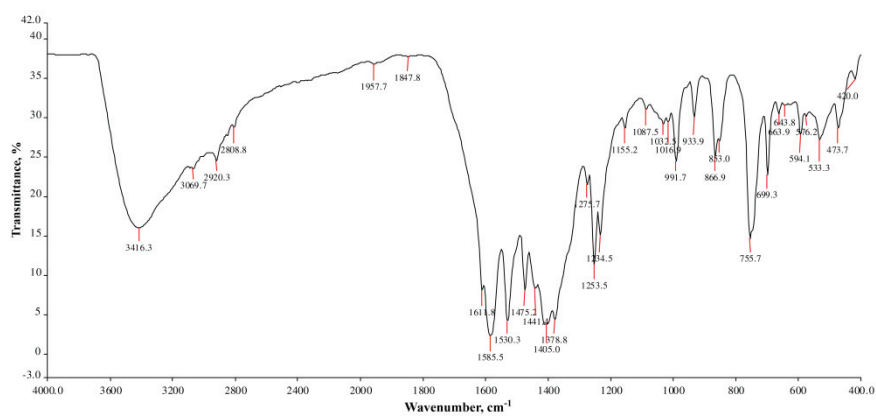Figure S-4. FTIR Spectrum of complex C4

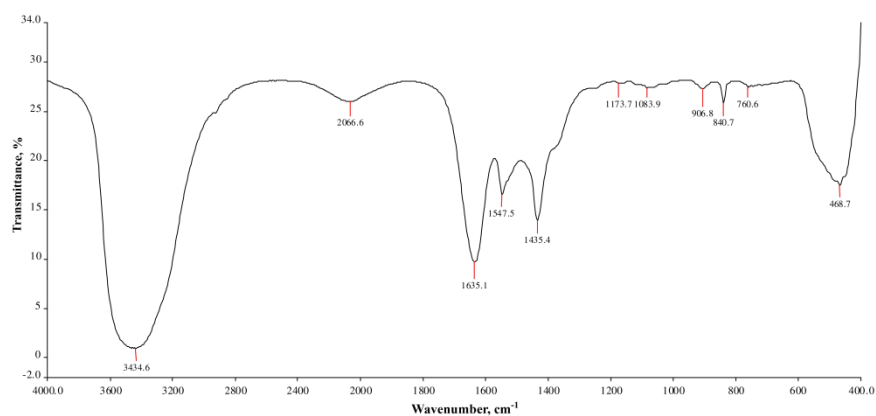Figure S-5. FTIR Spectrum of complex C5

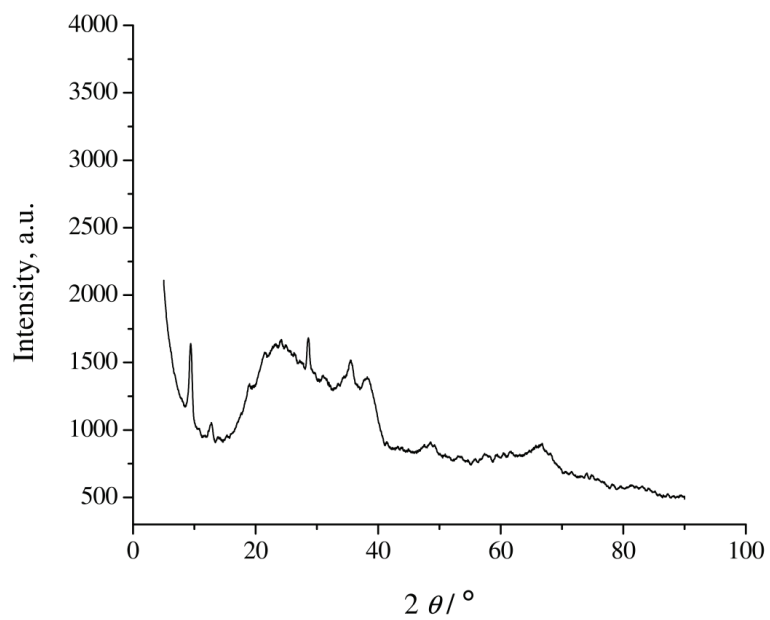Figure S-6. FTIR Spectrum of complex C9
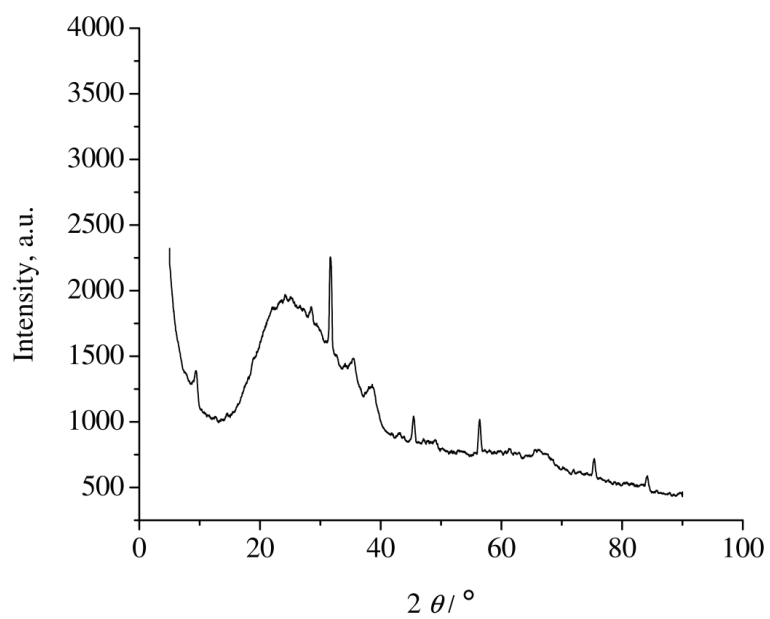
Figure S-7. XRD of complex C1
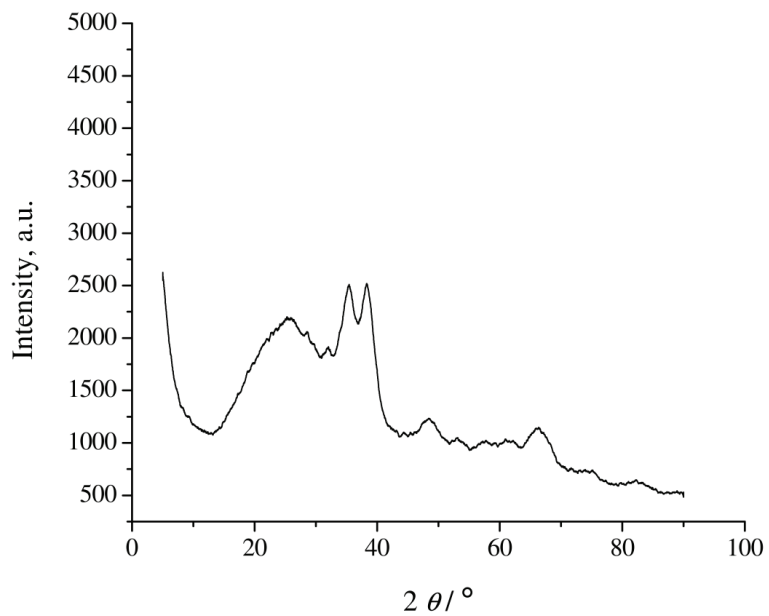

Figure S-8. XRD of complex C2
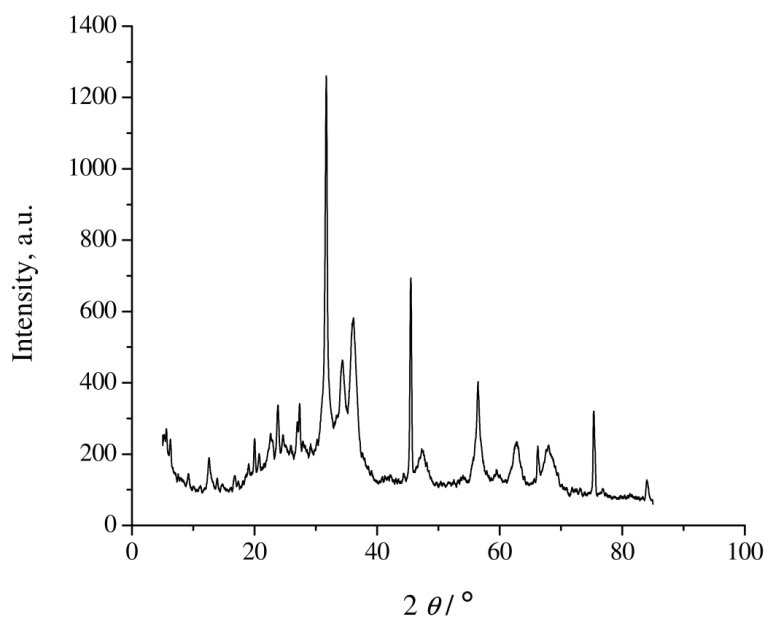
Figure S-9. XRD of complex C4

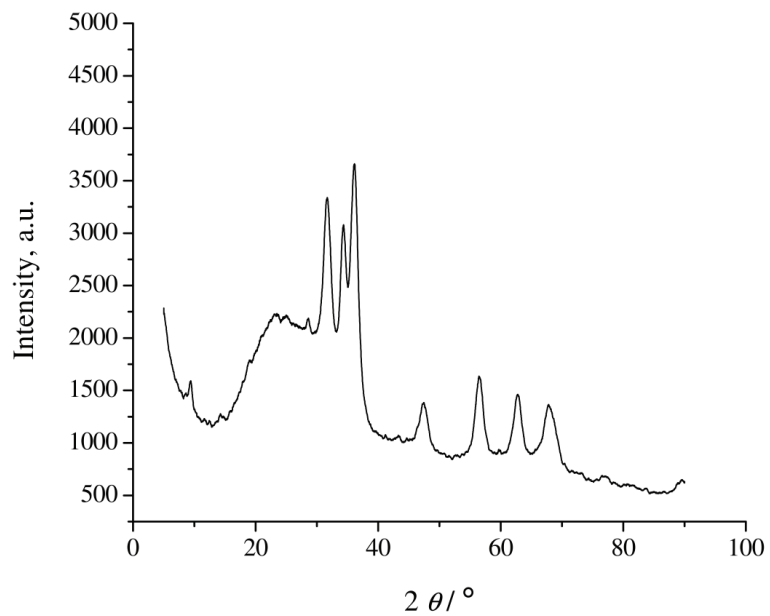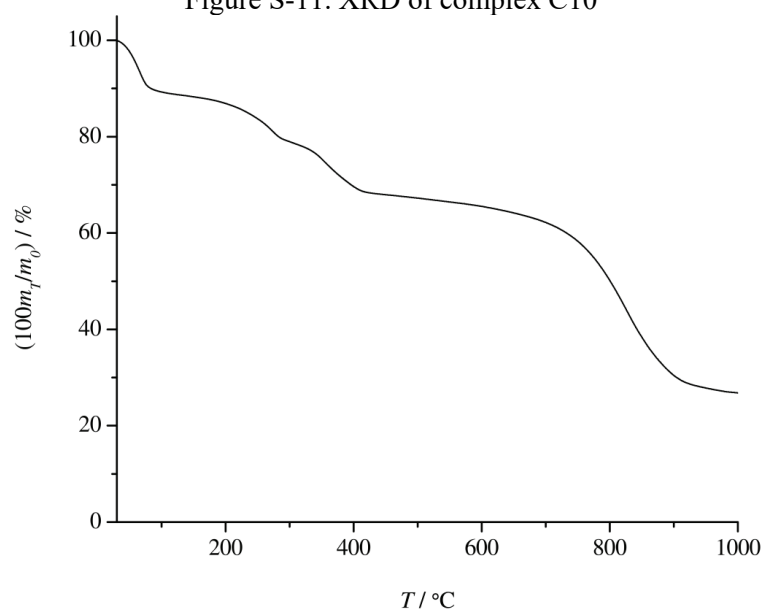Figure S-10. XRD of complex C9

Figure S-11. XRD of complex C10
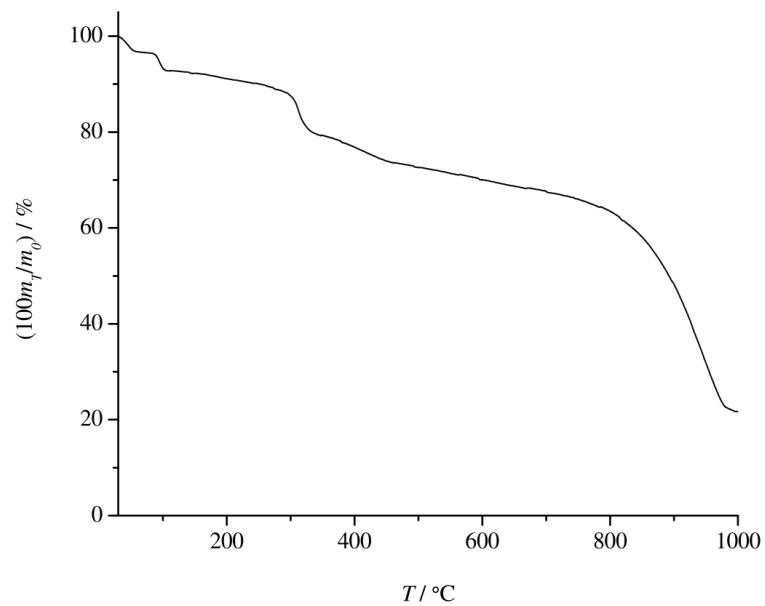

Figure S-12. TGA of complex C1
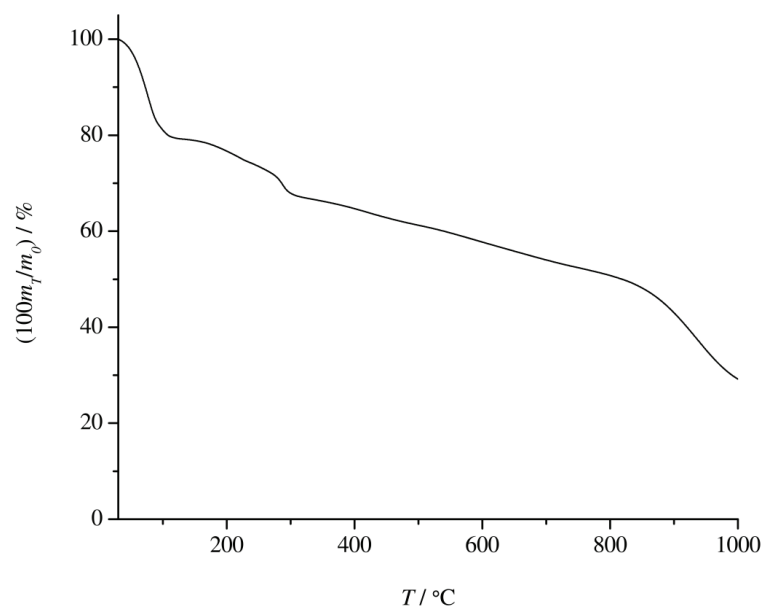
Figure S-13 TGA of complex C3

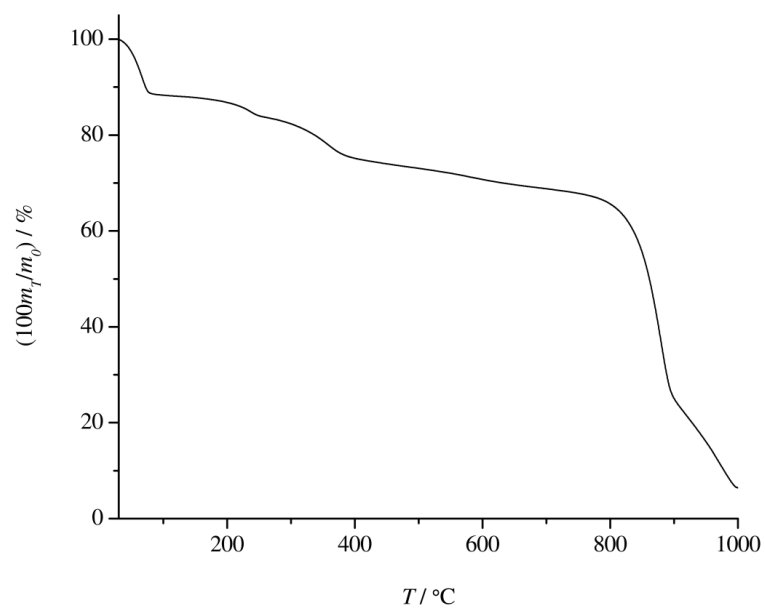Figure S-14. TGA of complex C4

Figure S-15. TGA of complex C9
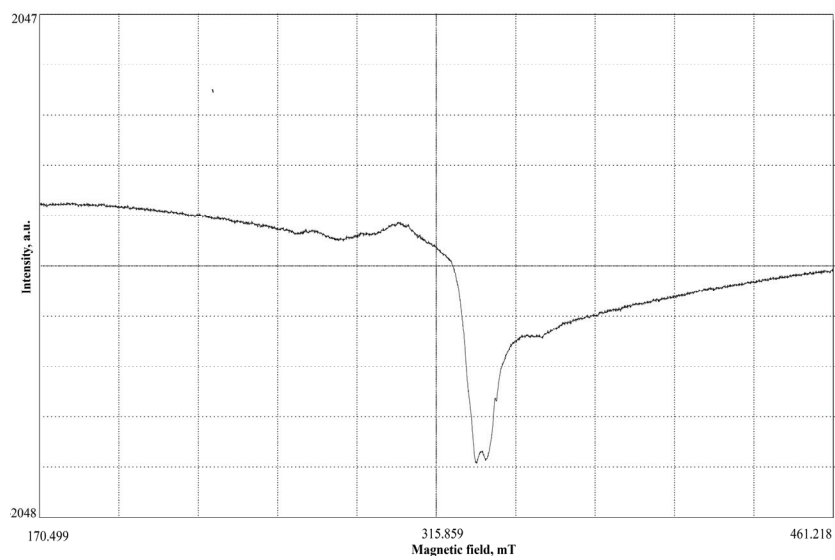
Figure S-16. ESR of complex C1
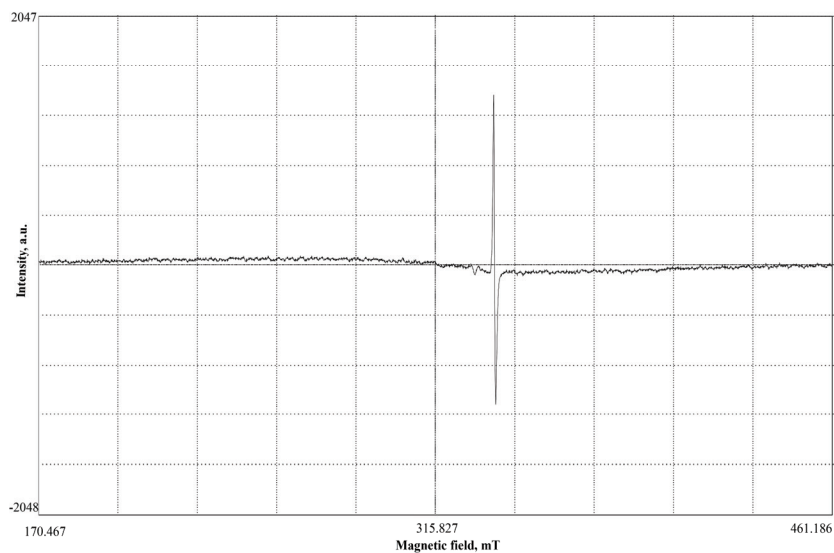
Figure S-17. ESR of complex C9
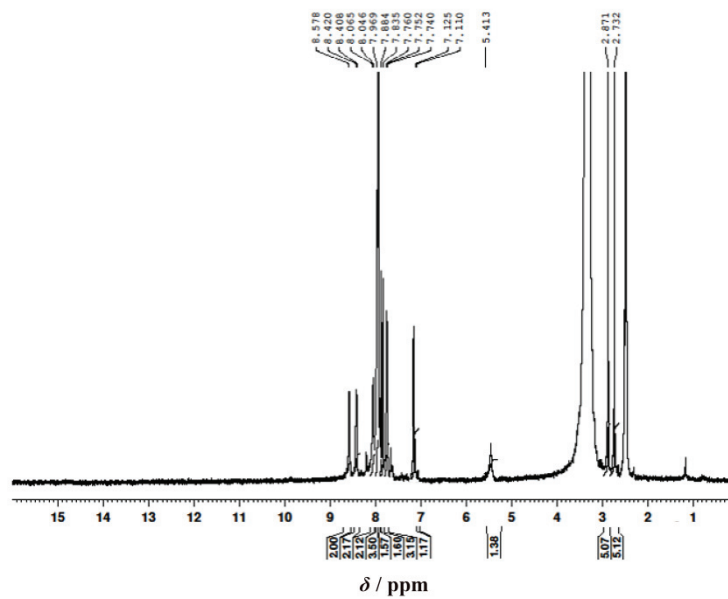
Figure S-18. ^{1}H NMR spectrum of complex C1
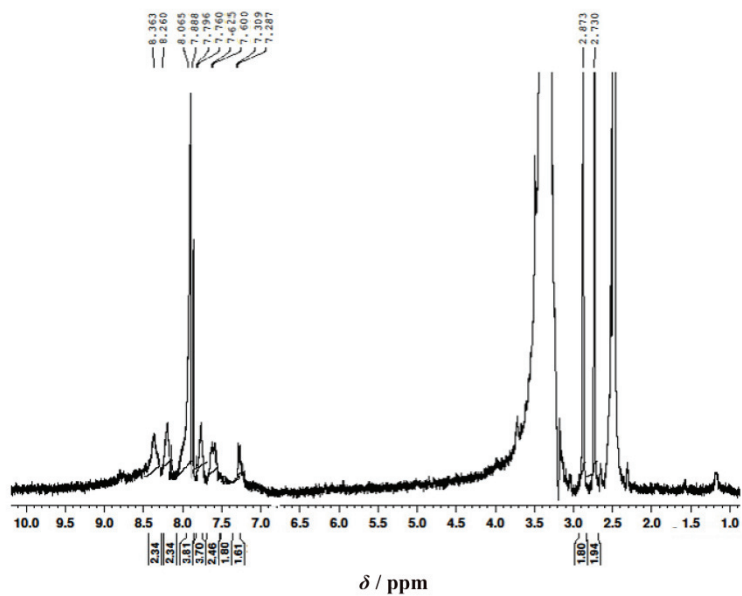
Figure S-19. ^{1}H NMR spectrum of complex C2
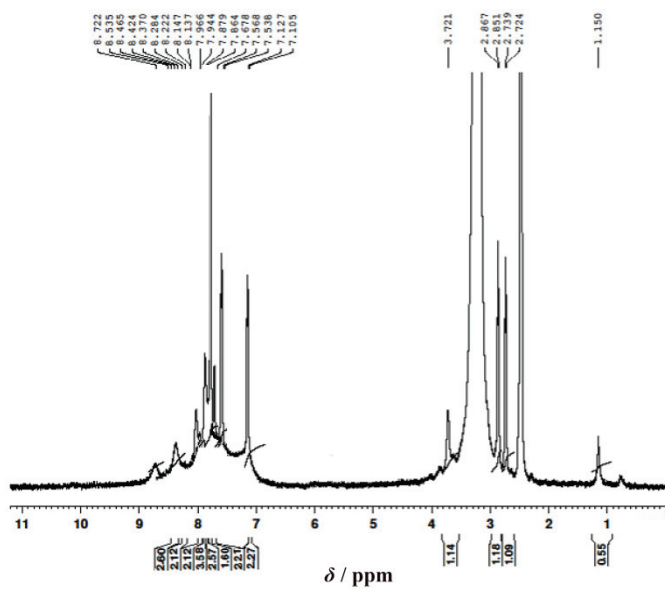
Figure S-20. ^{1}H NMR spectrum of complex C4
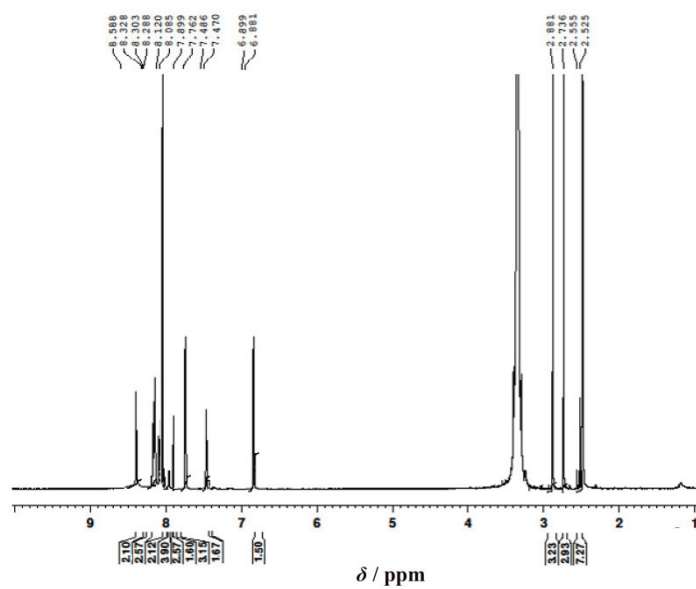
Figure S-21. ^{1}H NMR spectrum of complex C9
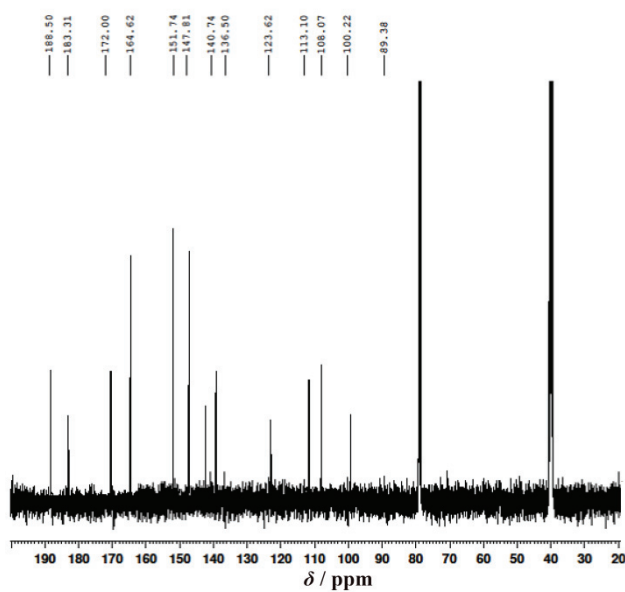
Figure S-22. ^{13}C NMR spectrum of complex C1

PATIL and ZANGADE
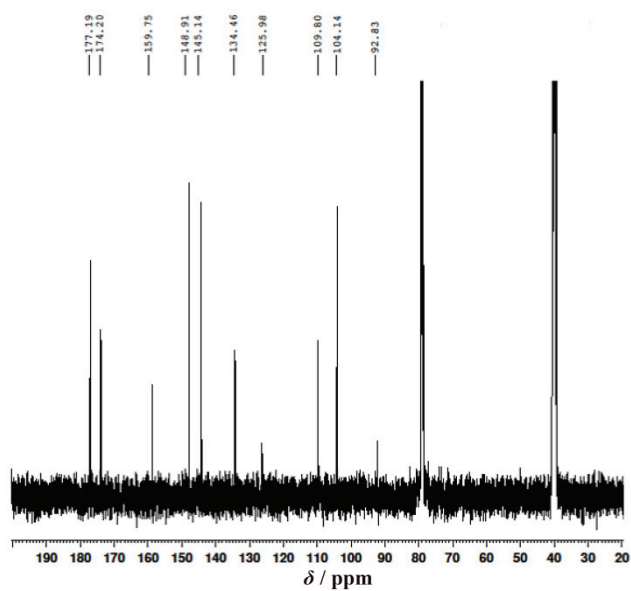
Figure S-23. ^{13}C NMR spectrum of complex C2
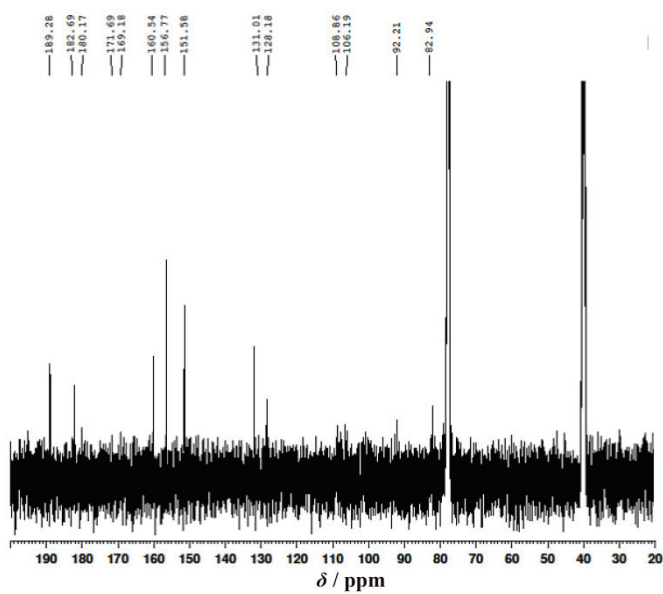
Figure S-24. ^{13}C NMR spectrum of complex C4
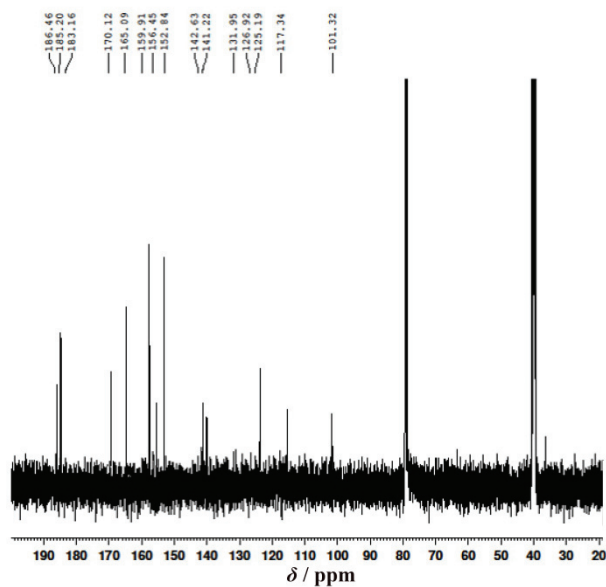
Figure S-25. ^{13}C NMR spectrum of complex C9
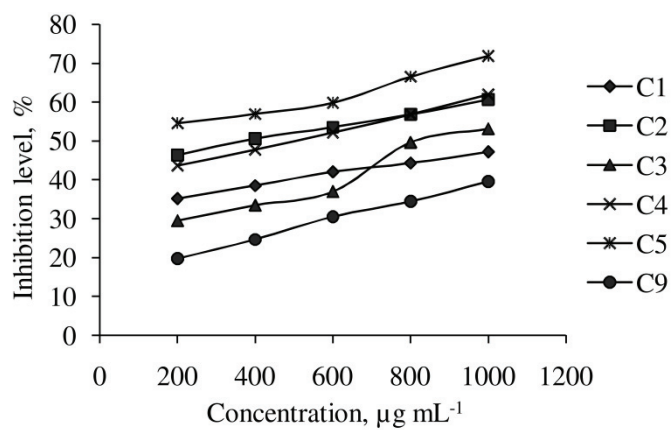
Figure S-26. Graph of sample concentration against the inhibition level

REFERENCE

1. P. Patil, P. A. Khan, S. Zangade, *Curr. Chem. Lett.* **9** (2020) 183–198
(http://www.growingscience.com/ccl/Vol9/ccl_2020_5.pdf)

Journal of the Serbian Chemical Society

A simple computational approach for pK_a calculation of organosulfur compounds

SYED TAHIR ALI*, ANEESA CHOUDHARY[1], SYED MAJID KHALIL[2]
and ARIF ZUBAIR[3]

[1]*Department of Chemistry, Federal Urdu University of Arts Science and Technology, Karachi, Pakistan,* [2]*Bosch Pharmaceutical Private Limited, Plot No. 209, Sector 23, Korangi Industrial Area, Karachi, Pakistan and* [3]*Department of Environmental Science, Federal Urdu University of Arts Science and Technology, Karachi, Pakistan*
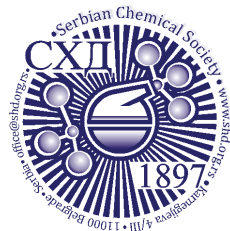
Abstract: The present work is related to predicting the pK_a values of organosulfur compounds through the density functional theory (DFT). In this study, 22 organosulfur compounds were considered to calculate the theoretical pK_a values. The main emphasis was given on the substitution of different groups on the sulfur atom. The computations were performed in the presence of dimethyl sulfoxide (DMSO) as solvent. Experimentally, the order of increase of acidity is; sulfides < sulfoxides < sulfones. The herein computed pK_a values also follow the same order. The theoretical pK_a values were computed using the DFT method B3LYP, with the basis sets 6-31G(d), 6-31+G(d,p) and the IEFPCM bulk solvation model. The majority of the pK_a values computed through the diffuse function basis set were in excellent agreement with the experimental ones. Hence this computational approach, B3LYP/6-31+G(d,p)/IEFPCM, could be utilized to predict the pK_a values of these types of organosulfur compounds.

Keywords: DFT method; diffuse function basis set; DMSO solvent.

INTRODUCTION

The acid dissociation constant (pK_a) is an important property of many organic compounds and it is strongly related to their applications. Fast and accurate methods for determining aqueous pK_a values of organic compounds would have a wide range of applications. Aside from experimental measurements, theoretical determination of the acidity of a compound has been an important and challenging objective of computational chemistry.[1,2] The computations (theoretical calculations) are a reconfirmation of experimental results. A

---

computation provides an idea of the structural information of a molecule in vacuum (gas phase), which is difficult to obtain through experiments. Theoretical calculations are also helpful in providing information for the determination of the preferred protonation site when more than one site is available.[3]

Organosulfur compounds have many important applications, which have already been reported in literature.[4–7] In this communication, we are presenting a very easy computational approach for theoretical calculation of pK_a values. This theoretical model is employed for three types of organosulfur compounds, *i.e.*, sulfides, sulfoxides and sulfones. Different kinds of substituents were selected that were attached on both sides of the sulfur atom. The structures of compounds considered for pK_a calculation are shown in Fig. 1. The significance of this computational model is that it could be uniformly applied for sulfides, sulfoxides and sulfones.
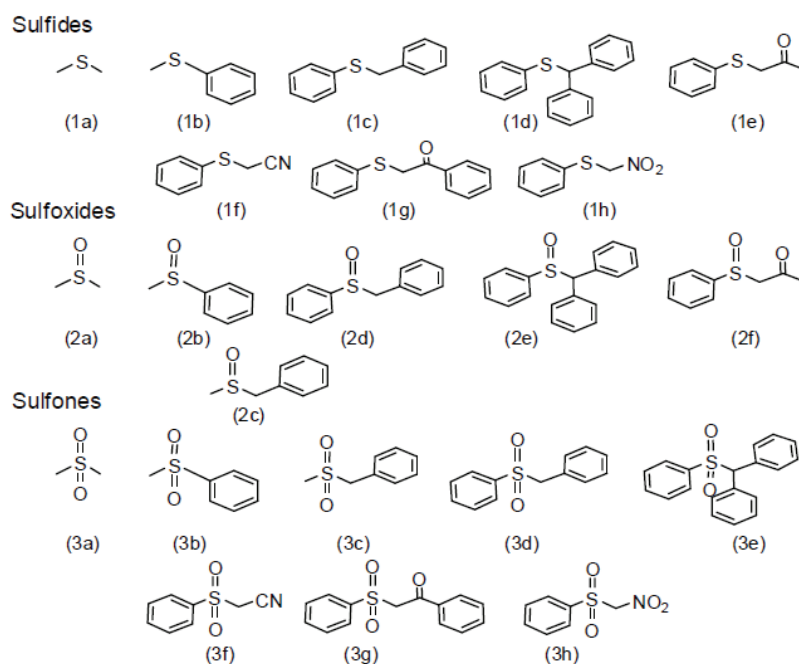
Fig. 1. Compounds considered for the theoretical pK_a calculations.

This computational protocol was developed in previous studies related to pK_a calculations.[8,9] In these studies, it was shown that the theoretically calculated pK_a values could be utilized to resolve discrepancies in experimental pK_a values. These computational studies were performed with different solvation models but only water was used as the solvent.

EXPERIMENTAL

The experimental pK_a values of different derivatives of sulfide, sulfoxide and sulfone were obtained from literature.[10-13] These experimental pK_a values are determined in DMSO as solvent. The series starts with the simple forms, *i.e.*, dimethyl sulfide, dimethyl sulfoxide and dimethyl sulfone. Other derivatives were set by variation of different groups (see Fig. 1). First, the geometries of all the considered compounds were drawn with the help of GaussView 6.[14] Then the molecular modeling software Gaussian 16[15] was employed for all quantum calculations. For the computation of the pK_a values, the Gibbs energy changes in the gas phase (ΔG_{gas}) were calculated through the DFT method, B3LYP, with the basis sets 6-31G(d) and 6-31+G(d,p). Solvation free energy changes (ΔG_{solv}) in DMSO have been obtained by single point computations on gas phase geometries, using the bulk solvation model – integral equation formalism polarizable continuum model (IEFPCM). The calculations of pK_a values is performed by using a well known thermodynamic cycle (Scheme 1; Eqs. (1) and (2)).[16] The Gibbs energy of the gas phase proton[17] was taken from the Sackur–Tetrode Equation as $G_{gas}(H^+) = -6.28$ kcal* mol^{-1}; for the Gibbs energy change of hydration of the proton, the experimental value,[18] $\Delta G_{solv}(H^+) = -270.0$ kcal mol^{-1}, was used. The usual correction term of 1.9 kcal mol^{-1} was applied for standard state conversion between 1 atm in the gas phase and 1 mol L^{-1} in solution.[19]
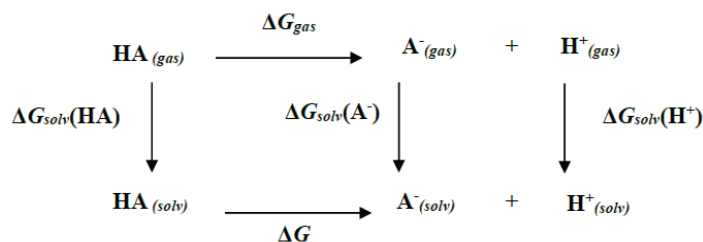
Scheme 1. The thermodynamic cycle utilized for Eqs. (1) and (2).

$$pK_a = \Delta G/(2.303RT) \tag{1}$$

$$\Delta G = \Delta G_{gas} + \Delta G_{solv}(A^-) + \Delta G_{solv}(H^+) - \Delta G_{solv}(HA) \tag{2}$$

RESULTS AND DISCUSSION

The data set of experimental pK_a values shows that changing the methyl group with a phenyl or a benzyl group increases the acidity of the considered organosulfur compounds. Electron withdrawing substituents also have the same effect (see Table I). Addition of oxygen atoms on sulfur also increases the acidity from sulfide to sulfoxides and sulfones (see Fig. 2).

Initially all structures were fully optimized with frequency calculations, by the B3LYP method using the basis set, 6-31G(d). Solvation energies were obtained by single point computations with the same basis set. The calculated pK_a values obtained through this computational approach and the experimental pK_a values are summarized in Table I.

---

* 1 kcal = 4184 J

TABLE I. Comparison of experimental and calculated pK_a values

Sulfide				Sulfoxide				Sulfone		
Comp.	Exp.	Calcd.[a]	Calcd.[b]	Comp.	Exp.	Calcd.[a]	Calcd.[b]	Comp.	Exp.	Calcd.[a]	Calcd.[b]
1a	45.0	55.7	45.7	**2a**	35.1	46.9	35.1	**3a**	31.1	38.2	31.3
1b	42.4	51.3	43.2	**2b**	29.0	35.3	28.6	**3b**	25.4	30.2	24.4
1c	30.8	37.6	32.0	**2c**	33.0	53.5	34.1	**3c**	29.0	36.5	28.6
1d	26.7	32.0	27.7	**2d**	27.2	33.8	27.6	**3d**	23.4	29.8	24.1
1e	20.8	24.5	18.6	**2e**	24.5	30.3	25.3	**3e**	22.3	32.1	23.4
1f	18.7	24.9	21.7	**2f**	15.1	21.9	12.8	**3f**	12.0	15.2	9.4
1g	16.9	25.2	15.4					**3g**	11.4	24.5	17.0
1h	11.8	15.7	8.7					**3h**	7.1	10.1	3.0
MAD		6.8	1.7			9.6	0.83			6.8	1.9
R^2		0.99	0.98			0.83	0.99			0.89	0.91

[a]B3LYP/6-31G(d)/IECPCM; [b]B3LYP/6-31+G(d,p)/IECPCM

Dimethyl Sulfide pK_a = 45.0 — Dimethyl Sulfoxide pK_a = 35.1 — Dimethyl Sulfone pK_a = 31.1
Oxidation of Sulfur increases the acidity
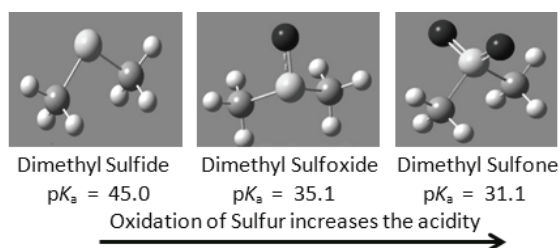
Fig. 2. Addition of oxygen atoms increases the acidity.

A comparison of the experimental and computed pK_a values shows that the pK_a values computed through B3LYP/6-31G(d)/IEFPCM procedure are large than experimental pK_a values. The mean absolute deviations (*MAD*) are also large (<7pK_a – units) in sulfide, (<9pK_a – units) in sulfoxide and (<7pK_a – units) in sulfone. However, the correlation coefficients (R^2) are somehow better in each series (>0.8).

Addition of a diffuse function in the basis set subsequently improved the results. The *MAD* values decreased significantly in each series (<2pK_a – unit) and the R^2 values also improved (>0.9). The data obtained through the B3LYP/6--31+G(d,p)/IEFPCM computational approach shows an excellent agreement between the experimental and computed pK_a values (see Table I). Hence, this computational model is excellent in predicting the pK_a values of these kinds of organosulfur compounds. All investigated data obtained through B3LYP/6--31+G(d,p)/IEFPCM computational model are presented in Fig. 3.

CONCLUSIONS

The DFT method was employed to calculate theoretical pK_a values of organosulfur compounds using two different basis sets. The diffuse function basis set provided the best calculated pK_a values and these are in excellent agreement with
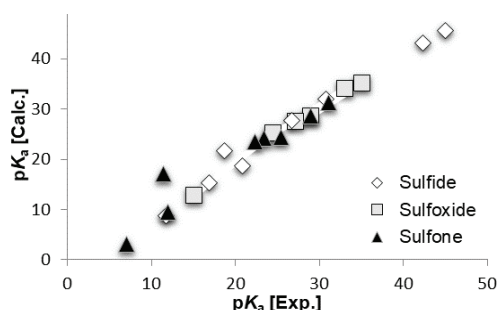
Fig. 3. Plot of experimental and computed pK_a through B3LYP/6-31+G(d,p)/IEFPCM.

the majority of the experimental pK_a values. Oxidation of sulfur and substitution of electron withdrawing and aromatic groups increase the acidity of considered organosulfur compounds. The predicted pK_a values showed the same phenomenon regarding the acidity of organosulfur compounds. Finally it was concluded that the proposed computational approach B3LYP/6-31+G(d,p)/IEFPCM is predictive and could be utilized to calculate theoretical pK_a values of these kinds of small organosulfur compounds. For large and flexible organosulfur compounds, conformational analysis will be required.

ИЗВОД

ЈЕДНОСТАВАН РАЧУНАРСКИ ПРИСТУП ИЗРАЧУНАВАЊУ pK_a ОРГАНОСУМПОРНИХ ЈЕДИЊЕЊА

SYED TAHIR ALI, ANEESA CHOUDHARY[1], SYED MAJID KHALI[2] и ARIF ZUBAIR[3]

[1]Department of Chemistry, Federal Urdu University of Arts Science and Technology, Karachi, Pakistan, [2]Bosch Pharmaceutical Private Limited, Plot No. 209, Sector 23, Korangi Industrial Area, Karachi, Pakistan и [3]Department of Environmental Science, Federal Urdu University of Arts Science and Technology, Karachi, Pakistan

Овај рад се односи на предвиђање pK_a вредности органосумпорних једињења помоћу теорије функционала густине (DFT). У овој студији су разматрана 22 органо-сумпорна једињења за израчунавање теоријских pK_a вредности. Нагласак је стављен на супституцију различитих група на атому сумпора. Израчунавања су урађена за при-суство диметил-сулфоксида (DMSO) као растварача. Експериментални редослед пораста киселости је: сулфиди < сулфоксиди < сулфони. Наше израчунате pK_a вредности такође следе овај поредак. Теоријске pK_a вредности израчунате су користећи DFT метод B3LYP, са базисима 6-31G(d), 6-31+G(d,p) и IEFPCM помоћни солватациони модел. Већина pK_a вредности, израчунатих помоћу дифузног базиса, су у изврсној сагласности са експерименталним. Отуда се овај рачунарски приступ, B3LYP/6-31+G(d,p)/IEFPCM, може користити за предвиђање pK_a вредности овог типа органосумпорних једињења.

(Примљено 18. маја, прихваћено 7. јула 2020)

REFERENCES

1. A. Onufriev, D. A. Case, G. M. Ullmann, *Biochemistry* **40** (2001) 3413 (https://doi.org/10.1021/bi002740q)

2. K. S. Alongi, G. C. Shields, *Ann. Rep. Comp. Chem.* **6** (2010) 113 (https://doi.org/10.1016/S1574-1400(10)06008-1)
3. G. J. Paul, J. S. Walter, *J. Chem. Phys.* **83** (1985) 2984 (https://doi.org/10.1063/1.449201)
4. M. K. Syed, C. Murray, M. Casey, *Eur. J. Org. Chem.* **25** (2014) 5549 (https://doi.org/10.1002/ejoc.201402584)
5. M. K. Syed, M. Casey, *Eur. J. Org. Chem*. **35** (2011) 7207 (https://doi.org/10.1080/09168451.2017.1407235)
6. B. Cheng, Y. Li, T. Wang, X. Zhang, H. Li, Y. Li, H. Zhai, *Chem. Comm.* **55** (2019) 14606 (https://doi.org/10.1039/c9cc08326j)
7. X. Yang, X. Li, K. Adair, H. Zhang, X. Sun, *Elect. Chem. Energy Rev.* **1** (2018) 239 (https://doi.org/10.1007/s41918-019-00044-4)
8. S. T. Ali, S. Karamat, J. Kóňa, W. M. F. Fabian, *J. Phys. Chem., A* **114** (2010) 12470 (https://doi.org/10.1021/jp102266v)
9. S. T. Ali, S. Jahangir, S. Karamat, W. M. F Fabian, K. Nawara, J. Kóňa, *J. Chem. Theor. Comput.* **6** (2010) 1670 (https://doi.org/10.1021/ct9003355)
10. F. G. Bordwell, *Acc. Chem. Res.* **21** (1988) 456 (https://doi.org/10.1021/ar00156a004)
11. F. G. Bordwell, G. E. Drucker, N. H. Andersen, A. D. Denniston, *J. Am. Chem. Soc.* **108** (1986) 7310 (https://doi.org/10.1021/ja00283a028)
12. X. M. Zhang, F. G. Bordwell, *J. Am. Chem. Soc.* **116** (1994) 968 (https://doi.org/10.1021/ja00082a018)
13. F. G. Bordwell, X. M. Zhang, *J. Am. Chem. Soc.* **114** (1992) 7623 (https://doi.org/10.1021/ja00046a003)
14. R. Dennington, T. A. Keith, J. M. Millam, *GaussView 6*, Semichem Inc., Shawnee Mission, KS, 2016
15. *Gaussian 16, Revision C.01*, Gaussian, Inc., Wallingford, CT, 2016
16. C. P. Kelly, C. J. Cramer, D. G. Truhlar, *J. Phys. Chem., A* **110** (2006) 2493 (https://doi.org/10.1021/jp055336f)
17. I. D. Cunningham, K. Bhaila, D. C. Povey, *Comp. Theor. Chem.* **1019** (2013) 55 (https://doi.org/10.1016/j.comptc.2013.06.031)
18. J. Ho, M. L. Coote, *Theor. Chem. Acc.* **125** (2010) 3 (https://doi.org/10.1007/s00214-009-0667-0)
19. M. D. Tissandier, K. A. Cowen, W. Y. Feng, E. Gundlach, M. H. Cohen, A. D. Earhart, V. C. James, T. R. Tuttle, *J. Phys. Chem., A* **102** (1998) 7787 (https://doi.org/10.1021/jp982638r).

Study on charge mobility of hexathiapentacene and its selenium analogs

SU-QIN ZHOU[1], QI-YING XIA[2]*, MENG LIANG[3] and XUE-HAI JU[3]**

[1]Faculty of Chemical Engineering, Huaiyin Institute of Technology, Key Laboratory for Attapulgite Science and Applied Technology of Jiangsu Province, Huaian 223003, P. R. China, [2]School of Chemistry and Chemical Engineering, Linyi University, Linyi 276005, P. R. China and [3]School of Chemical Engineering, Nanjing University of Science and Technology, Nanjing 210094, P. R. China

Abstract: The relationship between molecular geometries, crystal structures and charge mobilities of hexathiapentacene (HTP) and three of its derivatives (2Se-HTP, 4Se-HTP, 6Se-HTP) were studied using the density functional theory combined with a hopping mechanism at the molecular and crystal level. The effect of Se substitution on the charge mobility was discussed. The calculated results showed that the derivatives exhibit good planarity and the molecular geometries show little variation during the charge transfer process. The electron mobility is 1.20 cm^2 V^{-1} S^{-1} for HTP and 2.30 cm^2 V^{-1} S^{-1} for 6Se--HTP, which are much larger than the corresponding hole ones, indicating that HTP and 6Se-HTP are good candidates for *n*-type organic semiconductors. However, 2Se-HTP and 4Se-HTP have comparable hole and electron motilities and are suitable for ambipolar semiconductors.

Keywords: selenium substitution; organic semiconductor; density functional theory; hopping mechanism; ambipolar.

INTRODUCTION

Over the past decades, organic field effect transistors (OFET) have attracted more and more attention due to their advantages, such as low cost and ease of fabrication on a large scale.[1–4] The charge mobility of OFETs made from some small molecules by the vacuum deposition and solution processing method has already approached that of a polycrystalline silicon field effect transistor, the charge mobility of which is over 10 cm^2 V^{-1} S^{-1}. These OFETs are considered to have promising applications in radio frequency identification devices, organic light-emitting displays and sensor-based equipment.[5] All these potential applications are dependent on high charge mobilities. Therefore, it is still a challenging

---

task in the field of organic electronics to design and fabricate new organic semiconductors with high charge mobility, ease of storage, and stable to handle.

The electronic property, solubility and molecular packing in organic semiconductors could be regulated and controlled by the introduction of heteroatoms, such as halogens, sulfur and nitrogen atoms.[6,7] Among the heteroatoms in organic semiconductors, selenium is not as common as sulfur and nitrogen. The available investigations showed that the effects of sulfur being replaced by selenium are not really uniform. The difference in charge mobilities between tetrathiofuran and selenium-substituted tetrathiofuran is almost neglectable.[8] However, the charge mobility increases noticeably from 0.081 to 0.17 $cm^2 V^{-1} S^{-1}$ in DNTT/DNSS when the sulfur atoms of the latter are replaced by selenium.[9] In 2011, Lee and coworkers reported a series of metal chalcogenides of cadmium selenide nanocrystals and their charge transferring. The electron mobility was up to 16 $cm^2 V^{-1} S^{-1}$,[10] a value that is greater than that of the best dissolved organic nanocrystalline devices by one order of magnitude. In a word, the selenium compounds used in organic semiconductors are not as popular as sulfur- or nitrogen-containing compounds. The replacement of sulfur by selenium is an appropriate strategy to develop high-performance organic semiconductor materials.[11]

In 2006, Briseno and his colleagues studied the molecular structure, molecular packing of hexathiapentacene (HTP) and its application in light-emitting diodes.[12,13] Both face to face π–π interaction and S···S interaction contribute to the charge transfer. Since sulfur and selenium belong to the same group and the latter has more d-electrons, the replacement of sulfur with selenium is expected to improve the charge transfer property. To probe the influence of selenium substitution, the molecular and crystal structures, and charge mobilities of HTP and its selenium analogs (Fig. 1) were studied by the density functional theory method together with the charge carrier hopping model.
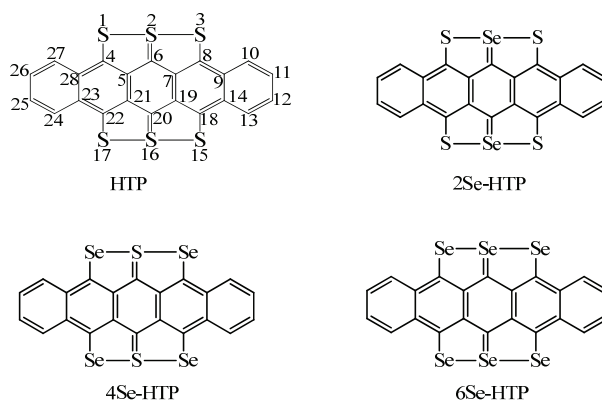

Fig. 1. Molecular structure and atomic numbering of HTP and its analogs with the same atomic numbering.

EXPERIMENTAL

The hybrid functional of B3LYP was proved to be appropriate for organic molecules with π conjugations.[14] Therefore, the reorganization energy in the charge transfer process was obtained at the B3LYP/6-311++G** level. Consequently, the optimized geometrical structures of the neutral molecules and the ionization energy, electron affinity, and energies of HOMO and LUMO of the corresponding cations and anions were calculated. Whereas, the PW91PW91/6-31G(d) was used for the molecular packing of the dimers and the charge transfer integral, since computational practice showed that this method produces rational results for the coupling integral.[15-16] All the above-mentioned quantum calculations were performed by the Gaussian 09 package.[17]

The crystal structure of HTP is from Cambridge Crystal Database. Both the crystal and molecular structure were optimized by the DFT-D method with PBE functionals. The dispersion corrected method (-D) has commonly been used to describe weak interactions.[18] As displayed in Table I, the optimized cell parameters are in good agreement with the experimental values, indicating the DFT-D method and the basis set used could be adopted for the system. Since sulfur and selenium are in the same group, it is reasonable to use the same method for predicting the crystal structures of the selenium analogs when the sulfur is substituted by selenium.[19] The calculations for the crystals were performed by the CASTEP module.[20]

According to the incoherent hopping mechanism, the charge carriers localize and jump between neighboring molecules to migrate across the organic layer.[21] The charge transfer rate between neighboring molecules is:

$$k_{\mathrm{i}} = \frac{2\pi t_{\mathrm{i}}^2}{h} \left(\frac{\pi}{\lambda_{-} k_{\mathrm{B}} T} \right)^{0.5} \exp \left(-\frac{\lambda_{-}}{4 k_{\mathrm{B}} T} \right) \tag{1}$$

where t_{i} is the transfer integral between neighboring molecules in each individual hopping pathway, and λ_{-} is the reorganization energy for electron transports, T is the temperature, h and k_{B} are the Planck and Boltzmann constants, respectively. The charge coupling t_{i} was calculated by considering the spatial overlap between two monomers according to:[22]

$$t_{\mathrm{i}} = \frac{h_{12} - 0.5(h_{11} + h_{22}) S_{12}}{1 - S_{12}^2} \tag{2}$$

where h_{ij} is the charge transfer integral and S_{ij} is the spatial overlap integral. The charge transfer mobility is evaluated by the Einstein Relation:

$$\mu = \frac{e}{k_B T} D \tag{3}$$

where e is the electron charge, k_{B} Boltzmann constant, and D diffusion coefficient that is a sum along the ith hopping pathway:[23]

$$D = \frac{1}{2n} \sum_{\mathrm{i}} r_{\mathrm{i}}^2 k_{\mathrm{i}} P_{\mathrm{i}} \tag{4}$$

where n is the space dimensionality, r_{i} is the centroid distance of the hopping channel i, k_{i} is the hopping rate in the i pathway, and P_{i} is the relative probability for charge carrier hopping determined by:

$$P_i = \frac{k_i}{\sum_i k_i} \tag{5}$$

RESULTS AND DISCUSSION

Geometrical structures

The optimized bond lengths of HTP are in good agreement with the single crystal X-ray diffraction structure (Table I), indicating that the B3LYP/6--311++G** method is appropriate for HTP. show The changes of the bond lengths from molecule to anion Δ(A–G) and to cation Δ(C–G) are shown in Figs. S-2 and S-3 of the Supplementary material to this paper, respectively. The maximum variations of bond lengths are 0.023 Å for HTP and 2Se-HTP, and 0.024 Å for 4Se-HTP and 6Se-HTP, indicating the variation of structure is small upon the molecule donating or accepting an electron. This is beneficial for the charge transfer. As seen in Figs. S-2 and S-3, the lengths of 1 to 3, 25 to 29 bonds, and bonds associated with labels 35 and 36 vary largely from molecule to anion. The bond lengths associated with labels 3, 13, 25, 29, 33 and 35 vary largely from molecule to cation. These bonds with large length variations are C–S, C–Se, S–S and Se–Se, indicating these atoms make large contributions to the charge transfer.

TABLE I. Experimental and calculated cell parameters of HTP and its selenium analogs

Compound	α / °	β / °	γ / °	a / Å	b / Å	c / Å
HTP[a]	72.46	88.89	84.17	3.894	14.33	16.55
HTP[b]	73.43	88.73	82.08	3.837	14.22	16.64
2Se-HTP	75.55	89.65	88.29	3.872	13.14	17.44
4Se-HTP	73.55	88.85	82.53	3.893	14.33	16.58
6Se-HTP	75.05	89.15	84.65	3.918	13.42	17.43

[a]Experimental values from the Cambridge Crystal Database; [b]This work

Frontier molecular orbitals

The electronic structures and energies of frontier molecular orbitals greatly influence charge transfer.[24] As seen from the contours of Fig. 2, the HOMO is symmetric, while the LUMO is asymmetric. The contours of HOMO distribute on almost all heavy atoms (non-hydrogen atoms) except for S or Se, while those of LUMO are on all heavy atoms. The delocalized distribution is favorable for electron transfer. The energies of HOMO and LUMO determine the injection of a hole and electron. A low LUMO is beneficial for the injection of electrons.[25] The energy difference (E_{gap}) between HOMO and LUMO is also an important factor for the injection of charge. A small E_{gap} value is beneficial for charge injection.[26] As seen in Table II, the E_{gap} values for 4Se-HTP and 6Se-HTP are relatively small, indicating that these compounds are adequate for *n*-type OSC.
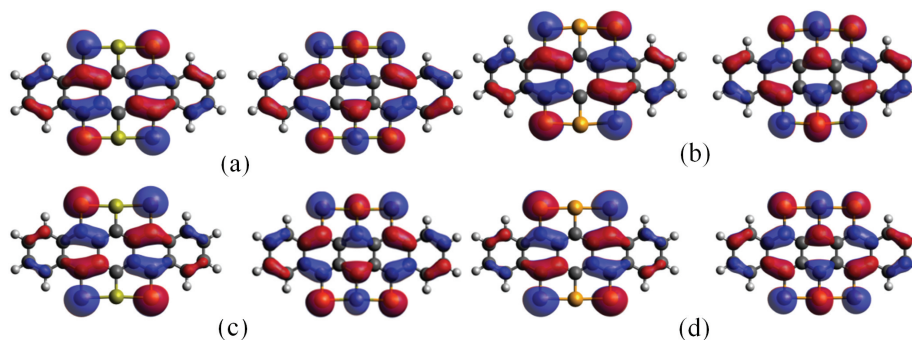
Fig. 2. Contours of LUMO (left) and HOMO (right) for HTP (a), 2Se-HTP (b), 4Se-HTP (c) and 6Se-HTP (d).

TABLE II. Energies of HOMO and LUMO, and their gap

Compound	E_{HOMO} / eV	E_{LUMO} / eV	E_{gap} / eV
HTP	−5.27	−3.51	1.76
2Se-HTP	−5.28	−3.48	1.80
4Se-HTP	−5.20	−3.52	1.68
6Se-HTP	−5.23	−3.50	1.73

Electron affinity, ionization energy and reorganization energy

The ionization energy, electron affinity and reorganization energy are listed in Table III. For a good electron injection, the electron affinity should be large enough. Similarly, a small ionization energy is favorable for hole transfer. After Se substitution, the ionization energy decreases, but the electron affinity increases excepted for 2Se-HTP, indicating the substitution of Se improves the hole and electron transfer.

TABLE III. Ionization potential (*IP*), electron affinity (*EA*) and reorganization energy (λ_e for electron and λ_h for hole) at the B3LYP/6-311++G** level; subscripts "v" and "a", following IP and EA, denote the corresponding vertical and adiabatic values

Compound	IP_v / eV	IP_a / eV	EA_v / eV	EA_a / eV	λ_e / eV	λ_h / eV
HTP	6.78	6.72	2.30	2.37	0.145	0.137
2Se-HTP	6.79	6.72	2.28	2.35	0.139	0.142
4Se-HTP	6.72	6.66	2.37	2.43	0.133	0.110
6Se-HTP	6.73	6.68	2.36	2.42	0.128	0.114

As one of the key factors for charge transfer, the reorganization energy is related to the molecular size and geometrical structure. Generally speaking, the larger the deformation is during charge transfer, the larger is the reorganization energy, and the smaller is the charge transfer rate. By summing up the absolute values of bond length variations (denoted as $\sum|\Delta r_{A-G}|$ and $\sum|\Delta r_{C-G}|$) of anion/ /molecule and cation/molecule (Tables S-1–S-4), it could be found that the values

of $\sum|\Delta r_{C-G}|$ are in the order: 2Se-HTP > HTP > 6Se-HTP > 4Se-HTP, which is in accordance with the order of the hole reorganization energy (λ_h). For electron transfer, the reorganization energy decreases after Se substitution, indicating Se substitution favors electron transfer.

Charge transfer integral and charge mobility

The charge transfer integral is closely related to the molecular packing and center-of-mass distance of neighboring molecules. The space group of the crystal is supposed to be similar when S is replaced by Se since both the elements have almost the same electronegativity (2.58 *vs.* 2.55) and thereby similar intermolecular force. As seen in Fig. 3, the molecules in HTP and its selenium analogs are packed in fishbone patterns after geometrical and cell parameter optimization. The dimers in hopping paths of P1 and P2 are in face-to-face π–π packing, which is proved by many literature references to be an efficient packing for charge hopping.[27]
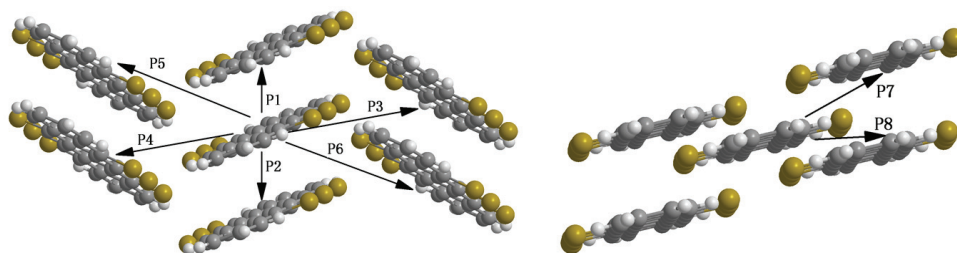
Fig. 3. Paths for charge hopping.

The charge transfer integrals in P1 and P2 hopping are the largest for both hole and electron transfer. As seen in Table IV, the maximum absolute values of charge transfer integrals for electron hopping are 37.3, 37.1, 53.4 and 55.1 meV for HTP, 2Se-HTP, 4Se-HTP and 6Se-HTP, respectively. Those for hole hopping are 101.9, 61.0, 123.2 and 119.3 meV, respectively. Moreover, the larger the center-of-mass distance is, the smaller is the overlap integral between the orbitals of neighboring molecules. The intermolecular orbital interaction will vanish, and the charge transfer integral will become zero when the center-of-mass distance exceeds a certain value. For example, the center-of-mass distance r_i is 3.84 Å in dimer P1 of HTP and the corresponding hole transfer integral is 101.9 meV. The center-of-mass distance in P3 (12.72 Å) is three times larger than in P1 and its transfer integral is only one fiftieth of the latter. While the center-of-mass distance in P8 is 15.23 Å and the transfer integral is nearly zero. In view of charge transfer integral, 4Se-HTP possess the maximum hole transfer integral and is a candidate for *p*-type OSC. 6Se-HTP has the maximum electron transfer integral and is a promising candidate for *n*-type OSC.

TABLE IV. Charge transfer integral (h_e for electron and h_h for hole) for neighboring molecule dimer; charge transfer integral at the PW91PW91/6-31G (d, p) level; S is the overlap matrix of the dimer

Compound	Path[a]	h_e / meV	S_e^{ij}	h_h / meV	S_h^{ij}	r^b / Å
HTP	1	37.3	−0.0065	101.9	−0.0201	3.84
	2	−37.1	0.0065	101.8	−0.0201	3.84
	3	−4.1	0.0004	2.5	−0.0003	12.72
	4	−4.3	0.0009	−1.7	0.0004	9.31
	5	−0.7	0.0003	3.0	−0.0004	9.63
	6	−5.1	0.0006	3.0	−0.0004	12.36
	7	−1.0	0.0001	0.6	−0.0001	14.22
	8	1.9	−0.0002	0.8	−0.0001	15.23
2Se-HTP	1	31.7	−0.0059	61.0	−0.013	3.87
	2	−31.7	0.0059	61.0	−0.013	3.87
	3	5.1	−0.0005	−3.1	0.0003	0.99
	4	−3.0	0.0004	−10.8	0.0019	0.99
	5	3	−0.0004	−10.5	0.0018	0.99
	6	−5.5	0.0006	−3.3	0.0004	0.99
	7	−1.3	0.0001	−1.0	0.000	6.21
	8	6.9	−0.0008	4.7	−0.0005	6.21
4Se-HTP	1	−53.4	0.0093	123.2	−0.024	3.89
	2	−53.4	0.0093	123.1	−0.024	3.89
	3	−4.4	0.001	−6.1	0.0011	0.62
	4	−4.4	0.0004	2.5	−0.0003	0.62
	5	−7.1	0.0008	3.9	−0.0005	0.62
	6	0.6	0.0002	3.9	−0.0004	0.62
	7	−0.6	0.0001	0.3	0.000	14.33
	8	0.7	−0.0001	−1.6	0.0002	15.33
6Se-HTP	1	−55.1	0.0096	119.3	−0.0228	3.92
	2	55.1	−0.0096	119.3	−0.0228	3.92
	3	4.8	−0.0005	2.9	−0.0003	12.57
	4	0.1	0.000	13.3	−0.0022	9.63
	5	1.3	−0.0002	12.1	−0.002	9.83
	6	6.5	−0.0007	3.7	−0.0004	12.33
	7	1.1	−0.0001	−0.5	0.000	13.42
	8	3.4	−0.0004	1.9	−0.0002	14.33

[a]See Fig. 3 for paths; [b]center-of-mass distance of neighboring monomers

As seen in Table V, the electron mobility is 1.20 cm^2 V^{-1} S^{-1} for HTP and 2.30 cm^2 V^{-1} S^{-1} for 6Se-HTP, which are much larger than their corresponding hole ones, indicating that HTP and 6Se-HTP are good candidates for *n*-type organic semiconductors. However, 2Se-HTP and 4Se-HTP have comparative hole and electron mobilities and are suitable for ambipolar semiconductors.

TABLE V. Hole and electron mobilities

Comp.	μ_h / cm^2 V^{-1} s^{-1}	μ_e / cm^2 V^{-1} s^{-1}	Comp.	μ_h / cm^2 V^{-1} s^{-1}	μ_e / cm^2 V^{-1} s^{-1}
HTP	0.14	1.2	4Se-HTP	0.61	0.92
2Se-HTP	0.19	0.28	6Se-HTP	0.41	2.29

CONCLUSIONS

The charge transfer features of HTP and its selenium analogs were investigated by DFT and the charge carrier hopping mechanism. The stabilities of the selenium analogs are increased, and the reorganization energies decreased compared to the parent those of HTP. In view of the contours and energies of the frontier molecular orbitals, HTP and its selenium analogs are suitable for *n*-type OSCs. 4Se-HTP and 6Se-HTP have lower LUMO and E_{gap}, which is more favorable for electron injection. The face-to-face π–π packing of HTP and its selenium analogs guarantees large charge transfer integrals and is thus beneficial for charge transfer. Both the electron mobilities of HTP and 6Se-HTP are larger than the hole ones, and HTP and 6Se-HTP are adopted for *n*-type OSCs. 2Se-HTP and 4Se-HTP have the similar magnitudes of electron and hole mobilities and are thus candidates for bipolar OSCs. The present study showed that selenium substitution for sulfur is one of the strategies to develop *n*-type or ambipolar semiconductors.

SUPPLEMENTARY MATERIAL

Additional data are available electronically at the pages of journal website: https://www.shd-pub.org.rs/index.php/JSCS/index, or from the corresponding author on request.

ИЗВОД

ТЕОРИЈСКО ПРОУЧАВАЊЕ ПОКРЕТЉИВОСТИ НАЕЛЕКТРИСАЊА КОД ХЕКСАТИОПЕНТАЦЕНА И ЊЕГОВИХ СЕЛЕНОВИХ АНАЛОГА

SU-QIN ZHOU[1], QI-YING XIA[2], MENG LIANG[3] и XUE-HAI JU[3]

[1]*Faculty of Chemical Engineering, Huaiyin Institute of Technology, Key Laboratory for Attapulgite Science and Applied Technology of Jiangsu Province, Huaian 223003, P. R. China,* [2]*School of Chemistry and Chemical Engineering, Linyi University, Linyi 276005, P. R. China u* [3]*School of Chemical Engineering, Nanjing University of Science and Technology, Nanjing 210094, P. R. China*

Теоријом функционала густине комбинованом са механизмом прескакања проучаван је однос између молекулских геометрија, кристалних сруктуре и покретљивости наелектрисања у хексатиапентацена (HTP) и његова три деривата (2Se-HTP, 4Se-HTP, 6Se-HTP) на нивоу молекула и кристала. Дискутован је ефекат супституције селеном на покретљивост наелектрисања. Израчунати резултати показују да деривати имају добру планарност и да геометрије молекула мало варирају током процеса преноса наелектрисања. Мобилност електрона је 1,20 cm² V⁻¹ S⁻¹ за HTP и 2,30 cm² V⁻¹ S⁻¹ за 6Se-HTP, што је много веће него за одговарајуће празнине, указујући да су HTP и 6Se-HTP добри кандидати за органске полупроводнике n-типа. Међутим, 2Se-HTP и 4Se-HTP имају упоредиве покретљивости електрона и шупљина и погодни су за амбиполарне полупроводнике.

(Примљено 11. маја, ревидирано 23. јула, прихваћено 29. јула 2020)

REFERENCES

1. H. Usta, A. Facchetti, T. J. Marks, *Acc. Chem. Res.* **44** (2011) 501
   (https://dx.doi.org/10.1021/ar200006r)
2. X. Wang, K. C. Lau, *J. Phys. Chem., C* **116** (2012) 22749
   (https://dx.doi.org/10.1021/jp309226z)
3. A. Datta and S. K. Pati, *J. Phys. Chem., C* **111** (2007) 4487
   (https://dx.doi.org/10.1021/jp070609n)
4. N. Z. Prlainovic, M. P. Rancic, I. Stojiljkovic, J. B. Nikolic, S. Z. Drmanic, I. Ajaj, A. D.
   Marinkovic, *J. Serb. Chem. Soc.* **83** (2018) 139 (https://doi.org/10.2298/JSC170408003P)
5. A. Tripathi, C. Prabhakar, *J. Chin. Chem. Soc.* **65** (2018) 918
   (https://dx.doi.org/10.1002/jccs.201700448)
6. Y. Song, C. Di, X. Yang, *J. Am. Chem. Soc.* **128** (2007) 15940
   (https://dx.doi.org/10.1021/ja064726s)
7. M. Melucci, L. Favaretto, M. Zambianchi, *Chem. Mater.* **25** (2013) 668
   (https://dx.doi.org/10.1021/cm303224a)
8. H. W. Lin, W. Y. Lee, C. Lu, *Polym. Chem.* **3** (2012) 767
   (https://dx.doi.org/10.1039/c2py00583b)
9. T. Yamamoto, K. Takimiya, *J. Am. Chem. Soc.* **129** (2007) 2224
   (https://dx.doi.org/10.1021/ja068429z)
10. A. L. Briseno, S. C. B. Mannsfeld, E. Formo, *J. Mater. Chem.* **18** (2008) 5395
    (https://dx.doi.org/10.1039/b809228c)
11. A. Bedi, S. P. Senanayak, K. S. Narayan, S. S. Zade, *Macromolecules* **46** (2013) 5943
    (https://dx.doi.org/10.1021/ma4008219)
12. A. L. Briseno, S. C. B. Mannsfeld, X. Lu, Y. Xiong, S. A. Jenekhe, Z. Bao, Y. Xia, *Nano
    Lett.* **7** (2007) 668 (https://dx.doi.org/10.1021/nl0627036)
13. A. L. Briseno, Q. Miao, M. M. Ling, *J. Am. Chem. Soc.* **128** (2007) 15576
    (https://dx.doi.org/10.1021/ja066088j)
14. K. Chaitanya, X. H. Ju, B. M. Heron, *RSC Adv.* **5** (2015) 3978
    (https://dx.doi.org/10.1039/c4ra09914a)
15. O. Castellano, R. Gimon, H. Soscun, *Energy Fuel* **25** (2011) 2526
    (https://dx.doi.org/10.1021/ef101471t)
16. Y. Hong, Y. R. Liu, H. Wen, *RSC Adv.* **8** (2018) 7225
    (https://dx.doi.org/10.1039/c7ra13670f)
17. *Gaussian 0*9, Revision A.02, Gaussian, Inc., Wallingford, CT, 2009
18. A. Krishtal, K. Vannomeslaeghe, A. Olasz, *J. Chem. Phys.* **130** (2009) 174101
    (https://dx.doi.org/10.1063/1.3126248)
19. Y. Hu, K. Chaitanya, J. Yin, X. H. Ju, *J. Mater. Sci.* **51** (2016) 6235
    (https://dx.doi.org/10.1007/s10853-016-9921-8)
20. M. D. Segall, P. L. D. Lindan, M. J. Probert, C. J. Pickard, P. J. Hasnip, S. J. Clark, M. C.
    Payne, *J. Phys.: Cond. Matt.* **14** (2002) 2717 (https://dx.doi.org/10.1088/0953-
    8984/14/11/301)
21. M. D. Hanwell, T. A. Madison, G. R. Hutchison, *J. Phys. Chem., C* **114** (2010) 20417
    (https://dx.doi.org/10.1021/jp104416a)
22. S. Mohakud, A. P. Andrews, S. K. Pati, *J. Phys. Chem., C* **114** (2010) 20436
    (https://dx.doi.org/10.1021/jp1047503)
23. W. Q. Deng and W. A. Goddard III, *J. Phys. Chem., B* **108** (2004) 8614
    (https://dx.doi.org/10.1021/jp0495848)

24. J. Yin, K. Chaitanya, X. H. Ju, *RSC Adv.* **5** (2015) 65192 (https://dx.doi.org/10.1039/C5RA06418J)
25. J. M. Hancock, A. P. Gifford, R. D. Champion, *Macromolecules* **41** (2008) 3588 (https://dx.doi.org/10.1021/ma800304m)
26. J. Yin, K. Chaitanya, X. H. Ju, *Can. J. Chem.* **93** (2015) 740 (https://dx.doi.org/10.1139/cjc-2014-0569)
27. M. Liang, J. Yin, K. Chaitanya, X. H. Ju, *J. Theor. Comput. Chem.* **15** (2016) 1650027 (https://dx.doi.org/10.1142/S0219633616500279).

Study on charge mobility of hexathiapentacene and its selenium analogs

SU-QIN ZHOU[1], QI-YING XIA[2]*, MENG LIANG[3] and XUE-HAI JU[3]**

[1]*Faculty of Chemical Engineering, Huaiyin Institute of Technology, Key Laboratory for Attapulgite Science and Applied Technology of Jiangsu Province, Huaian 223003, P. R. China,* [2]*School of Chemistry and Chemical Engineering, Linyi University, Linyi 276005, P. R. China and* [3]*School of Chemical Engineering, Nanjing University of Science and Technology, Nanjing 210094, P. R. China*

HTP

Fig. S-1. Bond labels of HTP. (Same labels for its selenium analogs).

*** Corresponding authors. E-mail: (*)xiaqiying@163.com; (**)xhju@njust.edu.cn

TABLE S-I. Bond lengths and their variations in the ionic states of HTP

Bond labels	Bond length, Å				Δr_{A-G}	Δr_{C-G}
	Crystal	Ground state	Anion state	Cation state		
1	1.746	1.749	1.771	1.746	0.022	–0.003
2	2.385	2.380	2.403	2.384	0.023	0.004
3	1.693	1.716	1.736	1.693	0.020	–0.023
4	1.419	1.420	1.419	1.419	–0.001	–0.001
5	1.426	1.406	1.415	1.426	0.009	0.019
6	1.450	1.446	1.427	1.450	–0.019	0.004
7	1.408	1.413	1.421	1.408	0.008	–0.005
8	1.383	1.378	1.374	1.383	–0.004	0.004
9	1.401	1.406	1.414	1.401	0.008	–0.005
10	1.383	1.378	1.374	1.383	–0.004	0.005
11	1.408	1.413	1.421	1.408	0.008	–0.005
12	1.450	1.445	1.427	1.450	–0.018	0.005
13	1.426	1.406	1.415	1.426	0.009	0.020
14	1.419	1.420	1.419	1.419	–0.001	–0.001
15	1.419	1.420	1.419	1.419	–0.001	–0.001
16	1.426	1.406	1.415	1.426	0.009	0.020
17	1.450	1.446	1.427	1.450	–0.018	0.004
18	1.408	1.413	1.421	1.408	0.008	–0.005
19	1.383	1.378	1.374	1.383	–0.004	0.005
20	1.401	1.406	1.414	1.401	0.008	–0.005
21	1.423	1.423	1.433	1.423	0.010	0.000
22	1.430	1.448	1.452	1.430	0.004	–0.018
23	1.430	1.448	1.452	1.430	0.004	–0.018
24	1.423	1.423	1.433	1.423	0.010	0.000
25	1.693	1.716	1.736	1.692	0.020	–0.024
26	2.383	2.378	2.401	2.384	0.023	0.006
27	1.746	1.749	1.771	1.746	0.022	–0.003
28	2.385	2.380	2.403	2.384	0.023	0.004
29	1.69	1.716	1.736	1.693	0.020	–0.023
30	1.38	1.378	1.374	1.383	–0.005	0.005
31	1.408	1.413	1.421	1.408	0.008	–0.005
32	1.450	1.445	1.427	1.450	–0.018	0.005
33	1.426	1.406	1.415	1.426	0.009	0.020
34	1.419	1.420	1.419	1.419	–0.001	–0.001
35	1.693	1.716	1.736	1.693	0.020	–0.023
36	2.383	2.378	2.401	2.384	0.023	0.006

TABLE S-II. Bond lengths and their variations in the ionic states of 2Se-HTP

Bond labels	Bond length, Å				
	Ground state	Anion state	Cation state	$\Delta r_{\text{A-G}}$	$\Delta r_{\text{C-G}}$
1	1.892	1.915	1.889	0.023	–0.003
2	2.446	2.467	2.453	0.021	0.007
3	1.720	1.741	1.696	0.021	–0.024
4	1.419	1.418	1.419	–0.001	0.000
5	1.410	1.418	1.430	0.008	0.020
6	1.446	1.427	1.450	–0.019	0.004
7	1.414	1.422	1.409	0.001	–0.005
8	1.378	1.373	1.382	–0.005	0.004
9	1.406	1.414	1.401	0.008	–0.005
10	1.378	1.373	1.382	–0.005	0.004
11	1.414	1.422	1.409	0.008	–0.005
12	1.446	1.423	1.450	–0.023	0.004
13	1.410	1.418	1.430	0.008	0.020
14	1.419	1.418	1.419	–0.001	0.000
15	1.419	1.418	1.419	–0.001	0.000
16	1.410	1.418	1.430	0.008	0.020
17	1.446	1.427	1.450	–0.019	0.004
18	1.414	1.422	1.410	0.008	–0.004
19	1.378	1.373	1.382	–0.005	0.004
20	1.406	1.414	1.401	0.008	–0.005
21	1.422	1.432	1.421	0.010	–0.001
22	1.453	1.458	1.435	0.005	–0.018
23	1.453	1.458	1.435	0.005	–0.018
24	1.422	1.432	1.421	0.010	–0.001
25	1.720	1.741	1.696	0.021	–0.024
26	2.446	2.467	2.453	0.021	0.007
27	1.892	1.915	1.889	0.023	–0.003
28	2.446	2.467	2.453	0.021	0.0067
29	1.720	1.741	1.696	0.021	–0.024
30	1.378	1.372	1.382	–0.006	0.004
31	1.414	1.422	1.409	0.008	–0.005
32	1.446	1.427	1.450	–0.019	0.004
33	1.410	1.418	1.430	0.008	0.020
34	1.419	1.418	1.419	–0.001	0.000
35	1.720	1.741	1.696	0.021	–0.024
36	2.446	2.467	2.453	0.021	0.007

TABLE S-III. Bond lengths and their variations in the ionic states of 4Se-HTP

Bond labels	Bond length, Å				
	Ground state	Anion state	Cation state	$\Delta r_{A\text{-}G}$	$\Delta r_{C\text{-}G}$
1	1.760	1.784	1.758	0.024	–0.002
2	2.473	2.495	2.475	0.022	0.002
3	1.862	1.883	1.839	0.021	–0.023
4	1.432	1.429	1.431	–0.003	–0.001
5	1.410	1.418	1.428	0.008	0.018
6	1.441	1.424	1.445	–0.017	0.004
7	1.415	1.424	1.412	0.009	–0.003
8	1.376	1.371	1.379	–0.005	0.003
9	1.406	1.414	1.403	0.008	–0.003
10	1.376	1.371	1.379	–0.005	0.003
11	1.415	1.423	1.412	0.008	–0.003
12	1.441	1.424	1.445	–0.017	0.004
13	1.410	1.418	1.428	0.008	0.018
14	1.432	1.429	1.431	–0.003	–0.001
15	1.432	1.429	1.431	–0.003	–0.001
16	1.410	1.418	1.428	0.008	0.018
17	1.441	1.424	1.445	–0.017	0.004
18	1.416	1.423	1.412	0.007	–0.004
19	1.376	1.371	1.379	–0.005	0.003
20	1.406	1.414	1.403	0.008	–0.003
21	1.418	1.428	1.417	0.010	–0.001
22	1.461	1.466	1.444	0.005	–0.017
23	1.461	1.466	1.444	0.005	–0.017
24	1.418	1.428	1.417	0.010	–0.001
25	1.862	1.883	1.839	0.021	–0.023
26	2.473	2.495	2.475	0.022	0.002
27	1.760	1.784	1.758	0.024	–0.002
28	2.473	2.495	2.475	0.022	0.002
29	1.862	1.883	1.839	0.021	–0.023
30	1.376	1.371	1.379	–0.005	0.003
31	1.415	1.424	1.412	0.008	–0.003
32	1.441	1.424	1.445	–0.017	0.004
33	1.410	1.418	1.428	0.008	0.018
34	1.432	1.429	1.431	–0.003	–0.001
35	1.862	1.883	1.839	0.021	–0.023
36	2.473	2.495	2.475	0.022	0.002

TABLE S-IV. Bond lengths and their variations in the ionic states of 6Se-HTP

| Bond labels	Bond length, Å				
	Ground state	Anion state	Cation state	Δr_{A-G}	Δr_{C-G}
1	1.908	1.932	1.906	0.024	–0.002
2	2.537	2.559	2.541	0.022	0.004
3	1.867	1.889	1.843	0.022	–0.024
4	1.431	1.428	1.431	–0.003	0.000
5	1.414	1.422	1.433	0.008	0.019
6	1.441	1.425	1.446	–0.017	0.005
7	1.417	1.425	1.413	0.008	–0.004
8	1.375	1.371	1.378	–0.004	0.003
9	1.406	1.414	1.403	0.008	–0.003
10	1.375	1.371	1.378	–0.004	0.003
11	1.417	1.425	1.413	0.008	–0.004
12	1.441	1.425	1.446	–0.016	0.005
13	1.415	1.422	1.433	0.007	0.018
14	1.431	1.428	1.431	–0.003	0.000
15	1.431	1.428	1.431	–0.003	0.000
16	1.415	1.422	1.433	0.007	0.018
17	1.441	1.425	1.446	–0.016	0.005
18	1.417	1.425	1.413	0.008	–0.004
19	1.375	1.371	1.378	–0.004	0.003
20	1.406	1.414	1.403	0.008	–0.003
21	1.417	1.427	1.416	0.010	–0.001
22	1.467	1.472	1.449	0.005	–0.018
23	1.467	1.472	1.449	0.005	–0.018
24	1.417	1.427	1.416	0.010	–0.001
25	1.867	1.889	1.843	0.022	–0.024
26	2.537	2.559	2.541	0.022	0.004
27	1.908	1.932	1.906	0.024	–0.002
28	2.537	2.559	2.541	0.022	0.004
29	1.867	1.889	1.843	0.022	–0.024
30	1.375	1.371	1.378	–0.004	0.003
31	1.417	1.425	1.413	0.008	–0.004
32	1.441	1.425	1.446	–0.016	0.005
33	1.415	1.422	1.432	0.007	0.017
34	1.431	1.428	1.431	–0.003	0.000
35	1.867	1.889	1.843	0.022	–0.024
36	2.537	2.559	2.541	0.022	0.004
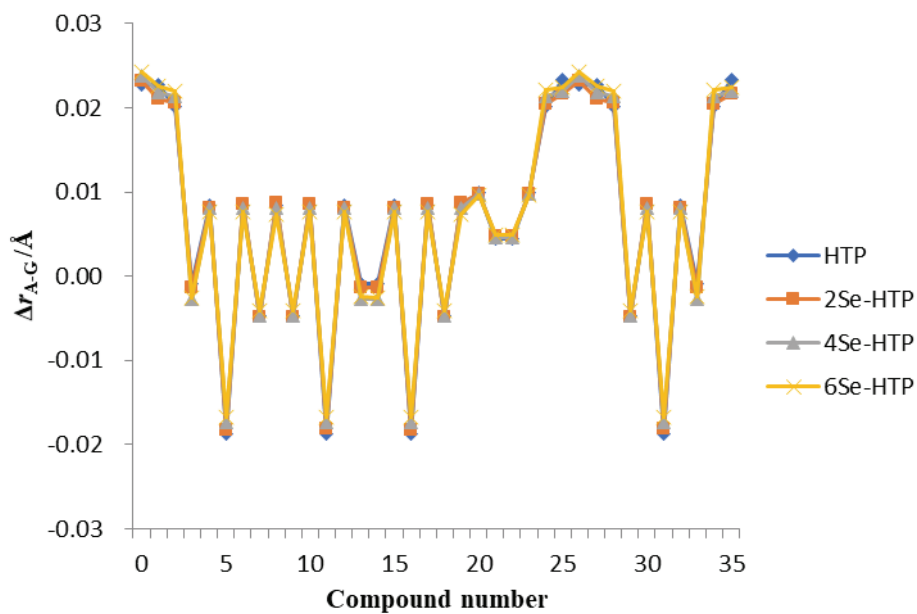
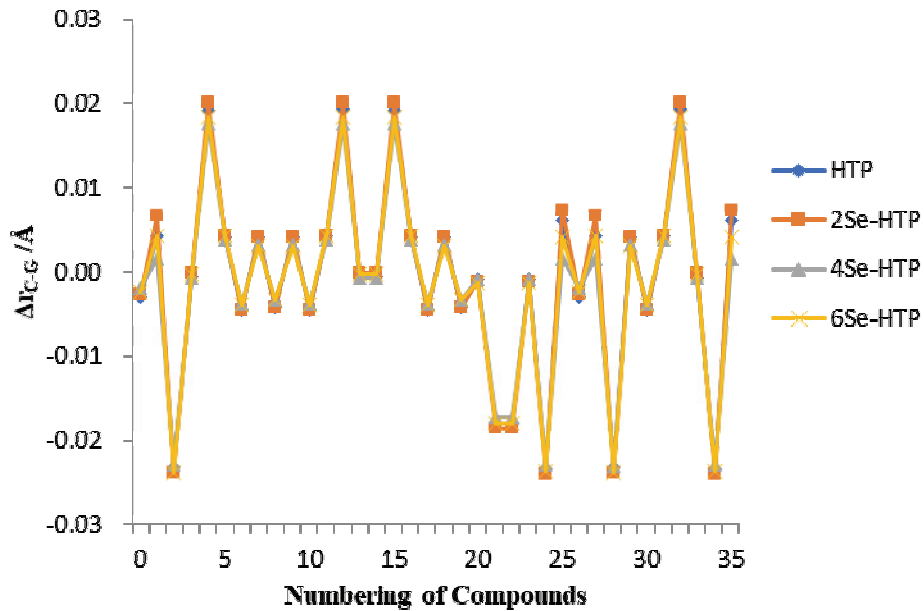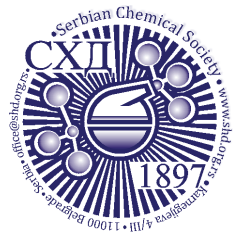Fig. S-2. Variations of bond lengths (Δr_{A-G}) from molecule to anion.

Fig. S-3. Variations of bond lengths (Δr_{C-G}) from molecule to cation.

Folic acid conjugation of magnetite nanoparticles using pulsed electrohydraulic discharges

VLADIMER MIKELASHVILI[1]*, SHALVA KEKUTIA[1], JANO MARKHULIA[1], LIANA SANEBLIDZE[1], ZAUR JABUA[2], LÁSZLÓ ALMÁSY[3] and MANFRED KRIECHBAUM[4]

[1]*Vladimir Chavchanidze Institute of Cybernetics of the Georgian Technical University, Z. Anjafaridze str. 5, Tbilisi, 0186, Georgia,* [2]*Georgian Technical University, Kostava str. 77, Tbilisi 0160, Georgia,* [3]*Institute for Energy Security and Environmental Safety, Centre for Energy Research, Konkoly Thege str. 29–33, Budapest-1121, Hungary and* [4]*Institute of Inorganic Chemistry, Graz University of Technology, Stremayrgasse 9/5, A-8010 Graz, Austria*

Abstract: The sonochemical coprecipitation reaction with moderate ultrasound irradiation in a low vacuum environment was used to obtain aqueous colloidal suspensions of iron oxide nanoparticles (IONPs). The synthesized magnetite nanoparticles were conjugated directly by folic acid using electrohydraulic discharges as a processing technique before modification of the surface of the nanoparticles. Electrohydraulic discharges were applied in two operational modes with high and low power pulsed direct currents between the electrodes. The physical and chemical properties of the obtained samples were studied using X-ray powder diffraction (XRD), Fourier transform infrared spectroscopy (FTIR), dynamic light scattering (DLS) and small angle X-ray scattering (SAXS). The investigation proved an inverse cubic spinel structure of magnetite with folic acid attachment to the magnetite surface (mean crystallite diameter in the samples, *D*, ranges 25–31 nm by XRD and SAXS). It was found that the processing with electrohydraulic discharges increased the colloidal stability of the folic acid-magnetite nanoparticle dispersions.

Keywords: iron oxide nanoparticles; sonochemical coprecipitation; pulsed arc discharge; surface functionalization.

INTRODUCTION

High-voltage pulsed discharge (HVPD) into a liquid medium is an efficient method used in plasma science and technology. The interaction of non-equilibrium plasma (where the temperature of the ions is much less than that of the electrons $T_e >> T_{ions}$ depending on the energy and discharge type) with a liquid medium finds many important applications in the area of mechanical processing,

fracturing technology in mining,[1] environmental remediation,[2] production of nanomaterials and health care.[3–5] During pulsed electrohydraulic discharges (PEHD) the released electrical energy is converted to mechanical energy. Moreover, different physical and chemical phenomena occur during discharge, such as heat emission, shock wave formation, ultraviolet/visible radiation, the formation of chemically active species ($O^•$, $H^•$, $^•OH$, $HO_2^•$), ions (O^-, H^+, H_3O^+) and molecular species (O_2, O_3, H_2, H_2O_2) that either recombine to form stable by-products or return to a lower energetic state emitting in the ultraviolet (UV) range.[6–8]

In recent years, among the variety of discharge types, underwater spark discharges were intensively used in the low-cost production of nanoparticles (NPs) in solution. Although many experimental setups for nanoparticle production have been reported exploring variation of discharging type,[3] parameters (voltage, current), electrode material and configuration, *etc.*, there are very few reports about the processing of the chemically synthesized surface of nanomaterial by high--voltage pulsed arc electrohydraulic discharge for deagglomeration,[9] and further modification of the bare surface of nanoparticles by bioactive molecules for medical application.

Nowadays, the use of iron oxide nanoparticles (IONPs) in diagnostics and therapy is one of the modern strategies in nanomedicine. Magnetic nanocolloids containing IONPs of magnetite (Fe_3O_4) and maghemite (γ-Fe_2O_3) are promising and popular biomedical materials due to their unique magnetic properties. Magnetite exhibits antibacterial activity due to the reactive oxygen species (ROS) generated by Fe_3O_4 NPs, they are hydrophilic and biocompatible. They can be encapsulated with a suitable coating substance for biomedical applications.[10–12]

The most common and cost-effective method for obtaining IONPs is chemical co-precipitation. Although this method is relatively simple, it is necessary to develop an effective strategy to improve the precise control of the main properties of the NPs, such as size, shape, stability, reproducibility and dispersibility of NPs in desired solvents, for bioapplications.[13] The bare iron oxide NPs have high chemical activity and are easily oxidized in air (especially magnetite).[14] Therefore, providing a proper surface coating and developing effective protection strategies to maintain the stability of magnetic iron oxide NPs are important directions of current research.

The method of conjugating folic acid as a specific targeting molecule to magnetite particle is the key to the successful application of magnetic nanoparticles (MNPs) in targeted drug delivery for cancer treatment. Numerous attempts have been made to develop therapeutic drug delivery systems to synthesize folic acid-linked nanoparticle components using surface activation of IONPs with functional molecules, such as chitosan,[15] poly(ethylene glycol),[16,17] poly(ethyleneimine) (PEI),[18] carbodiimide,[19] carboxymethyl dextran,[20] serum folate-bind-

ing protein,[21] which increase their specific uptake by the tumor and inhibit cell growth in microbes and cancer. FA are forms of a water-soluble B_9 vitamin which is a stable, non-immunogenic and low-cost apart from protein-targeting molecules, such as antibodies.

In this paper, continuing previous works,[22–24] a facile method is reported to directly conjugate folic acid (FA) molecules to iron oxide nanoparticles using surface activation with PEHD after their synthesis using *in situ* sonochemical coprecipitation in a low vacuum environment.

EXPERIMENTAL

Chemicals

All chemicals were of analytical grade and used without further purification. Chemicals used for the synthesis of magnetite nanoparticles: ferric chloride hexahydrate ($FeCl_3 \cdot 6H_2O$) (≥ 98 %), ferrous sulfate heptahydrate ($FeSO_4 \cdot 7H_2O$), ammonium hydroxide solution (NH_4OH, 25 % of NH_3 basis), and folic acid ($C_{19}H_{19}N_7O_6$) (water content (by Karl Fischer) – 9 %, purity (HPLC) >97 %) were purchased from Sigma–Aldrich.

Synthesis of bare magnetic nanoparticles

Bare iron oxide (Fe_3O_4) nanoparticles were prepared by sonochemical coprecipitation with moderate ultrasound irradiation using an iron salt ratio Fe^{3+}/Fe^{2+} of 1.9. First, $FeCl_3 \cdot 6H_2O$ (9 g) + 333 ml distilled water (DW) (0.1 M solution) was prepared in the jacketed reactor 1 (see Fig. 1, temperature 45 °C, mixing duration 20 min, vacuum environment), and $FeSO_4 \cdot 7H_2O$ (4.87 g) +175 ml DW (0.1 M solution) – in the jacketed ultrasonic reactor 2 (temperature 45 °C, duration 20 min, ultrasonication 30 % of 900 W homogenizer, pulse on 2 s, pulse off 1 s).
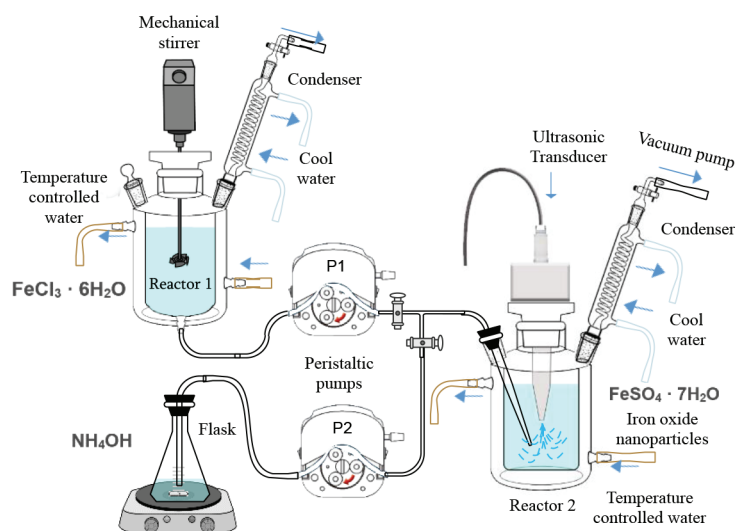

Fig. 1. Experimental set-up for the sonochemical coprecipitation reaction of IONPs with moderate ultrasound treatment in a low vacuum environment.

After dissolution, the iron salt solutions were passed by a peristaltic pump (P1) into the ultrasonic reactor (reactor 2), followed by further sonication. Then, a previously prepared 19 ml NH$_4$OH (25 %) + 35 ml DW (4 M solution) was added dropwise over 20 min at 45 °C in the middle area of reactor 2 using peristaltic pump P2 (see Fig. 1).

After the formation of the black precipitate, the obtained colloidal suspension was further sonicated for 30 min and gradually cooled to room temperature. This procedure resulted in 570 ml of a black suspension. This fluid was washed several times with an abundant quantity of DW with magnetic separation with a permanent magnet to reduce the pH to the physiological value (initial pH 12, after washing – pH 7.3) and remove the residues of the chemical synthesis. For each sample, 100 ml of the suspension was taken for the preparation of bare IONPs (sample: Bare-IONPs), FA-modified IONPs without PEHD processing (sample: IONPs-FA), FA-IONPs after PEHD processing in two operation modes (see description below) called IONPs-HC-FA and IONPs-LC-FA, respectively.

Electrohydraulic processing

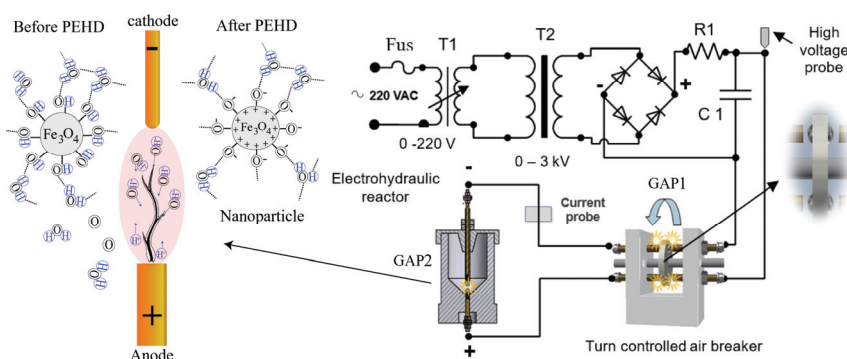A scheme of the electrohydraulic device is shown in Fig. 2.

Fig. 2. Electrohydraulic device scheme.

Electrohydraulic processing of 100 ml suspension containing IONPs was performed in a 300 ml volume reactor in a low vacuum. The entire fluid was processed for 5 min. Brass electrodes were immersed through the suspension in the middle of the discharge reactor.

The high voltage transformer T2 has maximum regulated voltage of 3 kV. After that alternating current is transformed to direct current by a diode bridge. The charge accumulated by the capacitor (C1) is transferred through an air gap (Gap 1) that regulates the discharge frequency (by rotating wheel controlled by motor) to the main discharge gap (Gap 2). A digital oscilloscope (Rigol DS1204B) monitors the discharge voltage (voltage transformer: Caltest CT4026) and current (current transformer: Ionphysics CM-01-L).

This device with controlled parameters allows the nanofluid to be processed in two modes:

1. High current (HC) mode (Fig. 3) – the distance between rods, $d = 0.7$ mm, discharge current, $A_{max} = 30$ A, voltage, $V = 1.3$ kV, frequency, $f = 2$ Hz, duration, $t_{max} = 20$ ms;

2. Low current (LC) mode – $d = 2$ mm, $A_{max} = 10$ A, $V = 1.6$ kV, $f = 2$ Hz, $t_{max} = 20$ ms.

The development of a spark discharge in time occurs by successive "germination" of streamers in the interelectrode gap (Fig. 2, GAP2) in which two types of ions (H$^+$ and OH$^-$) play the main role. A negative charge accumulated between the electrodes from OH$^-$ dissolve into the liquid, which easily gives off its electrons to the growing streamer channel and form

hydrated electrons (e_{aq}). The hydrated electrons have high reduction potential and induce H^+ reduction at the anode with H_2O and OH^- generation through electrolysis of water at the cathode, respectively, contributing to an increase in the pH value (Fig. 4):[1,7,8]

$$e \rightarrow e_{aq}; \; e_{aq} + H_2O_{aq} \rightarrow H_{aq} + OH_{aq}^-; \; e_{aq} + H_{aq}^+ \rightarrow H_{aq}$$
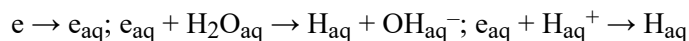
Discharges in water enhance the deprotonation reactions of suspended magnetic nanoparticles as their surface presents amphoteric behaviour:[25,26]

$$\equiv MOH + OH^- \rightarrow \equiv MO^- + H_2O$$
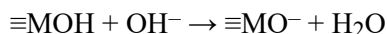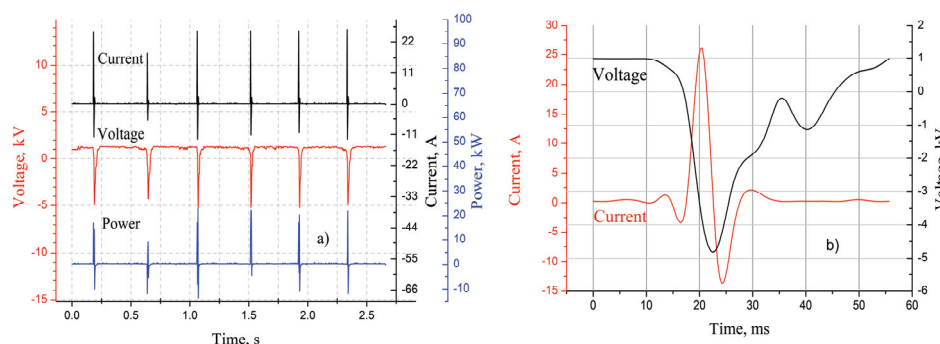
where M is the metal on the surface.

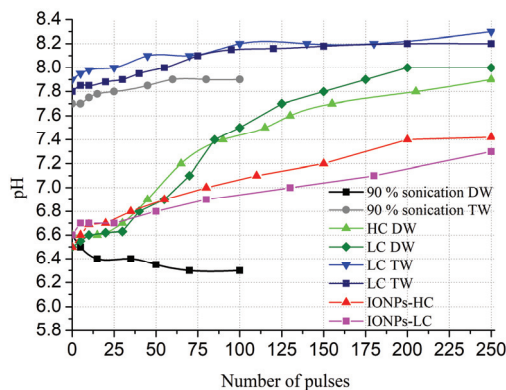Fig. 3. PEHD in HC mode. a) HC discharge set in 2.5 s; b) one discharge in HC mode.

Fig. 4. Comparison of change in pH during electrohydraulic discharge and ultrasonic processing. TW – tap water, DW – distilled water.

Accumulation of the superficial charge on the surface of nanoparticles (see Fig. 2) is due to the specific adsorption of ions (in the present case, Fe ions etching metals during discharge between brass electrodes) during pulsed discharge into water. If the pH is greater than the characteristic point of zero charge (concentrations of positive and negative sites are equal), the discharge develops a negative charge on the nanoparticle surface.

When the streamer passes through the liquid (in the present case, through water), the liquid ions, discharging onto a growing streamer as a "pull-out" electrode, form a thin gas cavity on its surface, which separates the already formed branch of the streamer from the surrounding liquid. The insulating cavity is formed by atomic and molecular oxygen and hydro-

gen, gaseous hydrogen peroxide, as well as electrically neutral free radicals H, OH, existing in the water vapor. Fluid molecules gaining acceleration from the discharge channel, move from discharge zone in all directions, forming a cavitation zone causing the first (main) shock wave. Then the cavity closes at high speed, creating a second spark discharge at given pulse parameters. A sharp increase in the channel temperature and sharp pressure jump induce additional decomposition/deagglomeration products in the liquid inside the channel.

Modification by folic acid

For direct modification (sample IONPs-FA), 100 ml washed precipitate sonicated for 10 min at 30 % energy (900 W, pulse – 2 s, on, 1 s, off) was taken. For 100 ml of suspension, 0.178 g of FA was taken. Previously, FA in 10 ml DW was stirred at 30 °C for 15 min and added by the peristaltic pump to the magnetic fluid and sonicated at 14 % power for 20 min at 30 °C (Fig. 1). After one day, the sample was washed by decanting and separation by a permanent magnet. The pH was increased to 7.4 by dropwise addition of NH_4OH (initial pH was 5.2) diluted in DW, and finally, centrifuged at 4000 rpm during 10 min. The same procedure was applied to the PEHD processed samples. To obtain IONPs-HC-FA and IONPs-LC-FA samples, the initial 2×100 ml of washed and sonicated suspension was processed separately by HC and LC - mode for 5 min each under vacuum and modified directly with FA (as described for sample IONPs-FA).

<div align="center">RESULTS AND DISCUSSION</div>

X-Ray diffraction (XRD)

The phase purity and crystal structure of the synthesized materials were identified *via* XRD analysis (Fig. 5) using a DRON 3M X-ray diffractometer, operating with CuK_α radiation ($\lambda = 1.541$ Å) filtered by a nickel foil, voltage – 40 kV, current 20 mA, and scanning speed 2°/min. The diffraction peaks at 2θ values of 30.56, 35.86, 43.46, 54.01, 57.38 and 63.00° were assigned to the crystal planes (220), (311), (400), (422), (511) and (440), respectively. All peaks match well with characteristic peaks of magnetite (Fe_3O_4) (JCPDS file No. 19-0629).
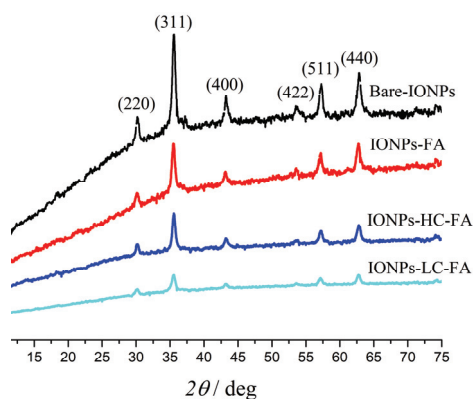

Fig. 5. XRD patterns of synthesized bare-IONPs, bare-IONPs conjugated directly by FA, bare-IONPs processed in the HC and LC mode and conjugated by FA after processing (IONPs-LC-FA and IONPs-LC-FA, respectively).

The X-ray diffraction pattern showed that the materials were crystalline, and no impurity peaks were observed. The average crystallite diameter ($D = 28\pm2$

nm) was calculated using the Scherrer Equation from the FWHM of the (311) peak at $2\theta = 35.86°$. The average value of the lattice parameter was found to be $a = 8.37$ Å. Although the presence of maghemite could not be excluded from the diffraction data, the black color of the suspensions and the large lattice parameter indicate a majority of magnetite phase in the prepared nanoparticles.

Fourier-transform infrared spectroscopy (FTIR)

In order to determine the functional groups on the surface of the obtained IONPs, FTIR analysis was performed using an Agilent Cary 670 (Mid-IR spectral range: 5000–400 cm^{-1}) on powder samples after drying in vacuum. The absorption bands of the synthesized iron oxide-NPs (Bare-IONPs) were observed at 3447, 1630, 895, 798 and 578 cm^{-1} (Fig. 6). The peak located at 578 cm^{-1} is associated with the stretching vibration mode of Fe–O characteristic for the magnetite NPs, while the absorption bands at 3447 cm^{-1} indicated the O–H stretching vibration, because the surfaces MNPs are covered with OH groups, as a result of the chemical co-precipitation. The H–O–H deformation peaks at 1630 cm^{-1} (for bare magnetite and also other samples) prove the presence of water adsorbed on the surface of the nanoparticles.[27,28] Comparing the spectrum of bare IONP with folic acid - conjugated IONP, it could be seen that several peaks appeared in the range of 1600–1100 cm^{-1} for the conjugated samples (Fig. 6c–e). These bands are attributed to carboxylic group (C=O) group vibrations of folic acid in the FA--conjugated samples (especially Fig. 6e), indicating FA attachment to the NP surface.
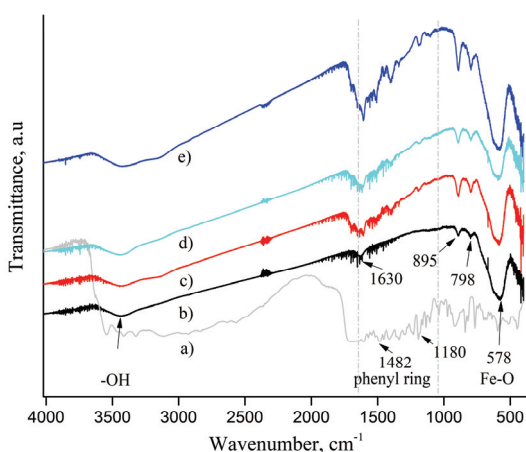

Fig. 6. FTIR spectra of FA (a), bare--IONPs (b), IONPs-FA (c), IONPs--LC-FA (d) and IONPs-HC-FA (e) samples.

Dynamic light scattering (DLS) and zeta potential

In order to determine the hydrodynamic size (D_{hyd}) distribution profile of primary nanoparticles and their aggregates in suspension, an Anton Paar Lite-

sizer™ 500 equipped with a 658-nm laser was used at 25 °C in the back scattering geometry. The refractive indices (*RI*) for the investigated particles (Fe_3O_4 phase) was set to $n = 2.3636$ and $n = 1.3310$ was set for the solvent (distilled water). For an assessment of the stability of the colloidal dispersions and thus the strength of electrostatic repulsion between similarly charged particles, the zeta potential (ζ) of the aqueous suspensions was measured using the same instrument with a scattering angle of 173° at 25 °C and adjusted voltage 200 V. As expected, bare uncovered IONPs possess high hydrodynamic diameter and smaller magnitude of the zeta potential because of the stronger agglomeration. All FA-conjugated samples have the same diameters, although IONPs-FA have a lower zeta potential (19.3 mV) because of partial, insufficient covering.

Small-angle X-ray scattering (SAXS)

The angular distribution of X-rays scattered by the samples injected into quartz capillary at very small (< 10°) angles and at 25 °C was performed on a SAXSpoint 2.0 instrument (Anton Paar GmbH) equipped with a MicroSource, Primux 100 copper X-ray generator ($\lambda = 0.154$ nm) and an Eiger R 1M Tilt 2D detector. In the case of isotropic scattering, the measured intensities are regrouped by radial averaging and presented as the intensity *I* as a function of momentum transfer or length of the scattering vector *q*:

$$q = \frac{4\pi \sin \phi}{\lambda} \tag{1}$$

where ϕ is the scattering angle and λ is the wavelength of the X-ray radiation. In order to obtain information of the scattering of the particles only, background subtraction was performed by the ATSAS software (Fig. 7).[29,30]
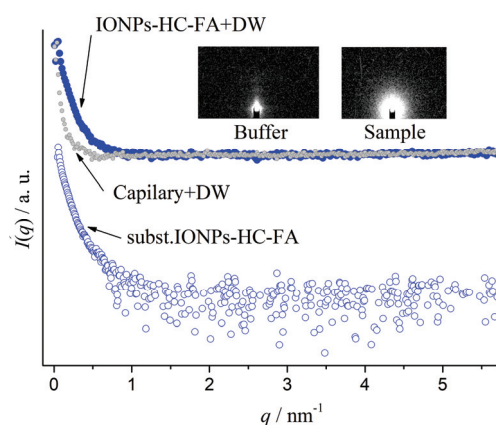

Fig. 7. Experimental image data by a 2D detector (insets) and the circularly averaged scattering curves before and after subtraction of the background scattering. (sample – IONPs-HC-FA diluted in DW) and buffer material (capillary with DW).

One of the most important parameters that provides an estimate of the overall size of a particle (the average electron density-weighted squared distance

to center-of-mass in a particle) is the radius of gyration, R_g (see Fig. 8), which describes the average size of the particles:[31]

$$I(q) = I(0)e^{\frac{-R_g^2 q^2}{3}} \qquad (2)$$

where $I(0)$ is forward scattered intensity. The linearity of the Guinier plot (ln I against q^2) is a sensitive indicator of the quality of the experimental data. Deviation from a straight line could indicate aggregation, or a large polydispersity of the scattering particles.

For evaluating the pair distance distribution function $p(r)$ (probable distribution of distances between electrons, Fig. 9), GNOM was used as an indirect Fourier transform program for small-angle scattering data analysis.[32,33]
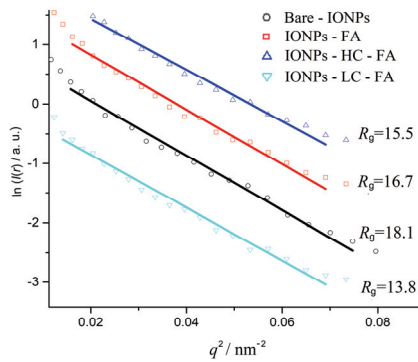

Fig. 8. Guinier plots for evaluating the radius of gyration R_g in the colloid dispersions.
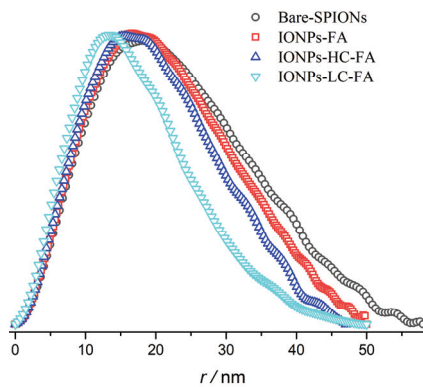

Fig. 9. Pair distribution functions $p(r)$ obtained by GNOM.

Using the output data of GNOM, an *ab initio* shape determination was performed using the bead-modeling program DAMMIF.[32] Starting from an arbitrary initial model, DAMMIF utilizes simulated annealing to construct a compact interconnected cluster of small spherical beads yielding a calculated scattering curve matching the experimental data. As expected, the reconstructed particle

shapes resemble aggregates of nearly spherical particles, Fig. 10. The IONPs-FA clusters have more irregular shapes, which could be related to the effect of the FA coating on the particle agglomeration process.

Bare - IONPs   IONPs - FA   IONPs - HC - FA   IONPs - LC - FA

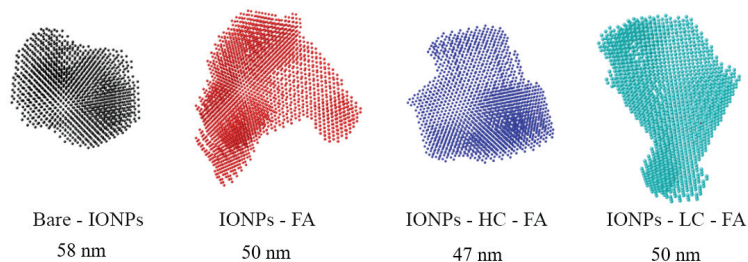58 nm   50 nm   47 nm   50 nm

Fig. 10. Bead models of bare and FA-conjugated magnetite clusters containing nanoparticles obtained by the DAMMIF. Numbers in nanometers – maximum cluster diameters (D_{max}).

The scattering curves and subsequent modeling indicate the presence of agglomerates for all the samples.[4,37] Small angle scattering data of agglomerated surfactant-stabilized magnetite nanoparticles in aqueous dispersions are often analyzed using empirical models, such as fractal dependences or the Beaucage model.[36–38]

The assumed-free size distributions of the particles and agglomerates obtained from the scattering patterns by the Monte-Carlo fitting method were evaluated using McSAS software.[39,40] For the Monte Carlo runs, the following parameter values were used: lower and upper q cut-off: 0.05–2.9 nm^{-1}, respectively; number of repetitions 10; model – sphere, distribution of sphere radii between 3–50 nm. The resulting volume-weighted size histograms are shown in Fig. 11, with uncertainties on the bars, and the red dashed line indicating the minimum level required for each bar to contribute in a measurable amount to the scattering pattern (*i.e.*, sensitivity limit).

The obtained distributions are very similar for all the samples, with some variations in the radius range of 20–60 nm, and most of the particles have radii 13–14 nm, which is in good agreement with the single particle or crystallite size obtained from the XRD data.

The analysis results are collected in Table I. The size distribution as given by McSAS analysis reveals two populations, the single nanoparticles, with mean diameter of 22 nm, and the agglomerates with a size distribution from 40 to 100 nm in diameter, with different cluster diameters D_{max} (Fig. 10).

The mechanism of FA conjugation depends on high values of surface charge density of the water-based iron oxide colloids, the pH of the medium, and the ionic strength of the dispersion. In addition, the presence of specific ions (also, the etching particles from brass electrodes in the HC-mode consisting of zinc and copper) at the solid–liquid interface can induce the formation of chemical bonds

favorable for FA conjugation in addition to the pure Coulombic attraction. This interaction is quite probable due also to the fact that FA interacts with the negative charge of the magnetite surface at increased pH values. Comparing dried powder samples of the same mass, the higher intensities of the FA characteristic peaks show that the sample IONPs-HC-FA has a better coating compared to the sample IONPs-LC-FA, in which the particles are less stable and may agglomerate and flocculate due to the smaller surface charge.
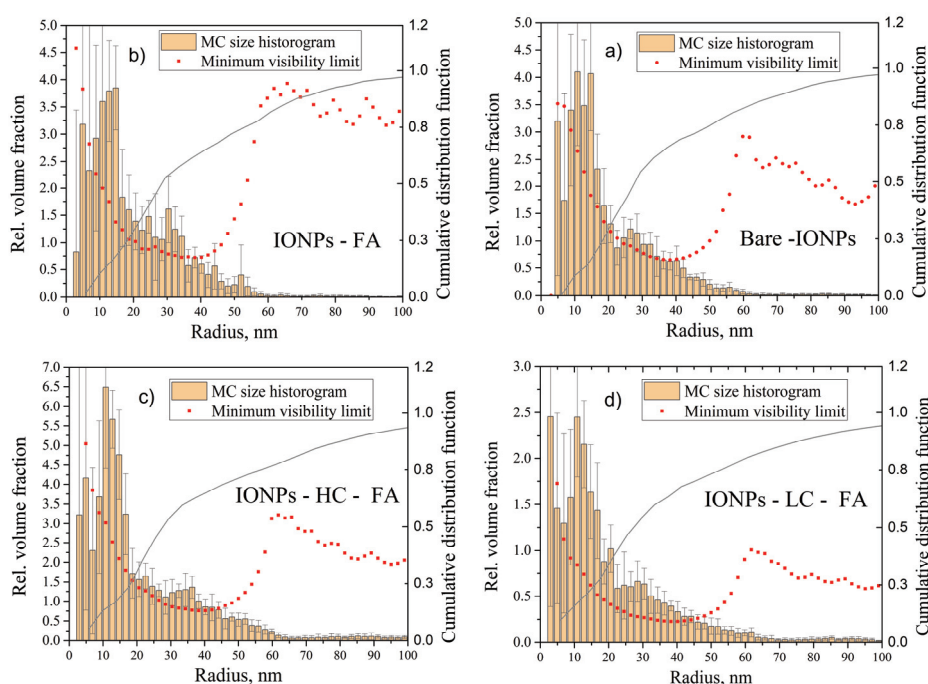

Fig. 11. Particle size distributions obtained using McSAS.

TABLE I. Results of DLS, Zeta potential and SAXS measurements

Material	D_{hyd} / nm	ζ_{mean} / mV	ρ / mS cm^{-1}	$R_g{}^a$ / nm	$D_{max}{}^b$ / nm	$r_{mean}{}^c$ / nm
Bare-IONPs	226.4	21.2	0.019	18.1	58	14
IONPs-FA	141	19.3	0.012	16.7	50	13
IONPs-HC-FA	141.73	25.6	0.013	15.5	47	13.4
IONPs-LC-FA	147.27	24.6	0.038	13.8	50	13.5

[a]Retrieved by PRIMUS; [b]evaluated by DAMMIF; [c]calculated by MsSAS

CONCLUSIONS

A simple, inexpensive and suitable for upscaling technology of preparation of functionalized iron oxide nanoparticles for biomedical use, using non-thermal plasma discharges in water (electrohydraulic discharges) has been developed.

Electrohydraulic discharges assist the modification of MNPs with a bioactive molecule such as folic acid, as proved by FTIR analysis. The presence of specific ions, increased pH and superficial charge around the electohydraulically processed IONPs induce the formation of chemical bonds favorable for FA conjugation in the IONPS-HC-FA dispersions that showed increased zeta potential and stability, compared to the IONPs-LC-FA dispersions and those prepared without electrohydraulic discharges.

ИЗВОД

КОНЈУГАЦИЈА МАГНЕТИТНИХ НАНОЧЕСТИЦА ФОЛНОМ КИСЕЛИНОМ КОРИШЋЕЊЕМ ИМПУЛСНИХ ЕЛЕКТРОХИДРАУЛИЧНИХ ПРАЖЊЕЊА

VLADIMER MIKELASHVILI[1], SHALVA KEKUTIA[1], JANO MARKHULIA[1], LIANA SANEBLIDZE[1], ZAUR JABUA[2], LÁSZLÓ ALMÁSY[3] и MANFRED KRIECHBAUM[4]

[1]*Vladimer Chavchanidze Institute of Cybernetics of the Georgian Technical University, Z. Anjafaridze str. 5, Tbilisi, 0186, Georgia,* [2]*Georgian Technical University, Kostava str. 77, Tbilisi 0160, Georgia,* [3]*Institute for Energy Security and Environmental Safety, Centre for Energy Research, Konkoly Thege str. 29–33, Budapest-1121, Hungary* и [4]*Institute of Inorganic Chemistry, Graz University of Technology, Stremayrgasse 9/5, A-8010 Graz, Austria*

Сонохемијска реакција копреципитације са умереним ултразвучним зрачењем у ниском вакууму коришћена је за добијање водених колоидних суспензија наночестица гвожђе-оксида. Синтезоване наночестице магнетита директно су конјуговане фолном киселином користећи електрохидраулична пражњења као технику обраде пре модификације површине наночестица. Електрохидраулична пражњења примењена су у два оперативна режима са импулсним једносмерним струјама велике и мале снаге између електрода. Физичка и хемијска својства добијених узорака проучавана су применом дифракције рендгенског зрака (XRD), инфрацрвене спектроскопије са Фоуријеовом трансформацијом (FTIR), динамичког расејања светлости (DLS) и рентгенског расејања малих углова (SAXS). Испитивањем је доказана инверзна кубна структура спинела магнетита са везивом фолне киселине на површину магнетита (средњи пречник кристалита, *D*, у узорцима, одређен помоћу XRD и SAXS, је био у опсегу 25–31 nm). Утврђено је да обрада електрохидрауличким пражњењем повећава колоидну стабилност дисперзија наночестица фолне киселине и магнетита.

(Примљено 11. априла, ревидирано 2. септембра, прихваћено 5. септембра 2020)

REFERENCES

1. L. A. Yutkin, *Electro-hydraulic effect and its application in industry*, Engineering, Leningrad, 1986, p. 252 (http://bourabai.ru/library/elektrogidravlicheski_effekt.pdf)
2. E. Leal-Quirós, *Braz. J. Phys.* **34** (2004) 1587 (http://dx.doi.org/10.1590/S0103-97332004000800015)
3. G. Saito, T. Akiyama, *J. Nanomater.* **2015** (2015) 1 (http://dx.doi.org/10.1155/2015/123696)

4. H. Li, K. Wang, X. Tuo, L. Almásy, Q. Tian, G. Sun, M. J. Henderson, Q. Li, A. Wacha, J. Courtois, M. Yan, *Mater. Chem. Phys.* **204** (2018) 236 (http://dx.doi.org/10.1016/j.matchemphys.2017.10.047)
5. S. Horikoshi, N. Serpone, *RSC Adv.* **7** (2017) 47196 (http://dx.doi.org/10.1039/c7ra09600c)
6. Ruma, H. Hosano, T. Sakugawa, H. Akiyama, *Catalysts* **8** (2018) 213 (http://dx.doi.org/10.3390/catal8050213)
7. S. Wakisaka, K. Tsuda, K. Takahashi, K. Satoh, *IEEE Trans. Plasma Sci.* **47** (2019) 1083 (https://doi.org/10.1109/TPS.2018.2866282)
8. H. Shiraishi, G. R. Sunaryo, K. Ishigure, *J. Phys. Chem.* **98** (1994) 5164 (https://doi.org/10.1021/j100070a037)
9. M. I. Lerner, I. A. Gorbikov, O. V. Bakina, S. O. Kasantzev, *Inorg. Mater. Appl. Res.* **8** (2017) 473 (http://dx.doi.org/10.1134/S2075113317030169)
10. P. M. Price, W. E. Mahmoud, A. A. Al-Ghamdi, L. M. Bronstein, *Front. Chem.* **6** (2018) 619 (http://dx.doi.org/10.3389/fchem.2018.00619)
11. T. Vangijzegem, D. Stanicki, S. Laurent, *Expert Opin. Drug Deliv.* **16** (2019) 69 (http://dx.doi.org/10.1080/17425247.2019.1554647)
12. S. Palanisamy, Y. M. Wang, *Dalton Trans.* **48** (2019) 9391 (http://dx.doi.org/10.1039/c9dt00459a)
13. A. Stepanov, R. Mendes, M. Rümmeli, T. Gemming, I. Nizameev, A. Mustafina, *Chem. Pap.* **73** (2019) 2715 (http://dx.doi.org/10.1007/s11696-019-00823-9)
14. A. Ali, H. Zafar, M. Zia, I. ul Haq, A. R. Phull, J. S. Ali, A. Hussain, *Nanotechnol. Sci. Appl.* **9** (2016) 49 (http://dx.doi.org/10.2147/NSA.S99986)
15. H. Arami, Z. Stephen, O. Veiseh, M. Zhang, *Adv. Polym. Sci.* **243** (2011) 163 (http://dx.doi.org/10.1007/12_2011_121)
16. T. Keskin, S. Yalcin, U. Gunduz, *Inorg. Nano-Metal Chem.* **48** (2018) 150 (http://dx.doi.org/10.1080/24701556.2018.1453840)
17. M. Erdem, S. Yalcin, U. Gunduz, *Hum. Exp. Toxicol.* **36** (2017) 833 (http://dx.doi.org/10.1177/0960327116672910)
18. H. Yoo, S. K. Moon, T. Hwang, Y. S. Kim, J. H. Kim, S. W. Choi, J. H. Kim, *Langmuir* **29** (2013) 5962 (http://dx.doi.org/10.1021/la3051302)
19. A. Ancira-Cortez, E. Morales-Avila, B. E. Ocampo-Garciá, C. González-Romero, L. A. Medina, G. López-Téllez, E. Cuevas-Yáñez, *J. Nanomater.* **2017** (2017) 1 (http://dx.doi.org/10.1155/2017/5184167)
20. Q. L. Jiang, S. W. Zheng, R. Y. Hong, S. M. Deng, L. Guo, R. L. Hu, B. Gao, M. Huang, L. F. Cheng, G. H. Liu, Y. Q. Wang, *Appl. Surf. Sci.* **307** (2014) 224 (http://dx.doi.org/10.1016/j.apsusc.2014.04.018)
21. J. Chen, S. Klem, A. K. Jones, B. Orr, M. M. B. Holl, *Bioconjug. Chem.* **28** (2017) 81 (http://dx.doi.org/10.1021/acs.bioconjchem.6b00526)
22. J. Markhulia, V. Mikelashvili, S. Kekutia, L. Saneblidze, Z. Jabua, D. Daraselia, D. Jafaridze, *J. Pharm. Appl. Chem.* **2** (2016) 33 (http://dx.doi.org/10.18576/jpac/020201)
23. J. Markhulia, S. Kekutia, Z. Jabua, V. Mikelashvili, L. Saneblidze, in *Proceedings of 7th International Multidisciplinary Scientific GeoConference SGEM 2017,* (2017), Sofia, Bulgaria, *SGEM2017 Conference Proceedings* **17,** SGEM, Sofia, 2017, pp. 51–58 (http://dx.doi.org/10.5593/sgem2017/61/S24.007)
24. J. Markhulia, S. Kekutia, N. Mitskevich, V. Mikelashvili, L. Saneblidze, N. Leladze, Z. Jabua, L. Sacarescu, M. Kriechbaum, L. Almásy, *Dig. J. Nanomater. Biostructures* **13** (2018) 1081 (http://www.chalcogen.ro/1081_MarkhuliaJ.pdf)

25. A. F. C. Campos, W. C. De Medeiros, R. Aquino, J. Depeyrot, *Mater. Res.* **20** (2017) 1729 (http://dx.doi.org/10.1590/1980-5373-MR-2017-0649)

26. E. Illés, E. Tombácz, *J. Colloid Interface Sci.* **295** (2006) 115 (https://doi.org/10.1016/j.jcis.2005.08.003)

27. F. Márquez, G. M. Herrera, T. Campo, M. Cotto, J. Ducongé, J. M. Sanz, E. Elizalde, Ó. Perales, C. Morant, *Nanoscale Res. Lett.* **7** (2012) 210 (http://dx.doi.org/10.1186/1556-276X-7-210)

28. M. Mahdavi, M. Bin Ahmad, M. J. Haron, F. Namvar, B. Nadi, M. Z. Ab Rahman, J. Amin, *Molecules* **18** (2013) 7533 (http://dx.doi.org/10.3390/molecules18077533)

29. D. Franke, M. V. Petoukhov, P. V. Konarev, A. Panjkovich, A. Tuukkanen, H. D. T. Mertens, A. G. Kikhney, N. R. Hajizadeh, J. M. Franklin, C. M. Jeffries, D. I. Svergun, *J. Appl. Crystallogr.* **50** (2017) 1212 (http://dx.doi.org/10.1107/S1600576717007786)

30. P. V. Konarev, V. V. Volkov, A. V. Sokolova, M. H. J. Koch, D. I. Svergun, *J. Appl. Crystallogr.* **36** (2003) 1277 (http://dx.doi.org/10.1107/S0021889803012779)

31. A. Guinier, G. Fournet. *Small-Angle Scattering of X-rays,* Wiley, New York, 1955 (https://pdfs.semanticscholar.org/e307/79ad3cf2fb2e2c0a4d6c6b9f6a92bafec4a8.pdf)

32. A. V. Semenyuk, D. I. Svergun, *J. Appl. Crystallogr.* **24** (1991) 537 (http://dx.doi.org/10.1107/S002188989100081X)

33. D. I. Svergun, *J. Appl. Crystallogr.* **24** (1992) 495 (http://dx.doi.org/10.1107/S0021889892001663)

34. D. Franke, D. I. Svergun, *J. Appl. Crystallogr.* **42** (2009) 342 (http://dx.doi.org/10.1107/S0021889809000338)

35. S. Zhu, Y. Leng, M. Yan, X. Tuo, J. Yang, L. Almásy, Q. Tian, G. Sun, L. Zou, Q. Li, J. Courtois, H. Zhang, *Appl. Surf. Sci.* **447** (2018) 381 (http://dx.doi.org/10.1016/j.apsusc.2018.04.016)

36. D. F. Coral-Coral, J. A. Mera-Córdoba, *DYNA* **86** (2019) 135 (http://dx.doi.org/10.15446/dyna.v86n209.73450)

37. V. I. Petrenko, O. P. Artykulnyi, L. A. Bulavin, L. Almásy, V. M. Garamus, O. I. Ivankov, N. A. Grigoryeva, L. Vekas, P. Kopcansky, M. V. Avdeev, *Colloids Surfaces, A* **541** (2018) 222 (http://dx.doi.org/10.1016/j.colsurfa.2017.03.054)

38. A. Taufiq, Sunaryono, N. Hidayat, A. Hidayat, E. G. R. Putra, A. Okazawa, I. Watanabe, N. Kojima, S. Pratapa, Darminto, *Nano* **12** (2017) 1750110 (http://dx.doi.org/10.1142/S1793292017501107)

39. B. R. Pauw, J. S. Pedersen, S. Tardif, M. Takata, B. B. Iversen, *J. Appl. Crystallogr.* **46** (2013) 365 (http://dx.doi.org/10.1107/S0021889813001295)

40. B. R. Pauw, C. Kästner, A. F. Thünemann, *J. Appl. Crystallogr.* **50** (2017) 1280 (http://dx.doi.org/10.1107/S160057671701010X)

Evaluation of laterite as a filter media to remove arsenic from groundwater

HAFZA RUQYA MAQSOOD[1], SHAH RUKH[2]*, MUHAMMAD IMRAN[1], AYAZ MEHMOOD[3], WAZIR AHMAD[1], AMAR MATLOOB[4], HAFIZ SHAHZAD AHMAD[1], AHMAD KHAN[5] and SUNDUS AROOJ BUTT[5]

[1]*Department of Soil and Environmental Sciences, MNS-University of Agriculture, Multan, Pakistan,* [2]*National Center of Excellence in Geology, University of Peshawar, Pakistan,* [3]*Department of Soil and Climate Sciences, University of Haripur, Haripur, Pakistan,* [4]*Department of Agronomy, MNS-University of Agriculture, Multan, Pakistan and* [5]*Institute of Soil Science, PMAS-Arid Agriculture University Rawalpindi, Pakistan*

Abstract: Arsenic in drinking water has a chronic effect on humans and thus is a global health issue. Most people of Pakistan use groundwater for drinking, and consequently, prone to As toxicity. The objective of this study was to evaluate laterite as an adsorbent media for As removal, and subsequent preparation of a low-cost As filter. Laterite was tested for As adsorption capacity through batch sorption experiments and fitting to the Langmuir model. Two identical filters were prepared using variable particle size of laterite and substrate material ratios (sand, activated carbon, and brick chips). Arsenic contaminated water was poured daily and collected at the bottom for analysis. The water samples were analyzed for As using an atomic absorption spectrophotometer coupled with a hydride generation assembly. Other water quality parameters *viz.*, electrical conductivity (*EC*), pH, chloride, total suspended solids (*TSS*), total dissolved salts (*TDS*), nitrate, calcium, magnesium, sodium, potassium, carbonate, bicarbonate and sulfate contents were also tested. Filter 1 had an As removal efficiency from 83 to 93 %, while Filter 2 had 67 to 85 % removal efficiency. Most of the water quality parameters remained under the WHO recommended limits indicating no harmful addition to the filtered water by substrates. It appears that laterite may serve as an economical option for As removal from contaminated groundwater.

Keywords: arsenic adsorption; Langmuir isotherm; low-cost adsorbent; drinking water treatment.

INTRODUCTION

Water pollution is one of the major threats people are facing all around the world. The World Health Organization (WHO) reported 768 million people had no access to safe drinking water, which ultimately causes widespread diseases in many areas of the world.[1] According to worldwide ranking of drinking water quality, Pakistan came 80th of 122 countries. Groundwater contamination is one of the major problems caused by both natural and anthropogenic activities. In developing countries, such as Pakistan, chemicals used in agriculture and inappropriate industrial and municipal waste disposal are of major public health concerns.

Arsenic ranks 20th in the earth crust metalloid ranking, about 12th in the human body and 14th in seawater.[2] Arsenic causes serious environmental and health issues throughout the world[3] and especially countries such as India, Bangladesh, China and Nepal have higher reported incidence.[4] Shallow groundwater of many Asian (Pakistan, Bangladesh, Vietnam, Thailand, Mongolia, China and India), European (Germany and Hungary), South American (Argentina and Chile) and North American countries (USA, Canada and Mexico) have As contamination. Arsenic contamination is widely reported in many parts of Pakistan. A collaborative study between the Public Health Engineering Department of Pakistan and UNICEF revealed the alarming situation of As-enriched groundwater throughout the Indus alluvial basin. Ironically, an As concentration as high as 906 µg L^{-1} has been reported for the district Muzaffargarh in Southern Punjab.[5] The results of the monitoring program indicated that many areas of Punjab and Sindh province have As contaminated groundwater that is being used as drinking water.[6,7] The rural community of these areas uses naturally As contaminated groundwater for drinking purposes.[8] Due to the relative mobility of As over a wide range of redox conditions, it can appear simultaneously in soil and water. In reduced conditions, As is relatively more mobile and form oxyanions that are harmful even at µg L^{-1} levels. Overall, As occurs in four oxidation states -3, 0, $+3$, $+5$, and of these oxidation states, $+3$ and $+5$ are most prevalent in aqueous environments.[9] It was reported that both organic and inorganic forms of As can exist in natural waters, whereby the inorganic forms (arsenate As(V) and arsenite As(III)) are more toxic than the organic forms.

In the environment, natural and anthropogenic sources are the two major pathways of As release. The terrestrial amount of As is 1.5–3 mg kg^{-1}.[10] Currently, different electronic devices contain As and on their disposal and recycling process release As into the environment. In addition, industrial activities result in As contamination.[11] Several anthropogenic activities cause increases in the As concentrations in groundwater and surface waters. These include power plants running on oil and coal, wood preservatives, electronics and glassware production, treatment of ores and metals, processing, and production, combustion of

waste, cement works, disinfectants and pesticides, waste disposal, dyes and colors and cotton drying agents.[12–15] Human activities, besides surface application of As-containing chemicals, pumping water also causes contamination of groundwater due to dissolution and washing of As bearing sediments. Since 1993, the WHO guideline value for As in drinking water was decreased from 50 to 10 $\mu g\ L^{-1}$. Similarly, the permissible limit for As in drinking water in Japan is 10 $\mu g\ L^{-1}$, whereas the maximum permissible concentration for As in Canadian drinking water is 25 $\mu g\ L^{-1}$. Indeed, on a global scale As is considered one of the most harmful inorganic contaminants in drinking groundwater.

Laterite is a red colored mineral rock, extensively found in various parts of the country.[16] Rocks containing high ferromagnetism minerals give rise to thicker layers of laterite having relatively higher concentration of iron.[16] The iron and aluminum contents are higher than the silicon content. Subsequently, natural laterite comprises minerals that are assemblages of goethite, hematite, Al hydroxide, kaolinite and quartz.[17] Due to its rich content of Fe and Al oxides, Laterite could be a potential adsorbent media for the removal of As from drinking water.

In India (Bengal, Purulia, Bankura and West Midnapore) and Bangladesh, laterite soils are extensively found and have been tested for the removal of arsenic from drinking water.[18–20] During the studies, laterite was used as a filtering material, which reduced the arsenic content by up to 99 % from the actual arsenic in the contaminated groundwater.[19] In Sri Lanka, naturally obtainable laterite was used as an effective adsorbent for the removal of arsenic from contaminated water.[21] The dominant form of arsenic in water is arsenate, which could also be removed using laterite as the adsorption material.[22] In one study, the operational conditions were accessed for the evaluation of the natural efficiency of laterite to remove As(V) from groundwater after determining the adsorption capacity through the Langmuir isotherm model, which was 0.565 mg g^{-1}. In another study, the acid treatment for the activation of four raw laterite samples with different compositions was optimized for their use their as adsorbents for the removal of arsenic from an aqueous system.[23]

Several studies were carried out on the preparation of indigenous filters for removing As from drinking water using low-cost adsorbing materials. Several natural sorbents, such as activated red mud and natural zeolite,[17,24] and a mixture of Fe, Al, manganese and titanium oxides and hydroxides with clay minerals and quartz grains,[25,26] were used for the sorption of inorganic As compounds from an aqueous solution.

The people living in rural areas are exposed to As toxicity, leading to serious health problems. Socio-economic constraints are creating hurdles in accessing As free water. A low cost and socially acceptable solution is required for the people living in affected areas. The present study was designed to evaluate local reserves

of laterite present in Pakistan as an adsorbent media for As removal from drinking water and develop a low-cost filter by using indigenous (laterite) material.

EXPERIMENTAL

To evaluation raw laterite as an adsorption media for As removal from drinking water and to prepare a low-cost filter, chemical analysis related to drinking water quality and a study of the As adsorption capacity of laterite was carried out.

Sampling and processing

Raw laterite was collected from District Rawalpindi (Near Nicholson Monument) ground and passed through 53-micron mesh size sieve. Fine sand was collected and thoroughly washed with distilled water before packing. Brick chips were collected, ground (passed through 2 mm sieve), and washed with distilled water before packing. Wood charcoal was collected, crushed, and treated with 25 % $CaCl_2$ to convert it into activated carbon[27] before packing.

Adsorption experiment

In triplicate, 3 g laterite sample was equilibrated in batch sorption experiments with 30 mL 0.01 M KNO_3 solution containing As (as Na_2AsO_4) 0, 0.1, 2.5, 5, 8, 10, 15, 20, 25, 40 and 100 mg L^{-1}. The suspension was shaken for 48 h at room temperature and centrifuged. A 0.45 micron cellulose membrane of was used to filter the supernatant, and the total As was determined. The sorbed amount of As was calculated from the change in the solution phase concentration. The adsorption isotherm data was fitted to the Langmuir model to calculate maximum adsorption capacity (b) and surface binding strength (K).[28,29] The following Langmuir equation was used:

$$x = \frac{bKc_w}{1 + Kc_w} \tag{1}$$

The linear form of the Langmuir model is:

$$\frac{c_w}{xm^{-1}} = \frac{1}{Kb} + \frac{c_w}{b} \tag{2}$$

where c_w is the equilibrium concentration, x is the adsorbed concentration, m is mass of soil, K is surface binding strength, and b is the maximum adsorption.

Filter preparation

For the filling of substrates, a clay pitcher was used due to its low cost, local manufacture, and easy availability. Layers of the substrates material were packed in the pitchers (Table I). During packing, an nylon mesh was placed between each layer to keep the layers intact. Laterite was the active As removal component. Sand was used for filtering any suspended particles and ensuring an equal distribution of flow. Activated carbon was used for its ability to remove organic pollutants while the function of brick chips was to stabilize the flow. The two major differences in the packing material of the filters were the size of the particle size of the laterite and the nature of the carbon used.

Drinking water quality parameters

Both non-filtered and filtered water were analyzed for various water quality parameters. Electrical conductivity and pH was measured using calibrated EC and pH electrodes.[30,31] Arsenic contaminated samples before and after filtration were analyzed for Na, K and Ca

using a BWB XP flame photometer following standard methods of APHA.[32] Chloride was measured by a Cl specific ion electrode using potentiometry,[33] CO_3^- and HCO_3^- were determined by the titration method,[34] using phenolphthalein and methyl orange indicators, respectively and 0.01 M H_2SO_4 as the titrant. Sulfate was determined in the samples using the turbidity method.[35] In this method, turbidity was produced by the addition of barium chloride crystals to acidified water samples, which was measured at 420 nm using Shimadzu UV–Vis spectrophotometer. The NO_3^- in water samples was determined by a colorimetric method.[36] The absorbance was measured at 410 nm after the addition of salicylic acid and H_2SO_4. The water quality parameters of the As-contaminated water used in this study are given in Table II.

TABLE I. Description of the materials used in the filters; values in parenthesis in second and third column are the mass of material used

Materials used	Filter 1	Filter 2
Laterite	Unit: 1 (6 kg)	Unit: 1 (6 kg)
	Unit: 2 (6 kg)	Unit: 2 (6 kg)
	53 μm particle size	2 mm particle size
Charcoal	Unit: 2 (2 kg)	Unit: 2 (2kg)
	Used as activated carbon	Used as raw charcoal
Sand	Unit: 1 (4 kg)	Unit: 1(4 kg)
	Unit: 2 (4 kg)	Unit: 2 (4 kg)
Brick chips	Unit:1 (0.5 kg)	Unit:1 (0.5 kg)
	Unit: 2 (1 kg)	Unit:2 (0.5 kg)

TABLE II. Water quality parameters for the unfiltered raw water used in the experiments; ND – not detected

EC / μS cm^{-1}	pH	Concentration, mg L^{-1}									
		As	SO_4^-	Cl	TDS	Na	K	Ca	NO_3^-	HCO_3^-	CO_3^-
8.5	7.8	0.093	120	5877	6500	50	55	44	0.45	47	ND*

Determination of As

Total As in the non-filtered and filtered samples was determined by using a Shimadzu AA-6300 atomic absorption spectrophotometer coupled with Shimadzua HVG-1 hydride vapor.

Generation assembly.[37] Initially, arsine (AsH_3) was produced by a premix of 0.4 % $NaBH_4$ and 0.5 % NaOH solutions mixed with 5 M HCl in a mixing chamber and gas–liquid separator chamber.[38] The detection limit was 2.42 μg L^{-1} as determined by analyzing 10 blanks and calculating the standard deviation ($\sigma = 0.26$). The detection limit was mean of 10 blank samples plus three times the standard deviation.

RESULTS AND DISCUSSION

Adsorption isotherm and model parameters

The adsorption capacity of laterite was tested as a potential adsorbent for As removal from the drinking water by employing the sorption batch method. The sorption isotherms were developed and Langmuir adsorption parameters were calculated by fitting adsorption isotherms in the Langmuir equation.

The isotherms for As depicted the sorption was initially fast with only a very small increase in the concentration of the equilibrium solution (Fig. 1). This trend of sorption isotherm was in line with the several previous studies in which a quick initial rise in sorption was observed, while later, the rise was moderate.[39] The maximum increase for As sorption was below 8000 mg kg^{-1}. It appears that oxides of Fe and Al play a vital role in the sorption of As. According to several studies, a strong adsorption relation of As with the Fe and Al oxides content has been observed.[40,41]
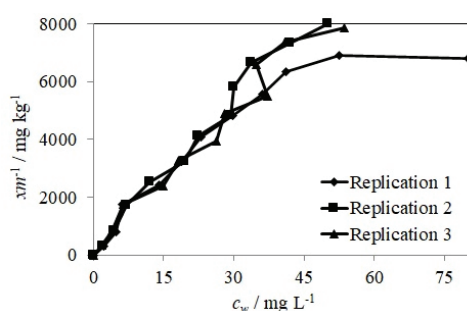

Fig. 1. Arsenic adsorption isotherms plotted between adsorbed concentration and concentration in the solution, indicating an initial fast adsorption and moderate adsorption later.

The fitted isotherms in the Langmuir equation, Eq. (1), showed $r^2 > 71$ as presented in Fig. 2. The maximum As adsorption capacity, b, was 20000 mg kg^{-1} and binding energy constant, K, was 0.011 L mg^{-1} as calculated from the linear regression Eq. (2). The results indicated high efficiency of laterite for the adsorption of As. As discussed earlier the major components in the laterite are Fe and Al oxides, which control the adsorption mechanism. Several studies showed the importance of Fe and Al oxides for the removal of As from aqueous solution. In most cases, the oxides were purchased from manufacturers, which resulted in increased the cost of the adsorbents. In one study, Fe$_2$O$_3$ and Al$_2$O$_3$ were used for the adsorption of As and observed maximum As adsorption was at pH 7 and values of b for Fe$_2$O$_3$ and Al$_2$O$_3$ were 660 and 117 mg kg^{-1}, respectively.[42] Similarly, synthetic Fe oxides–hydroxides (akaganeite) and modified akaganeite achieved a maximum adsorption capacity of 148.7 and 170.9 mg g^{-1} through the Langmuir isotherm.[43] As(III) and As(V) adsorption characteristics on laterite soil using both (Langmuir and Freundlich) adsorption models were observed with maximum adsorption capacities of 1.384 mg g^{-1} for arsenite and 0.04 mg g^{-1} for arsenate.[19]

Arsenic adsorption capacity in batch experiments was evaluated using a synthetic solution simultaneously containing arsenate and arsenite.[18] Additionally, it is apparent that the Langmuir isotherm better fitted the batch experiment results for calculating the adsorption capacity. The limitation regarding the use of synthetic and pure forms of the oxides of Fe and Al is its cost and availability in large quantities. Thus, laterite could be a better option as it is low cost and easy

availability. Furthermore, it has comparable adsorption capacity for As to those of sophisticated synthetically prepared Fe and Al oxides.
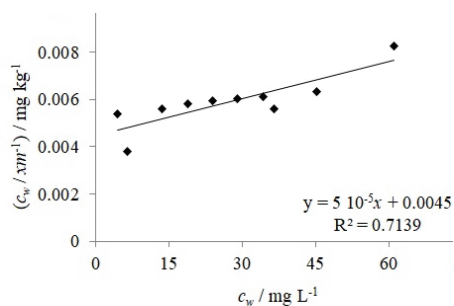

Fig. 2. The As removal by laterite isotherm fitted to the linear form of the Langmuir equation (Eq. (2)). Adsorption parameters for As were calculated from the regression equation.

After testing the adsorption capacity of laterite, a filter run test was performed by using laterite as the adsorbing medium in clay pitcher filters. Two different grain sizes of laterite were used with additional substrates. In one filter activated carbon was used while in other raw charcoal was used. The purpose was to improve the efficiency of the designed filter. Both filter sets were tested for a month by applying As containing tap water to mimic the natural environment.

Filter test and water quality parameters

In the trial, the designed filters were tested for 30 days by adding water daily. Detail of the application rate was briefly discussed in the methodology section. The collected samples were analyzed for EC, pH, TDS, K, Ca, Na, SO_4^-, NO_3^-, Cl^- and HCO_3^- (the results are presented graphically in Fig. S-1 of the Supplementary material to this paper and Fig. 2) and As.

Throughout the experiment, tap water was used with 93 µg L^{-1} As added. Arsenic was determined in the samples collected on the 1st, 15th and 30th day of the experiment. Details of the results are given in Table II. On the first day the removal efficiency was low, but it improved later on the 15th day and 30th day of the experiment. Arsenic adsorption was greatly increased in Filter 1. Filter 1 efficiently increased the adsorption concentration of As. On the first day, filter 1 had an efficiency of about 83 % and after 15 days its efficiency was increased to 92 % and at the end, after 30 days its efficiency increased to 93 %. Filter 2 also efficiently removed As from the drinking water. On the first day, Filter 2 showed an As removal efficiency of 67 % and after 15 days of continuous filtration and application of As contaminated water, it efficiency was about 80 % and after the 30th-day, the efficiency was up to 85 %. Both the filter adsorbates had a fast rise in adsorption. In Filter 1, fine laterite was used which was ground and passed through the 0.53 µm sieve. Furthermore, the activated carbon used in this filter was derived from treated wood charcoal. Sand (4 kg) was spread in the upper

layer for easy drainage of water. Six kg laterite material (6 kg) was used for As adsorption due to its high Fe and Al oxides contents that have a high adsorption capacity to remove As. Brick chips (2 kg) were used for transient water flow. In Filter 2, coarse laterite material, which had been ground and past through 2 mm size sieve was used. The wood charcoal was used without $CaCl_2$ treatment. The result indicates that Filter 1 performs well due to the fine laterite particles and activated carbon as compared to Filter 2. It revealed that Filter 1 had an efficiency of about 93 %. This filter reduces As concentration significantly. It is easy to use and can be prepared at home using indigenous materials. Furthermore, its operational cost is very low and can be regenerated easily. The prepared filter had an efficiency of 85 to 93 %. It is recommended for those areas where the As concentration in groundwater is around 70 $\mu g\ L^{-1}$ so that the As concentration in the filtered water can be reduced to below 10 $\mu g\ L^{-1}$. Initially, the filter was not fully saturated, and the water did not contact the whole matrix. Over time, all the matrix in both units became completely saturated and allows more matrix surfaces to contact the flowing water, which results in increased adsorption of As and ultimately greater efficiency. This suggests that initially, the filter needs to be equilibrated for a few days until all the matrixes in the units become completely saturated. After treatment, the filtrate can be consumed for drinking purposes. Role of pH on arsenic removal efficiency of laterite was studied and showed that at pH 10, more than 90 % As(III) was removed and less than 10 $\mu g\ L^{-1}$ could be maintained within 5 min by keeping the arsenite and laterite ratio to less than 10.[21]

Electrical conductivity indicates the amount of dissolved ionic constituents in water. Non-significant variation occurred in the *EC* of Filter 1 was observed throughout the experiment and it remained in the range from 2 to 2.8 $\mu S\ cm^{-1}$, whereas in case of Filter 2, the *EC* was reduced significantly from 10 to 5 $\mu S\ cm^{-1}$ and then remained below 4 $\mu S\ cm^{-1}$ throughout the experiment. These small variations in Filters 1 and 2 may be attributed to the seasonal variation in the groundwater that was used as the input source to the filters. Several studies showed that the *EC* of the groundwater sample was in the range from 14.44 to 12.22 $\mu S\ cm^{-1}$.[44] Similarly, a study reported the *EC* of the groundwater was 11.08 $\mu S\ cm^{-1}$ throughout the study.[45] The pH of Filters 1 and 2 was in the range of 7.3 to 8 and did not change significantly throughout the experiment. A study showed the pH values of drinking groundwater samples in the range of 6.09––7.05, with the lower value was in the acidic range, which later somewhat drop to the limit of 8.5, which is the endpoint of the safe limit.[46] The WHO recommends a pH range of about to 6.5 or higher for drinking water.[47] Although drinking water with a pH greater than 8.0 would be harmful and need treatment. Good quality water usually has pH values in the range of 6.5 and 8.5. This pH range is observed for some of the typical greatest basins of the world.[48]

Filter water samples from both filters were analyzed for their SO_4^- concentration and the results showed that the SO_4^- concentration in Filter 2 was slightly higher throughout the experiment. In the initial 10 days, the variation in the concentration of SO_4^- was higher but later both the filters showed the same trend with minor variations. Overall, the SO_4^- concentration was with the threshold level of 250 mg L^{-1}. No strict health guideline for SO_4^- has been established but if the SO_4^- concentration increases to above 500 mg L^{-1}, there is an increased probability of health problems.[49] Globally conducted surveys indicated the SO_4^- concentration of freshwater is around 20 mg L^{-1} while in rivers, the range is from 0 to 630 mg L^{-1}. In Belgium and Mexico, the SO_4^- concentration of groundwater is in the range of 2 to 250 mg L^{-1} while in Chile and Morocco, the SO_4^- concentration in the groundwater is in the range 0 to 230 mg L^{-1}.[48] The chloride concentration in both the filters varied significantly. Initially, Filter 1 had a high value on day 1 but during the remaining experiment duration, the Cl contents were almost constant and remained mostly below 100 mg L^{-1}. While the Cl concentration in water obtained from Filter 2 decreased over time but remained significantly higher than in the water from Filter 1. This may be attributed to the addition of Cl in the reservoir for groundwater collection when the Filter 2 experiment was performed. A study on Cl analysis of the water samples indicated the 13 samples had a statistically different concentration of Cl with a maximum value of 62 mg L^{-1}.[50]

The concentration of Na in Filters 1 and 2 varied initially up to 20 days, thereafter the variation was minimal. In Filter 1, Na was slightly higher compared to Filter 2 but the variation in Na concentration remained constant in Filter 1 while in Filter 2 the Na concentration increased with duration of the experiment. Overall, the Na concentration remained below 50 mg L^{-1}. Usually, the water from the highland springs showed lowered Na concentration, *i.e.*, around 2 mg L^{-1}. However, in some areas, the water samples had a Na content as high as 331 mg L^{-1}. Several studies reported that a concentration of Na above 100 mg L^{-1} in drinking water may result in hypertension.[50] The calcium concentrations in both filters was low and varied only slightly up to the 18th day of the experiment and then it increased in both the filters to the maximum Ca concentration in Filter 1 of 65 mg L^{-1} and in Filter 2 of 50 mg L^{-1}. In several studies were performed to examine the composition of bottled mineral water in which the Ca concentration varied from 2 to 384 mg L^{-1}.[50] The concentration of the K in the filters decreased with increasing days of the experiment. However, Filter 2 showed significantly higher values of K as compared to Filter 1. Overall, Filter 1 had K concentrations in the range of 9 to 44 mg L^{-1}, while in Filter 2, the K concentration varied from 32 to 56 mg L^{-1}. In one study, it was observed that the K concentration was as low as 0.3 mg L^{-1} in Perrier water samples while in some samples the concentration of K was around 54.4 mg L^{-1}.[50]

In the case of *TDS*, the Filter 1 concentration was lower as compared to Filter 2 and remained almost unchanged throughout the experiment. While in Filter 2, the TDS was initially very high and decreased with the experimental days. Studies reported a *TDS* of groundwater of around 1000 mg L^{-1} represents a very deep water level or water from uplands. A low *TDS* is known to be a characteristic of mountains and upload areas that represent areas of recharge.[51] It was reported that the range of particulate matter or suspended particles was consistently found as around 350 mg L^{-1}.[52] Globally, these particles also came into the low range in contrast with dissolved matter concentrations, which are found to be numerous hundreds of mg L^{-1}. It was reported that if the water contains a *TDS* of less than 1000 mg L^{-1} then it could be freshwater and good enough for both drinking and irrigational purposes.[52]

An important water quality parameter, NO_3^-, was also studied during the filter test. Overall, the concentration of the NO_3^- was within the permissible limits, but Filter 2 showed extreme variations as compared to Filter 1, which remained almost consistent throughout the experiment. It was reported that in different countries the level of NO_3^- does not exceed 10 mg L^{-1} in drinking-water. While in most European countries, 0.5 to 10 % of the population[53] uses well water having NO_3^- concentration above 50 mg L^{-1} for drinking water. In the Netherlands, the NO_3^- range is frequently below 0.1 mg L^{-1}.

The concentration of HCO_3^- in both the filters showed the same trends as it remained continuously variable throughout the experimental days. The concentration of HCO_3^- was in the range of 180–701 mg L^{-1}.

CONCLUSIONS

The study concludes that Filter 1 had higher adsorption due to fine laterite particle and activated carbon as compared to Filter 2. The removal efficiency of Filter 1 was 93 % compared to 83 % for Filter 2. The results revealed that the laterite mineral had a high adsorption capacity to remove As from drinking water and it could easily reduce the cost of filtered water. The 0.53 μm particle size fraction of laterite and activated carbon combination was found better. These filters can reduce the As concentration below WHO international safe limit of 10 μg L^{-1} from highly As contaminated drinking water having As up to 60 and 70 mg L^{-1}. It is easy to use and can be prepared at home using indigenous materials. Furthermore, its operational cost is meager and it can be regenerated easily. Most of the water quality parameters, such as *TDS* and Cl, remained well below the WHO guideline values.

SUPPLEMENTARY MATERIAL

Additional data are available electronically at the pages of journal website: https://www.shd-pub.org.rs/index.php/JSCS/index, or from the corresponding author on request.

И З В О Д

МОГУЋНОСТ КОРИШЋЕЊА ЛАТЕРИТА КАО ФИЛТАРСКОГ МЕДИЈА ЗА УКЛАЊАЊЕ АРСЕНА ИЗ ПОДЗЕМНИХ ВОДА

HAFZA RUQYA MAQSOOD[1], SHAH RUKH[2], MUHAMMAD IMRAN1, AYAZ MEHMOOD[3], WAZIR AHMAD[1], AMAR MATLOOB[4], HAFIZ SHAHZAD AHMAD[1], AHMAD KHAN[5] и SUNDUS AROOJ BUTT[5]

[1]Department of Soil and Environmental Sciences, MNS-University of Agriculture, Multan, Pakistan, [2]National Center of Excellence in Geology, University of Peshawar, Pakistan, [3]Department of Soil and Climate Sciences, The University of Haripur, Haripur, Pakistan, [4]Department of Agronomy, MNS-University of Agriculture, Multan, Pakistan u [5]Institute of Soil Science, PMAS-Arid Agriculture University Rawalpindi, Pakistan

Арсен (As) у води за пиће има хронични утицај на људе и стога представља глобално здравствено питање. Становници Пакистана углавном користе подземне воде за пиће, што је представља потенцијални извор тровања арсеном. Циљ ове студије био је да се процени латерит као адсорбциони медиј за уклањање арсена и накнадна израда јефтиног филтера за његово уклањање. Латерит је тестиран на адсорпциони капацитет арсена кроз експеримент шаржне сорпције и фитовање параметара Лангмировим моделом. Два идентична филтера су припремљена користећи различите односе величине честица латерита и материјала подлоге (песак, активни угаљ и уситњена опека). Вода загађена арсеном свакодневно је пропуштана кроз филтер и сакупљана за анализу. Узорци воде су анализирани на присуство As користећи атомски апсорпциони спектрофотометар упарен са системом за стварање хидрида. Остали параметри квалитета воде, као што су електрична проводљивост, pH, садржај хлорида, укупне суспендоване чврсте честице, укупне растворене соли, садржај нитрата, калцијума, магнезијума, натријума, калијума, карбоната, бикарбоната и сулфата такође су одређивани. Филтер 1 је имао ефикасност уклањања As од око 83 до 93 %, а Филтер 2 од око 67 до 85 %. Већина параметара квалитета воде остала је испод препоручених граница Светске здравствене организације, што указује на то да супстрат не утиче на квалитет филтриране воде. Може се закључити да латерит може послужити као економична опција за уклањање арсена из контаминиране подземне воде.

(Примљено 10. марта, ревидирано 24. августа, прихваћено 31. августа 2020)

REFERENCES

1. World Health Organization (WHO), *Expert consultation on rabies: second report*, Geneva, Switzerland, 2013
2. B. D. Mandal, K. T. Suzuki, *Talanta* **58** (2002) 201 (https://doi.org/10.1016/S0039-9140(02)00268-0)
3. S. Aredes, B. Klien, M. Palwik, *J. Clean. Prod.* **29** (2012) 208 (https://doi.org/10.1016/j.jclepro.2012.01.029)
4. A. Azizullah, M. N. Khattak, P. Richte, D. P. Häder, *Environ. Int.* **37** (2011) 479 (https://doi.org/10.1016/j.envint.2010.10.007)
5. R. T. Nickson, J. M. McArthur, B. Sherestha, Kyaw-Myint, D. Lowry, *Appl. Geochem.* **20** (2005) 55 (https://doi.org/10.1016/j.apgeochem.2004.06.004)
6. M. A. Tahir, H. Rasheed, S. Imran, *Water Quality Status in Rural Areas of Pakistan*, PCRWR, Ministry of Science and Technology, Pakistan, 2010
7. A. Farooqi, H. Masuda, N. Firdous, *Environ. Pollut.* **145** (2007) 839 (https://doi.org/10.1016/j.envpol.2006.05.007)
8. F. Hashmi, J. M. Pearce, *Sustain. Dev.* **19** (2011) 223. (https://doi.org/10.1002/sd.414)

9. P. L. Smedley, D. G. Kinniburgh, *Appl. Geochem.* **17** (2002) 517 (https://doi.org/10.1016/S0883-2927(02)00018-5)

10. J. Mähler, I. Persson, *Appl. Geochem*. **37** (2013) 179 (https://doi.org/10.1016/j.apgeochem.2013.07.025)

11. G. Chen, H. Shi, J. Tao, L. Chen, Y. Liu, G. Lei, X. Liu, J. P. Smol, *Sci. Rep*. **5** (2015) 17419 (https://doi.org/10.1038/srep17419)

12. J. V. Bothe, P. W. Brown, *Environ. Sci. Technol.* **33** (1999) 3806 (https://doi.org/10.1021/es980998m)

13. J. Matschullat*, Sci. Total Environ.* **249** (2000) 297 (https://doi.org/10.1016/S0048-9697(99)00524-0)

14. M. Berg, H. C. Tran, T. C. Nguyen, H. V. Pham, R. Schertenleib, W. Giger, *Environ. Sci. Technol*. **35** (2001) 2621 (https://doi.org/10.1021/es010027y)

15. S. H. A. Shah, *Geol. Bull. Univ. Peshawar* **17** (1984) 107

16. W. Schellmann, *Catena* **52** (2003) 77 (https://doi.org/10.1016/S0341-8162(02)00178-9)

17. H. S. Altundogan, S. Altundogan, F. Tümen, M. Bildik, *Waste Manage.* **22** (2002) 357 (https://doi.org/10.1016/S0956-053X(01)00041-1)

18. A. Maiti, J. K. Basu, S. De. *Chem. Eng. J.* **191** (2012) 1 (https://doi.org/10.1016/j.cej.2010.01.031)

19. S. K. Maji, A. Pal, T. Pal, *J. Environ. Sci. Health, A* **42** (2007) 453 (https://doi.org/10.1080/10934520601187658)

20. S. K. Maji, A. Pal, T. Pal, *J. Hazard. Mater*. **151** (2008) 811 (https://doi.org/10.1016/j.jhazmat.2007.06.060)

21. R. M. S. C. Ranasinghe, D. R. I. B. Werellagama, R. Weerasooriya, *Engineer* **47** (2014) 23 (http://doi.org/10.4038/engineer.v47i2.6865)

22. A. Maiti, S. Dasgupta, J. K. Basu, S. De, *Sep. Purif. Technol.* **55** (2007) 350 (https://doi.org/10.1016/j.seppur.2007.01.003)

23. A. Maiti, B. K. Thakur, J. K. Basu, S. De, *J. Hazard. Mat*. **262** (2013) 1176 (https://doi.org/10.1016/j.jhazmat.2012.06.036)

24. M. P. Elizalde-González, J. Mattusch, R. Wennrich, *J. Environ. Monitor.* **3** (2001) 22 (https://doi.org/10.1039/B006636M)

25. V. K. Gupta, V. K. Saini, N. Jain, *J. Colloid Interface Sci.* **288** (2005) 55 (https://doi.org/10.1016/j.jcis.2005.02.054)

26. T. S. Singh, K. K. Pant, *Sep. Purif. Technol*. **36** (2004) 139 (https://doi.org/10.1016/S1383-5866(03)00209-0)

27. O. Zanella, I. C. Tessaro, L. A. Féris, *Chem. Eng. Technol*. **31** (2014) 205 (https://doi.org/10.1002/ceat.201300808)

28. J. K. Syers, R. F. Harris, D. E. Armstrong. 1973. *J. Environ. Qual.* **02** (1973) 628 (doi:10.2134/jeq1973.00472425000200010001x)

29. C. L. Castro, D. L. Rolston, *Soil Sci. Soc. Am. J.* **41** (1977) 1085 (https://doi.org/10.2136/sssaj1977.03615995004100060014x)

30. J. D. Rhodes, in *Methods of Soil Analysis Part 2, Chemical and microbiological properties*, No. 9, A. L. Page, Ed., Am. Soc. Agron., Madison, WI, 1982, p. 167 (https://doi:org/10.2134/agronmonogr9.2.2ed.c10)

31. E. O. Mclean, in *Methods of Soil Analysis Part 2, Chemical and microbiological properties*, No. 9, A. L. Page, Ed., Am. Soc. Agron., Madison, WI, 1982, p. 199–225 (https://doi.org/10.2134/agronmonogr9.2.2ed.c12)

32. *APHA 1995. Standard Methods for the Examination of Water and Wastewater*, 19th ed., American Public Health Association Inc., New York

33. B. W. Hipp, G. W. Langdale, *Commun. Soil Sci. Plant Anal.* **2** (1971) 237 (https://doi.org/10.1080/00103627109366310)
34. S. G. Simpson, *Ind. Eng. Chem.* **16** (1924) 709 (https://doi.org/10.1021/ie50175a019)
35. M. A. Tabatabai, *Environ. Lett.* **7** (1974) 237 (https://doi.org/10.1080/00139307409437403)
36. D. A. Cataldo, M. Haroon, L. E. Schrader, V. L. Youngs, *Soil Sci. Soc. Am. J.* **41** (1975) 1085 (https://doi.org/10.1080/00103627509366547)
37. E. P. Welsch, J. G. Crock, R. Sanzalone, in *Quality assurance manual for the Branch of Geochemistry*, B. F. Arbogast, Ed., U.S. Geological Survey: U.S. Geological Survey Open-File Report 90-668, 1990, p. 36
38. C. Moreda-Pineiro, P. Moscoso-Perez, S. Lopez-Mahia, E. Muniategui-Lorenzo, Fernandez-Fernandez, D. P. Rodriguez, *Talanta* **53** (2001) 871 (https://doi.org/10.1016/S0039-9140(00)00578-6)
39. H. Zhang, H. M. Selim, *Environ. Sci. Technol.* **39** (2005) 6101 (https://doi.org/10.1021/es050334u)
40. H. J. Shipley, S. J. Yean, A.T. Kan, M. B. Tomson, *Environ. Toxicol. Chem.* **28** (2009) 509 (https://doi.org/10.1897/08-155.1)
41. K. P. Raven, A. Jain, R. H. Loeppert, *Environ. Sci. Technol.* **32** (1998) 344 (https://doi.org/10.1021/es970421p)
42. Y. Jeong, M. Fan, S. Singh, C. L. Chuang, B. Saha, J. Hans van Leeuwen, *Chem. Eng. Process.* **46** (2007) 1030 (https://doi.org/10.1016/j.cep.2007.05.004)
43. I. Polowczyk, P. Cyganowski, J. Ulatowski, W. Sawiński, A. Bastrzyk, *Water Air Soil Pollut.* **229** (2018) 203 (https://doi.org/10.1007/s11270-018-3866-2)
44. E. Yilmaz, C. Koc, *J. Water Resour. Prot.* **6** (2014) 63 (https://doi.org/10.4236/jwarp.2014.62010)
45. H. H. Oyem, I. M. Oyem, D. Ezeweali, *Res. J. Environ. Sci.* **8** (2014) 444 (https://doi.org/10.3923/rjes.2014.444.450)
46. I. E. Ahaneku, P. A. Adeoye, *Br. J. Appl. Sci. Technol.* **4** (2014) 440 (https://doi,org/10.9734/BJAST/2014/5079)
47. World Health Organization (WHO), *Guideline for drinking water quality*. 3rd ed., Geneva, 2010
48. UNEP, GEMS/Water data summary 1985–1987. Canada Centre for Inland, Burlington, 1990
49. World Health Organization (WHO), *Guidelines for drinking-water quality*, Vol. 1. *Recommendations*. 3rd ed., Geneva, Switzerland, 2004
50. H. E. Allen, M. A. Halley-Henderson, C. N. Hass, *Arch. Environ. Health* **44** (1989) 102 (https://doi.org/10.1080/00039896.1989.9934383)
51. S. B. Olobaniyi, J. E. Ogala, N. B. Nfor, *J. Mining Geol.* **43** (2007) 79 (http://dx.doi.org/10.4314/jmg.v43i1.18867)
52. S. M. Shahidullah, M. A. Hakim, M. S. Alam, A.T. M. Shamsuddoha, *Pak. J. Biol. Sci.* **3** (2000) 246 (https://doi.org/10.3923/pjbs.2000.246.249)
53. World Health Organization (WHO), Guidelines for Drinking Water Quality, Health Criteria and Other Supporting Information, Geneva, Switzerland, 1984.

Evaluation of laterite as a filter media to remove arsenic from groundwater

HAFZA RUQYA MAQSOOD[1], SHAH RUKH[2]*, MUHAMMAD IMRAN[1], AYAZ
MEHMOOD[3], WAZIR AHMAD[1], AMAR MATLOOB[4], HAFIZ SHAHZAD AHMAD[1],
AHMAD KHAN[5] and SUNDUS AROOJ BUTT[5]

[1]Department of Soil and Environmental Sciences, MNS-University of Agriculture, Multan,
Pakistan, [2]National Center of Excellence in Geology, University of Peshawar, Pakistan,
[3]Department of Soil and Climate Sciences, University of Haripur, Haripur, Pakistan,
[4]Depaertment of Agronomy, MNS-University of Agriculture, Multan, Pakistan and
[5]Institute of Soil Science, PMAS-Arid Agriculture University Rawalpindi, Pakistan

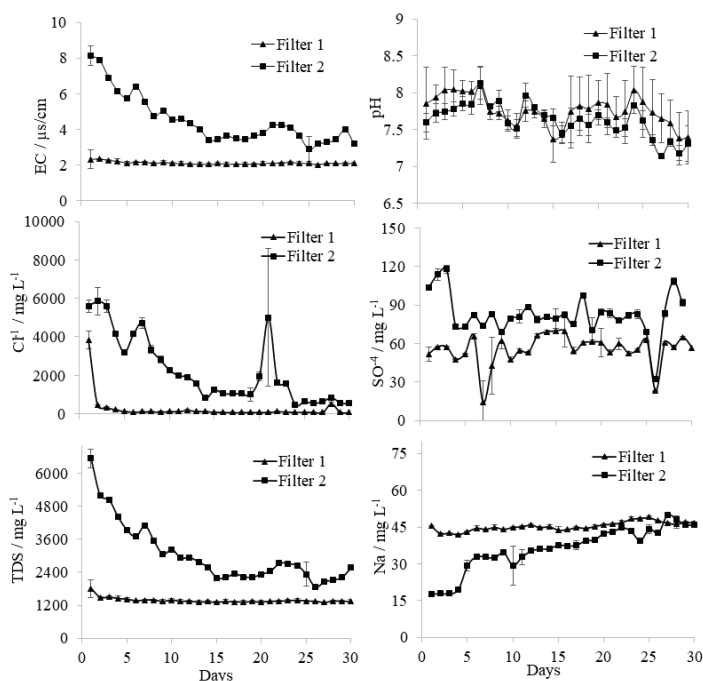Fig. S-1. The changes in parameters (EC, pH, Cl, SO_4^-, TDS and Na) with the experimental days.
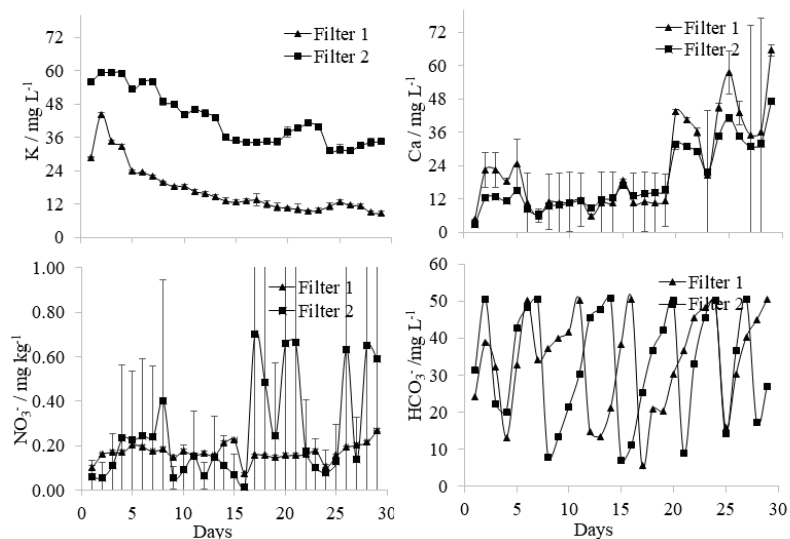
* Corresponding author. E-mail: shahrukh.nceg@uop.edu.pk

Fig. S-2. Variations in K, Ca, NO_3^- and HCO_3^- content with the experimental days.
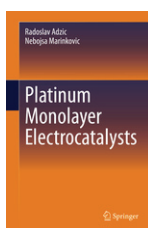
BOOK REVIEW
Platinum Monolayer Electrocatalysis

Authors: Radoslav Adžić and Nebojša Marinković

SLAVKO MENTUS[1,2]*

[1]*Faculty of Physical Chemistry, University of Belgrade, Studentski trg 12–14, 11158 Belgrade, Serbia and* [2]*Serbian Academy of Sciences and Arts, Knez Mihajlova 35, 11158 Belgrade, Serbia*

(Received and accepted 6 January 2021)

At first glance, this book captures attention with its splendid, dominantly orange colored hardcover. Within a volume of 167 pages, the reader encounters 11 chapters bearing the following titles: 1. Short Introduction to the Science of Electrocatalysis, 2. Electrocatalytic reactions, 3. Electrochemical Energy Conversion in Fuel Cells, 4. Studies of Electrocatalytic Reactions, 5. Important Electrosorption Reactions, 6. Important Electrocatalytic Reactions, 7. Platinum Monolayer Electrocatalysts, 8. Catalytic Properties of Pt Monolayer Electrocatalysts, 9. Performance Stability and Scale-Up Syntheses of Pt Monolayer Electrocatalysts, and, 11. Prospects for Platinum and Platinum Group Metal Monolayer Electrocatalysts.

One deals here with a scientific monograph based primarily on the authors personal research achievements. After a short introduction to the electrocatalysis, covering four reactions important for energy conversion in fuel cells in the first four chapters, in the fifth one the authors describe the properties of metal monolayers on electrode surfaces and underpotential deposition of metals. The period covered by this chapter begins with the Adžićs famous discovery of huge enhancement of electrocatalytic effectivenes of Pt surfaces upon adsorption of metal (Pb, Bi) submonolayers in 1970s. The main part of the book covers the descript-

---

* E-mail: slavko@ffh.bg.ac.rs

ion of very concept of Pt monolayer electrocatalysts, the ways of their synthesis and application. Through the description of numerous technically demanding investigations of four main reactions in energy conversion processes: oxygen reduction reaction and oxidation reactions of hydrogen, methanol and ethanol reactions on single-crystal surfaces, the book matter continues up to the recent application oriented systems. They involve stable, long-living core-shell structured electrocatalyst with durable, frugal Pt monolayers covering the cores of more abundant metals (Au, Pd and their alloys, and non-noble metals and alloys). In the concluding chapter the authors comment the predictions in scale-up syntheses and catalysts' stability in practical use.

What one might say about the temporary circumstances in which this book appeared?

The investigation of room-temperature fuel cells, the main subject of the book, experienced sudden acceleration after famous world oil crisis in 1970s. Since then, the developed countries funded many projects dedicated to the replacement of liquid fossil fuels in trafic by chemical sources of electric energy. With the oil market stabilization, this tension declined, however, in the period 1990–2000 a new threat splashed the world: climate changes caused by huge consumption of fossil fuels, which actualised the activities oriented to the development of new chemical power sources. Platinum seemed to be unavoidable electrocatalyst providing satisfactory effectiveness of fuel cells. In 2010s, an ambitious worlds action, supported by relevant UN bodies, to replace gradually all oil-driven automobile engines by electrically powered ones, seemed to be unattainable due to the too high demand of platinum in comparison to available Earth crust resources. This is the reason why automobile companies started to use Li-ion batteries rather than fuel cells, and a majority of both research grants and research institutions reoriented themselves toward the development of batteries. However, the authors of this book persisted in their research orientation, what resulted in many valuable new contributions in saving platinum as fuel cell electrocatalyst. This proved onself as reasonable performance, since metal resources required for Li-ion batteries became also critical, susceptible to rapid exhaustion in the next few decades. This new threat is the reason why the search for advanced fuel cell electrocatalysts is under permanent progress.

As the Springer's editor said, "Platinum monolayer electrocatalysts present a groundbreaking discovery that will likely have impact on future electrocatalysis. Unlike non-noble metal monolayer, platinum monolayer can have great stability and activity that can overcome three major obstacles of conventional platinum electrocatalysts – catalysts' cost, activity, and stability for a broad range of fuel cell applications." This is a reason why important automobile producers persisted in the development of fuel cells-driven automobiles. On dispasal stands the Platinum monolayer electrocatalyst developed by the authors of this book, produced

by N.E. ChemCat Corporation in Japan. It is licensed to two other companies. An actual difficulty for broader use of fuel cell powered automobiles, compared to battery driven ones, is the technically unsolved hydrogen distribution network, however this may be considered only as temporary obstacle.

This book may be highly recommended as an useful theoretical and practical guide to graduate, especially PhD students, preparing themselves for studies in surface science and electrocatalysis. Furthermore, reading this book, the researchers active in development of fuel cells will face the most recent research techniques available in worlds leading research institutions. Thanks to a selected literature surveys placed at the end of each chapter, the reader may follow a chronological development of fundamental concepts and practical aspect of functioning of electrocatalysts for contemporary room temperature fuel cells. Particularly, numerous practical examples illustrated by coloured graphs, discussed in a comprehensive language, offers a plenty part of knowledge presented in a concise and clear manner, as, otherwise, is really expected from the authors deeply personally involved in the subject matter of the book. I really enjoyed reading it.